Session 1

Monday August 22, 2022

1:30pm – 3:00pm

O1.1 – Assistive Technologies and Robotics

O1.2 – Imaging 1 – Bone

O1.3 – Metabolics/Energetics of Locomotion

O1.4 – Military and Veteran's Health

O1.5 – Sports Injuries 1

ELASTIC EXOSKELETONS MAY NOT OFFLOAD THE TRICEPS SURAE AS EXPECTED

Dylan G. Schmitz[1*], Sara E. Harper[1], and Darryl G. Thelen[1]
[1]University of Wisconsin – Madison, Department of Mechanical Engineering
email: *dgschmitz@wisc.edu

Introduction

Elastic ankle exoskeleton devices have shown success at reducing metabolic cost in walking [1,2] and running [3] by applying additional plantarflexion torque about the ankle in parallel with the triceps surae. Commonly, changes in the triceps surae forces are characterized by subtracting the external exoskeleton torque from the net ankle torque computed via inverse dynamics, predicting an overall reduction in triceps surae loading [2]. In this study, we used shear wave tensiometry to directly measure the Achilles tendon (AT) forces while walking with an elastic exoskeleton. We hypothesized that AT force would decrease as the external exoskeleton torque increased.

Methods

One male subject (26 yr, 190 cm, 95 kg) walked on a treadmill at 1.34 m/s wearing a bilateral passive elastic exoskeleton. The exoskeleton was engaged in stance and disengaged in swing with a mechanical clutch [1]. Three angular stiffnesses (20.7, 25.9, 35.8 N*m/rad) were applied for 30 sec trials and compared to the slack condition (0 N*m/rad). Exoskeleton force was measured with an in-line load cell (Futek lsb205). Joint angles were measured with IMUs (Xsens Awinda). The effective angular stiffness of the exoskeleton was computed by linear regression of exoskeleton torque versus ankle angle during stance. Force in the right AT was measured via shear wave tensiometry [4]. Muscle activity in the right soleus (SOL), medial gastrocnemius (MG), lateral gastrocnemius (LG), and tibialis anterior (TA) were measured with surface EMG (Delsys Bagnoli).

Results and Discussion

As expected, peak exoskeleton torque increased with increasing exoskeleton stiffness. By subtracting exoskeleton torque from measured triceps surae ankle torque during the slack condition, peak AT force was expected to decrease by 7% for the stiffest condition. Instead, peak AT force increased by 37% over the slack condition. A similar trend appeared in the plantarflexor muscle activity. While mid-stance SOL activity decreased with increasing stiffness, peak SOL and LG activity during push-off increased slightly, and peak MG activity increased substantially. Average TA activity during stance remained low throughout, suggesting that changes in co-contraction were minimal. These results make it clear that the exoskeleton did not offload the triceps surae as expected. In order to maintain a torque balance during gait, it is feasible that unobserved adaptation occurred at other joints. Further investigation is underway to see whether these trends hold across subjects and how the increased net plantarflexion torque is balanced.

These initial results suggest that the torque provided by an elastic exoskeleton may not have the expected effect on triceps surae forces. Simply applying a parallel plantarflexion torque about the ankle does not necessarily result in reduced triceps surae forces, but rather triggers a complex biomechanical response, including modified muscle coordination and perhaps adaptation in other parts of the body.

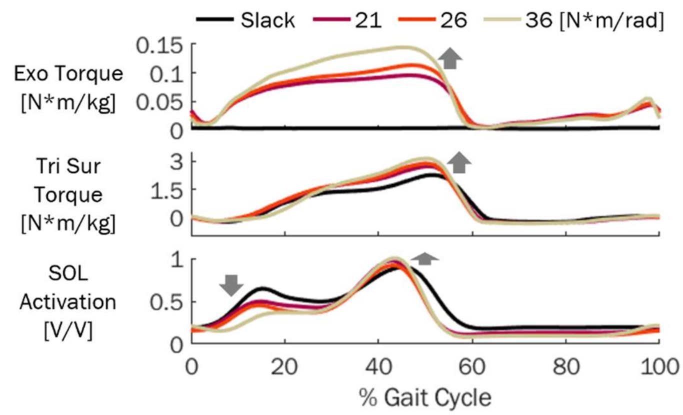

Figure 1: Triceps surae torque about the ankle, exoskeleton torque, and SOL activation for each condition.

Significance

These preliminary findings indicate that inverse dynamics and simple torque balance about the ankle are insufficient to characterize the changes in triceps surae forces due to an elastic exoskeleton. Likely, adaptations are more complex, potentially including changes in hip or knee kinematics, or perhaps modified energy storage and return in the arch of the foot [5]. A better understanding of how musculoskeletal loading adapts to an applied external torque will help us design more effective, more comfortable exoskeletons.

Acknowledgments

Funding: NSF DARE (2019621), NSF GRFP (DGE-1747503), NIH TL1TR002375.

References

[1] Collins et al., 2015. *Nature*. 522(212-215). [2] Nuckols et al., 2020. *Sci Rep.* 10(1-15). [3] Witte et al., 2020. *Sci Rob.* 5(40). [4] Martin et al., 2018. *Nat Commun.* 9(1592). [5] Welte et al. 2018. *J. R. Soc. Interface.* 15(20180270).

Table 1: Measured and computed data for exoskeleton stiffness, exoskeleton and triceps surae (TS) torque about the ankle, and muscle activity.

Exo Stiffness [N•m/rad]	Peak Exo Torque [N•m/kg]	Peak TS Torque [N•m/kg]	SOL Activity (mid-stance) [V/V]	SOL Activity (peak) [V/V]	MG Activity (peak) [V/V]	LG Activity (peak) [V/V]	TA Activity (stance) [V/V]
0	0	2.27	0.65	0.90	0.68	0.85	0.064
20.7	0.10	2.73	0.50	0.97	0.87	0.97	0.065
25.9	0.11	2.89	0.45	0.92	1.00	1.00	0.060
35.8	0.15	3.15	0.34	1.00	0.98	0.96	0.064

Exoskeletons need to react faster than reflexes to improve standing balance

Owen N. Beck,[1*] Max K. Shepherd,[2,3] Rish Rastogi,[1] Lena H. Ting,[1] & Gregory S. Sawicki[4]
[1]Wallace H. Coulter Department of Biomedical Engineering, Emory University & Georgia Institute of Technology
[2]Depts. Physical Therapy, Movement & Rehabilitation Sciences and [3]Mechanical & Industrial Engineering, Northeastern University
[4]George W. Woodruff School of Mechanical Engineering, Georgia Institute of Technology *email: obeck3@gatech.edu

Introduction

It is important for people to maintain balance as they perform activities of daily life. Failure to do so may cause harmful falls and lead to declining independence and quality of life. To improve human balance and mitigate fall-risk, researchers often propose interventions that enhance human biomechanics. A feasible way to improve user biomechanics is through the use of wearable assistive devices, such as exoskeletons. Exoskeletons typically act in parallel to user leg joints and can deliver balance-correcting torque following postural perturbations.

While exoskeletons have the potential to improve user balance in many situations, it remains unknown *how* these devices should deliver restoring torque following a perturbation. As people begin losing balance, the body's sensory receptors detect perturbations and spur corrective motor commands. Due to delays in the nervous system, reflexive responses take ~150 ms until restoring leg muscle forces of the balance correcting response are measurable (1). Exoskeletons can detect a perturbation and produce torque faster than the nervous system, but artificially fast torque production may disrupt important sensory information and impair the body's reactive response.

Accordingly, the goal of our study was to determine whether it is more effective for balance-improving exoskeletons to deliver assistive torque 1) faster than, or 2) coinciding with physiological time delays. Based on the notion that artificially fast exoskeleton torque would impair user reactive feedback response, we hypothesized that user standing balance capacity would be best when ankle exoskeletons produced plantar flexor torque at the same latency as the body's reactive postural response, versus artificially fast or no assistive torque conditions.

Methods

To test our hypothesis, we evaluated the standing balance capacity of ten participants across three different ankle exoskeleton conditions (Fast, Slow, Off). Specifically, participants tried to maintain standing balance without taking balance-correcting steps during backward support surface translations (Fig. 1). During these translations, we commanded the exoskeletons to detect perturbation onset using accelerometers and randomly perform one of the following actions: (Fast condition) produce a 30 Nm peak plantar flexor torque following a ~20 ms delay over a 50 ms rise-time followed by a decline in torque in 150 ms, (Slow condition) produce the same torque profile following an additional 100 ms delay after detecting perturbation onset, or (Off condition) maintain 1 Nm throughout the duration of the trial (Fig. 1). The magnitude of each support surface translation was updated for each trial using an adaptive Parameter Estimation algorithm (2). This algorithm continuously estimated the perturbation magnitude for each exoskeleton condition that elicited a 50% chance of the participant taking a step, which we termed 'Step Threshold' and used as our measure of balance capacity (3). We determined each participant and exoskeleton condition step threshold by fitting psychometric curves to the experimental data via maximum likelihood. We performed a repeated-measures ANOVA to test the influence of exoskeleton condition on step threshold.

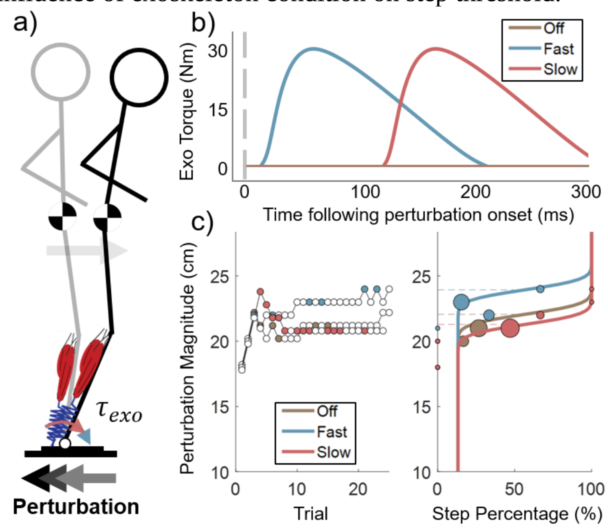

Figure 1. a) Depiction of a person experiencing a support-surface translation. b) Ankle exoskeleton torque (τ_{exo}) conditions. c) (left) Representative perturbation trials for a participant at each exoskeleton condition. Open and closed symbols indicate successful standing balance and stepping response per perturbation, respectively. (right) Psychometric curve fit for each exoskeleton condition, with symbol size proportional to number of trials at the indicated perturbation magnitude.

Results, Discussion, and Significance

The Fast exoskeleton condition improved step threshold 9% and 12% compared to the Off and Slow conditions, respectively (p=0.032. Average ± SD step threshold: Fast 25.4 ± 2.3 cm; Off 23.3 ± 2.4 cm; Slow 22.8 ± 2.4 cm) (Fig. 1). These data suggest that balance improving exoskeletons may be most effective if they can detect and correct postural disturbances faster than physiologically possible. Surprisingly, delivering plantar flexor torque at the same latency as postural reflexes did not improve participant step threshold compared to the Off condition, suggesting that exoskeletons controlled via physiological signals (*e.g.,* myoelectric control) may not improve user balance compared to the absence of an assistive device. Based on these data, we rejected our hypothesis stating that the Slow condition would yield the best user step threshold.

Moving forward we will assess neuromechanical data to propose mechanism(s) underlying our balance results. Perhaps the Fast condition is ideal because it quickly restores the person's center of pressure under their center of mass. Further, we are interested in the interplay of how artificially fast movements affect underlying muscle sensory receptors, and in turn the accompanying postural response.

Acknowledgments

Ga Tech McCamish Innovation Program & NIH HD46922.

References

[1] Ting et al., 2009. *Chaos*. [2] Frederick & Kingdom 2010. *Psychophysics*. [3] Palmer et al., 2021. *Front Aging Neurosci*.

OVERGROUND OPTIMIZATION OF ANKLE EXOSKELETON ASSISTANCE FOR SELF-SELECTED WALKING SPEED

Benjamin A. Shafer[1*], Aaron J. Young[1] and Gregory S. Sawicki[1,2]
[1] George W. Woodruff School of Mechanical Engineering and the Institute for Robotics and Intelligent machines (IRIM), Georgia Institute of Technology, Atlanta, GA 30332 USA
[2]School of Biological Sciences, Georgia Institute of Technology, Atlanta, GA 30332 USA
*Corresponding Author email: Ben.Shafer@gatech.edu

Introduction
As we age, our mobility decreases leading to decreased independence and quality of life. Self-selected walking speed (SSWS), a clinical measure of mobility, has been successfully increased in younger adults using a tethered ankle exoskeleton (exo) on a treadmill but the mechanism for this change is still unknown [1]. Humans intuitively minimize metabolic cost of transport (COT) when selecting walking speed, and rapidly discover novel optima when the COT landscape shifts [2]. In theory, ankle exo mechanical assistance could horizontally shift the COT landscape, placing the minimum at a faster speed, enabling users to converge on a faster SSWS. To increase translation for older adult communities outside the lab, we developed a novel, overground assistance optimization protocol applying an autonomous, commercially available ankle exo. We hypothesized optimal ankle torque assistance (Opt) will result in faster SSWS compared to walking in normal shoes (NoExo) by increasing minimal COT speed.

Methods
Users (N = 3M, 21+/-1 y/o, 66.6+/-2.89 kg, 1.79+/-0.05 m) were habituated to max-torque, spline-based ankle exo assistance (Fig. 1A) for 20 minutes on a treadmill and 200m overground. After habituation, we used a Surrogate Bayesian optimizer to generate torque control parameters seeking to maximize SSWS over 30 iterations by applying suggested optimal parameters and measuring the associated SSWS using a 4m walk test. Finally, SSWS was measured for NoExo and Opt in a validation session. To examine whether shifts in COT landscape drove changes in SSWS, users walked with Opt and NoExo conditions at 5 randomized speeds each (0.65, 1.0, 1.7, Opt SSWS, and NoExo SSWS) while we recorded metabolic cost. We normalized gross metabolic power by speed and mass to calculate COT (J/m/kg) then applied a quadratic fit to calculate the minimum COT speed for each condition.

Results and Discussion
Our novel overground HILO protocol to optimize ankle exoskeleton assistance provided torque profiles that increased SSWS by 8.4% compared to walking in normal shoes (Opt: 1.55+/-.05 m/s; NoExo: 1.43+/-0.06 m/s) (Fig. 1B). Opt exo assistance increased COT at all speeds, with larger increases at slower speeds, re-shaping the COT curve and increasing the minimal COT speed compared to NoExo by 8.3% (Opt: 1.43 m/s; NoExo: 1.32 m/s). Interestingly, SSWS for each condition was faster than the minimum COT speed, but the shift in the minima on the new COT landscape mirrored the shift in SSWS (SSWS: 0.12 m/s; Min. COT speed: 0.11 m/s).

These results suggest our protocol can be used to personalize exo assistance to increase walking speed performance in community settings by shifting the speed that minimizes COT. Interestingly, increasing SSWS does not seem tied to reducing metabolic effort. We note SSWS was systematically faster than minimal COT speed, suggesting other factors may be important (e.g., local muscle fatigue, stability).

Significance
This is the first demonstration that an exoskeleton can be optimized to impact SSWS while user's freely select gait overground. This feasibility study suggests a framework for individualization of exo assistance that can be successfully conducted outside the lab. Future interventions for older adults should focus on decreasing COT at faster speeds to further increase SSWS.

Acknowledgments
This work was supported by an NIH grant (R01NR014756).

References
[1] Song et al., 2019 *IEEE Trans Neural Syst Rehabil Eng* 29
[2] Selinger et al., 2015. *Curr Biol* 25

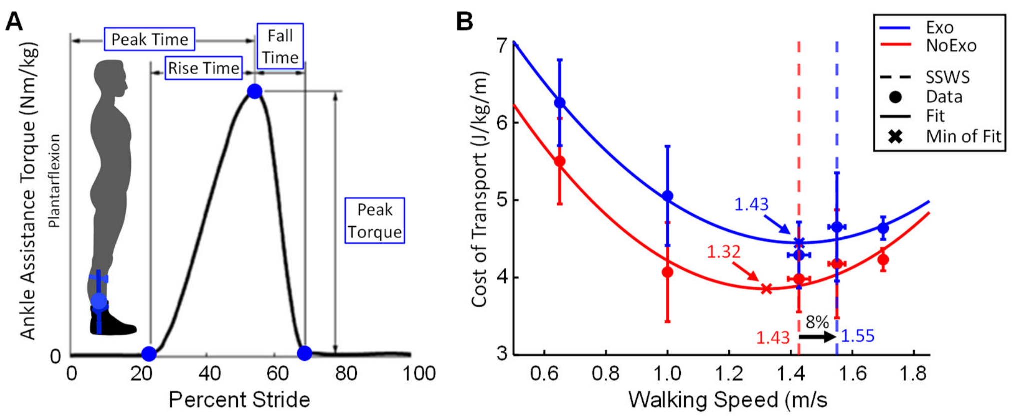

Figure 2: (A) Ankle exoskeleton torque profile and optimization parameters applied at each gait cycle. (B) Metabolic Cost of Transport (COT) across walking speeds with optimized ankle exoskeleton assistance (Exo) (blue) and NoExo (red). Across-participant (N=3) averaged data points shown for each condition and speed. A quadratic curve was fit for each condition across speeds. Self-selected walking speed (SSWS) averaged across participants is shown for each condition.

ACTIVE EXOSUIT CONTROLLER TO REDUCE BACK EXERTION WHILE MINIMIZING RESTRICTION

D. Adam Quirk[1*], Jinwon Chung[1], and Conor J. Walsh[1]
[1]Harvard University, School of Engineering and Applied Sciences
email: Walsh@seas.harvard.edu

Introduction

Back exoskeletons and exosuits are a promising technology to mitigate the risk of back injuries, by delivering assistive forces to reduce measures of back extensor exertion [1]. However, their adoption into occupational settings have been hindered by sources of discomfort arising from system weight and movement restriction [1,2]. Soft and lightweight "exosuits" effectively reduce weight [1]. While passive exosuits eloquently assist many tasks via springs, during dynamic flexion they can restrict motion if the spring is too stiff [3], or becomes too strained [2]. A benefit of active actuation is that it can deliver customizable assistance profiles to mitigating the risk restriction while preserving the ability to deliver high assistive forces when lifting. However, current active systems are heavy and rigid "exoskeletons" [1].

The purpose of this study was to test whether a soft, lightweight active back exosuit using an adaptive impedance force control could reduce back exertion as well as a high stiffness passive elastic system, without movement restriction.

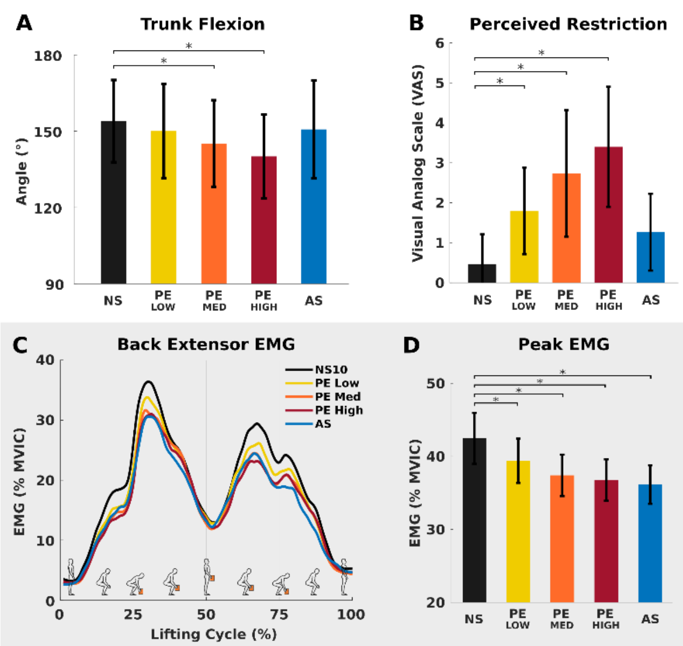

Figure 1: Measured (A) and perceived (B) restriction, and lifting assistance (reduced back extensor EMG (C&D)) afforded by exosuits. Significant post-hoc differences to no suit (NS) are conveyed by a *.

Methods

Fifteen healthy participants (♂=11) performed two highly constrained tasks to test the restrictive and assistive properties of four exosuit conditions and a no exosuit (NS) condition.

Exosuit conditions involved a soft lightweight (2.7kg) battery operated back exosuit delivering assistance with 3 passive elastics (PE) with low, medium or high stiffness or with a sensor based active exosuit (AS). The active suit deliver assistive forces via a generic adaptive impedance profile which considered an individual's phase of motion to deliver lower forces (similar to PE low) when flexing/lowering, to minimize restriction, while having higher assistance (similar to PE high) when extending/lifting to mitigate back extensor exertion.

Exosuit restriction was characterized as the magnitude of IMU measured peak trunk angular displacement, and the participant's level of perceived restriction (0-10 point) during a maximal trunk flexion task. Exosuit assistance was characterized by peak electromyography (EMG) amplitudes measured from 3 back extensor muscles when participants performed a 10kg squat and stoop style lifting task. Outcomes were compared using ANOVAs corrected for multiple comparisons ($\alpha<.0.02$).

Results and Discussion

For the maximum flexion range of motion task, both measured and perceptual restriction increased with increasing levels of exosuit assistive forces delivered during flexion. Only the AS and PE low did not restrict motion (Fig. 1A&B).

For the 10 kg constrained lifting tasks all exosuit conditions reduce peak back extensor EMG amplitudes (Fig 1C&D). Exosuits that delivered higher assistance during lifting lead to greater EMG reductions. The active and PE high reduce activity by 15 and 13% respectively compared to lifts with no exosuit.

The results of this study provides further evidence there exists an assistance-restriction trade-off when delivering forces via passive exosuits [2,3]. However, by utilizing an active adaptive impedance controller, our soft-active exosuit produced predictable yet favourable biomechanical effects. Strategically delivering lower assistive forces (comparable to PE low) during flexion, while simultaneously injecting higher forces (similar to PE High) during extending/lifting, our soft active exosuit successfully considered a user's desired movement direction to circumvent the assistance-restriction trade-off. Incorporating this active controller on a soft structure allowed us to develop a system that retained the favourable weight of a soft passive exosuit (2.7kg) [1]. However, through active actuation, this system was it was just as capable of reducing measures of back extensor exertion as a high stiffness passive elastic without discomfort arising from restriction [2].

Significance

The overall goal of this work is to improve the design of back exoskeletons and exosuits to enhance usability in a workplace. Collectively these data suggests the inclusion of active adaptive impedance controller to a soft-lightweight back exosuit can improve exosuit comfort via reductions to system restriction. It is hoped these efforts will improve translation of this technology to dynamic tasks in the workplace, enhancing system uptake and use time to further increase the potential of back exosuits to reduce the risk of developing occupational low back pain across a wide a range of tasks and activities [1].

Funding Acknowledgments

NIH BACPAC: 1UH2AR076731-01
Department of Defence: W81XWH2010609

References

[1] Toxiri, 2019. *IISE Trans on Occ & Ergo Hum Factors,7,*
[2] Kim, 2020. Applied Ergo., 89, 103194
[3] Frost, 2009, JEK., 19, e40

WALKING SPEED ESTIMATION USING A SINGLE IMU SENSOR FOR A WEARABLE ROBOT APPLICATION

Meet Mevada[1ǂ], Siddarth Vakacharla[1ǂ], Prakyath Kantharaju[1ǂ], Courtney Haynes[2], Courtney Bradford[2] and Myunghee Kim[1*]
[1]Department of Mechanical and Industrial engineering, University of Illinois at Chicago
[2]U.S. ARMY DEVCOM Army Research Laboratory
[ǂ]Equal contribution email: *myheekim@uic.edu

Introduction

Walking speed influences biomechanics and physiological response [1], and exoskeleton assistance must vary to accommodate changes in walking speed. [2,3]. Automatic speed recognition is critical to adapt exoskeleton assistance to walking speed. Current speed recognition algorithms, however, typically require a larger number of sensor modalities, or prior training data, making these methods not ideal for exoskeleton applications. In this study, we use a single chest accelerometer and dynamic walking principle to identify the walking speed. Furthermore, determining the optimal exoskeleton assistance is generally done on a treadmill, but the practical application is in the outdoor setting. We developed an algorithm that works both in an outdoor and indoor application with a similar methodology. We tested this method on overground and treadmill walking conditions. We also performed a sensitivity study to identify the optimal assistance parameter at each speed and illustrate the change in based on the metabolic landscape.

Methods

To estimate the walking speed, we used the vertical acceleration from a chest mounted accelerometer (Polar H10). The vertical acceleration, sampled at 200Hz, is first passed through a low pass filter and detrended to remove noise and the offset due to gravity. The detrended acceleration is then double integrated to obtain the vertical position. During the integration, the velocity and position are initialized to 0. After every stride, the signal is detrended to remove the effects of the integration constant. The apex and bottom point of the vertical position trajectory and subject height are then used to calculate the horizontal distance covered between these two points. Using this horizontal distance and the time between the apex and the bottom point (Fig. 1A), walking speed is calculated every 0.5 s.

In this pilot study, two subjects followed a 2-day protocol designed to observe the effect of ankle exoskeleton parameters of an ankle exoskeleton on the metabolic cost, and to test the speed estimation at 3 different speeds (1.0, 1.25, and 1.50 m/s) on a treadmill. We tested 3 exoskeleton parameters, Dorsi-stiffness, Plantar-stiffness, and maximum plantar-dorsi angle. On day one (acclimation day) the subject was asked to walk with an exoskeleton at three speeds for 7 min each. On the second day (data collection day) the subject walked at each speed for 19 min. During the walking period, each parameter was varied three times while keeping the others constant. Each set of parameters was tested for 2 minutes except for the first set which was for 3 minutes to include additional time to account for transient metabolic rate. Gaussian Process was used on the collected metabolic cost data to visualize the effect of parameters over a range of walking speeds (0.9 to 1.6 m/s).

Additionally, we performed a one subject pilot study to determine the accuracy of the walking speed estimation method for overground. We collected chest-mounted accelerometer and video-based motion tracking while the subject walked overground at 5 speeds spanning 1.0 - 1.5 m/s.

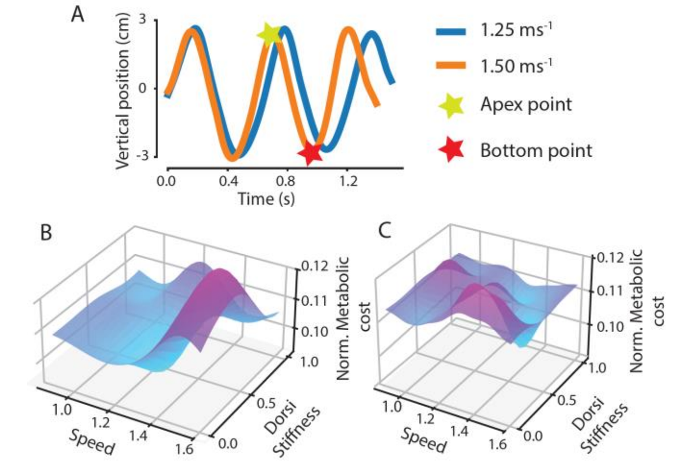

Figure 1: A. Comparison between vertical position trajectory obtained from integration of acceleration. B, C. Metabolic landscape for subjects 1 and 2 obtained from fitting Gaussian process with normalized metabolic cost, walking speed, and stiffness parameter.

Results and Discussion

The proposed speed estimation method had an average mean squared error of 0.004 m/s and 0.008 m/s and a maximum standard deviation of 0.058 m/s and 0.005 m/s for treadmill walking and overground walking, respectively. The high accuracy of the system makes it employable for indoor and outdoor usage. Figure 1BC shows that the optimal controller parameters were different with respect to walking speed. The optimal parameters were different for different speeds, especially the Dorsi stiffness. We also found that the metabolic cost reduction remains almost the same for some parameters such as maximum plantar-dorsi. This result suggests that we need to optimize certain parameters for each speed to maximize metabolic cost reduction while other parameters can remain the same.

Significance

Optimizing exoskeleton assistance for varying walking speeds could bring a greater reduction of metabolic costs. Several studies have shown speed as an important factor in deciding the optimum assistance, but few have incorporated it in indoor and outdoor applications. Our proposed speed estimation system solves this problem by using a dynamic walking model for estimating the speed and can be used for changing the optimal parameters accordingly.

References

[1] Sawicki, Gregory S., et al. JNER 17.1 (2020): 1-9.
[2] Bryan, Gwendolyn M., et al. JNER (2021).
[3] Song, Seungmoon,. et al. TNSRE 29 (2021): 786-795.

MUSCULOSKELETAL MODELS PREDICT THE EFFECT OF A SOFT ACTIVE EXOSUIT ON SPINAL MUSCLE ACTIVATIONS DURING LIFTING

Chenxi Yan[1,2], Jacob J. Banks[1,2], Brett T. Allaire[1], D. Adam Quirk[3], Jinwon Chung[3], Conor J. Walsh[3], Dennis E. Anderson[1,2*]
[1]Center for Advanced Orthopaedic Studies, Beth Israel Deaconess Medical Center, Boston, MA, United States
[2]Department of Orthopaedic Surgery, Harvard Medical School, Boston, MA, United States
[3]John A. Paulson School of Engineering and Applied Sciences, Harvard University, Boston, MA, United States
email: *danders7@bidmc.harvard.edu

Introduction

Lift assist exosuits are designed to mitigate spinal load and costly back injuries[1]. However, quantifying the efficacy of these devices is difficult as *in vivo* measures of spinal loads cannot be directly measured[2]. Thus, exosuits are sometimes deemed effective if they demonstrate a reduction in muscle activity measured by electromyography (EMG)[1]. Musculoskeletal computational models can estimate *in vivo* spinal loads, but their ability to appropriately represent the effect of an exosuit should be confirmed[3].

Therefore, the aim of this work was to quantify whether our participant-specific thoracolumbar musculoskeletal model is sensitive to exosuit assistive forces by comparing model-predicted muscle activity with recorded EMG[3]. We hypothesize model estimated back muscle activity will decrease when lifting with an exosuit, similar to known reductions in muscle activation directly measured by EMG.

Methods

Fourteen subjects were recruited for this study. Anthropometric measurements, motion capture (Qualisys AB), and bilateral EMG (Delsys Inc.; placed at T8 and L1 vertebral levels of erector spinae) were recorded from all participants. Participants performed squat and stoop floor lifts with boxes of 6 and 10 kg both without and while wearing a 2.7 kg soft active exosuit. The exosuit provided lifting assistance (up to 250 N) based on real-time kinematics via actuator controlled cords connecting a backpack harness to thigh straps.

Participant-specific musculoskeletal models were created from gender-specific "base" models with muscle parameters, anthropometry and spinal curvature adjusted to participant measurements[4]. The Active Suit conditions were modelled with an additional rigid mass attached to the back and actuators replicating known forces. Standard OpenSim tools[5] tracked the marker positions and assigned muscle activations using static optimization minimizing the activations cubed.

Bilateral averages from three consecutive lift repetitions for both EMG levels were computed, time normalized, and expressed as a lift phase. Peak EMG values and model muscle activations were computed for both the Box Pickup and Release lifting phases. Root Mean Square Error (RMSE) and cross-correlation analyses (*R*-values) were performed between the model and recorded EMG activations across all lifts. The differences in peak muscle activations between Active and No Suit conditions were compared via paired t-tests (α=.05) for both EMG levels, all four lifts, and both lifting phases.

References

1. Kermavnar et al. (2021) *Ergonomics* 64(6): 685-711
2. Dreischarf et al. (2016) *J. Biomch.* 49: 833-845
3. Hicks et al. (2015) *J. Biomch. Eng.* 137(2): 020905
4. Burkhart et al. (2020) *J Biomech*. 112:110044
5. Delp et al. (2007) *Trans. on Biomed Eng*. 54(11): 1940-1950

Results and Discussion

Results were similar across all lifts, therefore for brevity we will here focus on the squat lift with 6 kg. Muscle activation patterns from the model and EMG both exhibited lower activation levels during the Active Suit condition than the No Suit condition at the T8 (Fig. 1) and L1 level. Correlations and RMSE indicated the model predictions matched the experimental data well across both conditions and levels (average RMSE ≤ .10; R ≥ .90). Averaged peak activations at T8 in the Box Pickup phase were 19% (EMG, p =.01) and 12% (model, p < .01) lower with the Active Suit, and at L1 they were similar (EMG, p =.07) and 7% (model, p =.02) lower. Likewise, during the Box Release phase, peak activations were 18% (EMG, p < .01) and 8% (model, p < .01) lower at T8 with the Active Suit, and at L1 8% (EMG, p =.02) and a non-significant 3% (model, p = .13) lower.

Overall these trends support that musculoskeletal models can capture the effect of the active exosuit on spinal musculature recruitment. However, future work should aim at testing model assumptions to further improve the qualitative discrepancies between modelled and EMG measured muscle activity (Fig 1.).

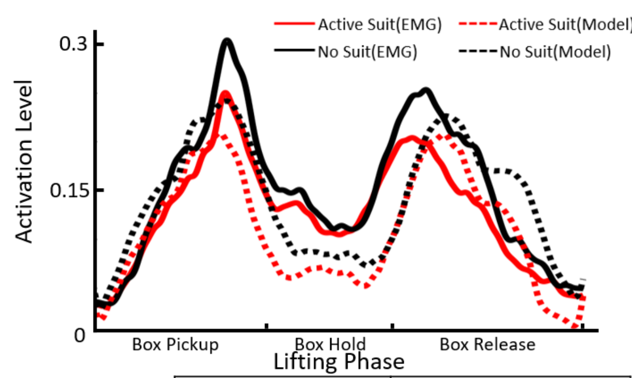

	Active Suit		No Suit	
Vertebral Level	T8	L1	T8	L1
R	.92 ± .03	.90 ± .03	.95 ± .02	.92 ± .02
RMSE	.09 ± .04	.10 ± .04	.10 ± .06	.10 ± .04

Figure 1. Average T8 model (dashed lines) and EMG (solid lines) muscle activations with (red) and without (black) suit during squat lifts with 6 kg. The table depicts the correlation (*R*) and RMSE values (mean ± SD) between EMG and model-based muscle activations

Significance

This study demonstrates that our musculoskeletal model can reasonably predict the assistive effects of a soft active exosuit on muscle activations. This supports the use of modelling to quantify how an exosuit impacts musculoskeletal outcomes such as vertebral loading. Furthermore, it represents a valuable tool to help clinicians and engineers predict how changes in exosuit force application and design can change spinal loads.

Acknowledgments

Funded via collaborative DOD CDMRP: W81XWH-20-1-0608

HOW DO ELASTIC EXOSKELETONS INFLUENCE MUSCLE SPINDLE FEEDBACK?

Amro Alshareef[1,2*], Jake Stephens[3], Lena Ting[3,5], and Gregory Sawicki[1,2,4]
[1]George W. Woodruff School of Mechanical Engineering, [2] Institute for Robotics and Intelligent Machines, and [3] Wallace H. Coulter Department of Biomedical Engineering, [4] School of Biological Sciences Georgia Institute of Technology, Atlanta, GA, USA
[5] Department of Rehabilitation Medicine, Emory University, Atlanta, GA, USA
email: *aalshareef6@gatech.edu

Introduction

With significant advancement in wearable technologies for assisting locomotion and augmenting balance, there is a growing need to understand the neural mechanisms underlying stable movement. It remains unclear whether exoskeletal devices that provide force either in parallel (e.g., elastic exoboots) or in series (e.g., cushioned running shoes) with muscle tendon units (MTU) interfere with or enhance the natural response of sensory organs during cyclical movement. In part due to the difficulty of directly measuring spindle firing in humans, a theoretical framework that can predict the relationship between muscle afferent feedback and contractile dynamics has yet to be fully validated. Indeed, most models of spindle firing still rely on a kinematic relationship with firing rates driven by fiber length and velocity. However, recent work suggests that the contractile force (F_c) and yank (Y_c) acting on the intrafusal fibers may more accurately predict spindle instantaneous firing rate (IFR) during passive MTU stretches [1]. Here, we aimed to construct a simple modelling framework pitting kinematic vs. kinetic drivers of spindle firing against each other in the context of altered external mechanical loading manifests from assistive technologies. Ultimately, we aim to test our model-based predictions in-vivo in both animal and human experiments to help reveal how spindles work and how exoskeletons alter their behaviour.

Methods

We developed a simple mechanical model (fig. 1a) comprised of series and parallel springs representing active and passive elements of the MTU (orange) and exoskeletal devices in parallel (blue) or in series (green). Sinusoidal length changes (L_{in}) were applied to the model while modulating active stiffness of the muscle to maintain a constant force amplitude, akin to a locomotion cycle. We independently varied parallel (fig. 1b) and series (fig. 1c) exoskeleton stiffness added to the MTU to determine their individual contributions to the predicted spindle IFR. The noncontractile part of the muscle force was determined according to [2]: $F_{NC} = k_{lin}(\Delta L_m) + Ae^{k_{exp}(\Delta L_m)}$, a function of muscle length change (ΔL_m). F_c was the result of subtracting the F_{NC} from the total force signal. F_c was then used to predict $IFR = (F_c + b_F)k_F + (Y_c + b_Y)k_Y + C$ [2].

Results and Discussion

With an exoskeleton (exo) in series (fig. 1b), the force on the MTU remained the same, but the length change of the muscle decreased as stiffness decreased. F_{NC} of the muscle therefore decreased, resulting in an increase in F_c to meet the F_{total}. As a result, IFR increased with added exo series compliance, when determined as a function of F_c, but decreased when determined as a function of L_m (fig. 1B).

With an exo in parallel, the total force was split between the exo and the MTU, and the length change of the muscle decreased as stiffness increased. F_{NC} of the muscle therefore increased, resulting in a decrease in F_c. As a result, IFR decreased as parallel exo stiffness increased, when determined as a function of F_c, but increased when determined as a function of L_m (fig. 1C).

Contrasting predictions from kinematic vs. kinetic models for spindle output IFR, when compared against in-vivo data from future animal and human experiments, should help decode mechanisms underlying spindle firing during cyclic contractions.

Significance

Adding known external mechanics with an exoskeleton either in parallel or series to a biological MTU can help reveal which muscle states contribute to spindle firing. As assistive devices become increasingly complex, a complete model of the human neuromuscular system is critical for human-machine integration. Further work in animal models (e.g., rat gastrocnemius muscle), augmented with exoskeletal assistance, will help clarify the relationship between varying muscle kinematic and mechanical parameters and resulting neural feedback [3]. With an understanding of this relationship, engineers and physiologists can join forces to develop exoskeletons more adept at addressing clinical challenges in motor (re)learning by controlling the neural feedback via exoskeleton tuning.

Acknowledgments

We would like to thank Dr. Tim Cope, Dr. Surabhi Simha, and Paul Nardelli for their feedback in developing this model.

Support form National Institutes of Health (NIH), Eunice Kennedy Shriver National Institute of Child health and Human Development (NICHD), R01HD090642.

References

[1] Blum et al. (2017) PloS Comput Biol. [2] Blum et al. (2020) eLife [3] Vincent et al. (2017) J Neurophysiol.

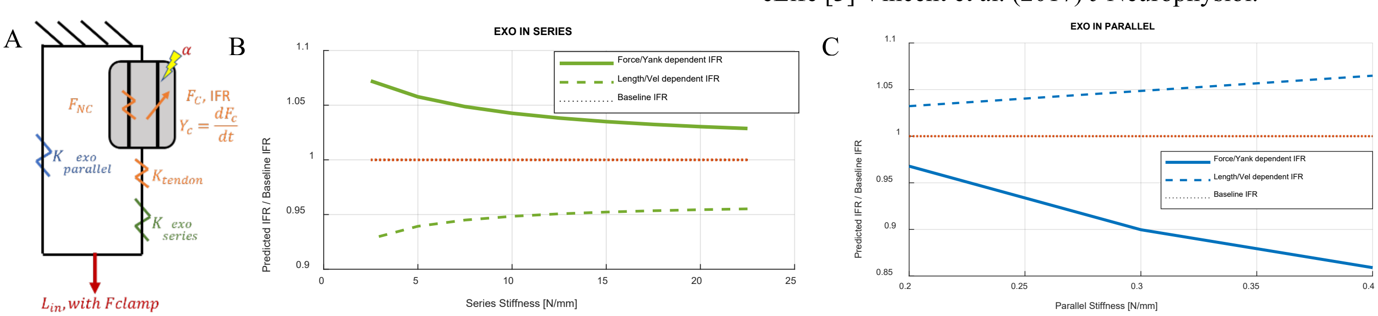

Figure 1: A) Mechanical Model of MTU with added parallel (K_{exo}) and series (K_{series}) elasticity. Comparison between the IFR prediction of a force and yank dependent spindle model vs a length and velocity dependent model with B) added series exoskeleton and C) added parallel exoskeleton.

INTEROSSEUS PROXIMITY DISTRIBUTIONS AS 4DCT-DERIVED CARPAL ARTHROKINEMATIC BIOMARKERS

Taylor Trentadue[1,*], Cesar Lopez[1], Ryan Breighner, David Holmes III, Sanjeev Kakar, Shuai Leng, Steven Moran, Andrew Thoreson[1], Kristin Zhao[1] | [1]Assistive and Restorative Technology Laboratory, Mayo Clinic, Rochester, MN | email: * trentadue.taylor@mayo.edu

Introduction

Scapholunate interosseous ligament (SLIL) injuries are among the most common wrist injuries and are a leading cause of wrist instability[1-3]. SLIL injuries may progress to the SL advanced collapse (SLAC) wrist pattern, which is associated with radiocarpal and midcarpal osteoarthritis. SLIL injuries can be challenging to diagnose: radiographs are limited by complex overlapping anatomy, and 3D computed tomography (CT) is unable to detect injuries that present only dynamically. 4DCT (3DCT over motion cycles) offers the ability to capture anatomy dynamically during motion. When reconstructed with sharp kernels, 4DCT captures bony anatomy; arthrokinematics may serve as biomarkers for ligamentous injury. The objective of this study is to quantify interosseous proximities at the radioscaphoid joint during wrist motion and describe the locations of interosseous proximity changes on the articulating surfaces.

Methods

We present data from the injured wrist of a 34-year-old male with a unilateral volar SLIL injury enrolled in clinical trial NCT03193996. Briefly, the trial involved bilateral wrist assessments preoperatively and one-year postoperatively; only the preoperative data are included in this study. 4DCT imaging and processing protocols have been described previously[4-6]. A third-generation, dual-source CT scanner (SOMATOM FORCE, Siemens Healthcare) was used to acquire neutral-static and dynamic CTs. Dynamic scans were acquired using a sequential, dual-source cardiac protocol over 1.5 seconds. This yielded 17 evenly-temporally distributed CT volumes (temporal resolution: 66 ms). We present data from one participant during flexion-extension.

Carpal bones were segmented and converted to 3D polygonal surface meshes. We present arthrokinematic data from the radioscaphoid joint. Nearest mesh-vertex distances between all vertices on the radius and scaphoid pairs within distance (2.5 mm)[7] and surface-normal opposition angular thresholds (60°) were calculated to reflect relative bone positions. Wrist angle was approximated as the angle between the radius and capitate[8]. Interosseous proximities can be visualized spatially using proximity maps and quantitatively using violin plots.

Results and Discussion

Interosseous proximity maps between the radius and scaphoid, displayed on the scaphoid facet of the radius, from neutral through flexion, maximum flexion, neutral through extension, and maximum extension are presented in **Figure 1 (top)**. The closest proximities at the radioscaphoid joint occurred along the dorsal-lateral corner and radial styloid. This was most prominent in wrist extension. This supports clinical experience, as patients are often symptomatic with wrist extension[9].

Time series interosseous proximity data and wrist flexion angle are presented in **Figure 1 (bottom)**. Generally, greatest proximities between the radius and scaphoid occurred when the wrist was flexed; closest proximities occurred when the wrist was extended. 4DCT time series data yield arthrokinematic data during a motion cycle that can be related to wrist position.

Closer proximities at the radioscaphoid joint may be related to SLAC wrist pattern development[10-12], where degenerative changes are often first noted at the radial styloid. These data support decreased interosseous distances along the lateral margin of the distal radius, including near the radial styloid, following SLIL injury. While injury localization is clinically significant, restoring joint space within normal limits is a pertinent biomechanical outcome for both injury diagnosis and long-term follow-up evaluation. Data can be compared to and interpreted relative to outcomes from the uninjured wrist.

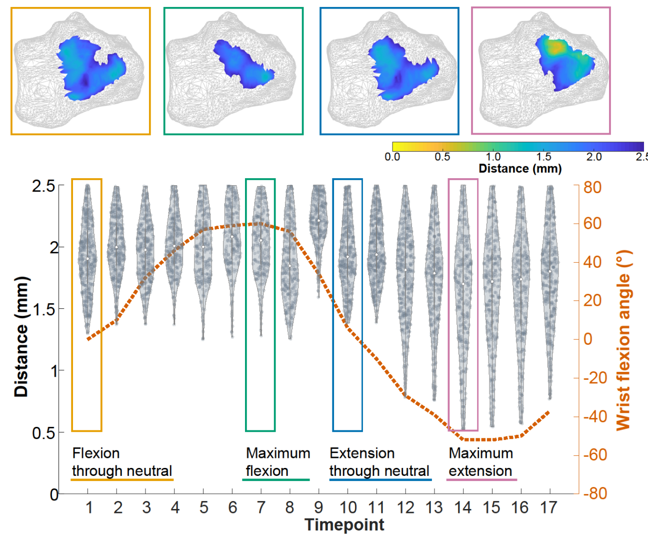

Figure 1: (top) Interosseous proximity maps showing radioscaphoid joint distances on the scaphoid facet of the radius at neutral, extreme flexion, neutral, and extreme extension. (bottom) Violin plot demonstrating radioscaphoid joint distances at each point in a flexion-extension motion cycle. White dots represent median radioscaphoid interosseous distances at the given timepoint. Colored boxes relate each proximity map to its corresponding distance distribution.

Significance

Assessing early radiocarpal degenerative changes on radiographs remains a clinical challenge[10]. Interosseous proximity maps may reveal anatomic areas of concern, and distance distributions during motion may highlight positions that put patients at risk of radiocarpal osteoarthritis development based on joint space alterations. Interosseous proximity maps and distance distribution data offer complementary information about wrist arthrokinematics, including localization of modified contact patterns and quantifications of joint proximities, respectively. Biomechanists, orthopedic surgeons, and radiologists may use the anatomical-based and distance-based visualizations to aid in diagnosis and understanding of SLIL injury during motion.

Acknowledgments

This work was supported by NIH NIAMS R01 AR071338, NIH NIGMS T32 GM065841, and NIH NIAMS T32 AR56950.

References

[1] Short. J Hand Surg Am. 2007. [2] Crawford. JBJS Rev. 2016. [3] Linscheid. J Hand Surg Am. 1983. [4] Leng. Med Phys. 2011. [5] Zhao. J Biomech Eng. 2015. [6] Kakar. J Wrist Surg. 2016. [7] Moeller. Thieme; 2000. [8] Neu. J Biomech. 2001. [9] Lee. Hand Clin. 2015. [10] McLean. Clin Orthop Relat Res. 2019. [11] Watson. J Hand Surg Am. 1984. [12] Watson. Hand Clin. 1997.

SUPER-RESOLUTION 3-D RECONSTRUCTION FOR CREATING BONE MODELS FROM LOW-RESOLUTION CLINICAL CT

Rebecca E. Abbott[1*], Ryan E. Breighner[2], Arin M. Ellingson[1]
[1]University of Minnesota, [2]Hospital for Special Surgery
*email: abbot364@umn.edu

Introduction

Routine clinical computed tomography (CT) scans are anisotropic, with high in-plane resolution, but large gaps (2-3mm) between slices. Bone models for shape-matching with biplane videoradiography (BVR) require CT volumes with high-resolution in all dimensions. When an individual has a previously acquired clinical CT scan, it would be desirable to use the existing scan and avoid exposing them to additional radiation.

While many imaging programs can resample a volume via interpolation, these methods do not incorporate information from the orthogonal series. This study presents a Super-Resolution Reconstruction (SRR) method for combining multiple orthogonal series from low-resolution clinical CT scans to create a high-resolution reconstruction [1]. We demonstrate that the SRR method improves segmentation, bone model morphology accuracy, and shape-matching accuracy.

Methods

A high-resolution cervical spine CT scan was obtained (23yo, F, 0.22x0.22x0.6 mm; Siemens AG) in 3 orthogonal planes. Image processing was performed using a custom program in MeVisLab (MeVis Medical Solutions AG) [2]. Clinical scans were simulated by downsampling the out-of-plane resolution to 3mm in all 3 orthogonal series. Two methods for increasing 3-D resolution were compared: 1) Resampled: resampling the axial series with Lanczos interpolation and 2) SRR: combining information in all 3 orthogonal series.

The SRR method begins with upsampling the 3 orthogonal series to a 0.22 x 0.22 x 0.6 mm grid using Lanczos interpolation. The coronal and sagittal series are inherently aligned to the axial and a voxel-by-voxel mean is computed for the full volume. Bone models of the C6 vertebra were segmented from the original, clinical, resampled, and SRR images in Mimics (Materialise). The bone models were taken through the pipeline for kinematic analysis with shape-matching in BVR [3]. Global kinematics were converted to Euler angles and filtered with a moving average filter (window=5).

Results and Discussion

Orthogonal reconstructions from the axial series (Fig 1: Left) show improved separation between vertebrae in the SRR volume, compared to the clinical and resampled volumes. A semi-automated segmentation tool (CT Bone Wizard in Mimics) successfully segmented the C6 vertebra from the original and SRR volumes, requiring less than 15 min. Manual segmentation was required for the clinical and resampled segmentations (>2 hrs). Morphology measures comparing the surface models (CloudCompare, Zephyrus) (Table 1) reveal the SRR model most accurately matched the original high-resolution model.

The Digitally Reconstructed Radiograph (DRR) created from the SRR volume produced a better match to the radiographs during shape-matching when compared to the clinical and resampled DRRs, as indicated by lower average normalized cross-correlation (NCC) cost and standard deviations (Table 1). Analysis of the kinematics show that the SRR method produced the most accurate tracking relative to the original (Fig 1: Right).

In summary, the SRR method decreased time and manual input required for segmenting the bone model and improved tracking when compared to the resampled volume. By incorporating between-slice information through fusion with the orthogonal series, more accurate reconstruction and visualization of the bone and joints are created.

Significance

The SRR method for creating bone models from low resolution CT scans allows us to include individuals in our studies who have previously acquired clinical CT images while avoiding exposing them to additional ionizing radiation.

Acknowledgments

NIH/NICHD R03 HD09771

References

[1] Greenspan, H. Comput J., 2009.; [2] König M. et al., SPIE, 2006.; [3] Akhbari, B. et al., J. Biomech., 2019.

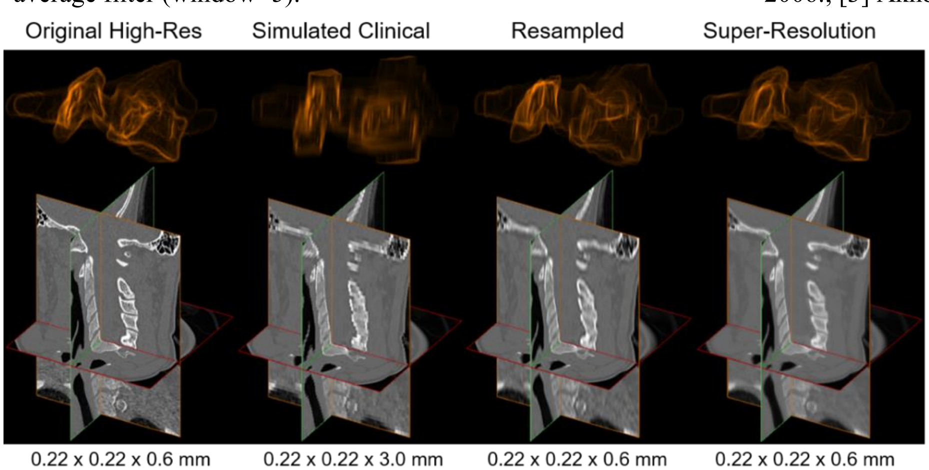

	Morphology (mm)			DRR Match
	Bias	Prec	MAE	NCC (std)
Original				0.87(0.04)
Clinical	0.18	1.14	0.59	0.93(0.09)
Resampled	0.29	0.71	0.46	0.97(0.04)
SRR	0.17	0.27	0.24	0.92(0.04)

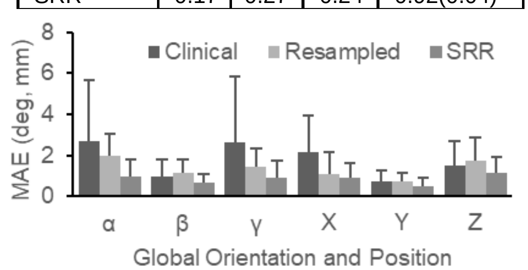

Figure 2. Left: Overlaid orthogonal views (below) and DRRs (above). The sagittal and coronal slices shown in the 3-D orthogonal views are reconstructed from the axial series. *Upper Right*: Table 1 - Comparison of bone model morphology and shape-matching performance. All metrics are referenced to the Original, except for the NCC. Bone morphology measures compare the surface models (STLs). Bias: average signed distance; Prec: standard deviation of bias; MAE: mean absolute error; NCC: mean normalized cross-correlation cost function between DRR and radiographs. *Lower Right*: Accuracy of C6 global kinematics relative to the original high-resolution model tracking for a flexion-extension trial. Error bars represent standard deviation of MAE.

IMAGING CHARACTERISTICS OF A WEIGHT-BEARING, CONE BEAM COMPUTED TOMOGRAPHY SYSTEM

Tadiwa H. Waungana[1,2,3*], Ying Zhu[2,3], and Sarah L. Manske[1,2,3]
[1]Biomedical Engineering Graduate Program, University of Calgary, Alberta, Canada
[2]McCaig Institute for Bone and Joint Health, University of Calgary, Alberta, Canada
[3]Department of Radiology, Cumming School of Medicine, University of Calgary, Alberta, Canada

email: *tadiwa.waungana@ucalgary.ca

Introduction

Cone beam computed tomography (CBCT) has been used to facilitate weight-bearing computed tomography (WBCT), which allows cross-sectional imaging of the lower extremities whilst the patient is standing in a fixed-flexion position [1-2]. This allows WBCT to provide an improved representation of load-bearing joints compared to traditional supine CT [3]. Cone beam systems are known to present with characteristic cone beam artifacts towards the peripheries of the field of the view (FOV)[4], reducing the FOV in which accurate measurements can be made. To establish their efficacy as a quantitative imaging modality, CBCT systems need to be assessed using methods that have been developed for quantitative measures of CT performance. Quality assurance CT phantoms are used to measure key performance metrics such as the spatial resolution, linearity of x-ray attenuation and uniformity. The purpose of this study was to characterize the performance of a cone beam, WBCT scanner and to establish its efficacy in quantitative analysis of bone mineral density (BMD) in weight-bearing imaging.

Methods

Four different CT phantoms were scanned using the HiRise CT imaging x-ray system (CurveBeam, Hatfield, PA) in the weight-bearing configuration (130 kVp, 6.5 mA). Individual image slices containing the relevant evaluation plates were extracted using 3DSlicer. The slant edge, geometrical accuracy and linearity evaluation plates were analysed using a semi-automated MATLAB code to quantitatively determine the spatial resolution, in-plane pixel spacing and linearity of x-ray attenuation respectively. Linearity was evaluated using vials of varying iodine concentration and the mean signal intensity measured at each vial. ImageJ and a bone density phantom consisting of uniform rods of varying hydroxyapatite (HA) concentrations were used to assess uniformity and determine the useable region along the height of the cone beam that was unaffected by cone beam artifacts.

Results and Discussion

Data obtained from the analyzed evaluation plates is summarized in Table 1.

Table 1. Summarized results from CT Phantoms

Spatial Resolution [µm]	318
Measured in-plane pixel spacing [µm]	262
Linearity slope [mg/mL] (R^2)	0.0157 (0.98)

The measured spatial resolution (10% MTF) was larger than the nominal pixel size (300µm), indicating that some blurring will be present when observing an object that is the same size as the pixel size. The signal intensity varied linearly with increasing iodine concentration over the tested range (R^2 = 0.98). The measured in-plane pixel spacing was smaller than the nominal pixel size, implying that errors may be present when estimating physical dimensions using the number of pixels traversed by an object in the image.

The signal intensity along a uniform HA rod varied by a maximum of 20.0% and 2.7% in the axial and coronal planes respectively. The latter was accompanied by a minimal increase in signal intensity in the inferior-superior direction of the coronal view. The useable height in the superior-inferior direction was estimated to be approximately 15.4 cm when looking at a central coronal slice. This indicates that approximately 79% of the total height of the FOV (40.124 cm diameter x 19.564 cm height) is absent of any cone beam artifacts and therefore useful for quantitative imaging.

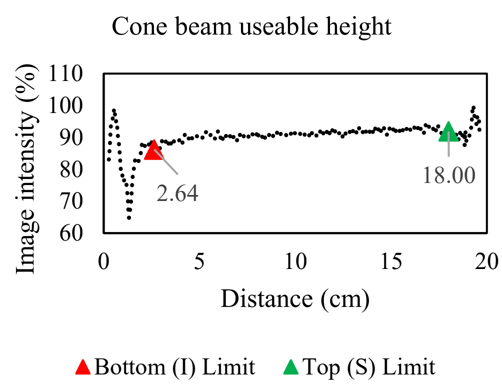

Figure 1: Plot of image intensity percentage versus distance from the inferior end of a uniform 100 HA cylindrical phantom rod. The distance between the two triangles represents the estimated range along the height of the cone beam that is largely unaffected by artifacts.

Overall, these results demonstrate that the performance of the WBCT system, in isolation, is not adequate to conduct quantitative analysis of BMD. Depending on the application, corrective algorithms (e.g., improved beam hardening correction algorithms) may need to be developed to account for the signal intensity variations across the useable FOV.

Significance

Recently, WBCT has been drawing increasing attention due to its direct application in the visualization of load-bearing joints. It combines the weight-bearing feature of traditional radiography with the cross-sectional benefits of clinical CT. Using WBCT to measure BMD alongside other anatomical measures (e.g., joint space) will therefore require post processing corrections.

Acknowledgments

CFI, University of Calgary Biomedical Engineering

References

1. N.A. Segal *et al.,* 2017. *J. Orth. Re.*
2. T.D. Turmezei *et al*., 2021. *Radiology*
3. E.K.J. Tuominen *et al*., 2013. *Am. J. Roent.*
4. J.F. Barret and N. Keat. 2004. *Radiographics*

AUTOMATED SEMANTIC SEGMENTATION OF CARPAL BONES FROM 4DCT IMAGE VOLUMES

Taylor P. Trentadue[1,*], Abhinav Goyal, Andrew Thoreson[1], Ryan E. Breighner, David R. Holmes III, Kristin D. Zhao[1]
[1]Assistive and Restorative Technology Laboratory, Mayo Clinic, Rochester, MN — email: * trentadue.taylor@mayo.edu

Introduction

The wrist is an anatomically complex region containing eight articulating carpal bones, with five metacarpal bases distally, and with the radius and ulna proximally. Carpal bones have complex relative motions and geometries[1,2]. Diagnosis of wrist ligament injuries is challenging: radiographs are limited by anatomic overlap, and 3DCT is limited to single, static acquisitions. Four-dimensional CT (4DCT), which captures 3DCT volumes over motion cycles, can be used to assess dynamic injuries[3-6].

While 4DCT provides great insight into osteokinematics, it has limitations: (1) a restricted proximal-distal field-of-view (FOV), yielding partial volumes of some bones; (2) motion cadence that may exceed the temporal resolution of the CT scanner, causing motion blur; and (3) certain diseases, such as osteoarthritis or osteopenia, contribute to narrowed joint space and poorly-defined cortical bone contours. These features complicate static-dynamic CT image registration.

Deep learning has improved our ability to process medical images. U-Net architectures can be used for semantic segmentation of 3D volumetric datasets, such as CT data. Briefly, U-Nets enable localization by concatenating higher-level spatial information from the encoding pathway with the more feature-rich representations in the decoding pathway[7].

We present a method for automated semantic segmentation of carpal bones acquired during 4DCT scans using a pipeline for automated generation of binary (bone versus non-bone) array masks for unlabeled training data and an autoencoder to learn the features inherent in the dataset. To assess performance, we compare U-Net segmentation to manual segmentation meshes.

Methods

4DCT data collections have been described previously[4-6,8]. Briefly, a third-generation, dual-source CT scanner (Siemens Healthcare) was used to acquire neutral-static and dynamic CT scans. Sequential dual-source scanning mode yielded high temporal resolution (66 ms) continuous images over motion cycles. Datasets from two cadavers (two motions in six ligament integrity conditions)[8] yielded 26,010 axial CT images.

To automate image mask generation, (1) images were thresholded to isolate bone cortex (>1300 HU); (2) contours were filled; and (3) MATLAB's circularity (C) and equivalent diameter (ED) object retention values were varied over 0.00 – 0.20 and 0 – 20, respectively, to optimize preprocessing for robust mask generation. An autoencoder was trained on the entire dataset to learn underlying feature representations. The encoding weights were then transferred to a standard U-Net, which contains a convolutional contraction pathway and an upsampling expansion pathway[7]. We shuffled and randomly selected 20% of each cadaveric dataset for validation. The U-Net was trained to minimize binary focal Jaccard loss[9] until validation loss plateaued for 10 epochs. Adjacent CT slices were stacked, segmented, and median- and joint-smoothed in 3D Slicer[10]. Meshes for the radius, scaphoid, lunate, and capitate were smoothed and converted to stereolithography (STL) files[11]. To assess automated segmentation performance, distances between manually-segmented static 3DCT meshes and U-Net's output segmentation (automated) meshes were compared for two bones captured entirely within the image FOV using CloudCompare[12].

Results and Discussion

Representative images from automated mask generation and U-Net segmentation are presented in **Fig. 1**. Jaccard loss and F1 scores for five C and ED combinations are presented in **Table 1**. The top-performing models had C=0.10, 0.15 and ED=10. Training and validation losses are presented in **Fig. 2**.

Fig. 1: Example raw, automated mask, and U-Net segmentation images.

Table 1: Model performance for five object retention value parameters.

C, ED	**0.10, 0**	**0.15, 5**	**0.10, 10**	**0.15, 10**	**0.10, 20**
Jaccard	0.53 (0.26)	0.42 (0.27)	0.03 (0.06)	0.02 (0.06)	0.51 (0.27)
F1	0.65 (0.27)	0.54 (0.29)	0.06 (0.10)	0.04 (0.09)	0.63 (0.29)

Median (25^{th} –75^{th} percentile) distances between automated and manually-segmented scaphoid and lunate meshes in one demonstrative volume were -0.13 (-0.33 – 0.00) and -0.30 (-0.44 – -0.18) mm, respectively. A difference mesh is presented in **Fig. 3**. Positive values indicate the automated mesh exceeded the manually-segmented mesh at the nearest vertex.

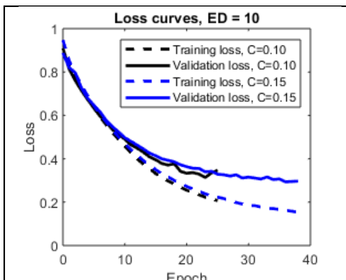

Fig. 2: Training and validation loss curves for the top-performing models (C=0.10, ED = 10; C = 0.15, ED = 10).

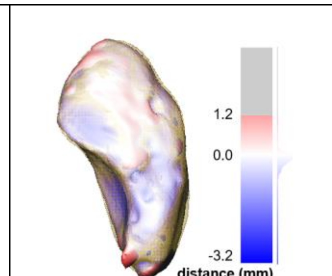

Fig. 3: Scaphoid distance difference mesh displayed on the automated mesh. Stippled beige vertices represent manual segmentation.

Significance

We have presented a pipeline for automated label generation of previously-unlabeled data. The use of an autoencoder and standard image processing pipelines enabled deployment of a supervised algorithm with minimal manual segmentation effort. Reconstructed meshes are comparable to manual segmentations, even in images with pronounced motion blur.

Acknowledgments

This work was supported by NIH NIAMS R01AR071338 and NIGMS T32GM065841.

References

[1] Rainbow. J Hand Surg Eur Vol. 2016. [2] Kobayashi. J Biomech. 1997. [3] Brinkhorst. Skeletal Radiol. 2021. [4] Kakar. J Wrist Surg. 2016. [5] Leng. Med Phys. 2011. [6] Zhao. J Biomech Eng. 2015. [7] Ronneberger. (abs). 2015. [8] Trentadue. (abs). 2021. [9] Duque-Arias. VISIGRAPP. 2021. [10] Kikinis. In: Jolesz F, ed. 2014. [11] Desbrun. SIGGRAPH. 1999. [12] CloudCompare (v2.10.2). 2022.

REPRODUCIBILITY AND REPEATABILITY OF A SEMI-AUTOMATED PIPELINE TO QUANTIFY TRAPEZIOMETACARPAL JOINT ANGLES USING DYNAMIC COMPUTED TOMOGRAPHY

Michael T. Kuczynski[1,2,3*], Kendra Wang[4], Justin J. Tse[2,3], Tomasz Bugajski[2], and Sarah L. Manske[1,2,3]
[1]Biomedical Engineering Graduate Program, Schulich School of Engineering, University of Calgary, Canada
[2]McCaig Institute for Bone and Joint Health, University of Calgary, Calgary, Canada
[3]Department of Radiology, Cumming School of Medicine, University of Calgary, Calgary, Canada
[4]Biomedical Engineering Undergraduate Program, University of Waterloo, Waterloo, Canada
email: *mkuczyns@ucalgary.ca

Introduction

Osteoarthritis (OA) commonly affects the joints of the hand, including the trapeziometacarpal (TMC) joint. OA is a complex and multifactorial disease, wherein biomechanics are a significant contributor [1] but challenging to study due to the joint's location. Dynamic computed tomography (CT) provides 3D visualization of joint motion and may improve our understanding of TMC-OA. Quantification of joint kinematics, such as joint angles, from dynamic CT often requires manually placed anatomical landmarks (AL). Previous motion analysis studies have shown that manually placed ALs can cause considerable variation in joint angles between individuals [2]. However, the repeatability and reproducibility of joint angles from dynamic CT scans using manually placed ALs has not been explored. Further, post-processing of dynamic CT datasets is often time intensive. The purpose of this study was to develop a fast, semi-automated pipeline to measure TMC joint angles from dynamic CT scans, and to evaluate the repeatability and reproducibility of manual AL placement on resulting joint angles. The accuracy of the developed image processing pipeline was evaluated by computing a target registration error (TRE) at each image registration step.

Methods

Ten cadaveric hands were acquired for scanning (4 female, 6 male, mean age: 81.6 ± 13.9 years). A device was designed to passively move thumbs in a radial abduction-adduction movement during scanning. Dynamic CT was acquired with 4cm longitudinal coverage, 4vol/s gantry rotation, 15s scan time, and 0.625x0.625x2.5mm voxels. Due to limited dynamic CT image quality, high resolution static CT scans (61μm^3 voxels) were acquired to generate bone masks and for segment coordinate system (SCS) definition. Intensity-based image registration was used to move bone masks to the dynamic CT image space where joint angles were calculated using a joint coordinate system representation previously described for the TMC joint [3]. Image processing was performed using custom Python scripts. SCSs were generated using ALs selected by three raters. Joint angle repeatability and reproducibility was evaluated using intraclass correlation coefficients (ICC), Bland-Altman plots, and frame-by-frame root mean square errors (RMSE). One specimen was used to determine image registration accuracy by implanting borosilicate fiducial markers (4.76mm diameter) into the first metacarpal bone and computing the TRE. Joint angles were computed on the remaining 9 specimens.

Results and Discussion

Mean joint angles calculated using our pipeline agreed with previous cadaveric and *in vivo* studies [3,4]. We found that intra-rater repeatability was high for flexion-extension (0.55-1.00) and abduction-adduction (0.81-1.00), and moderate for axial rotation (0.37-1.00). Inter-rater reproducibility was low to excellent for all angles (0.09-0.95). Joints with considerable degeneration were found to have poorer agreement between raters compared to joints that appeared healthy. Intra-rater RMSE was typically lower compared to inter-rater RMSE (Figure 1). Linear regression analysis of Bland-Altman plots suggested that differences introduced by differing raters are small and systematic (slope<0.06). Therefore, assessments of range of motion or comparisons between movements utilizing the same coordinate system will likely be unaffected by the choice of rater. Fiducial marker TRE was at or below voxel level, suggesting that a small portion of the error in the joint angle results between raters was due to the image registration.

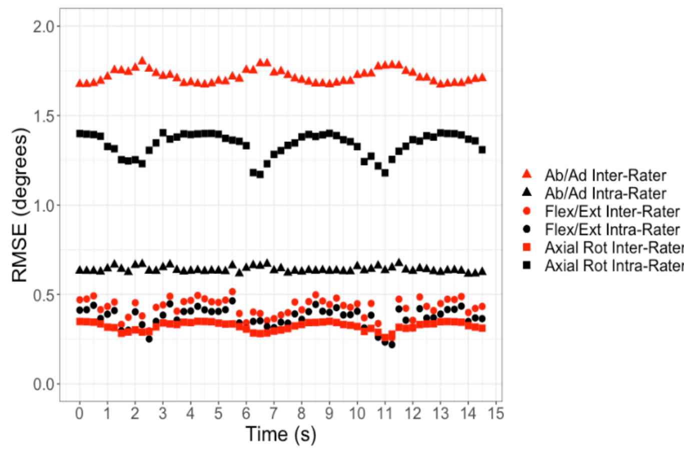

Figure 1: Sample frame-by-frame root mean square error (RMSE) of joint angles. Ab/Ad: Abduction-adduction, Flex/Ext: Flexion-Extension, and Axial Rot: Axial Rotation. Data in red represents inter-rater RMSE and data in black represents intra-rater RMSE.

Significance

We present an open-source, semi-automated pipeline to quantify joint angles from dynamic CT scans of the TMC joint that requires approximately 1.5 hours to completely process a single movement. This is a vast improvement from the previously reported 120 hours required for a single TMC joint [5]. Future work will be performed to determine whether the pipeline is sufficiently sensitive to differentiate between healthy and diseased TMC joint kinematics. Finally, this pipeline can be easily implemented for different motions, joints, and scan acquisition parameters, and can therefore enhance the utilization of dynamic CT to assess joint kinematics.

References

[1] Marshall M *et al.*, 2018. *Nat Rev Rheumatol*. 14(11).
[2] Della Croce U *et al.*, 1999. *Med Biol Eng Comput.* 37(2).
[3] Cheze L *et al.*, 2009. *Comput Methods Biomech Biomed Engin*. 12(3).
[4] Cooney W *et al.*, 1981. *J Bone Jt Surg*. 63.
[5] Wang K *et al.*, 2018. *J Hand Surg Eur Vol*. 43(10).

DOES A CYLINDER FIT TO THE TALAR DOME CAPTURE THE FUNCTIONAL AXIS OF THE TALOCRURAL JOINT?

Anja-Verena Behling[1*], Luke Kelly[1], Lauren Welte[2,3], Michael Rainbow[3]
[1]Human School of Nutrition Sciences, University of Queensland, Brisbane, Australia
[2]Department of Mechanical Engineering, University of Wisconsin-Madison, Wisconsin, United States
[3]Department of Mechanical and Materials Engineering, Queens University, Kingston, Canada
email: *a.behling@uq.net.au

Introduction

Due to the tightly congruent, dome-shaped articular surfaces of the talocrural joint, a cylinder fit to the articular surfaces has been used to inform ankle implant design[1]. This approach assumes that during movement, the functional axis of rotation is coincident in both location and orientation with the cylinder's axis; however, the agreement of the best-fit cylinder and functional axis has not been tested dynamically in vivo. Additionally, bone size likely affects the vertical location of the axes and is therefore important for ankle implants.

Here, we quantify the agreement of the cylinder and rotation axis during hopping using biplanar video radiography. We also determined whether the vertical distance of the axis from the tibia varies as a function of talus size.

Methods

CT scans (0.356mm x 0.356mm x 0.625mm) were obtained from nine asymptomatic feet (5 females, mean ± std, height 171 ± 11cm, weight 71 ± 15kg). We fit a cylinder through the talar dome, determining its orientation, radius, and location in the tibia coordinate system (Figure 1). We used biplanar video radiography (125 Hz) to capture the motion of the talus and tibia during hopping (156 bpm). The talus and tibia were tracked with Autoscoper using an established approach[2]. We computed the rotation axis of the talus relative to the tibia from contact to foot flat during the landing phase. Rotation axes were resolved in the tibia coordinate system. We calculated the intersections of rotation axes with the sagittal plane to obtain their location. Bland-Altman analyses were used to determine the level of agreement between the location and orientation of the cylinder and rotation axes. We regressed talus centroid size against cylinder radius and the vertical location of the rotation axis.

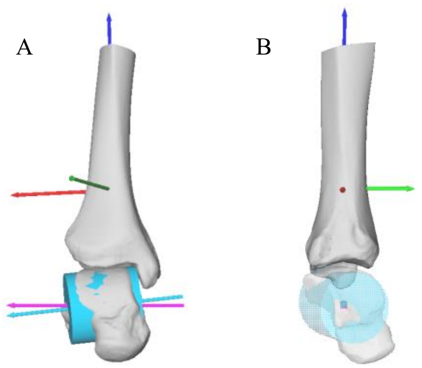

Figure 1: Illustration of the tibia and talus bone including the coordinate system (lateral red, anterior green, and vertical blue), a fitted cylinder including its axis orientation (1A) and center location (1B; teal), and a rotation axis with its orientation (1A) and location (1B; pink). N =1

Results and Discussion

Despite considerable inter-subject variation in the location and orientation of rotation axes and the cylinder, the overall alignment of the cylinder and rotation axis within each participant was good. The maximum difference in angle between the cylinder and rotation axis was ≤ 14.9º (mean = 12.6º; 95% confidence interval (CI) 9.2-13.4º).

The cylinder and rotation axis locations aligned well in the anterior-posterior (AP) and vertical directions (Table 1); however, the CI and limits of agreement (LoA) were larger in the vertical direction.

The orientation of the cylinder and the rotation axis matched best in the medio-lateral (ML) direction. The cylinder AP axis orientation consistently underestimated the AP orientation of the rotation axis (Bias = 0.12). Large LoA and CI values indicate poor agreement of orientation in the vertical direction between the cylinder and rotation axis and an overestimation of the rotation axis orientation in the vertical direction (Bias = -0.06).

Our results confirm that the functional axis of the cylinder is similar to the rotation axis in terms of its location and orientation. Our results are consistent with a previous study[1]. However, internal/external rotation (IR/ER) is not captured as well as other orientations by the cylinder axis.

Variable	Bias ± CI	LoA (lower, upper)
AP L [cm]	0.46 ± 0.90	-1.83, 2.76
Vertical L [cm]	-0.28 ± 1.17	-3.26, 2.70
ML O	0.01 ± 0.03	-0.06, 0.07
AP O	0.12 ± 0.05	0.01, 0.24
Vertical O	-0.06 ± 0.11	-0.34, 0.22

Table 1: Bland-Altman values for rotation axis-cylinder agreement (N = 9). L = Location; O = Orientation.

Talus size and cylinder radius were not related ($r^2 = 0.27$, $p = 0.15$). This suggests that talus size varies in regions other than the talar dome, resulting in a mismatch between talus size and cylinder radius. Moreover, rotation axis vertical location did not correspond to talus size or cylinder radius ($r^2 \leq 0.43$, $p \geq 0.06$).

Significance

Our data shows a cylinder approximates the functional axis in the ML direction, underestimates the AP direction, and does not capture the IR/ER direction. It is unclear if the small amount of AP and IR/ER range of motion during hopping (e.g., 5º), is functionally important and relevant for implant design, or how our results would vary for walking and running. More complex shapes might improve the agreement in the AP and IR/ER directions. Size is not a factor in predicting axis location, highlighting the importance of accounting for talocrural curvature when designing implants.

References

[1] Belvedere, et al., 2018. *J Orthop Res.* 37: 760-768.
[2] Miranda, et al., 2011. *J Biomech Eng*. 133(12):121002

CARPAL TUNNEL MORPHOLOGY QUANTIFICATION USING A CENTROID-TO-BOUNDARY DISTANCE ONE-DIMENSIONAL SHAPE SIGNATURE

Drew A. Anderson[1*], Michele L. Oliver [1], Karen D. Gordon[1]
[1] School of Engineering, University of Guelph, Canada
*email: dander04@uoguelph.ca

Introduction

Carpal tunnel morphology is important to understanding the aetiology of carpal tunnel syndrome (CTS) as well as risk factors such as deviated wrist posture. Previous studies have quantified the morphology of carpal tunnel cross-sections with measures including area, circumference, width, depth, tilt angle, and circularity ratio [1, 2]. These metrics provide global measures of shape but may not capture local tunnel boundary changes. Further insight may be gained by representing carpal tunnel cross-sections using one-dimensional (1D) shape signatures, a common method in shape analysis and classification [3]. A 1D representation of a tunnel cross-section can be generated by finding the centroid-to-boundary distance at constant angular intervals around the boundary of the cross-section. The objective of this study was to investigate changes in carpal tunnel morphology with wrist posture using 1D shape signatures.

Methods

Computed tomography scans were collected on ten cadaveric specimens (5 male; age=81±11) over a range of flexion-extension postures [4]. Proximal, middle, and distal cross-sections of the carpal tunnel were analysed in extension (–17.9 ± 3.1°), neutral (–0.40 ± 2.7°), and flexion (19.3 ± 3.5°) postures. Angles were calculated using inertial coordinate systems of the radius and third metacarpal. The 1D shape signature of each cross-section was determined as the magnitude between the centroid and the intersection points between the tunnel boundary and a ray rotated from 0° to 360° in 0.5° increments. The starting point was defined with the ray pointing medially in the orientation of the radius medial-lateral axis. The 1D shape signature can be visualized as a plot of distance vs. angle (**Figure 1**). Several metrics were applied to quantify differences between 1D shape signatures. The Euclidian distance was calculated between each 1D shape signature and a template function defined as the ensemble average of all shape signatures for that specimen. Phase shift was calculated using a circular cross-correlation between each shape signature and its respective template. Local maxima and minima peaks were found to calculate measures representing the width and depth of the carpal tunnel. The metrics were compared using an ANOVA with tunnel location and posture as factors.

Results and Discussion

The template function is defined to represent the average shape signature for each specimen. Therefore, the distance from the template indicates a global measure of shape change from the average. Tunnel location was significant ($p < 0.001$) in distance from the template with the middle cross-section having the lowest mean and proximal cross-section having the highest mean in each posture. This result indicates the greatest change in shape is at the proximal end of the tunnel across the range of flexion-extension postures. Posture was not a significant factor for distance from the template over the -17.9° to 19.3° range of flexion-extension postures. Further analysis may benefit from a

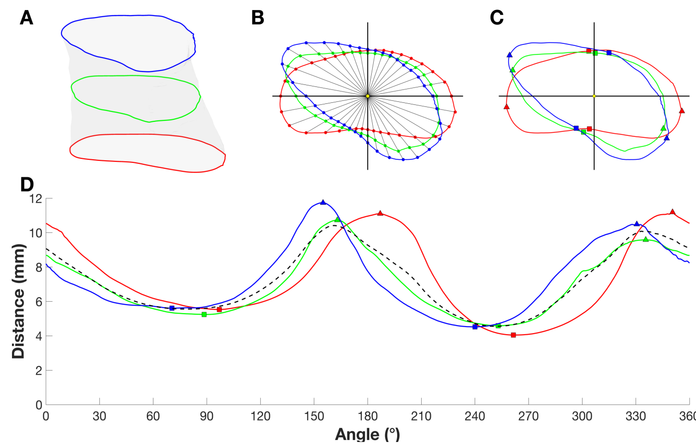

Figure 1: [A] Proximal (red), middle (green), and distal (blue) cross-sections. [B] Boundary points (10° increments shown for clarity) to calculate centroid-to-boundary distance. [C] Maxima (triangle) and minima (square) peaks from 1D plot used to calculate width and depth respectively. [D] Shape signatures and template function (black).

greater number of postures and assessing the effects of both flexion-extension and radial-ulnar deviation. Distance from the template increases with either an increase in the magnitude of the shape signature peaks or a phase shift relative to the template. No significant differences were observed for carpal tunnel width and depth measures taken from the peaks of the 1D shape signatures. Both location and posture were significant ($p < 0.001$) for phase shift. This result indicates there is a twist between the proximal and distal cross-sections, which changes with posture. Moving from extension to flexion, the proximal phase shift was minimal, while larger differences were seen for the middle and distal cross-sections which shifted further out of alignment with the template. These results collectively indicate that the distance from the template metric is most affected by the twist along the tunnel.

Significance

This study demonstrates the utility of a novel approach to quantifying carpal tunnel morphology. The reported metrics could be used as features for pattern classification and additional approaches such as spectral analysis may provide further insight. This study is the first to report twist between cross-sections along the carpal tunnel length. Further study of twist is warranted given flexion-extension posture was seen to affect the twist angle, and deviated wrist posture is considered to be a risk factor for CTS.

Acknowledgments

This research was supported by NSERC and DJO Global.

References

[1] Mogk & Keir, 2008. *Clin. Biomech.*, 23(9): 1112–1120.
[2] Pacek el al., 2010. *Hand,* 5: 77–81.
[3] Loncaric, 1998. *Pattern Recognit.*, 31(8): 983–1001.
[4] Anderson et al., 2022. *Clin. Biomech.*, 92: 105575.

INCREASING KINEMATIC FIDELITY IMPROVES PREDICTIONS OF WALKING METABOLIC COST

Ricky Pimentel[1], Adam W. Kiefer[2] Jason R. Franz[1]
[1]Joint Dept. of BME, UNC Chapel Hill and NC State, USA [2]Department of Exercise and Sport Science, UNC Chapel Hill, USA
email: rickypim@live.unc.edu

Introduction

Gold standard techniques to estimate metabolic energy cost (i.e., direct & indirect calorimetry) are time-consuming and complex procedures that require expensive equipment and trained personnel. These estimates are nevertheless critical, as reducing metabolic cost is often a goal of rehabilitation or assistive devices. Surrogate technologies (heart rate, accelerometry, etc.) rely on motion classification, regression equations, and body-worn devices which, even in controlled settings, still err from true energy cost.[1,2] New prediction techniques based on machine learning may estimate energy expenditure with shorter testing durations, less reliance on wearable devices, and improved precision.

Advancements in human pose estimation have improved our ability to measure whole-body kinematics from conventional video. This opens avenues for energy assessment technologies that can expand measurement capabilities outside the lab and improve throughput, thereby enhancing the personalized tuning of rehabilitation or assistive devices. Pose estimation algorithms typically identify keypoints (body points) as joint centers (i.e., hip, knee, etc.). However, some standard pose estimation algorithms omit anatomical points necessary to accurately describe human biomechanics.[3] For example, the default human models for DeepLabCut and OpenPose do not include keypoints distal to the ankle.

Our purpose was to determine how changing the number and locations of kinematic-based keypoints (i.e., increasing anatomical fidelity) affects the accuracy of machine learning predictions of walking metabolic cost. We hypothesized that: 1) human pose estimation can predict measured whole-body metabolic cost with moderate agreement ($R^2 \geq 0.3$); and 2) increasing anatomical fidelity (i.e., adding limb segments) will improve prediction accuracy.

Methods

We emulated pose-estimation techniques in this study by simplifying motion capture data during a series of walking trials. A convenience sample of 20 young adults (age: 24.7±5.2 years; height: 1.77±0.11 m; mass: 75.6±13.7 kg), walked for 12 different trials, each 5 minutes in length, at various speeds and push-off intensities known to elicit changes in whole-body metabolic cost.[4] We recorded whole-body kinematics via motion capture and net metabolic power via indirect calorimetry. Assuming steady-state exercise, we extracted marker trajectories from the final 2 minutes of each walking trial. We binned walking keypoint data into 15-second epochs: reducing motion capture data to mimic 3D pose-estimation-keypoints (Fig 1A) and calculating average metabolic cost for each epoch (8 in total). For simplicity across keypoint sets, we trained Support Vector Regression (SVR) machine learning models (6^{th} degree polynomial, from Scikit-learn[5] after basic hyperparameter tuning) for each keypoint set using a subject leave-out approach with 75% of the data used for training (first 15 subjects, 1,440 epochs), and 25% used for testing (final 5 subjects, 480 epochs). We report mean absolute error (MAE), root mean square (RMS) error, Pearson R^2, and concordance correlation coefficient (CCC) across keypoint sets on test data.

Results and Discussion

Consistent with our first hypothesis, using the Full, Torso, and Foot sets as inputs to SVR models predicted whole-body metabolic cost with moderate correlations ($R^2 \geq 0.321$). In partial support of our second hypothesis, the Torso set displayed the lowest RMS error (Fig. 1B), highest agreement (Fig. 1C), and closest fit to measured metabolic cost (Fig. 1D). Overall, keypoint fidelity had large effects on prediction accuracy.

Significance

Our results suggest that increasing anatomical fidelity of kinematic keypoints improves accuracy of metabolic cost predictions to within a mean absolute error of 0.9 W/kg or about 55 kilocalories per hour of walking for our subjects. However, at a certain point, incorporating keypoints from additional limbs can worsen predictions (as shown by adding arms in the Full set). Future model prediction accuracy may be improved by altering model architectures and including more training data.

Acknowledgments

This study was funded by NIH grant R01AG058615.

References

1. Nishida Y, et al. *Ann Nutr Metab.* 76, 62–72 (2020).
2. Pisanu S, et al. *J Nutr Metab.* 2020, e2327017 (2020).
3. Seethapathi N, et al. *ArXiv190710226* Cs Q-Bio (2019).
4. Pieper N, et al. *J Biomech.* 122, (2021).
5. Pedregosa F, et al. *J Mach Learn Res.* 12, 2825–30 (2011).

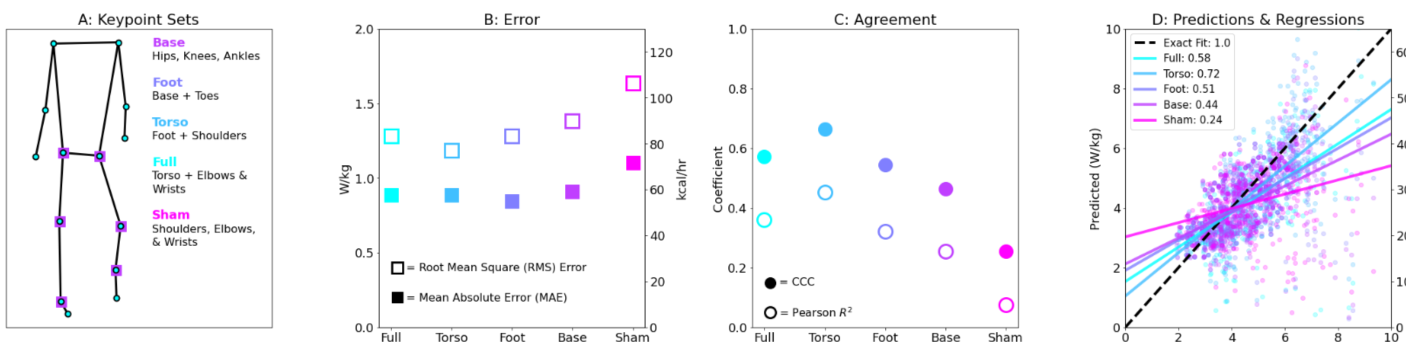

Figure 1: A) schematic of keypoint sets; B) prediction errors; C) prediction agreement; D) prediction outputs and linear regression slope coefficient

A SIMPLE MODEL OF BIPEDAL WALKING PREDICTS ENERGY-OPTIMAL GAITS ON A SPLIT-BELT TREADMILL

Surabhi Simha[1,2], Sina Mehdizadeh[2*], Max Donelan[2]
[1] Emory University & GeorgiaTech, Atlanta, GA, USA
[2] Simon Fraser University, Burnaby, BC, Canada
email: *smehdiza@sfu.ca

Introduction

Humans choose their gait pattern to reduce metabolic energy [1]. People also learn energy-optimal gaits when adapting to new conditions such as walking on unfamiliar terrains, with injury, or with a disorder such as stroke [2]. Split-belt treadmill walking is a common task to study adaptation in both healthy and pathological gait [3]. Experimental studies have found that to minimize energy in split-belt walking, people take longer steps on the fast belt and shorter steps on the slow belt. This allows people to take advantage of external assistance provided by the treadmill by letting the belt do net positive work on the body [3]. Despite the external assistance, the energy costs of optimal split-belt gaits are still higher than walking on a normal treadmill at the same relative speed [4]. In this computational study, we tested whether the same mechanisms that determine overground walking mechanics and energetics might also explain split-belt walking mechanics and energetics.

Methods

We developed a physics-based walking model similar to that used by Kuo, 2001 [5] (Figure 1). The model consists of a point-mass torso connected to two legs with distributed mass and curved massless feet. The two legs are connected to the torso via hip springs whose stiffnesses determine how the legs swing. The walker is powered by impulsive push-offs immediately prior to heel-strike. We integrated the equations of motion of the model and used numerical optimization to solve for the optimal walking gait. We solved for a gait cycle of one stride where the two steps can have unequal push-off impulses and hip spring stiffnesses, thus allowing for asymmetric step lengths and step times. The optimizer solves for the gait that minimizes a weighted sum of positive work at push off, negative work at heel-strike and swing cost by tuning the push-off impulses and hip spring stiffnesses. We chose the weighting of these costs in our cost function such that the optimal walking gait matched empirical observations from overground walking. We then used the same coefficients to optimize for walking on a split-belt treadmill where each belt moved at a range of different speeds.

Results and Discussion

Symmetric gaits are optimal on a tied-belt treadmill. Although our model can walk with asymmetric gaits, we found that when the belts are moving at the same speed, the minimum energy cost occurs when push-off impulses, hip spring stiffnesses, and step lengths are equal between the legs (Figure 1).

Asymmetric gaits are optimal on a split-belt treadmill. We also found that using the same model and cost function, increasing belt speed differences causes optimal gaits to have asymmetric step lengths with the leg on the fast belt having longer steps, i.e. positive step length asymmetry (Figure 1). This is a similar but more extreme trend to what is seen in human walking experiments [3,4].

Energy cost of optimal split-belt gaits are higher than walking on a normal treadmill. When the belt speed difference is increased, we found that push-off work always decreases. This explains how the split-belt treadmill can do work on people allowing them to reduce their work on the treadmill. However, the work at heel strike and swing cost increase with increase of belt speed difference. The reduction in push-off work is less than the combined cost increase due to the work at heel strike and swing cost. This might explain why walking on a split-belt treadmill is not cheaper than walking on a tied belt treadmill.

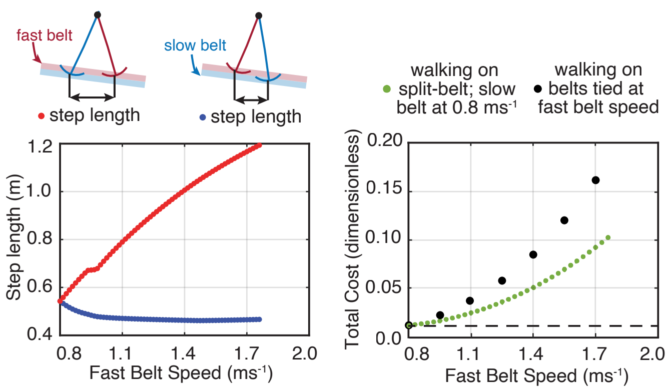

Figure 1: Left: the step lengths of slow (blue) and fast legs (red) at a range of belt speed, Right: energy cost over a range of speeds.

Significance

Our findings demonstrated that the same biomechanical determinants that explain overground walking mechanics and energetics can also help explain how people walk on a split-belt treadmill. The significance of this study is that we do not need new mechanisms and objectives to explain optimal gait after adaptation to new contexts such as split-belt treadmill walking.

Acknowledgments

This work was supported by a grant from NSERC.

References

[1] Zarrugh et al. 1974. *Eur J Appl Physiol Occup Physiol*, 33: 293-306.
[2] Selinger et al. 2015. *Current Biology,* 2t5: 2452-56.
[3] Sanchez et al. 2021. *J Neurophysiol,* 125: 344-57.
[4] Butterfield & Collins 2022. *J Biomech*, 132: 110905
[5] Kuo 2001. *J Biomech Eng,* 123: 264-69.

WALKING METABOLIC COST INCREASES WHEN SYNCHRONIZING STEPS TO UNSTRUCTURED VISUAL CUES

Anaelle E. Charles[1*], Nicholas Stergiou[1] and Aaron D. Likens[1]
[1]Department of Biomechanics, University of Nebraska at Omaha, Omaha, NE USA
Presentation Preference: [Podium]

email: anaellecharles@unomaha.edu

Introduction

Walking exhibits natural variation over several gait cycle repetitions that produces long-range correlations (LRCs) in gait parameters over time (i.e., pink noise) [1,3]. Those natural patterns have been associated with health, and their deterioration has been associated with disease (i.e., stoke and Parkinson's disease) [2,3]. Those observations are consistent with Optimal Movement Variability Hypothesis, the idea that healthy, adaptative movements take optimal forms. To restore healthy variation, previous studies have suggested synchronizing steps with variable external cues that exhibit cueing intervals embedded with LRCs. However, the influence of such external cues on the metabolic cost of walking has not been investigated. This study investigated the effect of synchronizing steps with visual cues embedded with various temporal structures on metabolic cost of walking. Specifically, we investigated three related research questions: (1) Do LRCs in gait reduce metabolic cost of walking? (2) If so, do external cues that promote LRCs in gait enhance that effect? (3) Do those external cues also reduce metabolic cost of walking?

Methods

Twenty-one participants (Male/Female = 16/5, Age = 25.8 ± 2.17 yrs) performed four 12-minute walking trials on a 200-m indoor track, wearing Noraxon FSR SmartLead footswitches on both their heels. The COSMED K5 recorded metabolic rate during all walking trials. First, participants completed a self-selected pace trial (SPW) to determine mean (M) and standard deviation (SD) of their typical stride interval. Those Ms and SDs were used to scale visuals cues for three remaining trials such that pacing matched each participant's preferred walking speed. Then, participants were instructed to synchronize their right heel strike with a bar moving vertically on a pair of augmented reality glasses. Participants walked under three visual conditions: pink noise, invariant (i.e., traditional metronome), and white noise cueing. The order of conditions was randomized for each participant. Strides were analyzed using Detrended Fluctuation Analysis [2] to compute the scaling exponent α, a measure of statistical persistence. Linear mixed effect (LMEs) models were used to examine effects of noise and α on metabolic cost of waking.

Table 1. Linear mixed effect modeling approach.

Model	Chi sq.	Df	*p*
Metabolic ~ Time+ Time^2			
Metabolic ~ Time+ Time^2+ condition	104.6516	3	<0.01
Metabolic ~ Time+ Time^2 + α condition	32.5187	1	<0.01
Metabolic ~ Time+ Time^2 + α *condition	13.9195	3	<0.01
Metabolic ~ Time * condition + Time^2 + α *condition	11.8693	3	<0.01

All models contained random intercepts.

Time Effects were only included as covariates

Results and Discussion

We fit a series of LMEs to understand the effects of noise and α on metabolic cost (Table 1). Baseline models included linear and quadratic time trends. Subsequent models included condition and α, along with their interactions. Time by condition interactions were also investigated. Model improvement was assessed by likelihood ratio test and revealed that the best fitting model contained effects of Time, Time^2, Condition, and α; an interaction between time and condition; and an interaction between condition and α. The analysis showed that all cues elevated metabolic cost (*p*s<.01); pink noise produced the smallest elevation; and all other cue types produced greater Mean Condition (MC) than pink noise. This analysis also found a generally negative relationship between α and metabolic cost such that higher α predicted lower metabolic cost. However, Condition and α were implicated in an interaction showing that all noise conditions strengthened the α-MC relationship. As time effects were not of central interest, they were not interpreted further.

These findings suggested that synchronizing steps to the Pink noise condition reduces metabolic cost compared to invariant and white noise visual cues. These results support the Optimal Movement Variability Hypothesis, which suggests that healthy movement is temporally structured, exhibiting long-range correlation overtime (pink noise structure). Moreover, these results demonstrate that optimal forms of movement variability promote more efficient locomotion.

Significance

Implementing visual cueing with a variable pink noise structure could promote effective interventions in gait rehabilitation protocols without increasing metabolic cost. Such protocols could help individuals with limited mobility such as recovering from stroke or suffering from Parkinson's disease who wish to recover a gait variability that is similar to healthy young adults.

Acknowledgments

This work is supported by NIH P20GM109090 to NS and AL, R15AG063106 to NS, R01NS114282 to NS, NSF-2124918 to NS and AL

References

[1] Hausdorff, J. M., & Peng, C.-K., 1996. *Physical Review E*, *54*(2), 2154.
[2] Kaipust, J. P., McGrath, D., Mukherjee, M., & Stergiou, N. (2013). *Annals of Biomedical Engineering*, *41*(8), 1595–1603.

[3] Stergiou, N., Harbourne, R. T., & Cavanaugh, J. T., 2006 *Journal of Neurologic Physical Therapy*, 30(3), 120–129

A REDUCED MODEL TO EXPLAIN VARIATION IN RUNNING ECONOMY WITH BIOMECHANICS

Kathryn Harrison[1*], Bethany Kilpatrick[1], Bradley Davidson[2], Eric Honert[1], Daniel Feeney[1]
[1]BOA Technology, Denver, CO
[2]Human Dynamics Lab, University of Denver, Denver, CO
email: *kate.harrison@boatechnology.com

Introduction

Running economy is critical to distance running performance.[1] A variety of kinematic, kinetic and spatiotemporal variables have been associated with running economy.[2–4] Athletes may attempt to alter these variables through training or equipment (e.g. footwear) to improve performance. It is difficult to select which of the multitude of variables associated with running economy are most important to address. Further, many of these variables covary, which could result in redundancy and inaccurate models. We propose that a subset of variables may be identified could parsimoniously explain the effect of biomechanics on running economy. Such a simplified model may allow athletes, coaches, and footwear designers to focus their attention on a smaller number of impactful varaibles.

Methods

Fourteen runners (6F) with a recent 5k time faster than 20 min (males) or 22 min (females) participated. Subjects were outfitted with a left side lower body marker set, and provided with standard running footwear for the study. They ran six 5 min trials on a force plate instrumented treadmill at 80-85% of their predicted maximum heart rate. Kinematic data were collected using a six-camera 3D motion analysis system. Energy expenditure per km was estimated using indirect calorimetry.

The twenty biomechanical variables of interest were ankle, knee, and hip joint negative and positive work, peak joint moments, joint range of motion, ground contact time and running speed. Kinetic variables were normalized to body mass. Biomechanical variables and energy expenditure were averaged within each trial. A mixed-effects linear regression model was created with the biomechanical variables as fixed effects, subject as a random effect, and energy expenditure per km as the dependent variable. For this full model, the variance inflation factor (VIF) for each variable was calculated. If any VIF was greater than four, the variable with the largest VIF was removed, until all VIF were less than four. Next, a backward stepwise selection procedure based on Akaike Information Criterion was conducted to identify a parsimonious model. Alpha for the model was set to 0.05.

Results and Discussion

The final model (p=0.0007) included just two variables, in addition to the random effect of subject (Table 1). Based on the final model, an increase in frontal plane ankle range of motion would result in a decrease in energy expenditure. Previous authors have proposed the importance of medial longitudinal arch (MLA) deformation to passively absorb and return energy during running.[5] Our results support this proposition, as an increase in frontal plane ankle range of motion may reflect a greater range of motion of the MLA, due to the kinematic coupling of forefoot dorsiflexion and ankle eversion.[6] These results may also help to explain the decrement to running economy observed with use of foot orthoses.[7]

Previously, greater knee abduction and hip adduction have been associated with greater metabolic cost.[3] However, both of these variables were eliminated from our final reduced model. Greater ankle eversion is moderately associated with less knee abduction during running, which is in turn associated with less hip adduction.[8] Thus, some of the variation in running economy explained by frontal plane motion of the proximal joints may already be explained by the frontal plane ankle range of motion.

A larger peak knee extension moment was also associated with better running economy. Similarly, Heise et al.[2] found that greater positive work at the knee was associated with better running economy. A greater knee extension moment could contribute to greater knee joint stiffness, which has also been associated with better running economy.[9] This may help to explain the anecdotal observation that many long-distance runners are "quad-dominant", in relation to gluteal and hamstring muscles.

Table 1. Biomechanical variables included in the reduced model to explain energy expenditure during running

Variable	Estimate	Std. error	p
Frontal plane ankle range of motion	-0.29	0.08	0.002
Peak knee extension moment	-2.22	0.79	0.009

Significance

We were successfully able to identify a subset of biomechanical variables to explain energy expenditure during running. Given just two variables, athletes and sport practitioners may be able to better focus training and equipment interventions to improve distance running performance. Interestingly, runners are often anecdotally advised that "over-pronation" and "quad dominance" should be avoided. This study challenges commonly held beliefs regarding the "ideal" biomechanics for long distance runners.

References

1. Conley DL, Krahenbuhl GS. *Med Sci Sports Exerc*. 1980;12(5):357-360.
2. Heise GD, Smith JD, Martin PE. *Eur J Appl Physiol*. 2011;111(8):1777-1785.
3. Pizzuto F, de Oliveira CF, Soares TSA, Rago V, Silva G, Oliveira J. *J Strength Cond Res*. 2019;33(7):1921-1928.
4. Lussiana T, Patoz A, Gindre C, Mourot L, Hébert-Losier K. *J Exp Biol*. 2019;222(Pt 6):jeb192047.
5. Crago D, Bishop C, Arnold JB. *J Sports Sci*. 2019;37(22):2613-2624.
6. Pohl MB, Messenger N, Buckley JG. *Gait Posture*. 2007;25(2):295-302.
7. Crago D, Arnold JB, Bishop C. *Int J Sports Physiol Perform*. Published online March 10, 2021:1-7.
8. Sakaguchi M, Ogawa H, Shimizu N, Kanehisa H, Yanai T, Kawakami Y. *European journal of sport science*. 2014;14:S302-S309.
9. Tam N, Tucker R, Santos-Concejero J, Prins D, Lamberts RP. *Int J Sports Physiol Perform*. Published online May 29, 2018:1-22.

WHY IS THE METABOLIC COST OF LOCOMOTION HIGHER ON SAND?

Jonathan R. Gosyne,[1*] & Gregory S. Sawicki[1,2]
[1]The George W. Woodruff School of Mechanical Engineering, [2]The School of Biological Sciences,
Georgia Institute of Technology, Atlanta, GA, USA
Email: *jonathan.gosyne@gatech.edu

Introduction

Locomotion on sand elicits a higher metabolic cost than on hard ground. Previous work attributes this to two main factors: sinkage into the sand itself, and the structural properties of the human leg. Losses due to sinkage into the sand are conventionally estimated as a function of kinematic properties such as depth, contact area, intrusion force, and ground material properties such as density or grain size. However, at the human muscle level, increased metabolic cost exceeds the expected penalty based on efficiency of positive mechanical work of 0.25. (i.e., more than a x4 penalty). Our previous work *in-silico* suggests that this discrepancy is due to increased MTU length changes and higher CE shortening velocities during locomotion over dissipative substrates, thereby requiring higher muscle activation to meet the force demands of the task. Here, we seek to test these predictions *in-vivo*. We hypothesize the added metabolic cost of hopping on sand is due to unfavourable muscle length and velocity operating points. This study presents the first muscle-level analysis of human locomotion on dissipative terrain and sets the stage for a new paradigm of terrain-capable wearable device design.

Methods

One participant (height = 1.82m, mass = 80kg) performed a 5-minute resting metabolic trial, followed by 3 maximum voluntary contraction trials of the soleus, tibialis anterior, and gastrocnemius, and then a first full mechanical baseline trial at 2.5Hz on hard ground to a set height and then finally 5 5-minute hopping trials to their preferred height on hard ground at 2.2, 2.5, 2.8, and 3.2 Hz and their preferred frequency in random order. After this, the participant performed 6 5-minute hopping trials to their preferred height on sand at 2.2, 2.5, 2.8 and 3.2 Hz in random order, and then matched the height and frequency of the hard ground mechanical baseline. Metabolic rates were monitored during trials to ensure that participant maintained sub-maximal aerobic effort for each condition, indicated by an RER<1.0. Indirect calorimetry, motion capture, ground reaction forces, surface EMG, and soleus cine B-mode ultrasound were collected. Biofeedback was provided to allow the participant to maintain a specified hop height for the necessary trials. Sand hopping was performed over a custom-built sand pit that uses dry, loose packed poppy seeds as simulated sand, and allowed for self-leveling through a combination of pivot enabled shaker panels and airflow to maintain a constant sand depth. We quantified muscular demand using surface EMG, as well as fascicle velocity and length change profiles using B-mode ultrasound.

Results and Discussion

Consistent with literature [1,3] and previous modelling and simulation work [2], we found a ~35% increase in metabolic cost at the mechanically matched condition (6.5cm, 2.5Hz) (fig. 1a). Similarly, consistent with previous work, we found a local frequency minimum for the self-selected height trials in sand (2.8Hz) and a trend that mimics that on hard ground, with a constant metabolic offset of ~39%. Increased cost was explained by shorter soleus fascicles (fig. 1c, e) and faster soleus shortening velocities (fig. 1d, f) that were reflected in increases soleus muscle activation (fig. 1b).

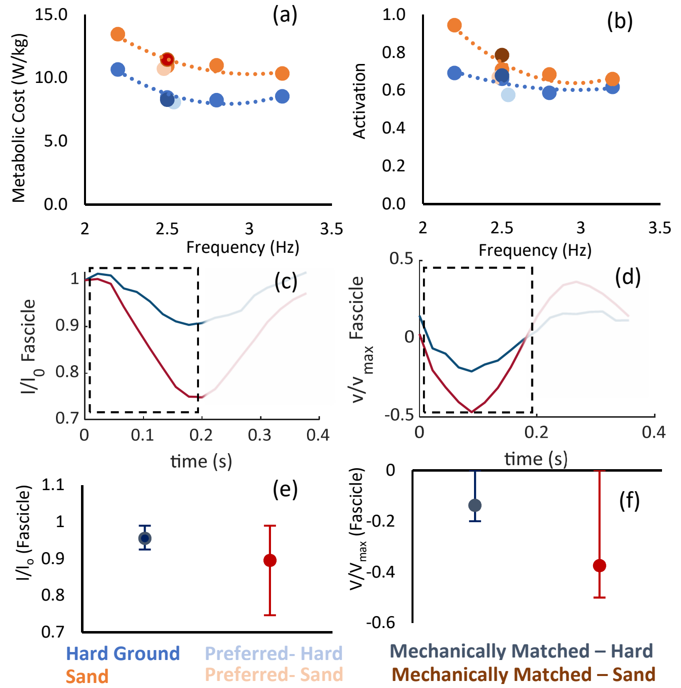

Figure 1. Initial data for metabolic cost and soleus (a) activation (b,d) length (length over cycle, max, min average) and (c,e) shortening velocity (velocities over cycle, max, min, average) (d,f). The mechanically matched conditions are used to make controlled comparisons in muscle dynamics on hard ground vs. in sand.

Significance

Human locomotion on deformable media has been studied for decades, but little has been done at the neuromuscular level to understand why it is more metabolically expensive, particularly when compared to the increased mechanical work required for locomotion in dissipative environments [1]. On the other hand, there have been many studies linking metabolic cost and center of mass, limb-joint and muscle-level neuromechanics on hard ground. Our study begins to bridge this gap, using a customized in-lab apparatus to perform the first comprehensive analysis of the human neuromuscular response to the complex non-linear behavior of propulsion on sand. Additionally, our results provide further evidence that neuromuscular effects that increase active muscle volume (higher fascicle velocities and shorter fascicle lengths) increase net metabolic power [4]. These results will help inform design of wearable devices that can mitigate energetic penalties associated with 'real-world' locomotion over dissipative terrain.

References

[1] T. M. Lejeune et al, *JEB,* 1998.
[2] J. R. Gosyne, et al in *ASB, 2020*
[3] A. E. Minetti et al, *JTB,* 1997
[4] O. N. Beck et al, RPB, 2020

Effects of real-time visual feedback on metabolic power during walking in people with transtibial amputation

Caelyn Hirschman[1], Janet Zhang[1] & Alena M. Grabowski[1,2]
[1]Applied Biomechanics Lab, University of Colorado Boulder, CO USA
[2]Eastern Colorado Healthcare System, Department of Veterans Affairs, Denver, CO USA
email: Caelyn.Hirschman@colorado.edu

Introduction

People with unilateral transtibial amputation (TTA) using a passive-elastic energy storage and return (ESAR) prosthesis have higher metabolic power [1] and greater biomechanical asymmetry during walking than non-amputees [2] and peak horizontal and vertical ground reaction forces (GRFs) produced by the affected leg (AL) are lower than those of the unaffected leg (UL) [2]. The use of a powered ankle-foot prosthesis (BiOM) can reduce metabolic power by 7-20% compared to an ESAR prosthesis during walking [3] and may reduce biomechanical asymmetry when users are trained to utilize the available stance-phase push-off power.

We provided real-time visual feedback (VF) of AL peak propulsive horizontal GRF (hGRF) during walking and hypothesized that participants with TTA using their own ESAR prosthesis would: 1. increase average AL peak propulsive horizontal GRF (hGRF) to meet targets 20% and 40% higher and incur greater metabolic power than baseline trials and 2. not retain increased AL peak propulsive hGRF when VF was removed, and thus net metabolic power (NMP) would return to baseline. We also hypothesized that participants using the BiOM prosthesis would: 1. increase average AL peak propulsive hGRF to meet targets 20% and 40% higher but would not incur greater metabolic power and 2. retain increased AL peak propulsive hGRF and incur the same metabolic power as VF trials.

Methods

Three subjects (2M, 1F) with unilateral TTA provided informed consent and walked on a dual-belt force treadmill (Bertec, Columbus, OH) at 1.25 m/s using their own ESAR prosthesis and the BiOM prosthesis while we measured vertical and horizontal GRFs (1000 Hz). We measured rates of oxygen consumption and carbon dioxide production via indirect calorimetry (ParvoMedics TrueOne2400, Sandy, UT) throughout each 5-min trial and averaged them during the last 2 min. We calculated NMP using a standard equation [4] and by subtracting metabolic power during standing. NMP was normalized to body mass when using a prosthesis.

During VF trials, we placed a monitor at eye level ~1.5 m in front of each subject and plotted real time peak propulsive hGRF. We asked subjects to match targets of 0%, +20% and +40% of their baseline AL peak propulsive hGRF. We measured baseline (0%) AL peak propulsive hGRF during the first 5-min walking trial without VF. Each VF trial was 5 min, followed by a 5-min rest and 5-min retention trial where VF was removed. Subjects completed this protocol over two days and trial order was randomized. We calculated AL peak propulsive hGRF and NMP during each trial. We report descriptive statistics of the percent differences of the mean compared to baseline walking using the ESAR prosthesis.

Results and Discussion

Compared to baseline walking trials using the ESAR prosthesis, subjects increased AL peak propulsive hGRF by 13.9-36.6% using the ESAR and 25.7-51.7% using the BiOM prosthesis during VF trials (Fig 1a). During VF, compared to baseline walking trials using the ESAR prosthesis, NMP increased by 15.1-21.9% using the ESAR and 9.6-25.8% using the BiOM prosthesis (Fig 1c). During retention trials, compared to baseline walking trials using the ESAR prosthesis, subjects increased AL peak proulsive hGRF by 5.2-5.3% using the ESAR and 20.8-24.6% using the BiOM prosthesis (Fig 1b). During retention trials, compared to baseline walking trials using the ESAR prosthesis, NMP increased by 5.6-7.3% using the ESAR and 5.1-5.9% using the BiOM prosthesis (Fig 1d).

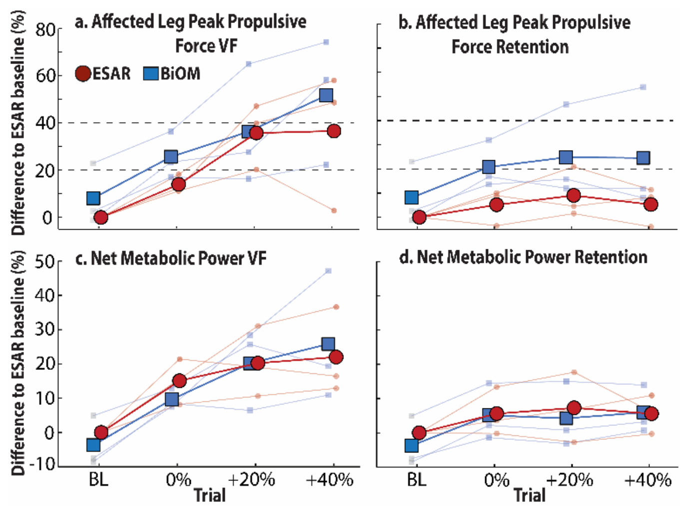

Figure 1. AL peak propulsive hGRF percent difference from baseline walking trials using the ESAR prosthesis for ESAR (red) and BiOM (blue) prostheses during visual feedback (VF) (a) and retention (b) trials. Dotted lines indicate +20% and +40% AL peak propulsive hGRF targets. NMP percent difference from baseline walking trials using the ESAR prosthesis for ESAR (red) and BiOM (blue) prostheses during VF (c) and retention (d) trials. Bold lines indicate the mean and faded lines, each subject.

Significance

Our results suggest that real time VF of AL peak propulsive hGRF could improve symmetry for people with TTA using an ESAR or BiOM prosthesis. However, subjects increased NMP during VF trials using ESAR and BiOM prostheses. AL peak propulsive hGRF was retained more so using the BiOM versus ESAR prosthesis during walking. Analysis of peak propulsive hGRF symmetry between legs may give further insight into the effects of using the BiOM compared to an ESAR prosthesis in conjunction with VF. Moreover, VF or some feedback may provide beneficial effects for people with TTA using the BiOM prosthesis during walking.

Acknowledgments

Funding from the VA RR&D Service RX002943-01A2.

References

1. Huang et al., *Physical Medicine and Rehabilitation,* 1979
2. Grabowski & D'Andrea, *J NeuroEngineering Rehabil*, 2013
3. Herr & Grabowski, *Royal Society B,* 2012
4. Brockway, *Hum Nutr Clin Nutr,* 1987

MECHANICAL ENERGY COST OPTIMISATION OF OBSTACLE NEGOTIATION MANOEUVRES

Katherine A. J. Daniels[1,2*] and J. F. Burn[2]
[1]Manchester Metropolitan University, UK
[2]University of Bristol, UK
email: *k.daniels@mmu.ac.uk

Introduction

When walking or running in straight lines over planar surfaces, humans and other animals tend to move in a way that minimises the energetic cost of transport (CoT) [1]. However, legged locomotion in the natural environment is rarely over uniform ground surfaces. Instead, gait must be adapted to accommodate varying terrain geometry and negotiate obstacles in the path of travel. Obstacle negotiation requires anticipatory control of whole-body dynamics across multiple steps to implement a traversal or avoidance manoeuvre whilst maintaining stability and forward progression [2, 3].

We hypothesised that the principle of energy cost minimisation in locomotion would extend to the energetic optimisation of obstacle negotiation. To test this idea, we systematically manipulated the relative mechanical energy cost of two different strategies for negotiating a lowered ground region and used a two-alternative forced-choice experimental paradigm to probe locomotor decision-making.

Methods

Thirteen young adults participated in the study (8 female/5 male). All were free of self-reported musculoskeletal, visual, and neurological impairments.

Each participant walked towards and crossed a lowered obstacle (a ‘hole in the ground’) of modifiable length and depth (Figure 1). A different obstacle length-depth combination was presented for each trial and the participant’s obstacle negotiation strategy (step over the hole *vs* step down into the base of the hole and then up the other side) was recorded. The participant then performed a second set of trials in which the same obstacle geometries were presented but this time the non-preferred alternative strategy was enforced for each length-depth combination. Whole-body kinematic data were recorded for all trials (10-camera Oqus system, Qualisys AB, Switzerland).

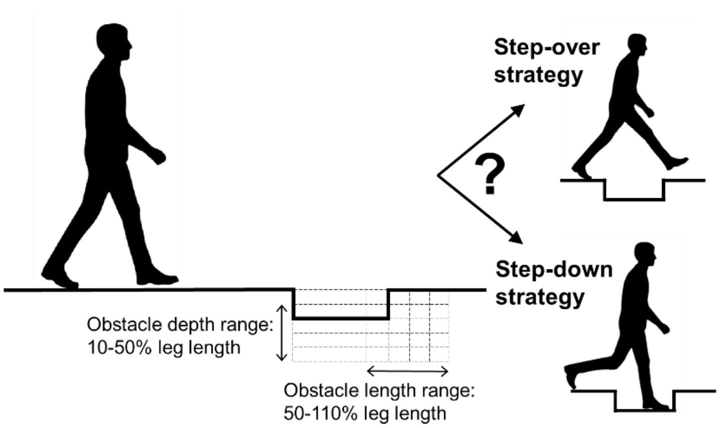

Figure 1: Experimental configuration. Obstacle length and depth were manipulated between trials.

Logistic regression models were constructed to model the relationship between the advantage in selecting a given strategy and the observed probability of that strategy being preferentially selected by the participants. Four candidate control objectives were explored: Minimising mechanical CoT for the complete manoeuvre, minimising mechanical CoT for individual crossing steps, maximising speed of travel, and conserving approach speed.

Results and Discussion

The energetically optimal obstacle negotiation strategy was dependent on both the length and the depth of the obstacle: CoT for the complete manoeuvre was minimised by stepping over the obstacle when it was short and deep and by stepping into the obstacle when it was long and shallow. Participants’ behaviour was consistent with strategy selection to minimise mechanical CoT for the entire multi-step obstacle crossing manoeuvre (β_0 p=.32, β_1 p<.001), but not with minimising CoT for any individual step, with maximising speed, or with conserving speed.

The kinematics of the two alternatives strategies diverged at the onset of the obstacle negotiation manoeuvre, indicating that strategy selection was based on anticipatory control rather than online control. Strategy selection was not affected by task exposure, which suggests that sensorimotor exploration over the duration of the experiment does not account for the observed behaviour.

We conclude that locomotor behaviour consistent with a control objective of minimising mechanical CoT for the complete manoeuvre was demonstrated for this obstacle negotiation task. Visual information regarding both the length and the depth of the obstacle guided strategy selection, and step-to-step energy cost variation was integrated into decision-making. Future work should explore the generalisability of our findings to other tasks, environments, and species.

Significance

Our results suggest that the principle of energy cost minimisation in locomotion can be extended to the anticipatory control of complex locomotor behaviours. These findings have implications for understanding the mechanisms underlying sensorimotor control of legged locomotion and for predicting locomotor behaviour in novel environments.

References

[1] Hoyt and Taylor, 1981. *Nature.* 292:16(239-40).
[2] Patla, 1997. *Gait Posture*. 5:1(54-69)
[3] Matthis et al., 2017. *Proc. Natl. Acad. Sci. USA*. 114:32(EE6720-29).

THE EFFECT OF BONE-ANCHORED PROSTHESIS USE ON BIOMECHANICAL FACTORS ASSOCIATED WITH KNEE OSTEOARTHRITIS: A PRELIMINARY ANALYSIS

Clare A. Severe[1,2], Brad D. Hendershot[1,3,4], Christopher L. Dearth[1,3,4], Benjamin K. Potter[1,4], Jonathan A. Forsberg[1,4]
[1]Walter Reed National Military Medical Center, [2]Henry M. Jackson Foundation for the Adv. of Military Medicine, Inc., [3]DoD-VA Extremity Trauma & Amputation Center of Excellence, [4]Uniformed Services University of the Health Sciences
email: clare.a.severe.ctr@mail.mil

Introduction

Knee osteoarthritis (KOA) is ~3x more prevalent within the contralateral limb among persons with vs. without unilateral transfemoral amputation (TFA) [1]. Persons with unilateral TFA often depend heavily on their sound limb during ambulation, potentially causing abnormal stresses on the limb [2]. To date, biomechanical evaluations of KOA risk in persons with TFA have focused on those who use traditional socket-based prostheses. However, osseointegration (OI) – direct skeletal attachment of a prosthesis – aims to eliminate socket-based complications [3]; in turn, perhaps reducing preferential use and reliance on the contralateral limb. This preliminary analysis compared biomechanical risk factors associated with KOA in persons with TFA before and after OI – i.e., using a socket-based vs. bone-anchored prosthesis, respectively. It was hypothesized that a bone-anchored prosthesis would facilitate greater/lesser loading on the prosthetic/sound limb, respectively, and thereby reducing KOA risk in the contralateral limb.

Methods

Eight male Service members with unilateral TFA (age: 38±9yr, height: 1.78±0.12m, mass: 99.2±24.0kg, time since amputation: 90±54mo) underwent a two-stage OI procedure (OPRA™ implant system), repeating a biomechanical gait evaluation (self-selected walking velocity [SSWV]), before and 12 months after OI. Data were assessed with an 18-camera optical motion capture system (Qualisys, Gothenburg, SE) and six instrumented force plates (AMTI, MA). At each time point, the Knee Injury and Osteoarthritis Outcome Score (KOOS) [4] and acute numerical pain scores were captured to assess self-reported changes in knee joint health, symptoms, and function. A subject-specific biomechanical model in Visual 3D (C-Motion, MD) was used to estimate the peak contralateral knee adduction moment (KAM), and bilateral vertical ground reaction force (VGRF) peak, impulse, and loading rate (LR). VGRF and KAM were normalized by body mass. Peak trunk-pelvis lateral flexion, SSWV, step width, and stance time were also calculated. All outcomes were compared at 12 months vs. baseline using paired t-tests ($p<0.05$).

Results and Discussion

Participants walked at similar SSWV at baseline (1.07±0.24m/s) and 12mo post-OI (1.11±0.15m/s). At a group level (Table 1), no changes were observed in peak KAM before and after OI ($p=0.853$). On the prosthetic side, GRF peak and impulse decreased between baseline and 12 months ($p=0.008$; $p=0.048$, respectively). Trunk lateral flexion toward the sound side decreased post-OI ($p<0.001$). There were no differences between time points in VGRF LR, step width, nor stance time ($p\geq0.167$). Of note, VGRF LR and impulse were qualitatively larger on the sound vs. prosthetic side at both baseline and 12 months. Self-reported outcomes were available at both time points for five of the eight participants. Three of these five participants reported an increase in pain of the contralateral knee at 12 months vs. baseline; two of these five participants reported a decrease in at least one sub-score of the KOOS between time points, indicating diminished functionality in at least one aspect of life. When considering the results, it should be noted that participants achieved independent ambulation (the ability to walk 50 ft or more without an assistive device) ~5 (1-9) months before their 12-month evaluation and thus further changes in gait mechanics may be likely over time.

Significance

While prior work has demonstrated improvements in general health outcomes with bone-anchored prostheses [5], this may be unrelated to KOA as the current results suggest that, within the first year, asymmetrical loading of the lower limbs persists with the use of a bone-anchored prosthesis, largely due to lesser loading of the prosthetic limb without a corresponding increase in loading of the sound limb. Although our hypothesis cannot be supported, gait may change with prolonged use of the bone-anchored prosthesis; additional follow-up time points (and a larger sample) will help better characterize long-term outcomes of OI for Service members with TFA.

Acknowledgments

This work was supported by Award W81XWH-17-2-0060. The authors also acknowledge the DoD OI program, and specifically those who supported biomechanical evaluations (JME, JCA, JRG, BRK, CEM, MLT, and HSM). The views expressed herein are those of the authors and do not reflect the views of HJF, USUHS, the Department of Defense, Departments of the Army/Navy/Air Force, nor the U.S. Government.

References

1. Norvell et al. *Arch Phys Med Rehab* **86**, 487-93, 2005
2. Guilak. *Best Pract Res CL RH* **25**, 815-23, 2011
3. Hagberg & Brånemark. *Prosthet Orthot Int* **25**, 186-94, 2001
4. Roos et al. *J Orthop Sport Phys* **78**, 88-96, 1998
5. Hagberg et al. *Arch Phys Med Rehab* **95**, 2120-7, 2014

Table 1: Mean±SD kinetic, trunk, and temporal-spatial outcomes at baseline and 12 months after OI, separated by limb side.

		Peak KAM (Nm/kg)	VGRF Peak (BW)	VGRF LR (BW/s)	VGRF Impulse (BW*s)	Trunk Lat. Flexion (º)	Step Width (m)	Stance Time (s)
Base-line	Prosthetic	N/A	1.03±0.04	0.05±0.02	68.3±11.3	4.6±3.8	0.19±0.05	0.85±0.17
	Sound	0.41±0.16	1.13±0.08	0.11±0.03	84.4±14.0	7.6±3.7	0.19±0.05	0.89±0.17
12 mo	Prosthetic	N/A	0.88±0.13	0.05±0.02	55.9±5.6	5.3±3.8	0.18±0.08	0.77±0.06
	Sound	0.40±0.10	1.14±0.08	0.11±0.05	82.9±11.3	4.4±3.3	0.18±0.06	0.85±0.10

ELBOW LOADING DUE TO BACK FACE DEFOMATION OF BALLISTIC SHIELDS

Julia E. de Lange[1], Liam J. Burrows[1], Jean-Sébastien Binette, and Cheryl E. Quenneville[1,*]
[1]School of Biomedical Engineering, McMaster University, Hamilton, Canada
email: *quennev@mcmaster.ca

Introduction

Behind armour blunt trauma (BABT) refers to bodily injuries that may occur as a result of the rapid deformation from projectiles on personal protective equipment. Ballistic shields, which are used by defence personnel for diffusing dangerous situations, are supported by the user's arm to protect against projectile penetration. In the process of absorbing or deflecting bullets, the shields deform, termed back-face deformation, potentially causing injury to the user.

Currently there are no standards in place to limit the allowable back-face deformation of shields, only to personal body armour [1]. These standards cannot be directly applied to shields as they were developed with respect to differing anatomical areas, with differing tissue properties and associated injury thresholds. The only injury criteria developed for the upper extremity in the same orientation as BABT are for automotive side impacts (approximately 5 to ten times slower) [2].

This study used a modified Anthropomorphic Test Device (ATD) upper extremity to quantify impact loading as a result of BABT at the elbow. Three different stand-off distances (defined as the space between the back of the shield and the front of the elbow force sensors) were investigated, a potential protective design measure.

Methods

A WorldSID 50th percentile ATD upper limb (Humanetics Innovative Solutions, Farmington Hills, MI, USA) was modified to facilitate the measurement of localized, high-rate forces typical of BABT impacts (Figure 1). Alignment was controlled using a laser to the centre of the elbow-mounted force sensor (recorded at 1 MHz, model 200C20, PCB Piezotronics, MTS Systems Corp., NY, USA), and an integrated 6-axis load cell in the forearm recorded forces and moments (at 100 kHz). A 7.62x51mm NATO ball projectile (9.6 g) was fired at nominal velocity of 838 ± 15 m/s, in accordance with the testing procedure associated with testing a Level III threat type [3].

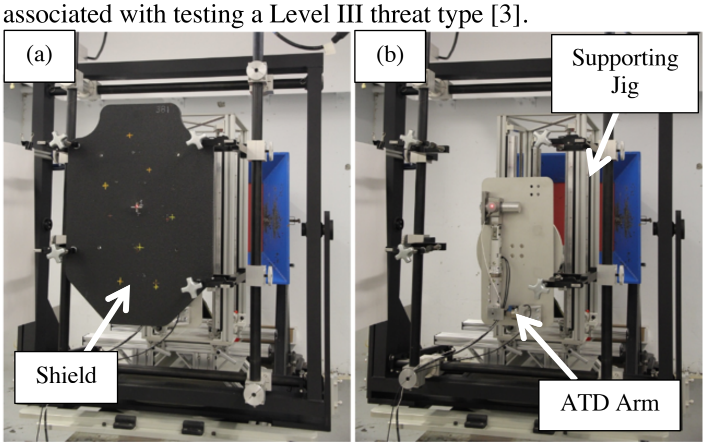

Figure 1: Ballistic testing setup (a) with a NIJ Level III ballistic shield, and (b) with the shield removed so the ATD arm is visible.

Two high-speed cameras (Fastcam SA-X type 324K-M2) at 30,000 fps captured the event to characterize the response of the shield. A one-way Analysis of Variance (ANOVA) with post hoc Tukey test was conducted on peak force, duration of impact and impulse to compare among stand-off distances ($\alpha = 0.05$).

Results and Discussion

Eleven shots were conducted, with an average impact velocity of 840.4 ± 3.2 m/s (Table 1). The peak back-face velocity of the shield was 208.9 ± 44.6 m/s. In terms of peak force (Figure 2), increasing stand-off distance significantly decreased the maximum force. The impact duration was significantly longer for the 20 mm stand-off as compared to 10 mm ($p = 0.02$). The impulse data was significantly lower at 20 mm as compared to the others ($p < 0.02$). The forearm moments were minimal for all tests (46.4 ± 32.6 Nm), highlighting the focal nature of these events.

Table 1: Summary of collected data.

Stand-off (mm)	Maximum Force (kN)	Impact Duration (ms)	Impulse (Nm*s)
10	19.0 ± 3.2	0.180 ± 0.045	1.303 ± 0.303
15	5.9 ± 1.1	0.623 ± 0.160	1.097 ± 0.142
20	2.0 ± 0.6	0.680 ± 0.355	0.452 ± 0.130

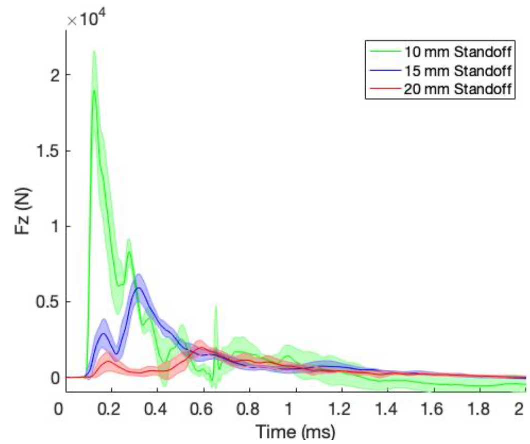

Figure 2: Force-time traces for each stand-off distance (mean ± SD).

Significance

Decreasing stand-off distance significantly increased force at the elbow, and therefore is a possible design approach to providing protection in future shields. The force-time curves generated herein will be used for developing injury thresholds at the elbow for shield deformation as it pertains to BABT.

Acknowledgments

The authors thank Defence Research and Development – Canada for funding this research, and Benoît Gauthier and Steven Kelly (DRDC) for their assistance during testing.

References

[1] NIJ Standard 0101.06, 2008.
[2] Bir, C. *et al*. (2004). J. Biomech. *37*(1), 73-79.
[3] NIJ Standard 0108.01, 1985.

TRUNK AND PELVIS MOVEMENT IN SLOPED WALKING FOR SERVICEMEMBERS WITH A TRANSFEMORAL OSSEOINTEGRATED PROSTHESIS

Jonathan R. Gladish[1,2], Julian C. Acasio[1,2], Brad D. Hendershot[2,3,4*], Christopher L. Dearth[2,3,4], Benjamin K. Potter[2,4] and Jonathan A. Forsberg[2,4]

[1]Henry M. Jackson Foundation for the Advancement of Military Medicine, Inc., Bethesda, MD, [2]Walter Reed National Military Medical Center, Bethesda, MD, [3]DoD-VA Extremity Trauma and Amputation Center of Excellence, Bethesda, MD, [4]Uniformed Services University of the Health Sciences, Bethesda, MD

email: bradford.d.hendershot2.civ@mail.mil

Introduction

Persons with vs. without lower limb loss (LL) report a high prevalence of secondary musculoskeletal conditions (e.g., low back pain), due in part to larger trunk-pelvic motions during activities of daily living [1,2]. Walking on slopes (vs. level ground) is especially challenging for persons with transfemoral (TF) LL using socket-based prostheses [3], further exaggerating compensatory mechanics involving large motions of the trunk and pelvis [4]. Osseointegration (OI), direct skeletal attachment of the prosthesis, is believed to alleviate discomfort presented by socket-based prostheses and improve functional outcomes [5]. While persons with TF LL have displayed improved metabolic cost and trunk sway in level-ground walking following a sufficient rehabilitation period [6], the effects of OI on sloped walking mechanics are not well-understood. The aim of this work was to compare trunk and pelvis motions during upslope and downslope walking among Service members with TF LL, before and after OI. We hypothesized that overall trunk and pelvic ROM will decrease after OI, and particularly in lateral flexion due a reduced hip-hiking strategy.

Methods

Six male Service members (mean±SD age: 34.3±11.1yrs, mass: 89.0±13.9kg, height: 179.0±7.1cm) with unilateral TF LL (one with contralateral transtibial limb loss) completed an instrumented, full-body biomechanical analysis while ascending and descending a 10° slope at a self-selected speed, prior to OI while using their traditional socket system (baseline; B) and again 12 months (12M) post-OI. Tri-axial global trunk and pelvis angles were calculated and ranges of motion (ROM) determined. Peak trunk relative to pelvis (trunk-pelvis) angles were also extracted. Paired t-tests ($p<0.05$) compared outcomes at B and 12M, separately for upslope and downslope walking.

Results and Discussion

For upslope walking (B: 1.03±0.13m/s; 12M: 0.99 ±0.13m/s), trunk axial rotation ROM decreased from B to 12M ($p<0.001$); there were no differences in trunk lean or lateral flexion ROM ($p>0.11$). Pelvis lateral flexion decreased from B to 12M ($p=0.04$); there were no differences in pelvic tilt or axial rotation ROM ($p>0.19$). There were no differences between time points in peak trunk-pelvis lean or lateral flexion angles. For downslope walking (B: 0.89±0.18m/s; 12M: 0.91±0.18m/s), trunk (all planes $p<0.001$) and pelvis (lean: $p<0.001$; lateral flexion, axial rotation: $p=0.01$) ROM decreased from B to 12M. There were no differences in peak trunk-pelvis lean angles, but the peak lateral flexion angle at 12M vs. B was greater on the OI side ($p=0.04$; 12M: 5.0±3.1°; B: 1.5±2.1°) and lesser on the non-OI side ($p=0.01$; 12M: 3.0±2.1°; B: 7.7±3.1°).

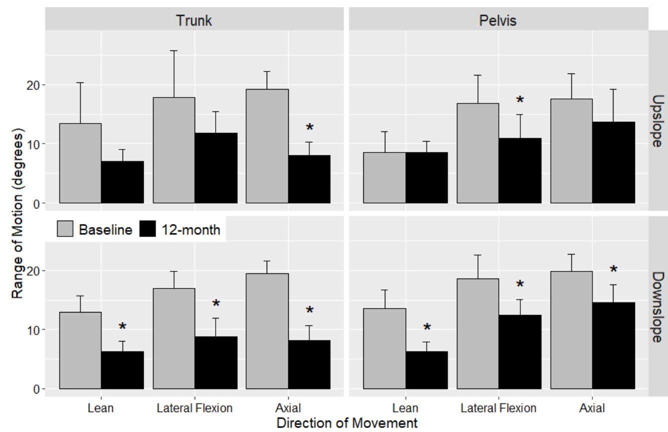

Figure 1: Tri-axial trunk and pelvis ranges of motion at baseline (gray) and 12-month (black) follow-up, for upslope and downslope walking. * denotes significant difference from Baseline value

Following OI, the decrease in lateral pelvic ROM (particularly in the upslope condition), along with the convergence of lateral peak trunk-pelvis angles, suggests a diminished hip-hiking strategy [4]. Moreover, decreased trunk and pelvic movements following OI in downslope, and to a lesser extent upslope, walking suggests decreased muscular and spinal loads [4] and, consequently, decreased risk for onset and/or recurrence of low back pain secondary to TF LL.

Significance

This preliminary analysis suggests that OI may improve overall trunk and pelvis mechanics during sloped walking, and thus decrease risk for musculoskeletal conditions secondary to TF LL. A larger sample and additional follow-up time points will help better characterize long-term outcomes of OI for Service members with TF LL.

Acknowledgments

This work was supported by Award #W81XWH-17-2-0060. The authors also acknowledge the DoD OI program, and specifically those who supported biomechanical and functional evaluations (JME, CEM, BRK, MLT, CAS, HSM). The views expressed herein are those of the authors and do not reflect the views of HJF, USUHS, the Department of Defense, Departments of the Army/Navy/Air Force, nor the U.S. Government.

References

[1] Farrokhi S. (2018) *Arch Phys Med Rehab* 99(2), 348-54. [2] Sagawa Jr Y. (2011) *Gait & Posture* 33(4), 511-26. [3] Bonnet X. (2021) *J Biomech* 129, 110843. [4] Acasio J. (2019) *J Biomech* 95, 109316. [5] Frossard L. (2010) *J Pros Orth* 22(1), 11-20. [6] Kooiman V. (2021) *ISPO World Congress*

EFFECT OF FATIGUE ON MOVEMENT PATTERNS DURING A LOADED RUCK MARCH

Audra E. Bloch[1*], J. Josiah Steckenrider[1], Rebecca A. Zifchock[1], Gregory M. Freisinger[1], Victoria G. Bode[2], and Seth Elkin-Frankston[2,3]

[1]United States Military Academy, Department of Civil & Mechanical Engineering, West Point, NY, USA

[2]Combat Capabilities Development Command Soldier Center, Natick, MA, USA

[3]Tufts Center for Applied Brain and Cognitive Sciences, Medford, MA, USA

email: *audra.bloch@westpoint.edu

Introduction

Physical fitness and preparation are key for success in the Army. Soldiers need to be able to move both themselves and their equipment for long distances while minimizing physical and cognitive fatigue. Physical exertion is the primary condition leading to fatigue [1], which often is encountered during loaded walking. Susceptibility to injuries may be associated with the fatigued state soldiers endure during a loaded ruck march. Previous work by Seay et al. suggested that increased load may cause an increased forward torso lean and a decrease in step length [2,3]. Additionally, extreme step width variability is associated with falling and balance issues [4]. Understanding the effect of fatigue on kinematic parameters can play a significant role in reducing health-related consequences including chronic injury, lost duty time, and significant medical costs [1,2,3]. Thus, the purpose of this study was to determine the effect of fatigue on the following gait parameters, and their variability, during a loaded ruck march: stride length, stride width, toe in-out angle, torso anterior-posterior (AP) angle, and torso side-to-side (SS) angle.

Methods

A sample size of 70 soldiers volunteered to participate in an IRB approved human performance study. The sample consisted of active-duty soldiers who had experience carrying heavy military loads over the course of a march. Measurements were taken during a 7-8 mile loaded march following a 72-hour field training exercise. It was assumed that fatigue increased over the course of the loaded march such that the percent of event completion could be considered as a proxy for fatigue status.

Participants walked in small groups of 6 – 9 and wore their own military equipment including their Army Combat Uniform, Fighting Load Carrier, rucksack, and rifle for the loaded marches. Additionally, participants wore two inertial measurement unit (IMU) sensors: one was secured to their chest plate and the other to their right ankle. Custom code written in MATLAB (Mathworks; Natick, MA) was used to process the data to identify the parameters of interest over the entirety of the loaded march.

The data over the entire ruck march was then processed as follows for each participant: (1) a baseline average from the first 5 minutes was calculated and then subtracted from the entire time series (except for torso SS angle), (2) rest periods were manually removed from the raw data, (3) remaining data were divided into four quarters based on the total completion time (to represent fatigue status) , and (4) the mean and standard deviation (to represent variability) was calculated for each quarter. One-way repeated measures ANOVA tests were conducted (Minitab, LLC; State College, PA) to examine the effect of fatigue status on each parameter. Significant ANOVAs were followed with planned pairwise comparisons between the first quarter of the march and each of the other quarters. Significance level was set at $p \leq 0.05$.

Results and Discussion

Of the ten kinematic parameters analyzed, two of the mean parameters and two of the variability parameters showed a significant difference from the first quarter of the march to the other quarters (Table 1).

Table 1: Quarter Comparisons, p-values

Kinematic Parameter	1-2	1-3	1-4
Stride Length Mean	0.77	0.09	0.00*
Stride Width Mean	0.00*	0.00*	0.00*
Torso AP Variability	0.25	0.92	0.01*
Torso SS Variability	0.12	0.01*	0.00*

*--Significantly different ($p<0.05$) compared to the first quarter

The purpose of this study was to determine the effect of fatigue on movement patterns during a loaded ruck march. The data collected did show a significant difference between quarters for variables that describe the magnitude and variability of motion.

Collectively, these results imply there are distinct mechanical responses to fatigue which become more pronounced over time. There is a decrease in stride length, increase in stride width, increase in stride width variability, and an increase in anterior-posterior and side-to-side torso lean variability. The kinematic adjustments made by the soldiers over the course of the loaded ruck march could lead to an increase in injury susceptibility. Additionally, real-time measurement of these parameters could be indicative of fatigue and therefore help prevent potential imminent injury. The results of this study do slightly differ from the findings of [2] and [3], fatigue did not influence the mean torso lean in either the AP or SS directions, but it did seem to increase their variabilities over the course of the loaded march.

It should be noted that, while this study benefitted from a large sample size and operational setting, it may be limited by individual rest periods, and the potential for slight sensor movements throughout the loaded march.

Significance

Over the course of a fatiguing loaded march, changes were observed in both stride kinematics and torso kinematics. These changes may be indicative of injury susceptibility, such as back and other musculoskeletal injuries, which are common in the military. This data can serve as a baseline condition and extend beyond the military setting for modeling efforts that seek to predict how the human body will respond to fatigue.

References

[1] Bustos, International Journal of Environmental Research and Public Health, 2021

[2] Seay, Military Medicine, 2014

[3] Wang, Military Medicine, 2012

[4] Brach, Journal of Neuroengineering and Rehabilitation, 2005

Approved for Public Release (PR2022_70896)

WALKING CHANGES AFTER LOADED RUCK MARCH, INDEPENDENT OF FACTORS RELATED TO A 72-HOUR SIMULATED FIELD MISSION

Amy Silder[1,2*], Trevor Viboch[1,2], Hedaya Rizeq[1,2], Victoria G. Bode[3], Seth Elkin-Frankston[3,4], and Pinata Sessoms[2]
[1]Leidos, Inc., San Diego, CA, USA
[2]Warfighter Performance Department, Naval Health Research Center, San Diego, CA, USA
[3]Combat Capabilities Development Command Soldier Center, Natick, MA, USA
[4]Center for Applied Brain and Cognitive Sciences, Medford, MA, USA
email: *silderam@gmail.com

Introduction

Soldiers are often required to carry heavy loads for long distances in austere environments, which can induce changes in gait [1,2] and muscular strength [1]. Both fatigue and walking with heavy loads can result in similar gait adaptations [2]. These adaptations can lead to an increased risk of injury and can adversely affect proprioception, neuromuscular coordination, and reaction times [3]. In an operational environment, a warfighter's ability to maneuver through their environment is paramount to combat effectiveness and overall mission success. While various studies have measured the acute effects of military load carriage on gait parameters, it remains unknown how the stress and fatigue associated with a multi-day mission affects gait and mobility.

The purpose of this study was to investigate the combined effects of a 72-hour simulated U.S. Army field mission on spatiotemporal gait parameters. We hypothesized that fatigue and stressors from the mission would induce greater changes in gait compared with changes from a loaded ruck march completed at the start and end of the simulated mission.

Methods

Fifty-six male Soldiers (22±3 y) completed a spatiotemporal gait assessment at four time points: immediately before and after two 11–13 km loaded ruck marches, which occurred before and after completion of a simulated 72-hour field mission on the grounds of Fort Devens, MA. All Soldiers carried 18–45 kg, were members of an infantry rifle squad, and remained with their squad for the duration of each march. The two marches were mostly level (~100 m elevation change) and took place on hard top. The squads were allowed to choose their pace and when they wanted to rest; each squad took 2–3 hours to complete the marches.

The gait assessments were performed pre- and post-ruck march and were completed in uniform without any additional load. Soldiers were instructed to walk with their arms at their side at a comfortable speed down and back along a 6-m pressure instrumented walkway (Zeno^{TM} Walkway, ProtoKinetics, PA). Speed, step length, step width, cadence, percent stance, and single support time were computed for each step using the location of the foot center and initial and final foot contact times. Two-way repeated measures analysis of variance was used to test for changes in gait that resulted from the ruck march, the 72-hour mission, and their interaction.

Results and Discussion

Contrary to our hypothesis, no significant differences in spatiotemporal gait patterns were detected between the start and end of the simulated 72-hour field mission. The lack of significant differences in gait across the multi-day mission is likely a result of the Soldiers being able to recover from the ruck march during the simulated field mission. It should be noted that this dataset includes only those participants who completed all four gait assessments. Approximately 10 additional individuals were not included in this analysis because they did not complete one or more of the gait assessments due to an injury acquired during the simulated mission.

Table 1: Mean (standard deviation) measured gait parameters

	Start of 72-hour Simulated Mission		End of 72-hour Simulated Mission	
	Before March	After March	Before March	After March
Speed (m/s)**	1.21(0.10)	1.15(0.14)	1.21(0.11)	1.16(0.13)
Step length (cm)**	71(5)	68(6)	72(5)	69(7)
Step width (cm)	13(3)	14(4)	13(3)	14(4)
Cadence*	102(4)	101(5)	102(4)	101(4)
Stance phase (%)	64(2)	65(2)	64(2)	64(2)
Single support (ms)	41(3)	42(3)	42(5)	42(5)

** Significant effect of ruck march, $P<.05$
* Significant effect of ruck march, $P<.001$

Soldiers did, however, walk slower, with shorter step lengths, and with a lower cadence after completing each ruck march. These are similar to the findings of others [e.g., 1,2] and suggest that heavy load carriage and fatigue have immediate and significant effects on gait. In situations where such changes are not resolved (e.g., daily marches), loaded and fatigued walking may expose Soldiers to increased risk for overuse injuries [4].

Further investigation is needed to determine if less experienced Soldiers or non-infantry units exhibit comparable patterns of recovery following similar missions.

Significance

Numerous physical, cognitive, and environmental factors can negatively affect a warfighter's effectiveness over time. If not properly addressed, these could lead to injury, casualty, or mission failure. The results of this investigation are significant in demonstrating that acute changes in gait that occur as a result of loaded ruck marches [1,2] seem to be temporary among trained infantry Soldiers. Current efforts are under way to combine these gait data with postural stability, strength, and other combat performance metrics obtained throughout the mission to determine if fatigue induced by a ruck march is indeed temporary or if other external factors may help explain gait and stability outcomes before and after the ruck marches.

Acknowledgments

Greg Freisinger, Paula Baluyut, Michael Rowling, Patrick Roscher, and the Measuring and Advancing Soldier Tactical Readiness and Effectiveness (MASTR-E) program

References

[1] Earl-Boehm et al., 2020. *Ergonomics*. 63(5):629-638.
[2] Wang et al., 2013. *R Q Exerc Sport*. 84(3):305-312.
[3] Ribeiro et al., 2007. *Eur J Appl Physiol*. 99:379-385.
[4] Knapik et al., 2012. *Int J Sports Med*. 33(11):940-946.

GAIT SYMMETRY AND STABILITY IN SERVICE MEMBERS WITH UNILATERAL TRANSFEMORAL AMPUTATION TWELVE MONTHS AFTER OSSEOINTEGRATION

Julian C. Acasio[1,2], Brad D. Hendershot[1,3,4], Christopher L. Dearth[1,3,4], Benjamin K. Potter[1,4], Jonathan A. Forsberg[1,4]
[1]Walter Reed National Military Medical Center, [2]Henry M. Jackson Foundation for the Adv. of Military Medicine, Inc., [3]DoD-VA Extremity Trauma & Amputation Center of Excellence, [4]Uniformed Services University of the Health Sciences
email: julian.c.acasio.ctr@mail.mil

Introduction

Persons with (unilateral) transfemoral amputation (TFA) are at an increased risk for falls, potentially leading to further injury [1]. Maintaining a steady and stable gait is difficult due to lower limb musculature loss; poor socket fit can exacerbate these issues [2]. To compensate, during gait the contralateral limb provides disproportionately larger propulsive and braking forces, which may lead to overuse injury [3]. Additionally, to increase passive stability (i.e., the ability to resist perturbations), persons with vs. without TFA walk slower, with shorter, wider, and more frequent steps [4], limiting community ambulation and the ability to make corrective steps [5]. Osseointegration (OI), a surgical procedure to bone-anchor the prosthesis, aims to eliminate socket-related issues and consequently may lessen gait compensations. The purpose of this study was to characterize gait symmetry and stability in Service members with TFA after OI. It was hypothesized gait will be more symmetrical with lesser passive stability post-OI.

Methods

Seven Service members (Mean±SD age: 34.6±10.5yr, body mass: 91.2±22.3kg, stature: 176.3±12.9cm) with unilateral TFA (77.9±52.9mo since injury) completed gait evaluations prior to (baseline) and 12mo post-OI. Participants walked without assistive devices at 1.0m/s on a 15m walkway with embedded force platforms. Kinematics were tracked via 51 retroreflective markers. Hip, knee, and ankle power and work were determined for the surgical (OI) and contralateral limb during leading, single support, and trailing phases; absolute normalized symmetry indices (NSI) [6] were computed. A unified deformable segment model approximated OI-side ankle power [7]. Step length and time NSI were determined. Minimum mediolateral margins of stability (MoS_{ML}) and base of support [8] evaluated passive stability. Paired t-tests (p<0.05) compared pre- vs. post-OI.

Results and Discussion

Outcomes generally remained similar between baseline and 12mo evaluations (Table 1). Notably, larger NSI were observed at 12mo vs. baseline in leading-limb hip work (p=0.014) and peak knee power generation (p=0.030). Similar trends were observed in leading-limb knee work (p=0.095) and step time (p=0.082) NSI. However, contrary to our hypothesis, the larger NSI post-OI indicate greater asymmetries; specifically, participants walked with near-zero contralateral hip work at 12mo (-0.002±0.041J/kg) vs. positive hip work at baseline (0.036±0.014J/kg, p=0.035). Meanwhile, contralateral peak knee power generation was larger at 12mo vs. baseline (1.204±0.778 vs. 0.703±0.511J/kg*s) and peak OI knee generation was lesser at 12mo vs. baseline (0.334±0.314 vs. 0.464±0.211J/kg*s); though, neither observation was statistically significant (p>0.18). Similarly, contralateral step time tended to decrease at 12mo vs. baseline (0.57±0.04 vs. 0.62±0.05s, p=0.052) while OI step time remained similar (0.64±0.06 vs. 0.65±0.06s, p=0.808). While these results suggest OI does not positively influence gait symmetry or stability (and may perhaps exaggerate some asymmetries), it is important to note that participants were still relatively early in their rehabilitation. Participants began independently ambulating ~5mo (range:1-9mo) before the 12mo evaluation; further gait adaptations are likely with time.

			Baseline	**12-month**	***p***
OI MoS_{ML} (cm)			13.7±2.6	12.7±3.3	0.544
Contralateral MoS_{ML} (cm)			13.6±2.1	12.3±2.3	0.302
Base of support (cm)			34.4±5.5	31.4±7.3	0.407
NSI	Step Length		10.2±8.8	8.0±8.5	0.636
	Step Time		4.9±4.9	11.6±8.0	0.082
	Leading Limb	Ankle	53.5±25.2	41.2±24.2	0.37
		Knee	44.1±25.9	66.3±19.5	0.095
		Hip	27.8±12.1	51.5±18.1	**0.014***
	Single Support	Ankle	46.3±32.7	44.8±33.1	0.933
		Knee	38.3±29.5	46.1±24.3	0.596
		Hip	37.3±29.7	51.9±37.4	0.436
	Trailing Limb	Ankle	46.7±37.1	41.5±26.8	0.767
		Knee	42.0±22.1	57.0±28.4	0.239
		Hip	42.0±24.8	45.1±27.4	0.831
	Peak Power Generation	Ankle	55.6±25.2	42.3±21.6	0.308
		Knee	41.7±20.6	67.3±18.3	**0.030***
		Hip	33.2±13.3	40.0±17.5	0.428
	Peak Power Absorption	Ankle	32.4±13.0	24.0±19.1	0.353
		Knee	30.9±9.9	37.8±26.7	0.531
		Hip	34.3±17.6	23.3±24.0	0.346

Table 1: Mean±SD minimum mediolateral margins of stability (MoS_{ML}), base of support, and normalized symmetry indices (NSI).
* indicates statistical differences 12mo vs. baseline.

Significance

In this preliminary analysis, gait symmetry and stability for Service members with TFA remained largely similar before and 12mo after OI, but continued characterization of long-term outcomes following OI are needed.

Acknowledgments

This work was supported by Award W81XWH-17-2-0060. The authors also acknowledge the DoD OI program, and specifically those who supported biomechanical evaluations (JME, JRG, BRK, CEM, CAS, MLT, and HSM). The views expressed herein are those of the authors and do not reflect the views of HJF, USUHS, the Department of Defense, Departments of the Army/Navy/Air Force, nor the U.S. Government.

References

[1] Miller et al., 2001. *Arch Phys Med Rehabil*. 82 (8): 1031-37. [2] Yazdani et al., 2021. *Curr Orthop Pract.* 32(5): 505-11. [3] Nolan & Lees 2000. *Prosthet Orthot Int.* 24: 117-25. [4] Sturk et al., 2019. *Disab Rehab Assist Tech.* 14(3): 226-35. [5] Acasio et al., 2017. *Gait Posture.* 52: 171-77. [6] Queen et al., 2020. *J Biomech*. 99: 109531. [7] Takahashi et al., 2012. *J Biomech.* 45(15): 2662-67. [8] Hof et al., 2005. *J Biomech.* 38(1): 1-8.

ASSESSING THE SOLDIER SURVIVABILITY TRADESPACE USING A SINGLE IMU

Matthew P. Mavor[1*], Victor C.H. Chan[1], Kristina M. Gruevski[2], Linda Bossi[2], Thomas Karakolis[2], Ryan B. Graham[1]
[1]School of Human Kinetics, Faculty of Health Sciences, University of Ottawa, Ottawa Ontario, Canada
[2]Defence Research and Development Canada, Government of Canada, Toronto, Ontario, Canada
email: *mmavo062@uottawa.ca

Introduction

Much of our understanding of what negatively affects the soldier survivability tradespace (i.e., performance, health, and susceptibility to enemy action) is from laboratory settings. However, most of an infantry soldier's occupational duties are performed outdoors in varying terrain/weather conditions [1]. Thus, to have the best understanding of how soldiers interact with their equipment in the field, a highly mobile outdoor motion capture method is needed.

One technology that could be deployed unobtrusively in the field are inertial measurement units (IMUs). By using a single IMU sensor, coupled with a deep learning human activity recognition (HAR) model, key movement patterns could be feasibly identified from soldiers operating in the field (e.g., [2]).

The goal of this work was to develop an indoor and outdoor-specific deep neural network (DNN) to perform HAR on a continuous data stream from a single IMU sensor. Using the predictions from the DNNs, tradespace metrics were calculated.

Methods

Seventeen male reservist infantry soldiers from the Canadian Armed Forces were recruited. Participant mean height, mass, age, and years served were 182.7 cm (±8.9), 81.7 kg (±9.2), 26.6 years (±7.2), and 3.8 years of service (±2.2), respectively.

Participants performed two repetitions of eight operationally-relevant movements indoors and two repetitions of an outdoor 60-metre section attack under four operationally-relevant load conditions: Slick ~5.5 kg, Full Fighting Order (FFO) ~22 kg, Small pack 38 kg (FFO + 16 kg small pack), and Pockets 38 kg (FFO + 16 kg non-ferrous plates in torso pockets) [3]. Movement patterns were collected concurrently using a whole-body IMU suit (240 Hz; Link, Xsens, Netherlands) and a single IMU sensor (100 Hz; S5, Catapult Sports Pty Ltd., Australia) worn on the back of the upper torso (~T8 vertebra) using a specialized sports pinnie. Triaxial accelerometer, gyroscope, and magnetometer signals from the single IMU were used to train the DNNs; IMU suit data were used to manually identify true class labels.

HAR was implemented using deep convolutional long short-term memory neural networks (DeepConvLSTM; [4]) in Tensorflow 2.3.0 [5], comprised of an input layer, four convolutional layers, two long short-term memory layers, and a fully-connected layer with a softmax activation function. Indoor- and outdoor-specific models were trained to classify eleven activities (reduced label set): null, stand, jump, descend, ascend, prone, kneel, stand-to-run, run, walk, and crawl. Hold-out testing was employed to train and evaluate the models, where participants were divided into training (~77%), validation (~10%), and testing (~13%) subsets. Hyperparameters were tuned using Bayesian optimization [6]; then, models were trained with a sliding window of 128 frames, stride length of 32 frames, batch size of 100 samples, and optimized using the root mean squared propagation algorithm.

HAR model predictions were processed through a two-step logical algorithm that applied real-world constraints, and to expand the reduced label set to a "full" label set consisting of 19 classes: the reduced set with contextualized descend and ascend classes (e.g., kneel-to-run vs. kneel-to-stand). The full label set was then used to calculate survivability tradespace metrics (i.e., exposure time, susceptibility to enemy action; [7]).

Results and Discussion

Table 1 presents the performances of the HAR models; Figure 1 depicts results from a section attack. On average, the HAR models' accuracy was 86.85%, which was increased to 90.7% (+3.85%) and 88.95% (+2.1%) for the reduced and full label sets, respectively following the logical algorithms. Compared to the true labels, the indoor model, on average, predicted exposure time and susceptibility within 0.37 seconds and 1.89%, respectively, whereas the outdoor model predicted exposure time and susceptibility within 0.14 seconds 0.83%, respectively.

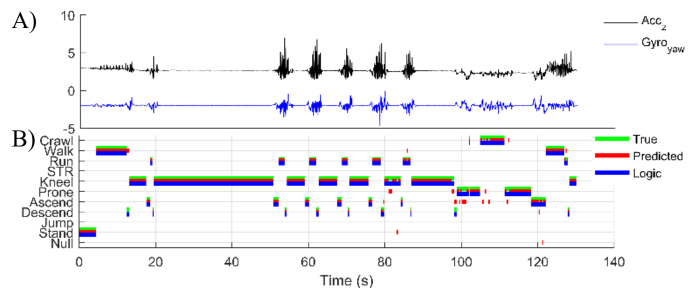

Figure 1: Example section attack from the outdoor DeepConvLSTM model. A) the raw vertical accelerometer and yaw gyroscope (note: data are offset for visualization). B) the reduced class labels from the ground truth, DNN predicted, and the logical algorithms.

Significance

Presented is a DNN method that can be employed by defence scientists to analyze IMU data collected in the field to obtain meaningful tradespace metrics with a high level of accuracy.

Acknowledgments

This work was funded by the Canadian Department of National Defence – Contract # W7719-195460/001/TOR.

References

[1] Armstrong & Bossi, 2021. *NATO AC/323(HFM-238)*. [2] Russell et al., 2021. *Sensors,* 21(2). [3] Mavor et al., 2019. *DRDC-RDDC*-2020-C001. [4] Ordóñez & Roggen, 2016. *Sensors,* 16(1). [5] Abadi et al., 2016. *12th USENIX*, 265-283. [6] Snoek et al., 2012 *Adv Neural Inf Process Syst.,* 25. [7] Billing et al., 2015. *J Strength Cond., 29(11S).*

Table 1. DeepConvLSTM HAR performance on hold-out test data, without and with logic.

	DeepConvLSTM without Logic			DeepConvLSTM with Logic	
	Accuracy	Weighted average F1-score	Loss	Reduced Label Set Accuracy	Full Label Set Accuracy
Indoor	86.5%	86.5%	0.752	89.8%	86.9%
Outdoor	87.2%	87.9%	0.696	91.6%	91.0%

Note: Reduced and full accuracy represent accuracy on the reduced label set (11 labels) and the full label set (19 labels).

LOADING ASYMMETRY BEFORE AND AFTER RUNNERS SUSTAIN A LOWER EXTREMITY BONE STRESS INJURY

Harper E. Stewart[1], Ryan S. Alcantara[3], Kathryn A. Farina[4,5], Alena M. Grabowski[6], Michael E. Hahn[4,5], Rodger Kram[6], Jill L. McNitt-Gray[1,2]

[1]Department of Biomedical Engineering, [2]Department of Biological Sciences, University of Southern California, Los Angeles, CA, [3]Department of Bioengineering, Stanford University, Stanford, CA, [4]Bowerman Sports Science Center, [5]Department of Human Physiology, University of Oregon, Eugene, OR, [6]Department of Integrative Physiology, University of Colorado, Boulder, CO.

email: hestewar@usc.edu

Introduction

Lower extremity bone stress injuries are prevalent in long distance runners. As training pace and mileage increase, ground reaction forces and number of loading cycles increase, potentially raising the risk of bone stress injuries. In a previous case study of an NCAA runner, greater asymmetry in peak vertical ground reaction forces (peak vGRF) was observed (injured > uninjured) 3 weeks prior to a metatarsal stress fracture [1]. Based on this initial finding, we hypothesized that runners who sustained bone stress injuries would exhibit comparable asymmetries in peak vertical ground reaction forces (vGRF) in weeks prior to injury.

Methods

This prospective, multi-institutional study of over 50 NCAA Division I mid- and long-distance runners was conducted over three years, in accordance with institutional IRBs. Kinetic and kinematic data of 5 athletes who sustained a lower-extremity bone stress injury during the study were compared before and after sustaining the injury. vGRF data were collected while running at 5, 5.5, 6.5, and 7 min/mile (3.8, 4.1, 4.9, 5.4 m/s) training paces using a force-treadmill sampled at 1000 Hz (Treadmetrix Park City, UT and Bertec, Columbus, OH). A 4th order zero-lag lowpass filter with a 14 Hz cutoff was used. Peak vGRF was defined as the highest vertical force during ground contact. The 20% trimmed mean of the peak vGRF was calculated for each leg (injured and uninjured) at each collection and compared over the duration of the study (Fig. 1) [2]. Trimmed means are a robust statistical measure, which mitigate the influence outliers [2]. Peak vGRF between legs before and after injury were compared within athlete at the fastest speeds (5, 5.5 min/mi) over a 2-year span. Symmetry index was calculated: $SI\ (\%) = (Inj - Uninj)/(0.5 * (Inj - Uninj)) * 100\%$.

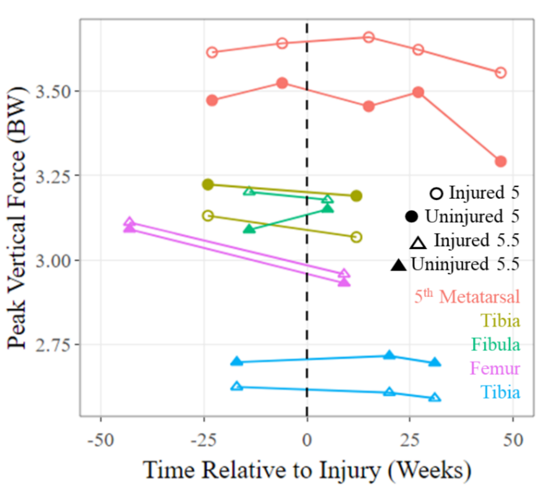

Figure 1: Peak vGRF for each leg (injured, uninjured) before and after sustaining a bone stress injury for individual runners. Markers indicate the 20% trimmed mean of peak vGRF during each collection relative to the date each athlete sustained a bone stress injury (time =0).

Results and Discussion

Three of the five athletes who experienced a lower extremity bone stress injury exhibited a greater peak vGRF on the leg eventually experiencing the injury (Fig 1.). Only the athlete who sustained a fibular bone stress injury had greater asymmetry between legs (3.6%) prior to injury and returned to greater symmetry after injury (0.9%). Trimmed mean magnitudes of peak vGRF across athletes were between 2.5 and 3.7 BW; however, the difference between legs within a collection was observed to be less than 0.25 BW. The athletes who sustained the metatarsal, fibular, and femoral injuries had consistently higher peak vGRFs on the leg with a bone stress injury across all collections indicated by the positive SI%. However, athletes who sustained tibial injuries had higher peak vGRFs on their uninjured leg across all collections. Our findings don't support the hypothesis of greater asymmetry in peak vGRF between the injured and uninjured legs prior to injury.

Table 1: Symmetry index for each data collection with weeks to injury.

5th MT		Tibia		Fibula		Femur		Tibia	
Wks Inj	*SI (%)*	*Wks Inj*	*SI (%)*	*Wks Inj*	*SI (%)*	*Wks Inj*	*SI (%)*	*Wks Inj*	*SI (%)*
-23	4.0	-24	-2.9	-14	3.6	-43	0.7	-17	-2.8
-6	3.3	12	-3.9	5	0.9	9	0.9	20	-4.1
15	5.8							31	-4.0
27	3.5								
47	7.7								

Significance

The results indicate that asymmetry in the peak vGRF is not a consistent method to prospectively identify injury risk. Different injury locations may require different types of analysis in order to detect kinetic differences prior to injury. Limitations of this work include focusing on biomechanical loading factors without considering physiological characteristics such as nutrition and hormones, which may also impact the likelihood of a bone stress injury. Future work will involve examining injured vs uninjured runners to determine the natural variability in a competitive season and determining variables which indicate a pending bone stress response.

Acknowledgments

Supported by the PAC12 Student-Athlete Health and Well-Being Grant Program (#3-03_PAC-12-Oregon-Hahn-17-02), Los Angeles Chapter of ARCS, and USC WiSE.

References

[1] R.S. Alcantara, et al. (2020) ASB [Abstract]

[2] R.Wilcox. (2017) Modern Statistics

Kinematic predictors of failed drop-vertical jump landings in adolescent athletes

Nicholas J. Romanchuk[1], Lisa E. Ek Orloff [2], Céline I. Girard [1], Michael J. Del Bel[3] and Daniel L. Benoit[1,2,3]
[1] Ottawa Carleton Institute for Biomedical Engineering, University of Ottawa, Canada
[2] School of Human Kinetics, University of Ottawa, Canada
[3] School of Rehabilitation Sciences, University of Ottawa, Canada
email: dbenoit@uottawa.ca

Introduction

The anterior cruciate ligament (ACL) is the most frequently damaged knee ligament, with injury rates continuing to rise among adolescent athletes [1]. In fact, females between 13-17 years of age now possess the highest injury incidence of any sex-age strata [2]. Although there have been several studies investigating the biomechanical links between jump landings and injury risk [3], limited research has explored the kinematic differences between successful and failed single-leg landings. Failed trials are generally discarded following data collection to reduce variability and improve reliability; however, significant clinical findings may be elucidated from these trials. Identifying the biomechanical factors that lead to failed landings may provide specific targets for injury prevention and sport performance programs. Thus, the purpose of this study was to *i*) determine if kinematic variables can predict whether a participant will successfully land a drop vertical jump (DVJ) and, *ii*) determine which variables are the most important predictors of a successful jump landing.

Methods

Thirty-three uninjured adolescent (<19 years old) athletes completed single-leg DVJs from a platform aligned with their tibial plateau. Participants were required to stick and hold the landing. Trials during which participants shifted foot position to regain balance or touched the ground with the contralateral leg were categorized as failed. Full-body kinematics were collected using a 10-camera infrared motion analysis system at 200Hz (Vicon, Nexus, Oxford, UK) and ground reaction force data (GRF) were collected using a force platform at 2000Hz (Bertec Corp., Columbus, USA). Sex, limb-dominance, joint angles, and centre-of-mass (CoM) position were extracted at the point of ground contact.

In total, 862 jump landings were recorded and categorized as 'successful' (n=501) or 'failed' (n=361). Participants were divided into training (80%) and testing (20%) datasets using stratified random sampling across sex. Variable selection was performed using recursive feature elimination and leave-one-out cross-validation (LOOCV). Once the optimal number of predictors was chosen, a logistic regression model was fit on the training dataset. Model performance was assessed on the left-out testing dataset using accuracy, kappa statistic, negative prediction value, and precision.

Results and Discussion

Based on recursive feature elimination with LOOCV, the four variable model had the highest cross-validation accuracy. Thus, the logistic regression model was fit on the training data using four variable recursive feature elimination. The variables selected were: limb dominance, hip flexion in the landing limb, head-arms-trunk (HAT) CoM lateral distance from base-of-support (BoS), and HAT CoM total distance from BoS (Table 1).

The logistic regression model had an accuracy of 70.6%, a kappa statistic of 0.412, a negative prediction value of 69.6% and a precision of 71.7% on the training dataset. When evaluated on the testing dataset there was a slight decrease in performance with an accuracy of 66.6%, a kappa statistic of 0.33, a negative prediction value of 62.0% and a slight increase in precision of 73.9%.

It should be noted that since the variables used in the model were extracted at the first point of ground contact, and therefore prior to the participant 'failing' the landing, this model represents a true prediction. Furthermore, the 'failed' landings represented a wide range of movement patterns, encompassing situations where participants shifted their landing foot slightly or fell completely. With these considerations, we believe that an accuracy of 66.6% on a left-out testing dataset is meaningful, and higher than what we would expect to occur due to random chance. In addition, the HAT CoM positioning relative to the BoS were the strongest predictors of failing a landing.

Table 1. Odds ratios and *p*-values for each predictor

	Odds Ratio	*p*-value
Limb Dominance	0.6112	<0.0001
Hip Flexion (landing limb)	0.7304	0.0002
HAT Lateral Distance	2.6477	<0.0001
HAT Total Distance	1.7941	<0.0001

Significance

Based on our findings, it appears that HAT CoM positioning relative to the BoS, hip flexion and limb dominance are strong predictors for whether a jump will be failed or landed successfully. The present study provides further evidence that failing a landing is initiated prior to ground contact, since included variables were extracted as the foot was first making contact with the force plate. Thus, injury prevention programs aimed at reducing injuries during jump landings should place an emphasis on controlling how athletes prepare for the landing rather than the kinematics following ground contact. In addition, considering the predictive importance of HAT CoM positioning relative to the BoS, interventions should also focus on modulating HAT positioning prior to landing.

Acknowledgments

The authors would like to thank Saskia Hanssen and Laura Boonstra for their contributions in data collections. They would also like to thank the NSERC, the Arthroscopy Association of North America, CHEO Research Institute and the University of Ottawa Department of Surgery for their support.

References

[1] Gornitzky et al., 2016. *Am J Sports Med.* 44:2716-2723.
[2] Herzog et al., 2017. *JAMA Pediatr*. 171:808-810.
[3] Hewett et al., 2005. *Am J Sports Med.* 33:492-5

PEAK KNEE EXTENSION TORQUE IS RELATED TO TOTAL BONE MINERAL DENSITY AMONG FEMALE COLLEGIATE FIELD SPORT ATHLETES

Katie Collins[1], Ashley Triplett[1], Matthew Harkey[1], D.S. Blaise Williams III[2], Brad Winn[2], Christopher Kuenze[1]
[1]Athletic Injury and Rehabilitation Laboratory, Michigan State University, East Lansing, MI, USA, [2] Nike Sport Research Laboratory, Beaverton, OR, USA
email: colli784@msu.edu

Introduction

Weight-bearing exercises such as running and walking promote healthy tissue adaptations including increased bone mineral density (BMD) and reduced adiposity [1]. Maintenance of healthy BMD is important for female athletes as women are more likely to experience injuries such as stress fractures [1]. In addition, maintenance of healthy adiposity may be important as fat mass can influence injury risk such as knee injury among young women. Strength outcomes (e.g. peak knee extension torque) are known to mediate BMD, and higher adiposity has been related to poorer strength. However, it is unclear if this relationship exists among female collegiate field sport athletes. This may be an especially important concern for female athletes, considering both BMD and adiposity are related to injury (e.g., stress fracture, acute injury). Therefore, the purpose of this investigation was to determine the relationship between isokinetic knee extension peak torque, total body BMD, and total body % adiposity. We hypothesized that peak knee extension torque would be strongly related to total BMD, peak knee extension torque would be moderately related to total % adiposity, and total % adiposity would be moderately related to total BMD.

Methods

Individuals were eligible for this study if they were between ages 18-25 years old, a member of an NCAA athletics team (i.e., women's soccer, women's field hockey), and did not have a diagnosed injury within 4 weeks of study enrollment. All participants provided written, informed consent prior to engagement in any study-related activities. Biologically female athletes were included in this analysis.

All participants completed an isokinetic knee extension strength assessment at 60°/ second on their dominant limb using an isokinetic dynamometer (Biodex, System 4, Biodex Medical Systems Inc., NY, USA). Participants were asked to complete 5 successful isokinetic trials for knee extension and flexion. Peak knee extension torque was extracted at the peak instance across 5 trials. All participants also underwent a whole-body Dual-energy X-ray Absorptiometry (DXA) scan (Horizon DXA, Hologic, Inc., AZ, USA) to determine total body BMD and % adiposity. BMD was calculated as bone mineral content relative to area (g/cm^2). Percent adiposity was calculated as total % body fat. Both analyses report whole body values that exclude the head.

Descriptive statistics (means, standard deviations) were calculated for participant demographics and variables of interest (BMD, % adiposity, peak torque). Partial correlations were used to determine the relationship between peak knee extension torque of the dominant limb, total BMD and % adiposity. Pearson's correlation coefficients were interpreted as weak: 0.1 - 0.3, moderate: 0.4 - 0.6, and strong: ≥ 0.7. Alpha was set *a priori* $P < 0.05$.

Results and Discussion

Thirty-five female NCAA field sport athletes completed a single preseason assessment for isokinetic knee extension strength and body composition and were therefore included in this analysis. Demographic information and outcomes of interest (BMD, % adiposity, torque) can be found in Table 1. Total body BMD was significantly related to dominant limb peak knee extension torque (r=0.451, P=0.007). Total body % adiposity was not significantly related to dominant limb peak knee extension torque (r=-0.315, P=0.066). Finally, total body BMD was not significantly related to total % adiposity (r=-0.057, P=0.743). Peak knee extension torque was moderately related to total BMD, though we had hypothesized a strong relationship. Peak knee extension torque and total BMD were not significantly related to total % adiposity.

The participants included in this study demonstrated similar total BMD [1], knee extension torque, and % adiposity as previously reported in female NCAA athletes. Dominant limb peak knee extension torque was moderately and positively related to total body BMD, meaning that greater peak knee extension torque was related to higher BMD, in accordance with previous investigations [2], though we had hypothesized a strong relationship. Total % adiposity was not related to BMD, which was similar to a previous investigation of female collegiate athletes [1]. However, % adiposity was not significantly related to peak knee extension torque, which was not in accordance with our hypothesis or previous investigations. Though, % adiposity was relatively low among our sample compared to normative age and sex specific values which may have limited observations.

Table 1. Participant Demographics and Outcomes

Age (years)	20.3 ± 1.4
Height (cm)	168.0 ± 5.3
Mass (kg)	64.8 ± 7.0
Field Sport (hockey, soccer)*	16 / 19
Peak Knee Extension Torque (Nm)	137 ± 27.4
Total Body Bone Mineral Density (g/cm^2)	1.15 ± 0.07
Total Body Adiposity (%)	24.2 ± 3.6

Table 1: Participant demographics and variables of interest are reported as mean ± standard deviation unless otherwise indicated. *reported as frequency.

Significance

Peak knee extension torque is moderately related to total body BMD among female NCAA field sport athletes. Future longitudinal investigations are needed to better understand how changes in strength, BMD, and % adiposity may influence injury risk among female collegiate athletes.

Acknowledgments

Financial support for this project was provided by the Nike Sport Research Laboratory.

References

[1] Mudd et al., 2007. J Athl Train. 403: 18059997.
[2] Snow-Harter et al., 1990. J Bone Miner Res. 5: 2382585.

AGREEMENT BETWEEN GFT & HYBRID-III HEAD KINEMATICS FOR DIFFERENT IMPACT SCENARIOS IN ICE HOCKEY

Olivia M.G. Aguiar, Jeremiah Zacharias, Omid Vakili, Stephen N. Robinovitch
Department of Biomedical Physiology and Kinesiology, Simon Fraser University, Burnaby, Canada
Email: oaguiar@sfu.ca

Introduction

In elite ice hockey, 62% of concussions involve impact to the head delivered by an opposing player's shoulder (42%), elbow (15%), or hand (5%) [1]. Helmet-mounted sensors, such as the GForceTracker™ (GFT), can be used to examine the frequency and magnitude of head impacts during game play. Previous studies have compared head kinematics recorded by GFT to "gold standard" Hybrid-III (H-III) head forms, and found that helmet make/model, impact direction, and sensor location affected the agreement between GFT and H-III [2]. The accuracy of the GFT may depend on the nature of the object that impacts the head. In this study, we examined the effect of impacting body parts (shoulder, elbow, hand) on agreement between GFT and H-III for peak resultant measures of head acceleration and velocity.

Methods

Eleven ice hockey players delivered checks to an instrumented dummy "as hard as comfortable" with each of their shoulder, elbow, and hand (Fig 1). A kickboxing dummy was equipped with a 50th percentile male H-III neck and head form, instrumented with nine uniaxial accelerometers in a 3-2-2-2 array recording at 20kHz. A CCM Vector 08 hockey helmet was instrumented with three GFT sensors in the back, right lateral, and top aspects of the helmet. The helmet was secured to the dummy. Players wore protective gear and delivered checks to the front (face cage) of the dummy's head. GFT recorded linear accelerations (a_{max}, g) at 3kHz and angular velocities (ω_{max}, rad/s) at 0.8kHz. H-III angular acceleration signals were integrated to provide velocities for comparison with the GFT.

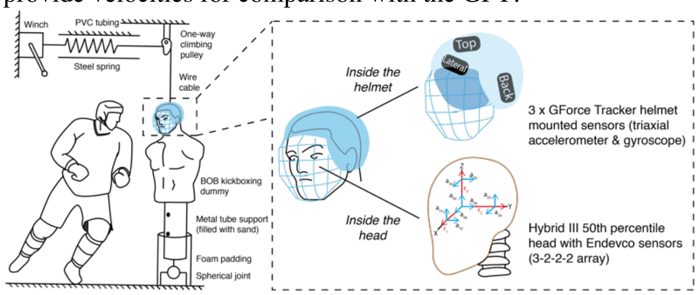

Figure 1: Experimental set up.

Peak resultant measures from the raw GFT and H-III were used for analysis. Absolute percent errors (APE) were calculated to determine the agreement between measures from each GFT sensor and the H-III. Generalized Linear Mixed Models were used to examine the effect of impact scenarios (shoulder, elbow, hand) on the agreement between GFT and HIII. Player code was treated as a random effect. Tukey post-hoc tests were used to compare differences in mean APE between impact scenarios. Significance was set to α=0.05 a priori.

Results and Discussion

A total of 132 impacts were collected and analyzed. There were differences in the mean APE for a_{max} and/or ω_{max} between impact scenarios for each sensor ($p<0.003$; Fig 2). Mean elbow APE for a_{max} were up to 1.73-fold greater than the hand ($p=0.009$) for the back and top sensors. In addition, the mean shoulder APE for a_{max} were 1.29-fold smaller than the elbow ($p=0.009$) for the back sensor, and 1.74-fold smaller than the hand ($p=0.001$) for lateral sensor. Mean elbow APE for ω_{max} were 1.42 to 1.71-fold greater than the hand ($p<0.034$) and 2.10 to 2.62-fold greater than the shoulder ($p<0.0001$) for the lateral and back sensors. Mean hand APE for ω_{max} were 1.49 to 1.54-fold greater than shoulder ($p<0.017$) for the lateral and back sensors. All other comparisons did not reach statistical significance.

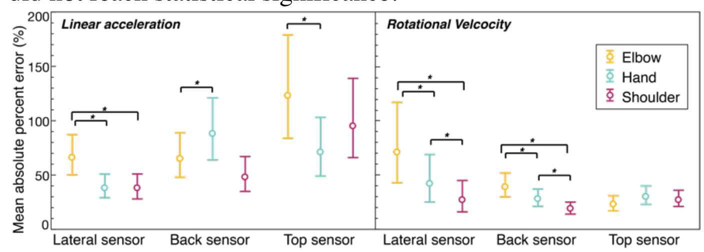

Figure 2: Mean absolute percent error for each sensor by impacting body part. Bars show 95th confidence intervals. Asterisks show $p<0.05$.

This study evaluated the effect of impact scenarios on GFT-H-III agreement for a_{max} and ω_{max}. We found that the accuracy of GFT was affected by the impact scenario, and that elbow-to-head impacts typically resulted in greater GFT errors than the shoulder or hand. This may be due to difference in the surface compliance of the impacting body parts, which influence the dynamic response of the helmeted head [3].

We also found the mean GFT errors were greater for a_{max} (range=38-123%) than ω_{max} (19-71%) across impact scenarios. Previous studies also reported smaller error for measures of ω_{max} than a_{max} [2]. We see three potential reasons for the observed errors: (1) the raw GFT measures were not transformed from the helmet shell to the centre of gravity of the head; (2) the GFT were fixed to the helmet via tape. Recorded kinematics may represent helmet dislocation, rather than head movement [4]; (3) impacts were delivered to the face cage, which produces larger errors in head kinematics than impacts to the helmet shell [4].

Significance

The impact scenario in hockey influences the accuracy of head kinematics measured by helmet-mounted sensors. Field studies should identify which specific body parts impact the head [6], to guide the development of impact-specific correction algorithms that minimize sensor error [2]. Future studies should consider using mouthguard-mounted sensors, which are less error-prone [6]. Available sensors must be validated for on-ice measures.

Acknowledgments

Funded by NSERC RGPIN/04065-2015.

References

[1] Hutchison et al., 2015. BJSM.
[2] Allison et al., 2015. J Athl Train.
[3] de Grau et al., 2019. Proc IMechE Part P: J Sports Eng Tech.
[4] Jadischke et al., 2013. J Biomech.
[5] Aguiar et al., 2020. J Biomech.
[6] Tierney, 2021. Sports Biomech.

ERGOMETER ROWING PLACES THE HIP AT RISK OF INJURY: A BIOMECHANICAL, CLINICAL, AND COACHING ASSESSMENT WITH IMPLICATIONS FOR INJURY PREVENTION AND EXERCISE PRESCRIPTION

Jordan P. Ankersen[1,2*], Bradley S. Lambert[2], Stephanie Gardner[2], Michael R. Moreno[1], Joshua D. Harris[2], Shari R. Liberman[2]
[1]Texas A&M University, College Station, TX; [2]Houston Methodist, Houston, TX
email: *ankjp@tamu.edu

Introduction

Rowing ergometers have gained popularity for row training and as purportedly low-impact means of improving general fitness. However, previous studies have shown high rates of acute and overuse injuries of the hip and lumbar spine. The purpose of the present study is to utilize 3D motion capture paired with clinical and coaching assessments to (1) determine if ergometer-based rowing results in hip flexion (HF) and internal rotation (HIR) associated with elevated risk of hip injury; (2) determine the impact of fatigue on hip range of motion (ROM), pull force, and row form; and (3) characterize the prevalence of hip pain/disfunction in recreational rowers.

Methods

Seventeen healthy amateur rowers (m=8, F=9; age=38±9.1 years; VO2max=44.4±7.8 ml·kg·min-1) volunteered to participate in this investigation. Following a standardized warmup, each subject performed a maximal effort 2000-meter row on an ergometer equipped with a load cell (Futek®) to record pull force. Kinematics were recorded using a 12-camera motion capture system (Vicon®). Data was recorded at the 200m, 600m, 1000m, 1400m, and 1800m distances. Risk thresholds were set at 90° of HF [1-3] and 10° of HIR [4]. Three professional rowing instructors (average 11.5 years rowing/coaching) evaluated row technique at the 200m and 1800m distances using a 1-4 rating scale (1, poor technique – 4, excellent technique) for the catch, drive, finish, and overall technique. Prior to beginning the bout, rowers completed an International Hip Outcome Tool (iHOT-12, VAS: 0 pain/disfunction – 100 no pain/no disfunction) survey [5]. A mixed-model ANOVA repeated on row distance followed by a Tukey's post-hoc test for pairwise comparisons was used to compare biomechanical assessments during the bout. A Mann-Whitney test for non-parametric data was used to compare rowing form scores between the 200m and 1800m distances. Type-I error was set at a=0.05 for all analyses.

Results and Discussion

No effect of row distance was observed for either HF or HIR (**Figure 1**). For HF, the group significantly exceeded the 90° risk threshold throughout the 2000m row ($p<0.001$, 111.0±5.3°) with all patients above the threshold throughout the rowing bout. For HIR, the group did not differ from the 10° risk threshold. Following the 200m measurement (8.2±0.4 N/kg), peak force was observed to significantly decrease at the 600m (7.4±0.4 N/kg, $p=0.004$) and 1000m (7.5±0.4 N/kg, $p=0.005$) measurements followed by a subsequent increase at the 1800m measurement (8.4±0.5 N/kg) to a value similar to the 200m measurement (**Figure 2**). Rowing form decreased from the 200m to 1800m measurement (overall; 200m, 2.2±0.3 | 1800m, 1.9±0.2; $p=0.012$). The mean iHOT-12 score for the group was 89.5±7.6 with more than 50% of the participants reporting some degree of discomfort/disfunction (<100).

Additionally, average peak force across the entire row was observed to be comparable, on average, to 23-29% peak deadlift pull force (31.2-36.8 N / kg body mass) observed in resistance trained and non-resistance trained young males [6]. Comparably, this would equate to roughly 26 sets of 10 repetitions at a submaximal workload. Taken together, study results indicate that the repetitive high degrees of hip flexion coupled with moderate pull forces and declining form with fatigue may place rowers at an increased risk of hip overuse injuries or FAI. Therefore, caution should be exercised when considering performing or prescribing repeated bouts of high intensity or fatiguing rowing. These findings may also assist in refining the concept of "low-impact" exercise as it pertains to joint-specific injury risk.

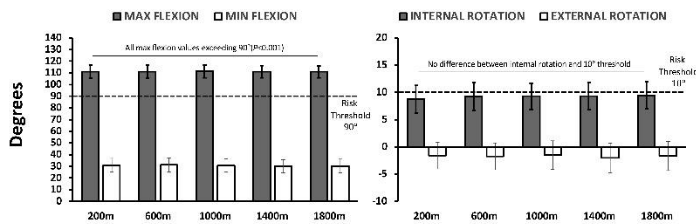

Figure 1: Data are presented as means±95% CI for hip ROM (degrees) at each recording point for the 2000m row. The dashed line represents risk thresholds for FAI.

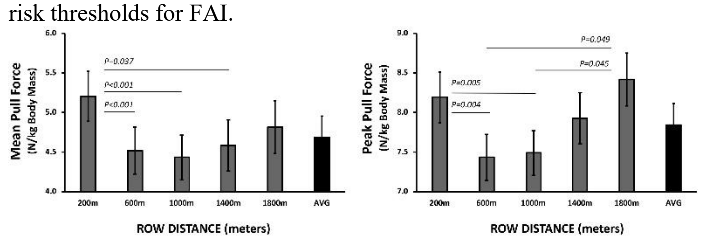

Figure 2: Data are presented as means±95% CI for mean (left) and peak (right) row pull force per stroke. Significant differences in force between distance intervals are indicated by solid lines and accompanied by P-values.

Significance

The present findings will aid physicians, athletic trainers, and others in educating patients, athletes, coaches, and general population adults about the potential risks associated with ergometer rowing, specifically as it relates to hip injury.

References

[1.] Boykin RE et al., 2013. *Clin Orthop Relat Res*. 471(8):2517-2522 .
[2.] Thornton JS et al., 2017. *Sports Med.* 47(4):641-661.
[3.] Larkin B et al., 2015. *Clin Orthop Relat Res*. 473(4):1284-1288.
[4.] Satpathy J et al., 2015. *J Hip Preserv Surg.* 2(3):287-294.
[5.] Griffin DR et al., 2012. *Arthroscopy.* 28(5):611-616
[6.] Zemkova E et al., 2019. *Am J Mens Health.* 13(1):1557988319828622.

A PCA AND HIERARCICAL CLUSTERING ANALYSIS OF THE RELATIONSHIP BETWEEN PELVIS GEOMETRY AND BONE STRESS INJURY INCIDENCE IN COLLEGIATE CROSS COUNTRY RUNNERS

Jack A. Martin[1,2,3*], Bryan C. Heiderscheit[1,2]
University of Wisconsin-Madison [1]Badger Athletic Performance Program, Depts. of [2]Ortho. & Rehab. and [3]Mech. Engr.
*email: jamartin8@wisc.edu

Introduction

Anthropometric factors like bone cross-sectional area [1] and section modulus [2] have been implicated in bone stress injury (BSI) among runners, but these are specific to individual bones, and difficult to measure. Instead, pelvis shape may play a role in force magnitudes experienced by bones throughout the lower body via differences in alignment relative to ground reaction and joint contact forces, such that pelvis geometry could be a predictor of BSI. Additionally, differences in pelvis shape may correlate with bone shape and size throughout the lower body.

The purpose of this study was to explore whether 1) runners can be grouped based on frontal plane pelvis geometry using principal component analysis (PCA) and hierarchical clustering, 2) these groups exhibit differences in BSI incidence, and 3) trends exist between pelvis geometry and BSI incidence.

Methods

Preseason whole body dual x-ray absorptiometry bone mineral density (BMD) scans (GE Healthcare Lunar iDXA) from 53 collegiate cross country runners (32F) were analyzed in MATLAB. Whole body BMD images were first aligned with each other using image transformations (translation, rotation, scale). Next, a pelvis region of interest (ROI) was selected for one runner. Pelvis ROIs were then defined for other runners by using an additional image transformation (translation, rotation, scale) that found the best match for the initial pelvis ROI in other BMD images. This process was repeated for mirrored versions of each runner – treated as additional subjects to reduce the effects of postural and structural asymmetries – such that 106 pelvis ROIs were included in subsequent analyses. BMD values were normalized to the maximum value observed in each pelvis ROI to remove the influence of absolute bone density, reformatted into a 1-D array, and compiled across runners into a single matrix.

PCA was performed to reduce the dimensionality of the data and examine how frontal plane pelvis geometry varied across runners (Fig. 1). PCs accounting for 90% of the variance in the data were retained for clustering. Hierarchical clustering (Euclidean distance; Ward algorithm) was used to divide runners into groups with similar pelvis geometry based on PC coefficients. Subsequent BSI incidence and pelvis/proximal femur geometry were compared across these clusters. Based on initial observable trends, geometry was assessed using a dimensionless shape factor: (pelvis height + ischial width)/(iliac width + trochanteric width).

Results and Discussion

Clustering identified four distinct groups of runners (Fig. 1). The first split between groups of runners was related to sex, with Clusters 1-2 being 100% female, and Clusters 3-4 being 91% male (Table 1). Further splits appeared to relate to BSI incidence in male-dominated clusters, but not in female-dominated clusters. Greater shape factor (relatively narrower greater trochanter spacing, narrower iliac crests, wider ischia, and greater pelvis height) was associated with lower BSI incidence across male-dominated clusters, but female-dominated clusters exhibited less distinction in shape factor and BSI incidence (Table 1).

These results indicate that pelvis structure may relate to risk of running-related BSI throughout the lower body. Future work will examine potential causal links between pelvis geometry and BSI risk. However, this relationship may be overshadowed by other factors in females, similar to previous findings linking anthropometry to BSI risk [3]. Thus, any attempt at predicting risk will also need to account for other factors such as running mechanics, training load, and energy availability.

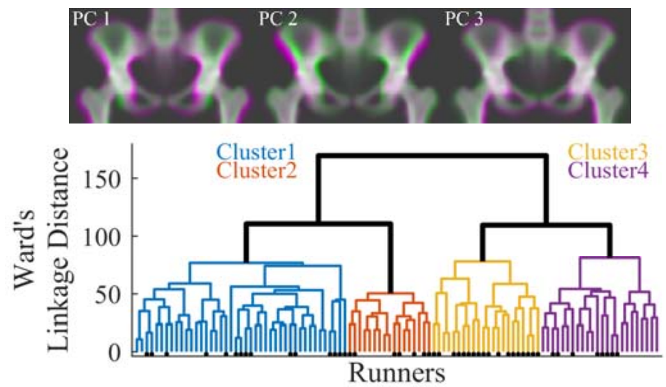

Figure 1: Upper) Pelvis ROI; principal components 1-3; green/magenta indicate high/low PC values. Lower) Cluster tree based on pelvis and proximal femur geometry. Endpoints along x-axis represent individual runners (with mirrored repeats); black dots at endpoints indicate BSI.

Table 1: Cluster splits, BSI incidence, and shape factor describing pelvis and proximal femur geometry: (pelvis height + ischial width) /(iliac width + trochanteric width) (normalized to range; mean ± SD).

Cluster	Females	Males	BSI Incidence	Shape Factor
1	43	0	15/43 (35%)	0.56 ± 0.21
2	17	0	7/17 (41%)	0.77 ± 0.15
3	4	18	18/22 (81%)	0.21 ± 0.10
4	0	22	8/24 (33%)	0.52 ± 0.21

Significance

This work presents a methodology that can be used to distill complex imaging data down to simple metrics describing variability in a population. This process is necessary both for linking clinically measureable factors to complex trends, and for selecting a subset of factors most likely to be usable in predictive models for injury risk and related screening tools. The results of this particular study have pointed to a potential link between pelvis shape and BSI risk, which may be combined with other available information to create a predictive model.

Acknowledgments

This work was supported by a grant from the Virginia Horne Henry Fund for Women's Physical Education and Movement.

References

[1] Crossley et al. 1999. *MSSE* 31: 1088. [2] Beck et al., 2000. *Bone.* 27: 437-444. [3] Bennell et al., 2004. *MSSE* 36: 397-404.

THE EFFECT OF LATERAL TIBIAL POSTERIOR SLOPE ANGLE ON INTERNAL TIBIAL ROTATION AND ANTERIOR TIBIAL TRANSLATION DURING SIMULATED JUMP LANDINGS

So Young Baek[1], Mélanie L. Beaulieu[2], Edward M. Wojtys[2], James A. Ashton-Miller[1]
[1]Department of Mechanical Engineering, [2]Department of Orthopaedic Surgery, University of Michigan, Ann Arbor, MI USA
Email: soy@umich.edu

Introduction

Approximately 200,000 anterior cruciate ligament (ACL) ruptures occur annually in the U.S.A. [1]. Depending on sex, the most important morphological risk factors for non-contact ACL injuries are a large alpha angle in the distal femur, a steeper tibial lateral tibial slope (LTS) angle and femoral notch anteromedial ridge thickness [2]. Since experimental studies of simulated jump landings in cadaver knees have already shown a high correlation between anterior tibial translation (ATT), internal tibial rotation (ITR) and peak ACL strain [3], we wondered how much an increased LTS angle affects ATT and ITR during hard landings. Our expectation was that a steeper LTS would increase both ATT and ITR because the large compression landing force on the knee should cause anterior sliding of the lateral tibia relative to the lateral femoral condyle. Because earlier studies of the effect of increasing compression on knee kinematics constrained axial tibial rotation [e.g., 4], the effect of LTS on ITR and ATT during landing are unknown. We tested the hypothesis that a steeper LTS increases ATT and ITR during a hard jump landing, both of which would increase peak ACL strain.

Methods

Seven pairs of knees from young male adult donors of similar age and weight [mean (SD) age: 25.71 (5.53) yrs, weight: 71.51(4.81) kg] were acquired. Knees were scanned in the sagittal plane with a 3T magnetic resonance scanner using a 3D proton-density sequence, which was used to measure the LTS using a previously published method [5] with OsiriX (version 3.7.1 lite, open source). Then, the knees were dissected to leave an intact knee capsule, and tendons of the quadriceps, medial and lateral hamstrings, and medial and lateral gastrocnemius muscles. The distal tibia and fibula and proximal femur were potted, mounted in polymethylmethacrylate, and mechanically tested using a modified Withrow-Oh testing apparatus [3] to simulate 100 repeated single-leg pivot landings with 1-3 times body weight [BW] measured via series 6-axis AMTI load cells at mid-tibia and femur. Simultaneous impulsive knee compression, knee flexion moment and internal tibial torque combined with realistic trans-knee muscle forces and tensile stiffnesses were applied.

To examine the relationship between LTS, ITR and ATT under increasing impact loading magnitudes, two sets of 25 impact trials of ~700 N (1 BW ±10%) were applied to a randomly selected knee of each pair after which another set of 25 trials was conducted with 1,400 N (2 BW ±10%). Similarly, on the other knee, two sets of 25 impact trials with ~1,800 N (2.5 BW ±10%) followed by two more sets of 25 trials with ~2,100N (3 BW ±10%) were applied.

Two-factor linear mixed effect models were used to determine the effects of LTS on ATT and ITR during increasing impact loading. The normalized impact force in BW and LTS were considered fixed effects, and subject (n=7) and side of the knees (right or left) random effects. Random intercepts were chosen from the linear mixed model with ATT, ITR, and LTS to simulate ATT and ITR being zero relative to their quiescent values in the absence of a landing impact force.

Results and Discussion

Figure 1 shows that as LTS increased, ATT and ITR also increased during increasingly large simulated landings. ATT was proportional to LTS (coefficient = 0.38, SE =0.089, $p<0.001$) under increasing impact force (coefficient = 0.46, SE =0.0095, $p<0.001$). Meanwhile, LTS also had an increasing effect on ITR (coefficient=0.94, SE = 0.20, $p<0.001$) relative to impact force (coefficient=0.43, SE=0.013, $p<0.001$). Lastly, the LTS coefficient shows that a steeper LTS increased ITR proportionally more than it did ATT.

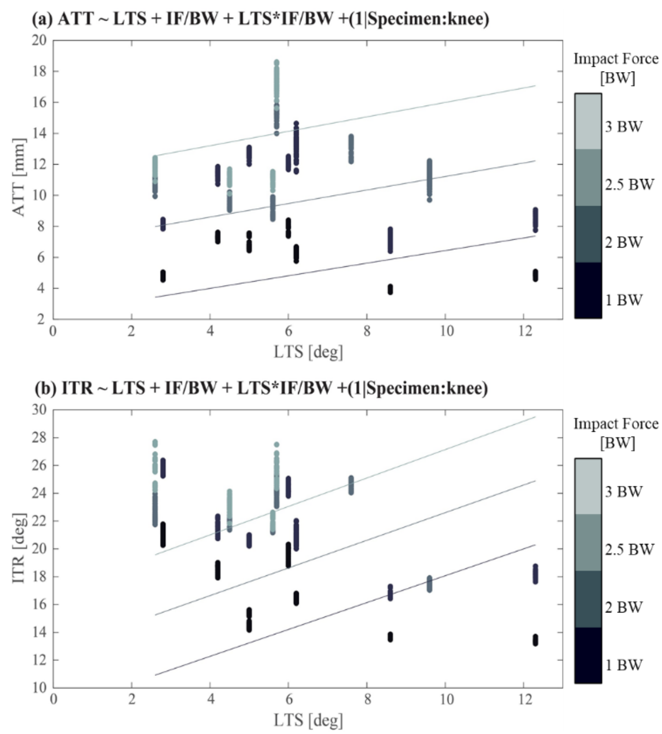

Figure 1: scatter plots of LTS versus (a) ATT and (b) ITR with each impact force. The lines on the plots indicate the linear mixed model if normalized impact force is constant at 1BW, 2BW and 3BW.

Significance

The results demonstrate that an increased LTS significantly increased ITR and ATT during landings. So, it is reasonable that an increased LTS increases peak ACL strain during hard landings (given [3]), thereby increasing the possibility for material fatigue failure of the ACL under too many such landings [given 6, 7].

References

[1] Musahl and Karlsson *N. Engl. J. Med*. 380 (2019)
[2] Barnum et al. *Am J Sports Med.* 49, 2021
[3] Oh et al. *Am J Sports Med.* 40 (2012)
[4] Meyer et al. *J. Biomech.* 41, 2008
[5] Hudek et al. *Clin Orthop Relat Res.* 8 (2009)
[6] Lipps et al. *Am J Sports Med.* 41 (2013)
[7] Chen et al. *Am J Sports Med.* 47 (2019)

Acknowledgements

NIAMS grant R01 AR 054821

Session 2

Monday August 22, 2022

3:30pm – 5:00pm

O2.1 – Ergonomics & Occupational Biomechanics 1

O2.2 – Insights on Slips, Trips, Falls

O2.3 – Knee Osteoarthritis

O3.4 – Thematic Poster Session 1 – Assistive Technologies

THE EFFECT OF CHAIR RECLINE ON NECK MUSCLE FUNCTION DURING SEATED COMPUTER WORK

Whitney L. Wolff[1], Constantin M. Heinemann[1], James A. Ashton-Miller[2], and David B. Lipps[1]
[1]School of Kinesiology, [2] Department of Mechanical Engineering, University of Michigan, Ann Arbor, MI USA
Email: wolffw@umich.edu

Introduction

Neck pain occurs in approximately half of all adults at some point in their life [1] and is commonly associated with seated computer work [2]. The U.S. Occupational and Safety Administration eTools website (https://www.osha.gov/etools/computer-workstations/positions) recommends an upright neck and torso posture during seated computer work. Maintaining such a posture requires back, shoulder, and neck muscle activity because the primary contributors to torque about the neck are the gravitational flexion moment due to the head and the resultant net muscle extension moment required to equilibrate it. The greater the head and neck flexion posture, the greater the gravitational moment about the 7th cervical vertebra (C-7) [3] and the greater will be the upper trapezius (UT) cervical extensor spinae activation [4]. Andersson, et al. showed that the more one reclines the torso and seat back, the more back extensor muscle activity and disc pressures are reduced [5]. We explored if working on a computer in a reclined position might elicit a postural set that also reduces UT muscle activity and thereby benefit those with idiopathic chronic neck pain (CNP). Therefore, a goal of this study was to determine how increasing chair back recline angle affects the activation, and therefore, stiffness, of the UT and sternocleidomastoid (SCM) during computer work in people with CNP. We hypothesized that a chair recline angle of 25° and 45° with neutral or self-selected head/neck postures will significantly decrease the UT activation and stiffness when compared to the conventional upright (0°) chair back recline angle and flexed head/neck posture.

Methods

The Neck Disability Index (NDI) was used to identify participants for this study. Increasing NDI scores indicate greater impairment due to CNP. Seven adults with mild-to-moderate CNP (3M, 4F, NDI 7-19 out of 50) participated in this study (mean (SD): age: 48 (19.8) years, height: 1.7 (0.1) m, weight: 68.7 (9.4) kg). Surface electromyography (EMG) (Trigno, Delsys) and shear wave elastography (SWE) images (Supersonic Aixplorer) were obtained from the SCM 2 cm distal to the halfway point on the belly of the muscle, as well as 3 subdivisions of the UT: 2 cm distal to the halfway point between the acromion process and C-7 (UT1), halfway between UT1 and the scapular spine (UT2), and 2 cm lateral to the 4th cervical vertebra (UT3) [6]. Maximal voluntary contractions (MVC) in neck flexion/extension, right/left lateral bending, and shoulder elevation were completed at the beginning of the experiment.

The participants were seated at a standardized computer work station in chair while seatback recline and head/neck posture were altered: nine randomly presented work postures that combined three chair back recline angles of 0° (e.g., no recline), 25°, or 45° with self-selected, neutral, or 10° flexion head/neck postures. The participants sat statically in each posture for ~4 minutes while SWE images were taken of the SCM and UT with simultaneous EMG recordings. Mean shear wave velocity (SWV, m/s) and EMG (%MVC) of the SCM, UT1, UT2, and UT3 were compared using separate ANOVAs for each muscle and data type where muscle side (right, left), recline angle (0°, 25°, 45°), and head/neck posture (self-selected, neutral, flexed) were fixed factors. Significance was set at α=0.05.

Results and Discussion

There was a significant main effect of head/neck posture on UT3 stiffness (p=0.006), with the neutral head/neck posture eliciting greater stiffness than the flexed head/neck posture (p=0.01) **(Figure 1)**. There were no other significant main effects of recline angle or head/neck posture on muscle stiffness (all p>0.091), however, the effect of head/neck posture on SCM stiffness was trending towards significance (p=0.091) with neutral posture eliciting a greater stiffness than self-selected. There were no main effects of recline angle or head/neck posture on any muscle EMG values (all p>0.123).

These results suggest that head/neck posture has more influence on UT3 muscle stiffness than chair recline angle alone. Although a neutral head/neck position reduces the gravitational moment of the head and neck about C-7, this alone may not be ideal ergonomically. The role of other neck muscles should also be considered.

Limitations included the small sample size and lack of healthy controls to determine if the observed changes are strictly due to the effect of CNP on neck muscle recruitment. We will therefore be expanding sample sizes to include 15 adults with CNP and 15 age-, height- and weight-matched healthy controls.

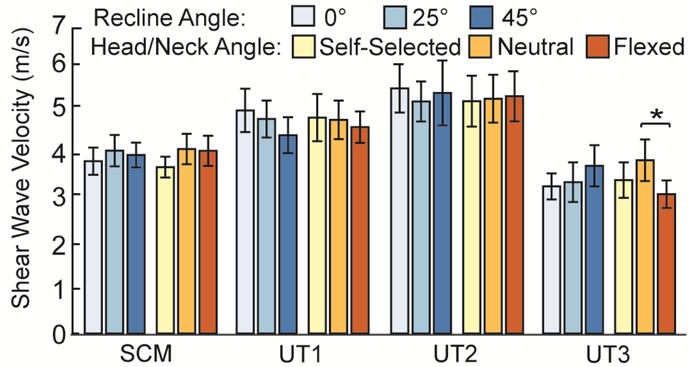

Figure 1: Mean SWV for the SCM, UT1, UT2, and UT3 during seat back recline angles of 0°, 25°, or 45°, with self-selected, neutral, or flexed head/neck postures. Error bars denote standard deviation (SD), and the asterisk (*) denotes p<0.05.

Significance

Our study supports the need to optimize the ergonomics of seated computer work, specifically for people with CNP. The standard instruction to sit with a neutral head/neck posture may not be beneficial or effective in decreasing the load placed on the neck extensors in individuals with CNP, because we observed increased stiffness of the UT3 subdivision in these patients.

References

[1] Côté, P., et al. *J Manip Physiol Ther.* 32 (2009).
[2] Côté, P., et al., *Spine*, 33 (2008)
[3] Vasavada, A., et al. *Ergonomics.* 58 (2015).
[4] Schuldt, K., et al. *Ergonomics.* 29 (1986).
[5] Andersson, et al. *Ortho Clin North America.* 6 (1975).
[6] Jensen, C., & Westgaard, R. *J Elec Kin.* 5(1995)

THE EFFECT OF TRAINING & WORKSTATION QUALITY ON DISCOMFORT DURING THE COVID-19 PANDEMIC

McAllister, Megan J.[1], Costigan, Patrick A.[1], Davies, Joshua P.[1], Diesbourg, Tara L.[2]*
1 School of Kinesiology and Health Studies, Queen's University, Kingston, Ontario, Canada
2 Public and Environmental Wellness, Oakland University, Rochester, Michigan, USA
*Email: tdiesbourg@oakland.edu

Introduction

Technological advancements have made telework a viable option for employees and employers alike[1]. Early in 2020, this option was put to the ultimate test in order to prioritize employee health and protection from the novel coronavirus (COVID-19).

Prior to the pandemic, researchers reported that voluntary telework, employer support, and proper workstation setups outside of the workplace are the keys to a successful telework experience[1,2,3]. The most important of these being that telework was voluntary[2,3]. When COVID-19 struck, employees were required to work from home if possible. There was no voluntary opting-in and no time to prepare a space in the home to accommodate full-time teleworking.

This study evaluated the transition to telework on university faculty and staff. We investigated the effectiveness of ergonomics training and workstation setup at mitigating work-related discomfort in the at-home work environment. We also evaluated the feasibility of using a survey to assess ergonomic risk factors in a home-based workstation based solely on self-reported availability of office equipment without any accompanying assessment. We hypothesized that workers who had received ergonomic assessments and training on-campus would have improved home-office workstations and would experience less discomfort as a result.

Methods

We sent a survey to all Queen's University employees who were forced to transition to telework due to the COVID-19 pandemic.

***Workstation Score**:* We provided a list of equipment and workstation configurations instructing respondents to "Select all that apply" and used this information to create a score representative of workstation quality. A workstation consisting of an office chair, a monitor, a keyboard, and a mouse received a categorical score of 0 ("baseline"). A workstation consisting of less equipment (i.e., working directly on a laptop with no external keyboard) received a categorical score of -1. Conversely, a workstation consisting of more equipment (i.e., a height-adjustable desk or an additional monitor) received a categorical score of +1.

Discomfort: We used a pain map to assess current discomfort and pre-pandemic discomfort from 21 body regions using Visual Analog Scales. Responses were subdivided into groups according to whether their discomfort was new (did not exist before beginning to work from home), or worsening (pain has worsened since beginning to work from home). We used a clinically relevant threshold of +/-15 to indicate whether pain had increased or decreased.

Training: Anyone who indicated that they had received an individualized ergonomics assessment from an experienced professional in the past was in the "In-person" group, while those who completed self-directed online searches were classified into the "Online" group. Finally, those having no training were placed into the "No training" group.

Statistical Analysis: To test the association between workstation score, ergonomic training, and new and worsening pain, we conducted a total of six loglinear analyses (new pain for arm, neck, and back, and worsening pain for arm, neck, and back). We also used correlations and chi-square to assess the relationships between individual variables.

Results and Discussion

In total, 131 participants completed the survey and were included in the analysis. We found that working conditions were worse when employees were working from home (Fig. 1), with 65% of respondents reporting that they spend more time at their computer than before the pandemic and 53% reporting that they change positions less.

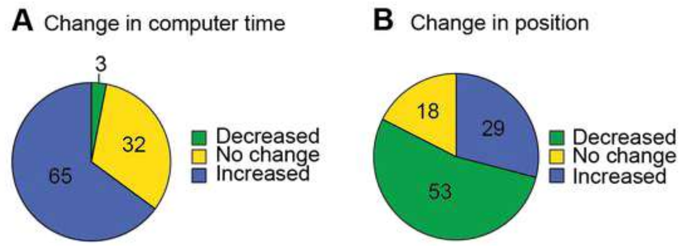

Fig. 1: Change in work habits when working from home. A: Change in time working at the computer. B: Change in number of position changes throughout the workday.

Furthermore, 51% of respondents reported worsening pain in one or more body regions and 24% of respondents reported new pain in one or more regions. Only 7% of respondents reported an improvement in pain since working from home (Fig. 2).

While descriptive variables point towards trends that should be investigated further, none of the statistical analyses revealed meaningful differences between groups or scores.

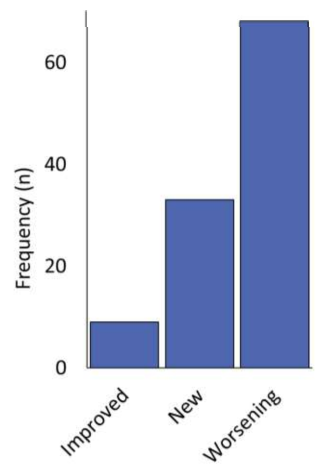

Fig. 2: Change in pain since working from home.

Significance

Working from home alters how much you move throughout the workday and places you at an increased risk for MSDs. To ensure that the equipment is used properly and suits the worker, telework employees should be supported by a program that provides adjustable office equipment, ergonomics training, and virtual assessments. Without all three elements, discomfort might persist or worsen when a worker transitions to teleworking.

Acknowledgments

This work was supported by a Vanier Canada Graduate Scholarship (M.J.M.) and by funds provided by Oakland University's School of Health Sciences.

References

[1] Montreuil & Lippel, 2003. *Saf Sci.* 41: 339.
[2] Jaakson & Kallaste. 2010. *New Technol. Work Employ.* 25: 196
[3] Ng. 2010. *Facilities.* 28: 137.

NEUROMUSCULAR ACTIVITY AND PERCIEVED DISCOMFORT COMPARISON BETWEEN ACTIVE CHAIRS, A TRADITIONAL CHAIR AND STANDING

Michelle Léger[2]*, Cynthia Dion [1]*, Michelle Cardoso[1], Wayne Albert[2],
[1]Département de Kinésiologie, Université de Moncton, Moncton, NB, Canada
[2]Faculty of Kinesiology, University of New Brunswick, Fredericton, NB, Canada
Email: **michelle.leger@unb.ca**

Introduction

It is estimated that approximately 80% of the Canadian population will experience at least one chronic low back occurrence in their lifetime [1], with 33 to 62% being seated workers [2]. To counter the negative effects of prolonged sitting, active chairs have been created to reduce sedentary time and perceived discomfort while seated. An active chair is defined as when the sitter is providing the action to move the chair, using alternating muscle groups, while the mechanism of the chair accommodates that action.

Methods

Twenty-four healthy participants were recruited for this study and asked to visit the laboratory on two separate occasions. The study compared four different workstations: 1- an active chair with a split seat pan design (AC1); 2- an active chair with a multiaxial design (AC2); 3- a traditional office chair (Control) and; 4- a standing workstation (Desk). The order of the four workstations were randomized, and the participants completed two tasks at each workstation in 15-minute intervals for a total of 60 minutes. During each 15-minute interval, participants began with a 10-minute typing task and then proceeded to a 5-minute web browsing task. The active protocol was to alternate between a pedaling/side-to-side motion and sliding forward/front-to-back motion to the sound of a metronome operating at 40 bpm during the web browsing task.

Electromyography (EMG) was used to measure neuromuscular activity of eight unilateral muscles (right): external oblique (EO), splenius capitis (SC), thoracic erector spinae (T9), lumbar erector spinae (L3), rectus femoris (RF), vastus lateralis (VL), vastus medialis (VM) and gastrocnemius (G). The raw signal was rectified (RMS converted) and Butterworth band pass filtered from 20-500 Hz to remove unwanted frequencies. Peak activity was found for each muscle during the MVC trials and used to normalize all subsequent EMG data. During each 15-minute collection period, the EMG data was compiled into 1-minute intervals to determine the percentage change from MVC during the computer tasks.

A Rate of Perceived Discomfort (RPD) questionnaire was used to monitor the participants' perceived discomfort while computing. RPD questionnaire recorded discomfort on a 100-point scale for thirteen different body parts bilaterally: shoulders, upper back, lower back, buttocks, upper and lower legs, and neck. To determine discomfort change, all values were compared to RPD baseline. The statistical analysis consisted of a repeated measure mixed analysis of variance (ANOVA) with a Tukey correction.

Results and Discussion

For EMG results, it was found that when the participants were seated in the AC2, they required significantly more SC and T9 neuromuscular activity when performing both side-to-side and front-to-back motions compared to the control chair. When standing, participants contracted their external obliques significantly more compared to sitting. Standing also required the participants to contract their external obliques up to 12% of their maximal voluntary contraction.

Participants associated standing with a significantly higher-level of lower leg discomfort compared to all three chairs. However, after 30 minutes of sitting the participants rated the buttocks area with a significantly higher level of discomfort on the AC1 compared to the other workstations. The AC1 chair scored low in the low back discomfort but high in buttocks discomfort; this would suggest that the active component of the chair may not be the cause of the buttocks discomfort but rather contributed to a lack of seat pan support around the buttocks.

All biomechanical changes found in this current study contribute to a reduction in perceived discomfort caused by spine unloading tension over time. If participants worked at each of the workstations for longer periods of time, it is hypothesized that the active workstations would outperform the control chair in reported perceived discomfort.

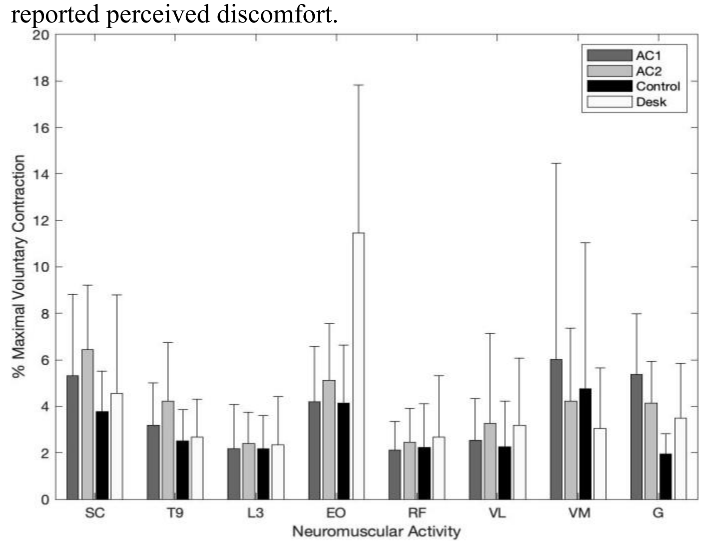

Figure 1: EMG findings for each of the four workstations (AC1, AC2, Control Chair, and The Desk) for eight unilateral muscles during the last minute of the 60min standing task. The increase in EMG activity is a sign that more neuromuscular activity was being required/engaged.

Significance

The study provided insight into the optimal biomechanical benefits of sitting in an active chair. During the typing task (no movement was required in the active chairs) little significance was found between the active chairs versus the control chair and standing workstation, which indicates that individuals did not move their lower limbs when given the choice to actively move or not. Engaging the active chair components would be best utilized when doing a low cognitive task like web browsing or talking on the phone.

References

[1] Rubin, D. I. (2007). *Neurologic Clinics*, *25*(2), 353–371
[2] Spyropoulos, P., Papathanasiou, G., Georgoudis, G., Chronopoulos, E., Koutis, H., & Koumoutsou, F. (2007). *Pain Physician*, *10*(5), 651–659.

TASK DEPENDENCE OF CENTRE OF PRESSURE VARIABILITY

Puneet Singh[1]*, Michelle Léger[2]*, Cynthia Dion[1]*, Wayne Albert[2], Michelle Cardoso[1]
[1]Département de Kinésiologie, Université de Moncton, Moncton, NB, Canada
[2]Faculty of Kinesiology, University of New Brunswick, Fredericton, NB, Canada
Email: puneet.singh@moncton.ca

Introduction

The center of pressure (COP) variability is frequently used as an index for postural stability in standing. An increase in COP variability can lead to increase in postural instability [1], which over time could lead to the development of fatigue, pain/discomfort or increase the risk for falls. It has been shown that aging [2], environmental factors [3], and sensorimotor deficits, [4] can also affect COP variability. We hypothesized that there is more than one component (time, task, and discomfort) which influences the COP variability. However, it is not well understood how different components influence the COP variability. The purpose of this study is to investigate the relationship between COP variability and component dependence.

Methods

Twenty-four healthy participants were recruited for this study and were asked to stand at a standing workstation for 60-minutes. The participants completed two tasks in 15-minute intervals for a total of 60 minutes. During each 15-minute interval, participants began with a 10-minute typing task and then proceeded to a 5-minute web browsing task.

Equipment:

<u>Standing pressure pad data</u> was collected using a Boditrak pressure mapping system. A sampling frequency of 5Hz was used for the standing trial sessions.

<u>Kinematic data</u> was collected using a Qualisys Miqus motion-capture system to quantify head, shoulders, hips, pelvis, knees, trunk-pelvis, and trunk thigh joint angle (flexion/extension, lateral bend, and rotation). A total of 71 retro-reflective markers were taped on the participant's skin. Each bony landmark had a retro-reflective marker, totalling 40 markers, and eight reference clusters (31 markers), were placed on the upper arms, left hip, thighs, shank, and trunk.

<u>Perceived discomfort (RPD) questionnaire</u> was used to monitor the participants perceived discomfort while computing. RPD questionnaire recorded discomfort on a 100-point scale for thirteen different body parts bilaterally: shoulders, upper back, lower back, buttocks, upper and lower legs, and neck. To determine discomfort change, all values were compared to RPD baseline.

<u>Statistical analysis</u> consisted of pairwise comparison and Pearson's correlation. Comparison between the group was performed using two-tailed t-test if data was normally distributed otherwise Wilcoxon signed-rank test was used. In the correlational analyses we used Pearson's correlation technique.

Results and Discussion

Time vs. COP variability: To test whether COP variability had an effect over time, we compared the COP variability during both tasks during the first 15-minutes and the last 15-minutes of the standing trial. No significance was found **(typing task: *p* = 0.33, *z* = 0.97; web browsing *p* = 0.18, *z* = 1.34)**.

Task dependence vs. COP variability: To test whether COP variability was task-dependent, we compared the COP variability for both tasks performed. The mean COP variability was **0.99 ± 0.52** for the typing task, and **2.05 ± 1.52** for the web-browsing task. We observed that the mean COP variability during the web-browsing task was significantly higher than the mean COP variability during the typing task **(Figure 1A; *p* = 6.9e-5, t (23) = 4.83)**. This was consistent across all four 15-minute increments (for a total of 60mins) and the last time increment is shown in **Figure 1B (*p* = 0.006, z = 2.74).** Our findings suggest that COP variability is affected by the computer task performed. The differences between the results of typing task and web-browsing task may be a consequence of higher postural control strategy.

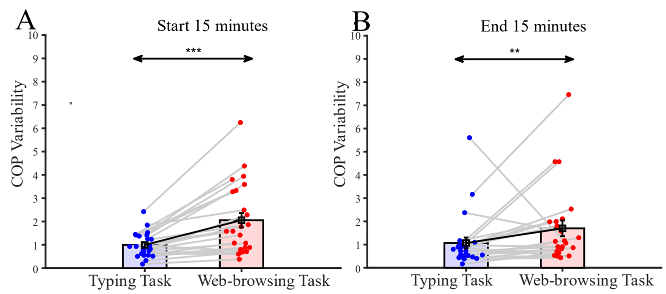

Figure 1: Centre of pressure (COP) variability in the typing task and web-browsing task (n = 24). **(A)** COP variability differences between typing tasks (blue) and web-browsing task (red) during the first 15 minutes. **(B)** COP variability differences between tasks during the last 15 minutes. Each dot represents a subject, and the grey line connects same subject.

Discomfort score vs. COP variability: Changes in COP variability maybe caused by perceived discomfort. We analyzed the correlation between CoP variability to the change in the reported discomfort scores (reported scores at the start of trial minus reported scores at the end of trial). We observed no correlation between the discomfort scores and the COP variability **(r = 0.17, *p* = 0.42)**.

Joint angles vs. COP variability: We are currently working to see if the COP variability can be influenced by the variability in joint angles. To test this, we simultaneously measured the COP variability and joint angles while working at a standing workstation. Results are currently pending.

Significance

Our results showed that the COP variability was more dependent on the task performed, compared to time (60mins of standing) or reported perceived discomfort scores during the 1hour standing task. Examining the joint angles and COP variability may provide better insight regarding changes in postural control, especially when observing task dependency.

References

[1] Yamagata, Momoko, et al., Clinical interventions in aging 12 (2017): 499.
[2] Amiridis, Ioannis G., et al., Neuroscience letters 350.3 (2003): 137-140.
[3] Redfern, Mark S, et al., Human factors 39.3 (1997): 445-455.
[4] Hughes, Michael A., et al., Archives of physical medicine and rehabilitation 77.6 (1996): 567-57

LUMBAR SPINE FIDGETS, LOW BACK PAIN, AND PRODUCTIVITY IN PROLONGED SITTING AND STANDING

Liana M. Tennant*, Jackie D. Zehr, Jessa Buchman-Pearle, Jack P. Callaghan
University of Waterloo, Department of Kinesiology and Health Sciences
email: *liana.tennant@uwaterloo.ca

Introduction

Fidgets of the lumbar spine early in standing and often in sitting may reduce transient low back pain (LBP) related to prolonged sedentary postures [1-4]. Evidence is mixed whether fidgets are a symptom of LBP; fewer fidgets early in standing may predispose individuals to LBP [3], whereas greater overall fidget frequency may minimize sitting-induced LBP [1]. The literature mostly supports equal productivity in sitting and standing, but many studies do not delineate between participants experiencing LBP, nor do they evaluate controlled complex deskwork tasks [5]. Our aim was to explore how lumbar fidget frequency and LBP interacts with data entry performance in prolonged sitting and standing. We hypothesized that standing-induced LBP would worsen data entry performance over time, and that standing-induced LBP developers would show unique fidget frequency patterns consistent across both sitting and standing.

Methods

Sixteen back-healthy adults (8 males, age: 25 ± 3 y, height 1.69 ± 0.09 m, mass 67.1 ± 11.9 kg) completed two hours of data entry, typing, and an abridged GRE on a PC. Each task was done twice, non-sequentially, in 15-minute time blocks in a randomized order while standing and sitting on different days. Data entry results are reported. Lumbar posture was measured with accelerometers at S1 and L1 at 250 Hz. LBP was recorded on a 100 mm visual analog scale after each block. Participants were classified as pain-developers if LBP was ≥ 10 mm from baseline at any time [3]. Pain was measured bilaterally; peak pain is reported.

Accelerometer data were filtered at 1 Hz using an effective 4th order low-pass filter. Sagittal lumbar angle was calculated as the difference in accelerometer inclination. Lumbar fidgets were identified using established methods [2, 4]. Each frame of angle data was compared to the moving average. A fidget was identified if $|\bar{x}_{w_i}-x_i| > 3SD_w$, where $\bar{x}_w$ and SD_w are the average and standard deviation of a moving window (size w = 50 s), centred on point x_i, with a maximum fidget duration of 4 s. Fidget frequency was normalized to time. Mixed general linear models were used to investigate the effect of posture (sit v stand), time (block 1 v block 2), and pain classification (standing pain developer [PD] v non-pain developer [ND]) on productivity and fidgets ($\alpha < 0.05$). Non-parametric analyses were used to investigate LBP because the data were positively skewed [6].

Results and Discussion

Six participants were classified as PDs. In partial support of our hypothesis, there was an interaction effect such that productivity was unchanged in NDs across postures, whereas PDs were more productive in sitting compared to standing ($p = 0.001$, n = 14) (Figure 1A). Contrary to our hypothesis, there was no interaction between pain classification, posture, and productivity over time ($p = 0.31$). Productivity improved by 0.50 entries/min across all participants between blocks ($p = 0.018$), suggesting learning occurred. There were no other significant effects ($p > 0.20$).

A significant 3-way interaction between pain classification, posture, and time was observed ($p=0.009$) (Figure 1B); LBP did not change over time in NDs, whereas standing PDs had greater LBP in standing, which increased over time compared to sitting ($p = 0.024$).

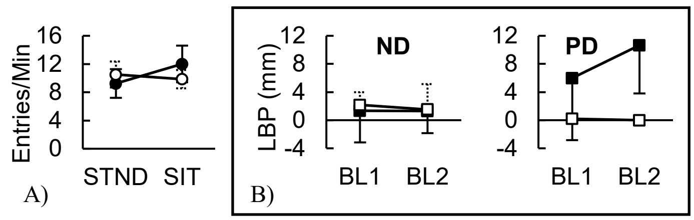

Figure 1: A) The interaction between posture and pain status (PDs (●) and NDs (○)) on productivity. B) The 3-way interaction between time, posture (sit (☐) and stand (■)) and pain developer status (PD vs ND).

Contrary to our hypothesis, there were no main or interaction effects of pain classification, posture, or time on fidget frequency between LBP classification groups ($p > 0.35$, n = 15) (Table 1).

Table 1: Lumbar fidgets (fidgets/min) in sitting and standing.

Posture	Block	Pain	N	Mean	SD	Min	Max
Sit	1	ND	10	0.709	0.283	0.265	1.127
		PD	5	0.663	0.599	0.066	1.591
	2	ND	10	0.636	0.382	0.066	1.326
		PD	15	0.690	0.237	0.398	0.994
Stand	1	ND	10	0.617	0.354	0.133	1.392
		PD	5	0.703	0.383	0.265	1.193
	2	ND	10	0.650	0.360	0.132	1.260
		PD	5	0.570	0.405	0.199	1.260

Our findings contrast with previous reports that there is little difference in productivity in sitting and standing; however, these studies mostly examine a typing-only task [5]. Since only PDs demonstrated improved productivity when sitting, pain distraction in our complex task (requiring attention, mousing, and typing) may have contributed to the reduced performance observed in standing.

Significance

Our results imply that productivity may be affected by posture among those who develop standing-induced LBP during complex computer tasks, while standing. This finding is important because it is usually presumed that productivity is unaffected by posture. This result could have implications for sit-stand workstation recommendations. More nuanced examination of the relationship between fidgets and LBP is likely required to parse out relationships in fidget behaviour between sitting and standing.

Acknowledgments

Funding was provided by NSERC (RGPIN-2016-04136). JC is supported by a Canada Research Chair (950-228146).

References

[1] Greene et al., 2011. *Ergonomics*. 62:11 p. 1415-1425
[2] Dunk & Callaghan, 2010. *Work*. 35:1 p.3-14
[3] Gallagher & Callaghan, 2015. *Hum Mov Sci*. 44 p.111-121
[4] Gallagher et al., 2011. *Gait Posture*. 34:4 p.490-495
[5] Karakolis et al., 2016. *Ergonomics*. 59:10 p.1275-1287
[6] Noguchi et al., 2012. *J Stat Softw*. 50:12 p.1-23

EXPLORING THE BIOMECHANICAL BASIS FOR A STRENGTH ASYMMETRY BETWEEN DOMINANT AND NON-DOMINANT ARMS

Fahima Wakeely, Michael Watterworth, Ryan C. A. Foley, and Nicholas J. La Delfa*,
Ontario Tech University, Oshawa, ON
email: *nicholas.ladelfa@ontariotechu.ca

Introduction

When designing manual work tasks, considering task demands in the context of human strength capability is vital to assessing workplace musculoskeletal injury risk. This is particularly true for the upper extremities, which are often relied upon to produce manual forces in occupational manufacturing tasks [1]. Other than grip strength, the effect of hand-dominance on any type of upper extremity strength is relatively underexplored, despite workers commonly utilizing both dominant (D) and non-dominant (ND) limbs in the workplace. Currently, right-side capability is assumed to be 10% stronger across all joints of the upper extremity; however, this generalized heuristic fails to account for handedness or sex effects, as well as task-relevant factors (e.g. force direction or hand location). It is unknown how these factors coalesce and contribute to bi-lateral differences in strength at the end-effector of the arm (i.e. manual arm strength -MAS). As such, the primary purpose of this study was to examine MAS between the D and ND arms. A secondary purpose was to elucidate potential biomechanical sources for these strength asymmetries through analysis of bi-lateral shoulder moments and angles during maximal manual force production in several exertion directions throughout the reach envelope.

Methods

Twenty-four healthy participants (12 M and 12 F) between the ages of 18-30 were recruited. Equal counts of left-handed and right-handed individuals for both sexes. Handedness was determined via the Edinburgh Handedness Inventory which utilizes 10 items to assess hand preference for everyday tasks [2]. While seated with their torso restrained, participants grasped a vertically oriented handle affixed to a 6-DOF force transducer and produced maximum manual forces in the six primary exertion directions (superior, inferior, medial, lateral, anterior, and posterior) with both their D and ND arms, separately. The handle was situated at 80% of reach length in three different hand locations. MAS was taken to be the peak force obtained from each trial, and shoulder joint moments (flex/ext, add/abd, int/ext rotation and angles were computed for when the peak force occurred. Statistical effects were evaluated using 4-way mixed-design ANOVAs for each of the six exertion directions. Hand dominance (2 levels: D vs ND) and hand location (3 levels: Ovrd, Shld, Umb) served as the within-subjects variables, while handedness (2 levels: right-handed, left-handed) and sex (2 levels: male, female) served as between factors. A 4-way mixed ANOVA evaluated effects of sex, handedness, exertion direction, and hand location on shoulder moment (n=3) differences. Shoulder joint angles (n=3) were explored descriptively.

Results and Discussion

For MAS, there was a 3-way interaction between dominance, hand location, and handedness for the pull direction ($F_{(2,2)}=6.58$, $p=0.003$). Both right-handed individuals at the shoulder height hand location, and left-handed individuals at the umbilicus height hand location, had a strength discrepancy of 23% in favor of the D hand for the pull exertion. Right-handed individuals showed greater shoulder moments on their D hand by 4 Nm, whereas, the left-handed individuals' shoulder joint moments were 0.5 Nm larger on their ND hand. Right-handed individuals' D arm had an internal humeral rotation of 12.4° greater than their ND at the shoulder hand location. Male MAS was 20% stronger in their D arm in comparison to their ND arm. Comparatively, females were much more balanced in strength between arms. Regarding shoulder moments, male's dominant shoulder moment was 3 Nm stronger than their ND. Whereas, for women the difference was only 1 Nm. Surprisingly, the ND arm in left-handed males showed stronger MAS, but their D hand had a larger shoulder moment.

The results of the study confirmed the hypothesis that the D limb values were larger than the non-dominant limb, and this effect was exaggerated for right-handed individuals. This evaluation provides critical context on the effect of hand dominance in MAS, as differences assumed to transfer from the grip strength literature may not be sufficient. Left-handed participants had significantly different joint moment profiles from right-handed participants, suggesting that differing control strategies between right- and left-handed individuals could explain discrepancies in force capability between the hands observed at the different hand locations.

Significance

This study works towards a better understanding of how handedness can impact ergonomics task assessments and risk of injury. Current assessment approaches rely on dated heuristics (i.e. 10% rule), which may not be robust for manual force exertions in different directions and across the reach envelope. Furthermore, evaluation of joint kinetics and kinematics are a relatively underexplored area of strength assessment in ergonomics, but can highlight specific mechanisms for strength asymmetry, and highlight potential vulnerabilities for different populations (e.g. left-handers working in a right-hand centric world). The research can help inform how ergonomists and engineers set limits for upper extremity work involving both the dominant and non-dominant hand, and future work will explore how these effects can be accounted for in ergonomics tool that estimate acceptable manual forces [3]

Acknowledgments

This work was funded by NSERC (Discovery Grant) and CRE-MSD (Seed Grant).

References

[1] National Research Council. (2001). Musculoskeletal disorders and the workplace. National Academies Press.

[2] Oldfield, R. C. (1971). The Edinburgh inventory. *Neuropsychological*, 9(1), 97-113

[3] La Delfa, N. J., & Potvin, J. R. (2017). *J Applied Ergonomics,* 59, 410-421

QUANTIFYING THE EFFECTS OF PATIENT BMI AND SCAN LOCATION ON UPPER EXTREMITY POSTURE AND JOINT STRENGTH CAPABILITY IN SONOGRAPHERS USING DIGITAL HUMAN MODELING

Cameron J. Lang[1], Alan C. Cudlip[1], Michael WR. Holmes[1*]
[1]Faculty of Applied Health Sciences, Brock University, St. Catharines, ON, Canada.
email: mholmes2@brocku.ca*

Introduction

The prevalence of work-related musculoskeletal injuries within the medical sonographer population is among the highest of all healthcare professions. Between 65-91% of sonographers reported regularly working whilst in pain, with 91% claiming to have visited a physician for treatment due to work-related pain, including fibromyalgia, bursitis, carpal tunnel syndrome, rotator cuff tendonitis, and myofascial pain (1).

Typical scanning postures combine repetitive motions, awkward postures and sustained loading, all factors known to contribute to upper extremity musculoskeletal disorders (2). To obtain high quality images, the sonographer must precisely maneuver a hand-held transducer over the desired body part for an average of 10-60 minutes per scan (3). Increases in patient body circumference may extend sonographer reach distance, change posture and require additional postural demands as static joint loading is increased during scans. The purpose of our study was to quantify the physical demands associated with sonographer scans using digital human modeling, and to evaluate how these demands vary based on differing patient anthropometrics. We hypothesized taller and heavier patients will increase demands on the sonographer, and exposures will differ by scan location.

Methods

This study used SantosHuman (v. 1.5.2018.408), a Digital Human Modeling Software (DHM), to quantify sonographer exposures in common scanning postures across patient avatars. On-site visits at a local hospital were used to develop an identical sonography environment. Eight scan locations were selected for analysis, consisting of bilateral locations for the breast, kidney, shoulder and leg. The sonographer avatar (50th percentile, normal weight female) was placed on the chair in a seated position while the patient was oriented on the bed; orientation was dependent on scanning location (Figure 1). Each scan was composed of 18 patients divided evenly by sex; within each sex a combination of three heights (5th/50th/95th percentile) and three body mass indices (BMI; healthy BMI of 21, overweight BMI of 28, obese BMI of 31), resulting in 144 scans. The Arm Force Field (AFF) (4) and Rapid Upper Limb Assessment (RULA) (5) were used to quantify sonographer exposure in each scenario. AFF scores document percentage of population with capable strength; RULA scores higher than three signifies that the task is unacceptable and injury risk is probable.

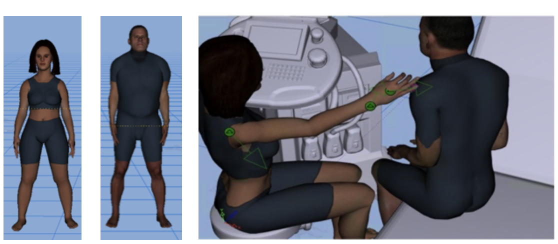

Figure 1: Avatar images from a 5th percentile height 'normal' weight female (left), a 95th percentile 'obese' male (middle); representative environment for a left shoulder scan using a 50th percentile normal weight male (right).

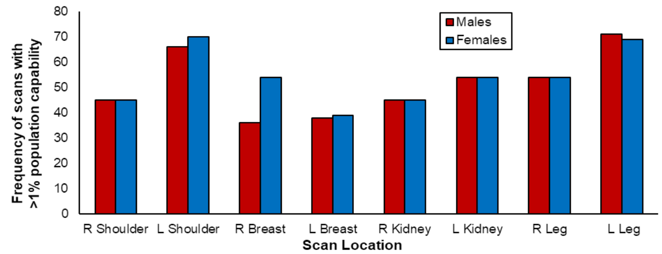

Figure 2: Differences in AFF population strength capabilities with >1% capability, by both males and females across scan locations.

Results and Discussion

The AFF tool demonstrated that most scans longer than 15 minutes in duration exceeded population strength. Scans completed on the left leg identified only an 18.5% sonographer strength capability when in 15-minute scans, and <1% capability for 30+ minute scans. More than 80% of left shoulder and leg conditions resulted in <1% population capability (Figure 2). Having an increased BMI also demonstrated a decrease in strength capability. In our case, a 15-minute scan showed capabilities similar to scans 30 minutes or greater (<1%).

RULA indicated a moderate to high risk. Across all scans, the average score recorded was 4.0 (± 0.9), indicating a need for ergonomic intervention. The highest recorded value was taken from the bilateral kidney and right shoulder at 5.9. This signifies a risk of injury and requires ergonomic intervention. These findings provide meaningful information to ergonomists and task designers for sonography tasks. A moderate to high risk associated with scans was observed across task scenarios but were primarily driven by scan location.

Significance

This work highlights sonographer exposures and clearly signals the need for additional examination into these tasks. This information is not only crucial for preventing further injury to sonographers but DHM can be used as a standard for further research on the safety of healthcare workers. DHM is an excellent tool for simulating risk exposure in a workplace. However, in our work, patient orientation needed to be manipulated in some scans due to the inability of the sonographer to reach specific areas.

Acknowledgments

This work was supported by CRE-MSD and the Canada Research Chairs program. Niagara Health for assistance in data collection.

References

[1] Muir et al., 2004. J Diag Med Son, 20(5).
[2] Randall et al., 2012. J ACVR and IVRA, 54(4), 459-456.
[3] Smith et al., 1997. J Am Soc Echo, 10(4), 357-362.
[4] La Delfa & Potvin., 2016. J of Biomech, 49, 602-605.
[5] McAtamney & Cortlett., 1993. Appl Ergon, 24(2), 91-99.

SLIP-AND-FALL RISK POSED BY SLOPED WALKING SURFACES

Corbin M. Rasmussen[1*], Abderrahman Ouattas[1], and Nathaniel H. Hunt[1]
[1]Department of Biomechanics, University of Nebraska at Omaha, Omaha, NE USA
email: *cmrasmussen@unomaha.edu

Introduction

Walking surfaces can be diverse, posing unique challenges to maintaining balance. Sloped surfaces, for example, elicit greater shear ground reaction forces compared to level ground [1,2]. Consequently, greater coefficients of friction are needed throughout stance phase to maintain traction, increasing the likelihood of a slip if not met [3,4]. However, it is unclear how the fall risk posed by sloped surface slips compares to level slips. Thus, we aimed to quantify the slip-and-fall risk of various slope directions and grades, and the phase-dependent vulnerability of slips throughout stance. We hypothesized that *fall rates* would 1) be highest on cross-slopes and 2) increase with slope grade. Further, we expected *slip vulnerability* (Equation 1) to be highest at 3) early stance on level and downhill slopes, 4) midstance on cross-slopes, and 5) late stance on uphill slopes.

Methods

Twenty-one young adults (mean ± SD 24.6 ± 3.4 yrs., 1.72 ± 0.09 m, 72.9 ± 12.8 kg, 9 females) participated in this study. All subjects wore a full-body marker set, standardized shoes, fall-arresting harness, and a Wearable Apparatus for Slip Perturbations (WASP) on both feet [5]. Subjects performed 27 walking trials at 1.3 m/s on a Computer Assisted Rehabilitation Environment (CAREN), all of which ended with a WASP-delivered slip at early, mid, or late stance phase of one leg. During each trial, the CAREN treadmill platform created level, uphill, downhill, or cross-slope walking surfaces at 5° or 10° grades. Slips during cross-slope conditions targeted either the uphill or downhill foot relative to slope direction.

Falls were determined via in-line load cell above the worn harness; if 30% or more of a subject's body weight is supported by the harness post-slip, that trial was coded as a fall [6]. We defined *fall rate* as the number of fall trials divided by the total trials within a direction or grade condition and *slip vulnerability* (SV) as the *fall rate* (FR) at one slip onset phase normalized to the total fall rate across all phases within a direction condition (Equation 1).

$$SV_{slope} = \frac{FR_{phase,\ slope}}{FR_{slope}} \tag{1}$$

Results and Discussion

Our first hypothesis was partially supported, with cross-slopes (9.6%) and uphill slopes (50.8%) leading to the highest fall rates on 5° and 10° grades, respectively (Fig. 1). As a whole, 5° slope fall rates were only marginally higher than the level fall rate (Down: 7.9%, Up: 6.3%, Level: 6.3%; Fig. 1) however all 10° slopes were markedly higher (Down: 44.4%, Cross: 44.0%, Level: 6.3%; Fig. 1). Increasing slope grade indeed led to higher fall rates, as 45.8% of all slips on 10° slopes caused falls. Interestingly, this increase was non-linear, illustrated by a small change at 5° (8.4%).

Overall, early stance slips were the most likely to cause a fall. Slip vulnerability was highest during early stance on level and downhill slopes (2.63 and 1.39, respectively), supporting our third hypothesis. However, slip vulnerability on uphill and cross-slopes was also highest during early stance (1.90 and 1.70, respectively), opposing our last two hypotheses. Mid-stance slips in all directions had markedly lower vulnerability than early stance (Down: 0.88, Up: 0.80, Cross: 0.36), indicating that they pose far lower fall risk. Falls resulting from late stance slips only occurred on cross-slopes and were unlikely compared to the overall cross-slope fall rate (0.29).

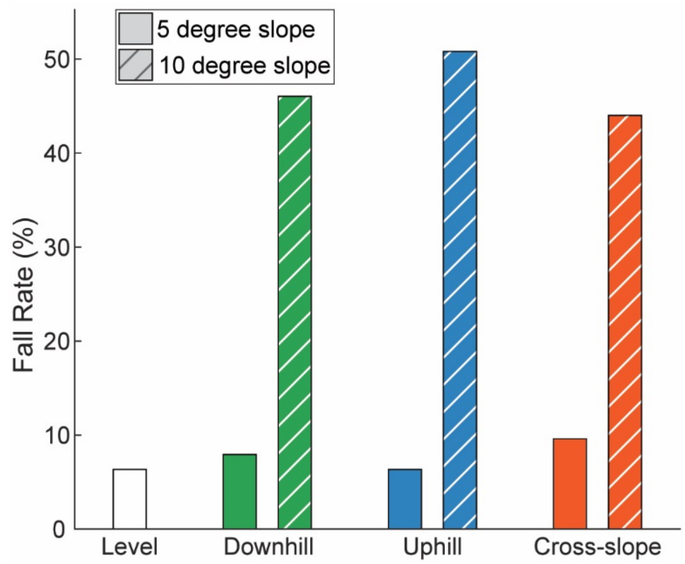

Figure 1: Fall rates across slope directions and grades.

Our results illustrate the threat to upright posture presented by sloped walking surfaces. Slope grade appears to exert a large influence on fall risk regardless, perhaps surprisingly, of slope direction. Slips occurring at or immediately after heel-strike are most dangerous on all slope directions, aligning with the peak required coefficient of friction during stance phase [3].

Significance

To our knowledge, this is the first direct examination of fall rates following slips on sloped surfaces. The consistently high slip vulnerability posed by early stance slips regardless of slope direction suggests they should be a primary target of fall prevention measures. Our results motivate further study into the balance recovery strategies used after slips on slopes, which may differ from those already described on level ground, to inform fall prevention training.

Acknowledgments

Study funded by NIH grants R15AG063106 and P20GM109090.

References

[1] McIntosh et al., 2006. *J Biomech.* 39: 2491-502.
[2] Dixon & Pearsall, 2010. *J Appl Biomech.* 26: 17-25.
[3] Redfern & DiPasquale, 1997. *Gait Posture.* 6: 119-25.
[4] Rasmussen & Hunt, 2021. *J Biomech.* 125: 110572.
[5] Rasmussen & Hunt, 2019. *J Neuroeng Rehabil.* 16: 118.
[6] Yang & Pai, 2011. *J Biomech.* 44: 2243-9.

PAIN PERCEPTION DURING LATERAL FALLS: INFLUENCE OF FALL SIMULATION PROTOCOLS, BODY COMPOSITION & IMPACT DYNAMICS

Sukirat K. Bhullar[1*], Steven P. Pretty[2] and Andrew C. Laing[3]
email: *skbhullar@uwaterloo.ca

Introduction

Pain and discomfort influence independence, mobility, and quality of life in older adults. While only 1-2% of falls suffered by older adults result in fractures, a much larger proportion results in minor injuries with residual pain and discomfort[1]. Individual literatures exist on the effects of noxious stimuli on pain perception, and impact dynamics during lateral falls; however, no studies have combined these respective fields. The goal of the current study was to investigate how faller characteristics (e.g., anthropometrics) and fall types influenced the perception of pain using the Visual Analog Scale (VAS). It was hypothesized that (1) the lateral fall's characteristics (type of fall simulation protocol) would influence the pain perceived during the fall, with individuals experiencing decreased pain during controlled pelvis release trials. Additionally, it was hypothesized that (2) the participant's anthropometric characteristics (BMI and trochanteric soft tissue thickness) would be negatively correlated with the pain perceived at the hip, (3) while impact dynamics (amount of force applied) would be positively correlated.

Methods

Thirty young adults completed fall simulation protocols including highly controlled pelvis, dynamic kneeling, and squat releases. Following each trial, participants reported pain levels on the VAS, while peak net force, peak localized force, and peak pressure were extracted. One-tailed bivariant Pearson correlations were performed to assess the strength and direction of relationships between hip pain, anthropometric, and impact dynamics. A two-way ANOVA assessed the influence of fall type and trochanteric soft tissue thickness on impact dynamics.

Results and Discussion

In contrast to hypothesis 1, individuals experienced the least and greatest amount of pain during squat and pelvis release falls, respectively (Figure 1). While individuals' anthropometrics were generally not correlated with hip pain, during squat release trials, there was a positive trend between trochanteric soft tissue thickness and pain magnitude (hypothesis 2). Impact dynamics were also not correlated with the pain experienced during the fall simulation protocols (hypothesis 3).

Generally, pain at the hip evaluated with the VAS did not relate to mechanics as expected. There are several potential explanations for this. The pelvis release fall was initiated after an electromagnet was released, while the participants self-initiated the kneeling and squat release falls giving them time to prepare and shift their bodies into less painful positions. These fall initiation differences may have led to a heightened expectation of pain during the pelvis release fall[2] resulting in individuals reporting more pain. Impact kinematics should be assessed to strengthen our understanding about the adjustments made by individuals to their positions during the fall simulations. Additionally, skin nociceptors have a lower pain threshold than muscle nociceptors[3] indicating that deeper soft tissues may not influence the pain perceived at the skin. Thus, the anthropometric characteristics were not correlated with the pain perceived at the hip. Lastly, pain was assessed using the VAS, which may have been unfamiliar and unclear to some of the participants. They were asked to complete multiple VAS scores for multiple body regions reducing their focus from the hip. Participants also could not reference their previously completed VAS after each fall simulation protocol was completed, providing an explanation for why baseline VAS scores were greater than those reported after the fall simulation protocols. Additional practice trials, prior to the baseline fall simulations, could assist participants in becoming more familiar with the VAS.

Overall, the study reveals the effects of different lateral falls, anthropometric characteristics and impact dynamics on pain perception. This provides important implications from clinical perspectives.

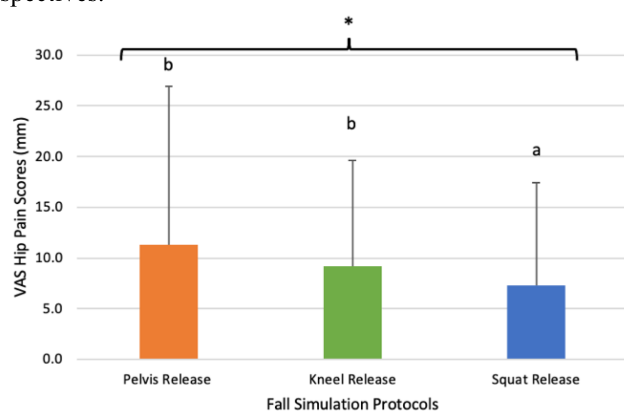

Figure 1: Pain perceived during squat release (a) was significantly less than the other fall simulation protocols (b). There was no significant association between the pain perceived during pelvis and kneel release falls (* indicates significant ANOVA main effects; letters refer to significant differences between groups based on Tukey's post hoc tests at $\alpha = 0.05$).

Significance

Pain is often a precursor to injury, and is a factor that influences mobility, performance, and behaviour. A sensitive measure of pain severity could help provide insights into the effectiveness of injury prevention interventions (e.g., wearable hip protectors, safety floors), and assist in product development cycles. It would also be interesting to see how pain is influenced by age towards determining whether nociceptive sensitivity decreases for older adults. Future research is being undertaken to address these questions.

Acknowledgments

This research was supported by NSERC (RGPIN-2015-03636, 2020-05517).

References

[1] Berry et al., 2008. *Curr Osteoporos Rep*. 6: 10.1007/s11914-008-0026-4

[2] Reicherts et al., 2017. *Soc Cogn Affect Neurosci*. 12: 10.1093/scan/nsw181

[3] Finocchietti et al., 2011. *Eur J Pain*. 1: 10.1016/j.ejpain.2012.05.0100

Kinematic factors that best discriminate falls from recoveries following unconstrained slips

Abderrahman Ouattas[1*], Corbin M. Rasmussen[1] & Nathaniel Hunt[1]
[1]Department of Biomechanics, University of Nebraska at Omaha, Omaha, NE USA
email: * aouattas@unomaha.edu

Introduction

More than 25% of older adults fall each year in the US[1]. Slips alone account for 25% of all falls[2]. Successful recovery depends on the severity of the slip and the individual's capacity to react effectively and regain balance. When someone loses traction on a slippery surface, slips are unconstrained and the slipping feet can travel in a variety of directions[3,4]. Furthermore, slips can occur simultaneously to one or both feet, which challenges the ability to support body weight and maintain an upright trunk. Previous laboratory research has mainly focused on single limb slips at heel strike where motion of the slipping foot is constrained to the sagittal plane. Better understanding of the biomechanics of unconstrained, double-limb slips can guide future interventions to train proper recovery strategies.

To explore the impact of frontal plane versus sagittal plane kinematic measurements to discriminate slip-related falls from recoveries, as well as upper versus lower body kinematics, we compared the accuracy of four Linear Discriminant Analysis (LDA) models. Each model was informed by either sagittal or frontal plane measurements predetermined from either the lower or upper body during reactive responses immediately after slip initiation. We hypothesized that the frontal plane lower body model would show the highest classification accuracy.

Methods

Three unconstrained, bilateral slips were administered with the Wearable Apparatus for Slip Perturbations at early, mid, and late stance of the dominant leg of ten younger (5M, 5F, 24.7 ± 3.1 years, 1.71 ± 0.09 m, 73.6 ± 12.9 kg) and ten older (5M, 5F, 72.4 ± 3.8 years, 1.68 ± 0.12 m, 79.7 ± 14.8 kg) adults as they walked at 1.3 m/s . A load cell attached to the harness was used to classify falls if participants applied more than 30% of body weight to the harness[5]. Full body kinematics were recorded using an 18-camera motion capture system (Motion Analysis Corp., Santa Rosa, CA) and sampled at 100 Hz.

Peak and minimum frontal and sagittal plane feet velocities relative to the CoM and angular momentum (L) of the trunk and arms were analyzed from slip initiation (i.e. feet start to slide) until slip stop (i.e. the absolute sum of both feet velocities reach zero) to classify falls and recoveries using leave-one-out LDA. Stepwise elimination was used to reduce the number of factors before running LDA.

Results and Discussion

Using the load cell data, in addition to video observations for verification, we detected 20 falls and 40 recoveries.

Frontal plane feet velocities relative to the CoM were able to best classify both falls and recoveries (LDA Classification Accuracy = 73.3% cross validated; Wilks' Lambda = 0.696, $p<0.001$) better than all other LDA models (Fig 1-A). Sagittal plane feet velocities relative to the CoM were the second-best classifiers of falls and recoveries (LDA Classification Accuracy = 66.7% cross validated; Wilks' Lambda = 0.853, $p=0.011$), followed by sagittal plane trunk L (LDA Classification Accuracy = 65% cross validated; Wilks' Lambda = 0.913, $p=0.022$) and frontal plane arms L (LDA Classification Accuracy = 61.7% cross validated; Wilks' Lambda = 0.875, $p=0.006$).

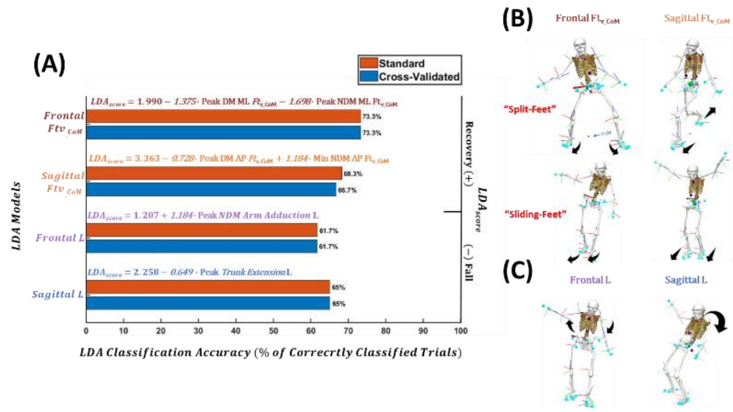

Figure 1. (A) LDA Classification Accuracy for the four models. Visual demonstrations are color-coded based on LDA models. **(B)** A visual demonstration of the main biomechanical behaviors observed for frontal & sagittal plane feet velocities relative to the CoM models. **(C)** A visual demonstration of the main biomechanical behaviors observed for frontal and sagittal plane upper body L.

The main two biomechanical behaviors we observed that led to severe falls were: 1) frontal-plane sliding feet: both feet traveling in the same direction (laterally\medially) and opposite to the CoM, and 2) frontal split feet: both feet traveling faster than the CoM and opposite to each other (Fig 1-B). Frontal plane L showed a significant effect of peak non-dominant (left in this case) arms adduction on falls, while sagittal plane L showed a significant effect of peak trunk extension on falls (Fig 1-C). Our hypothesis was supported - peak frontal plane feet velocities relative to the CoM classified falls and recoveries better than the three other LDA models. However, the accuracy of all models was generally low compared to the null accuracy of 66.7% (i.e. predicting all trials as recoveries) and future studies should consider the interaction between kinematic factors to investigate motor coordination of the reactive responses after unconstrained simultaneous double-limb slips.

Significance

Overall, maintaining similar frontal and sagittal feet velocities relative to one another and to the CoM, a flexed trunk, and larger abducted arms after slip onset is associated with a higher probability of recovery after sudden unconstrained simultaneous double-limb slips. However, we are uncertain if other factors may have contributed to the observed recoveries, particularly, given that we have not acquired muscle activation and inverse dynamics data.

Acknowledgments

NIH 2P20 GM109090-06; NIH R15AG063106-01.

References

1. Bergen G, et al. *Morb. Mortal. Wkly. Rep*, 65, 993–998, 2016.
2. Berg WP, et al. *Age Ageing*, 26, 261-268, 1997.
3. Rasmussen CM, et al. *J Neuroeng Rehabil*, 16, 118, 2019.
4. Ouattas A, et al. *44th Virtual ASB*, 2020.
5. Yang F & Pai Y. *J Biomech*, 44, 2243–2249, 2011

SUSCEPTIBILITY TO WALKING BALANCE PERTURBATIONS MAY GENERALIZE ACROSS CONTEXTS

Andrew D. Shelton[1*] Ellora M. McTaggart[1], Jessica L. Allen[2], Vicki S. Mercer[3], Jeremy R. Crenshaw[4] and Jason R. Franz[1]
[1] Joint Department of Biomedical Engineering, UNC Chapel Hill & NC State University, Chapel Hill, NC, USA [2]Department of Chemical and Biomedical Engineering, West Virginia University, Morgantown, WV, USA [3]Division of Physical Therapy, UNC Chapel Hill, Chapel Hill, NC, USA [4]Department of Kinesiology and Applied Physiology, University of Delaware, Newark, DE, USA
E-mail: adshelt@email.unc.edu

Introduction

Falls are a significant public health challenge and most often occur during locomotor activities such as walking. Accordingly, walking balance perturbations are commonplace in research settings to study instability and falls risk in a variety of populations. Indeed, our group has shown that observational measures during steady state walking do not necessarily predict susceptibility, or a measurable change in a particular stability measure, to perturbations [1]. However, the context of intrinsic and extrinsic factors contributing to walking instability and falls during daily activities can be diverse. It is presently unclear if the instability elicited by walking balance perturbations is context specific. Our purpose was to leverage a suite of walking balance perturbation paradigms in a cohort of young adult participants to address this knowledge gap. Given the fundamental mechanical and sensory differences between common perturbation contexts – namely, optical flow perturbations, mechanical waist-pull perturbations, and treadmill-induced slip perturbations – we hypothesized that susceptibility to balance perturbations does not generalize across different contexts. We evaluated this hypothesis by testing the prediction that susceptibility to perturbations (measured herein using change in margin of stability from unperturbed walking [ΔMoS]) would not significantly correlate between the three walking perturbation contexts.

Methods

19 young adults (23.7 ± 3.84 yrs, 11 F) completed four treadmill walking trials at their preferred overground walking speed in randomized order: two minutes of unperturbed walking, treadmill-induced slip perturbations (200 m/s duration, 6 m/s^2) applied randomly 5 times bilaterally at heel strike [2], waist-pull perturbations (100 m/s duration, 5 % body weight) applied 5 times bilaterally toward the swing leg at toe off, and two minutes of continuous mediolateral optical flow perturbations applied using a nominal amplitude of 35 cm. Subjects wore 36 motion capture markers on their trunk, pelvis, legs, and feet, from which we calculated MoS. Specifically, MoS was calculated in the anteroposterior (AP; MoS_{AP}) and mediolateral (ML; MoS_{ML}) directions at the instant of heel strike (that directly following perturbation onset for slip and waist pull perturbations). A repeated measures ANOVA tested for significant effects of condition. We also calculated bivariate Pearson correlations between the ΔMoS of each perturbation in the mediolateral and anteroposterior directions, and in the direction acted upon by each perturbation.

Results and Discussion

We found significant main effects of condition on MoS_{AP} and MoS_{ML}. Independent of perturbation context, MoS_{AP} decreased compared to unperturbed walking (p-values<0.001) but did not differ between perturbations (Fig. 1A). Similarly, MoS_{ML} was significantly smaller for all perturbed walking trials compared to unperturbed walking ($p<0.001$). However, we also found that MOS_{ML} was significantly smaller for treadmill-induced slips than either optical flow ($p = 0.017$) or waist-pull perturbations ($p = 0.004$) (Fig. 1B). In contrast to our predictions, we found significant correlations between ML susceptibility to all three perturbation contexts (ΔMoS_{ML}, $r \geq 0.53$, p-values≤0.020) (Fig. 1C-E). In contrast, we found no such correlations for AP susceptibility (ΔMoS_{AP}, $r \leq 0.387$, p-values≥0.102). In the direction acted upon by each perturbation, we found a significant correlation for susceptibility only between optical flow and waist-pull perturbations, which both target ML instability ($r=0.53$, $p=0.020$). AP susceptibility (i.e., ΔMoS_{AP}) to treadmill-induced slips did not correlate with ML susceptibility (i.e., ΔMoS_{ML}) to either optical flow ($p=0.934$) or lateral waist-pull perturbations ($p=0.992$). This may arise from a fundamental disconnect between AP and ML stability control in walking. Indeed, we found no correlation between MoS_{AP} and MoS_{ML} during normal, unperturbed walking ($p=0.652$).

Significance

We find that mediolateral susceptibility to walking balance perturbations, at least that quantified using MoS, generalizes across perturbation contexts (*i.e.*, sensory and mechanical) and extends to those primarily designed to elicit AP instability. This may introduce a paradigm shift in our use of perturbations to understand and mitigate risks for walking-related falls.

Acknowledgments

Supported by NIH 1R21AG067388.

References

[1] Qiao M, et al. (2018) *Gait & Posture*, **62** p. 80-5
[2] Crenshaw J, et al. (2014) *Gait & Posture*, **40** p. 363-8

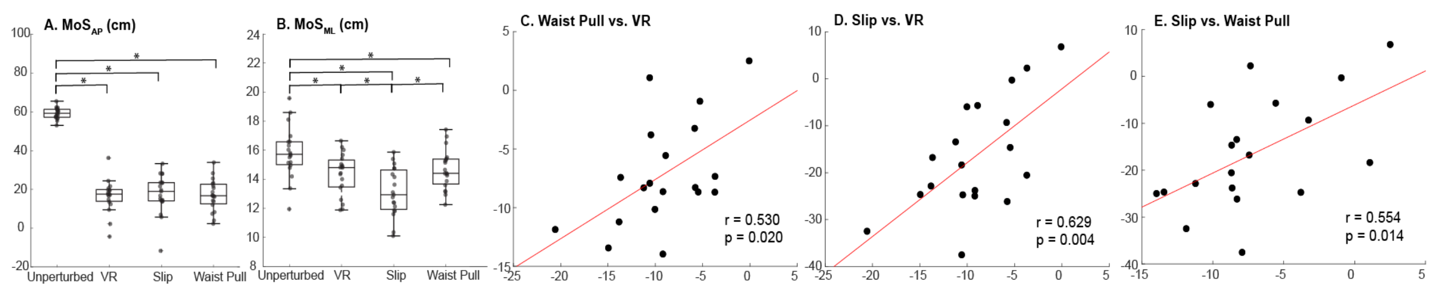

Figure 1: (A) Anteroposterior margin of stability (MoS_{AP}) and (B) Mediolateral margin of stability (MoS_{ML}) across the four walking trials. Asterisks (*) indicate significant pairwise comparison. (C-E) Correlations between the percent change in MoS_{ML} between each perturbation context.

DISTAL-TO-PROXIMAL REDISTRIBUTION OF PROPULSION DOES NOT CORRELATE WITH MARGIN OF STABILITY DURING FAST OR TYPICAL WALKING

Francesca Wade[1], B. Daniels[1], D. Clark[2,3], R. Seidler[1,4], T. Manini[3], D. Ferris[5], and C. J. Hass[1,4]
[1]Department of Applied Physiology & Kinesiology, University of Florida
email: *fwade21@ufl.edu

Introduction

Slower walking speed and greater instability are both characteristics of gait in older adults and are associated with increased fall risk [1]. Dynamic margin of stability (MoS) is a useful measure of gait instability, and it is sensitive to walking speed and age [2]. Musculature about the ankle primarily contributes to propulsive force, which regulates walking speed, yet older adults rely more on contributions from the hip [3]. It is unclear how individual joint contributions to forward propulsion are related to MoS, but a prevailing thought is that older adults use a more cautious gait to increase stability.

Here, we investigate how the contributions of the ankle and hip to forward propulsion relate to MoS during steady state (SS) and fast walking (FW) in a cohort of younger (YA) and typically-aging older adults (OA). We hypothesized that increased MoS will be associated with increased hip contributions to propulsion and that these correlations will be stronger in OA and FW.

Methods

YA (n = 18, mean ± SE age: 23 ± 4y; height: 1.69 ± 0.11m; mass: 69.14 ± 12.90kg) and OA (n = 20, age: 75 ± 4y; height: 1.70 ± 0.10m; mass: 74.91 ± 15.63kg) provided written informed consent. Participants performed two tasks: (1) walking at their "typical comfortable pace" (SS), and (2) walking at their "fastest safe speed without running" (FW), over a 10m walkway with 12 embedded force plates (2000Hz, AMTI). 18 cameras (100Hz, Vicon) simultaneously captured the motion of reflective markers, placed according to the Plug-in Gait marker set. A 4th order low-pass Butterworth filter (9Hz cut-off) was applied to marker and force data. For each gait cycle, projected CoM position was calculated [4]. At foot contact, anterior-posterior MoS (MoS_{AP}) was determined as the maximum distance between the projected CoM and the anterior toe marker, and mediolateral MoS (MoS_{ML}) was determined as the minimum distance between the projected CoM and the heel marker. Peak hip power, peak ankle power, and peak anterior ground reaction forces (aGRF) were extracted from the Plug-in Gait model output during each propulsive phase. The propulsive phase was defined from aGRF crossing 0 to the point of loss of foot-ground contact. Finally, we calculated the redistribution ratio (RR) [5]. An RR of 0 indicates positive propulsive work was fully performed about the ankle, while an RR of 2 indicates positive propulsive work was from the hip.

Statistical analysis: A repeated measures mixed effects ANOVA was run to identify the effect of walking speed (FW or SS) and age (OA or YA) on peak hip power, peak ankle power, peak aGRF, MoS_{AP}, MoS_{ML}, and RR. Pearson's correlations were run to identify any relationship between MoS_{AP}, MoS_{ML}, and RR for both FW and SS separately for OA and YA. Significance was set at the level $\alpha = 0.05$.

Results and Discussion

We found that preferred walking speed was similar between OA (mean ± SE: 1.18 ± 0.04 m/s) and YA (1.25 ± 0.04 m/s, p = 0.269), and yet during FW, OA (1.66 ± 0.07 m/s) walked significantly slower than YA (1.97 ± 0.07 m/s, p = 0.004). Interestingly, faster walking speed reduced both MoS_{ML} (Fig 1A, p = 0.034) and MoS_{AP} (Fig 1B, p = 0.01) for OA, but not for YA. Our data did not support our initial hypothesis; neither MoS_{AP} nor MoS_{ML} were correlated with hip or ankle power, regardless of walking speed (all p >.203).

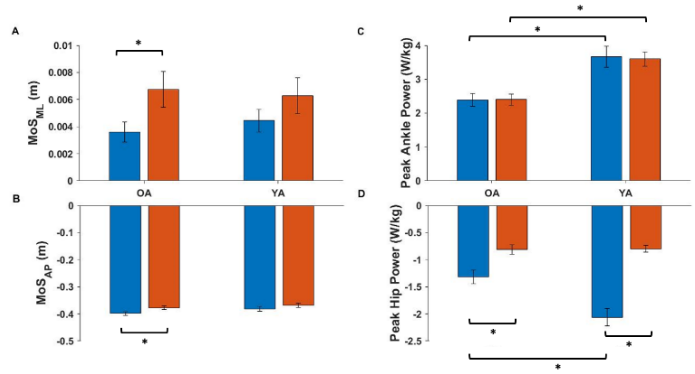

Figure 1: Dynamic MoS in both mediolateral (A) and anterior-posterior (B) directions and peak ankle (C) and hip (D) power for OA and YA during fast (blue) and typical (orange) walking.

Peak aGRF increased during FW for both OA and YA (all $p < 0.001$), while OA had lower peak aGRF than YA across all walking speeds (all $p \leq 0.003$). This age-associated decrease in aGRF may be due to the reduced peak ankle power generated by OA during both FW (p = 0.002) and SS ($p < 0.001$) trials (Fig 1C). OA also had lower hip power during FW (Fig 1D, p = 0.001). OA had a significantly higher RR than YA for both SS (mean difference: 0.237 ± 0.047, $p < 0.001$) and FW (mean difference: 0.156 ± 0.072, p = 0.037). This suggests OA were compensating by increasing hip contributions to forward propulsion.

We hypothesized that individuals with lower MoS_{AP} and MoS_{ML} would have a higher RR, and that faster walking speed would strengthen this relationship. However, we found no correlations between redistribution ratio, walking speed, nor MoS_{AP} or MoS_{ML}, regardless of age (all $p \geq 0.210$).

Significance

Our findings challenge the idea that older adults alter their gait mechanics to produce more stable gait, as no relationship between dynamic MoS and RR, MoS and hip power, nor MoS and ankle power were found, regardless of age group studied. Future studies are needed to understand why this distal-to-proximal redistribution of forward propulsion happens with aging.

Acknowledgments

This project is supported by NIH U01AG061389.

References

[1] Osoba et al., 2019. *Laryng Investig Otolaryng.* 4(1): 143-153
[2] Kongsuk et al., 2019. *Gait Posture.* 73:86-92
[3] DeVita & Hortobagyi, 2000. *J Appl Phys.* 88(5):1804-1811
[4] Hof, 2008. *Hum Mov Sci.* 27:112-125
[5] Browne & Franz, 2018. *Plos One.* 13(8):e0201407

UNPREDICTABLE DISCRETE MEDIOLATERAL TREADMILL PERTURBATIONS INCREASED SELF-PACED WALKING SPEED

Cesar R. Castano[1*] and Helen J. Huang[1,2,3]
[1]Mechanical and Aerospace Engineering Department, University of Central Florida, Orlando, FL
email: Castanocesar@knights.ucf.edu

Introduction

Humans often adjust their gait kinematics when walking in uncertain environments. On unstable surfaces, studies revealed that subjects walk more slowly and take shorter, faster, and wider steps compared to more stable surfaces [1,2]. A treadmill that shifts side-to-side can apply discrete mediolateral perturbations at a specific gait event on a stride-by-stride basis differentially affected gait stability [3]. Implementing similar perturbations on a self-paced treadmill would allow subjects to change their walking speed and step kinematics more freely [4]. Applying perturbations of different unpredictabilities during self-paced walking may better represent what would happen in real-world settings since subjects can freely change their walking speed and gait kinematics while experiencing the perturbations.

Here, we investigated how the unpredictability of discrete mediolateral treadmill perturbations would affect self-selected walking speed and step kinematics. Our hypothesis was that more unpredictable perturbations would lead to more cautious gait strategies. We predicted that more unpredictable perturbations would result in decreases in walking speed and step length and an increase in step frequency and step width compared to walking with more predictable perturbations.

Methods

We recorded lower limb movements using a motion capture system as young adults (n = 8, 4 female, 4 male) walked on an instrumented self-paced treadmill (M-Gait, Motek Medical). We changed the magnitude of mediolateral treadmill shifts and/or the timing of the perturbation during the gait cycle to create different levels of perturbation unpredictability. There were 5 conditions: 1) no perturbations, 2) same magnitude (3 cm shift) and same timing at left leg loading response (least unpredictable), 3) same magnitude (3 cm shift) with different timings (left leg loading response, terminal stance, and mid-swing), 4) different magnitudes (1cm, 3cm, or 5cm shifts) with the same timing, the left leg loading response, and 5) different magnitudes and different timings (most unpredictable). During each perturbation condition, subjects experienced 200 perturbations. We calculated mean step kinematics (walking speed, step length, step frequency, and step width) and their variability using standard deviation to examine gait strategies. We used a repeated-measures ANOVA followed by a Tukey's honest significance different (HSD) test to identify significant statistical differences between conditions.

Results and Discussion

Most subjects walked faster, not slower, for the perturbation conditions compared to the no perturbation condition (Fig. 1). As expected, subjects took faster and wider steps for the most unpredictable perturbation compared to the no perturbation condition. Walking speed, step frequency, and step width variabilities were the greatest for the most unpredictable perturbation. The mean step length, however, was similar across perturbation types while there was only a noticeable difference in step length variability for the most unpredictable perturbation compared to the no perturbation condition.

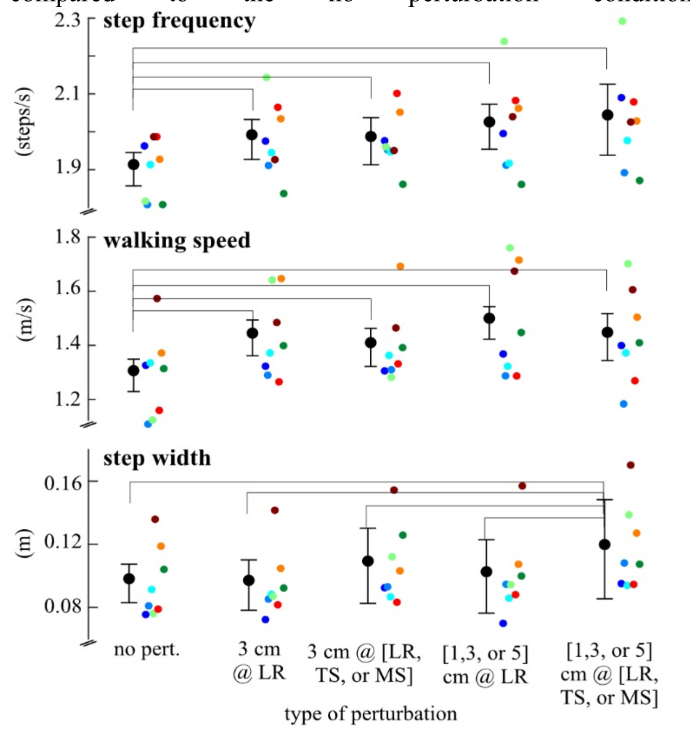

Figure 1: Average walking speed values for all conditions (n=8). The black circles and error bars show the group averaged and standard deviation walking speed. The colored dots correspond to individual subjects. Brackets indicate significant differences, Tukey HSD p<0.05.

These results partially support our hypothesis that subjects would use more cautious gait strategies for more unpredictable discrete perturbations during self-paced treadmill walking. Instead of walking more slowly which is often associated with more cautious gait [1,2], subjects adopted faster self-selected walking speeds for the perturbation conditions compared to the no perturbation condition in our study. The faster walking speeds occurred because of increases in step frequency as step lengths remained similar. Evidence of a more cautious gait was the increased step width with more unpredictable perturbations.

Significance

These findings provide new insights about gait strategies when responding to unpredictable and unstable surfaces. The surprising result that subjects used faster self-selected walking speeds when responding to the discrete mediolateral perturbations suggests that these perturbations could potentially help train older adults and clinical populations to increase their walking speeds.

Acknowledgments

This work was supported by NIH R01AG054621 to HJH.

References

[1] Menant JC et al. 2009. *Gait Posture.* 29: 392–397.
[2] Reimann H et al. 2018. *KinesiologyReview.* 7(1):18–25.
[3] Li J & Huang HJ. 2022. *J. Neurophysiol.* 127, 38-55
[4] Castano CR & Huang HJ. 2021. *PLoS One.* 2021;16: e0251229.

CORRELATION BETWEEN TROCHANTERIC SOFT TISSUE STIFFNESS AND HIP FRACTURE RISK DURING SIDEWAYS FALLS

Kitaek Lim[1], Seungsu Kim[1], and Woochol Joseph Choi[1]
[1]Injury Prevention and Biomechanics Laboratory, Dept of Physical Therapy, Yonsei University, South Korea
email: wcjchoi@yonsei.ac.kr

Introduction

While the stiffness of a falling body (i.e., pelvis) is a biomarker of hip fracture in a fall (the greater the stiffness, the higher the risk), accurate measure of body stiffness requires simulation of falls (thereby, it is not easy to figure out one's body stiffness) [1]. The stiffness of the trochanteric soft tissue is also considered a biomarker of hip fracture (the lesser the stiffness, the higher the risk), and quick and proper measure of the soft tissue stiffness is possible using a commercially available hand-held indentation device [2]. Correlating information between the two biomarkers should be useful to predict the hip fracture risk during a fall. In this study, we conducted falling experiments with humans to seek such information.

Methods

Twenty-three healthy young adults participated in pelvis release experiments that simulate an impact stage of a fall [3]. Participants lay sideways, where an electromagnet attached to the ceiling raised the pelvis, so the skin surface barely touched a Plexiglass plate (Figure 1a). Then, the electromagnet was turned off, causing the pelvis to fall. During trials, deformation of the trochanteric soft tissue was measured through an ultrasound probe (L4-7EL, SonoaceX8, Samsung-Medison, Seoul, South Korea), and corresponding compressive force was measured using a force plate (OR6-7-2000, AMTI, Waltham, MA, USA). Deformation of participants' pelvis during impact was also recorded using eight motion capture cameras (Vero v2.2, VICON, Oxford, UK).

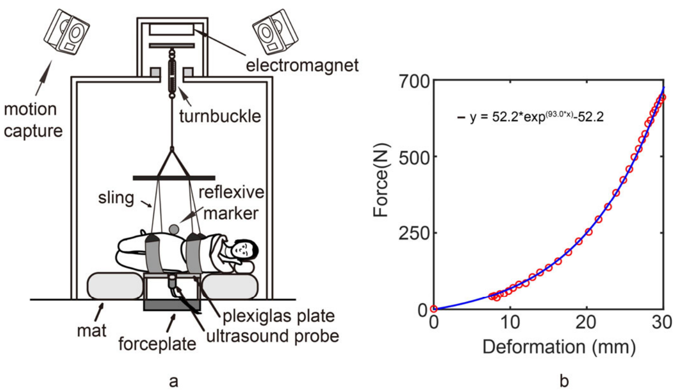

Figure 1: Experimental setup (a) and sample force-deflection data of the pelvis with a fitted curve (b).

Trochanteric soft tissue stiffness. We first fitted the force-deformation data of the trochanteric soft tissue during impact with different functions. We then defined the stiffness as a slope of the tangent line (a) at maximum deformation for each fitted curve: first polynomial (Ks_{1st}), second polynomial (Ks_{2nd}) and exponential (Ks_{exp}) curve, and (b) at a compressive force of 0.4 N for the exponential ($Ks_{0.4N}$) curve. We also measured the trochanteric soft tissue stiffness (Ks_{myoton}) using a hand-held indentation device (MyotonPro, Myoton AS, Tallinn, Estonia).

Body stiffness. We fitted the force-deflection data of the pelvis during impact with an exponential function (Figure 1b). We then defined the body stiffness (K_b) as a slope of the tangent line at an impact force of 4,000 N - a force magnitude that humans experience during a fall onto a hard surface from standing height [1].

Linear regression analyses were used to predict the body stiffness with the trochanteric soft tissue stiffness. All analyses were conducted with MATLAB routines (R2021B, MathWorks Inc.) and SPSS 25 (IBM corp., Armonk, NY, USA).

Results and Discussion

There was a significant correlation between Ks_{1st} and K_b, and $Ks_{0.4N}$ and K_b ($r^2 = 0.536$, $p = 0.005$; $r^2 = 0.256$, $p = 0.016$, respectively) (Figure 2). In particular, the K_b decreased 35.3 kN/m for every 1 kN/m increase in Ks_{1st} ("$K_b = -35.3{*}Ks_{1st}+1365.1$"). This suggests not only that the trochanteric soft tissue stiffness can predict the body stiffness (hip fracture risk) during a fall, but also that the hip fracture risk may decrease with an enhancement of the "natural" padding (i.e., strengthening muscles covering the hip).

However, there was no correlation between Ks_{2nd} and K_b, Ks_{exp} and K_b, and Ks_{myoton} and K_b ($r^2 = 0.023$, $p = 0.5$; $r^2 = 0.02$, $p = 0.53$; $r^2 = 0.024$, $p = 0.488$, respectively).

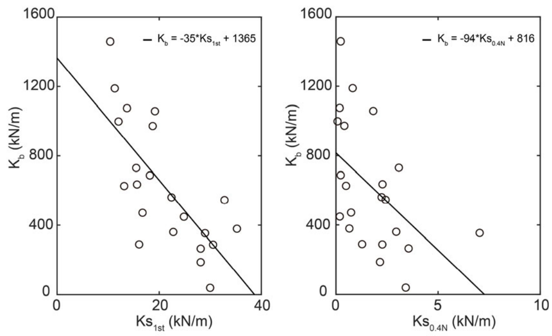

Figure 2: Correlation between the trochanteric soft tissue stiffness and the body stiffness during sideways falls.

Significance

Our study presents a linear relationship between the trochanteric soft tissue stiffness and body stiffness during sideways falls, informing that soft tissue stiffness can be a good predictor of hip fracture risk. However, the soft tissue stiffness measured by a commercially available clinical device is ineffective in predicting the body stiffness.

Acknowledgments

This research was supported by the "Brain Korea 21 FOUR Project", the Korean Research Foundation.

References

[1] Lim and Choi, 2020, *Osteoporos Int*, 31(9): 1713-1719
[2] Lim and Choi, 2019, *J Biomech*, 93: 28-33
[3] Lim and Choi, 2021, *J Biomech*, 117: 110254

QUANTIFYING BIOMECHANICAL PERFORMANCE OF A TRI-COMPARTMENT OFFLOADER BRACE IN ADULTS WITH KNEE OSTEOARTHRITIS

Chris A. McGibbon[1*], Emily Bishop[2] and Janet Ronsky[2]
[1]Faculty of Kinesiology and Institute of Biomedical Engineering, University of New Brunswick, Fredericton, New Brunswick
[2]Dept Mechanical and Manufacturing Engineering, University of Calgary, Calgary, Alberta
email: *cmcgibb@unb.ca

Introduction

Knee pain and muscle weakness are major contributors to mobility disability experienced by people with knee osteoarthritis (kOA). The Levitation "Tri-Compartment Offloader" knee brace (TCO, Spring Loaded Technology, Inc. Halifax, NS) was designed to reduce knee pain and improve function in people with multi-compartment kOA [1]. The TCO uses novel spring technology to provide an assistive knee extension moment during weightbearing knee flexion. Preliminary simulations assuming an "ideal brace" [2] show the mechanism for unloading the tibiofemoral (TF) and patellofemoral (PF) joints is directly related to the brace action reducing the knee extension moment. The degree to which this is achievable during a challenging task for people with kOA, such as rising from and sitting to a chair [3], depends in part on how well the brace transmits moments to the knee. However, there are no published approaches for evaluating the quality of force transmission of a knee extension assist brace.

We sought to answer the following questions: Does the TCO brace reduce joint contact forces in adults with kOA during a repeated chair rise task? And if so, which biomechanical variables explain the performance of the TCO brace?

Methods

Nine participants (6 male, age 61.4±8.1 yrs; BMI 30.4±4.0 kg/m2) with medial TF and PF OA (Kellgren-Lawrence grades 2-4) were enrolled and tested following informed consent. Six degree-of-freedom motion analysis data were captured for a 5-times repeated chair rise-and-lower task to compare three bracing conditions: 1) without brace (OFF); 2) brace in low stiffness mode (LOW); and 3) brace in high stiffness mode (HIGH).

A 3D inverse dynamics model of the lower-leg and foot was used to compute net knee joint reaction forces and moments, and a sagittal plane model of the knee was used to resolve PF and TF contact forces [2]. For the LOW and HIGH brace conditions, the TCO was modelled as: 1) an ideal brace by assuming perfect alignment of the brace and anatomical knee, and 2) as an actual brace by tracking the brace's 3D position during the movement trials. The brace effect was measured as the difference between joint contact forces (TF and PF) in the braced and unbraced (OFF) conditions. Paired t-tests (α=.05) were used to test for significant brace effect for LOW and HIGH braces.

To understand the influence of biomechanical factors on brace performance, we calculated brace performance index (BPI) as the ratio of the actual brace effect to the ideal brace effect and its correlation with brace performance parameters, shown in Fig. 1. Relationships between performance indicators and body weight (BW) were also examined using Pearson correlation analysis.

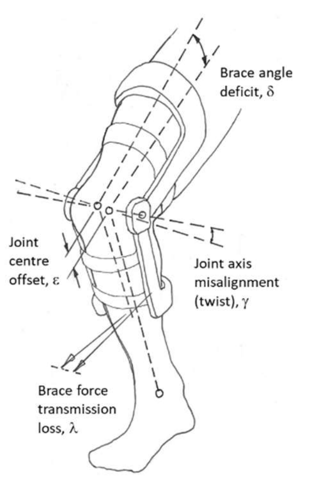

Figure 1. Brace performance parameters

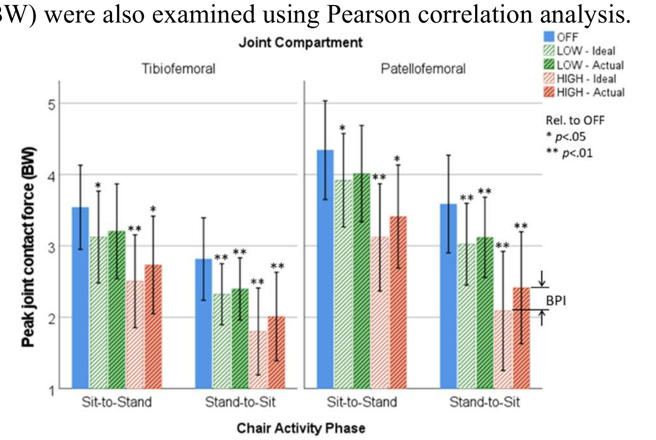

Figure 2: Mean peak joint contact forces (units of BW) for LOW and HIGH braces. BPI is illustrated as the ratio of ideal to actual brace effect.

Results and Discussion

Compared to the OFF condition, the HIGH (actual) condition showed a significant reduction in TF and PF contact forces (by 25-30%) for both the sit-to-stand (TF: p=.007; PF: *p*=.02) and stand-to-sit (TF: *p*=.005; PF: *p*=.008) phases, while the LOW (actual) condition showed significant reduction (by ~10-15%) only for the stand-to-sit phase (TF: *p*=.005; PF: *p*=.009) (Fig. 2).

The HIGH condition BPI ranged between 75-80% and the LOW condition BPI ranged between 80-85% (Fig. 2). This means the braces were able to deliver about 75-85% of the assistance they had the potential to deliver.

BPI decreased with increasing brace deficit angle δ for both the LOW (r=-.96, p<.001) and HIGH (r=-.95, p<.001) conditions, but was not related to any other parameters. Brace axis misalignment γ (LOW: r=-.77, p=.016; HIGH: r=-.91, p=.001) and joint centre offset ε (LOW: r=-.69, p=.04; HIGH: r=-.72, p=.028) were lower in participants with higher BW.

Significance

The LOW brace significantly reduced joint contact forces during the stand-to-sit phase while the HIGH brace significantly reduced joint contact forces during both phases of the activity. The primary performance parameter for both the LOW and HIGH stiffness brace was the amount of brace bend (spring engagement) achieved relative to the anatomical knee flexion angle. The TCO had less relative motion on the leg for those with higher BW, but higher BW did not likewise improve BPI.

Acknowledgments

This work was supported by a Mitacs Accelerate Fellowship.

References

[1] Budarick et al., *Rehabil Res Pract*. 2021: 5923721
[2] McGibbon et al., *Front Bioeng Biotech*. 2021(8): 604860
[3] Verlaan L et al. *Biomed Res Int*. 2018: 351949

AT-HOME ASSESSMENT OF WALKING AND CHAIR STAND MOVEMENTS USING WEARABLE SENSORS IN KNEE OSTEOARTHRITIS: A RELIABILITY STUDY

Michael J. Rose[1*], Tuhina Neogi, MD, PhD[2], Brian Friscia, MS[1], Kaveh A. Torabian[1], Michael P. LaValley, PhD[3], Mary Gheller, MS[2], Lukas Adamowicz, MS[4], Pirinka Georgiev[4], Lars Viktrup, MD, PhD[5], Charmaine Demanuele, PhD[4], Paul Wacnik, PhD[4], and Deepak Kumar, PT, PhD[1,2]

[1]Department of Physical Therapy & Athletic Training, Boston University (BU), Boston, MA, USA; [2]Section of Rheumatology, BU School of Medicine, Boston, MA, USA; [3]Department of Biostatistics, BU School of Public Health, Boston, MA, USA; [4]Early Clinical Development, Pfizer Inc., Cambridge, MA, USA; [5] Neuroscience Business Unit, Eli Lilly and Company, Indianapolis, IN, USA;
email: *rosemich@bu.edu

Introduction

The COVID-19 pandemic has accelerated the adoption of digital health technologies for remote monitoring in clinical trials [1]. For trials in people with knee osteoarthritis (OA), function measures such as gait and chair stand are considered important outcomes [2]. Wearable sensors could allow remote monitoring of these outcomes. However, the reliability of wearable sensor metrics of gait and chair stand in participants' homes and the agreement between metrics collected in the laboratory and at-home have not been reported to date. Hence, our objective was to assess the reliability of wearable sensors for remote monitoring of gait and chair stand in people with knee OA.

Methods

We used data from a substudy (n=20) embedded within an ongoing, single-arm clinical trial of an exercise intervention in people with knee OA (clinicaltrials.gov NCT04243096). All assessments took place before the initiation of the intervention. Participants completed two visits, an in-person lab visit, and a remote at-home visit, with the order of visits randomized. Participants were provided a wearable system for the remote visit consisting of three inertial sensors (Opal, APDM, Portland, OR, USA). During the remote visit, researchers guided the participants via video conference. Participants self-applied the sensors on each foot and on the lower back. They performed two trials each of a standardized gait task (self-selected walk for two laps of a 7-meter path totaling 28 meters of walking) and chair stand task (five chair stands as quickly as possible with arms across the chest) in their home. Then, the participants removed the sensors, waited for 15-minutes, re-applied the sensors, and performed two more trials of each task. At the end of the visit, participants completed a survey on their experience. Participants performed two trials of the same tasks during the in-person lab visit after a researcher placed the sensors on the participants. Spatiotemporal gait metrics (e.g., gait speed, cadence, stride length, stance and swing as a % of gait cycle time) and duration of chair stand were extracted from the sensor data using software (MoveoExplorer) provided by the sensor manufacturer.

The mean of sensor metrics across each set of two trials was used in the analyses. Intra-class correlation coefficients (ICC) and Pearson's correlation were used to determine the reliability of sensor metrics during the remote visit. ICCs and Bland-Altman plots (with 95% limits of agreement) were used to examine agreement between sensor metrics from the remote (first two trials) and lab visits.

Results and Discussion

Participant characteristics are given in **Table 1**. All ICCs were good to excellent (between 0.85 and 0.96) for the test-retest reliability during the remote visit and R^2 ranged between 0.81 and 0.95. ICCs were moderate to excellent (between 0.63 and 0.91) for agreement between remote and lab visits. Bland-Altman plots (such as in **Figure 1**) showed slight bias in all metrics, likely due to participants walking slightly faster during the lab visit than the remote visit. Feedback from the participants showed that they were highly accepting of the remote visit.

Table 1. Participant characteristics

	Participants (n=20)
Mean Age (SD), years	70.5 (4.7)
Mean BMI (SD), kg/m^2	30.6 (4.7)
Mean KOOS Pain (SD)	60.2 (10.6)
Mean KOOS ADL (SD)	68.8 (14.2)
Female, n (%)	17 (85%)
White, n (%)	19 (95%)
Without a college degree, n (%)	2 (10%)
Annual Income <$50,000, n (%)	4 (20%)
Currently Employed, n (%)	11 (55%)

SD = Standard Deviation, KOOS = Knee injury and Osteoarthritis Outcome Score

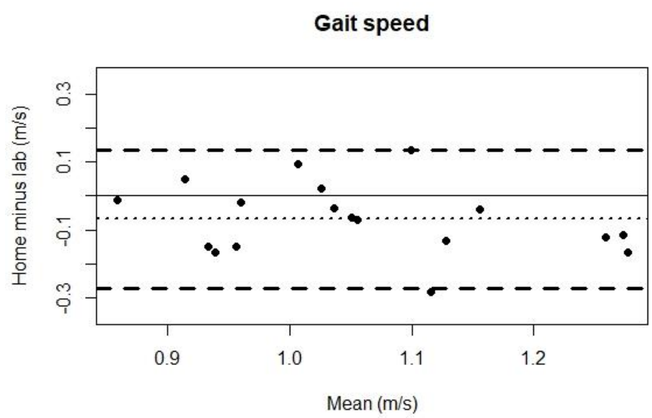

Figure 1: Bland-Atlman plot for gait speed. Lines show mean difference (dotted) and 95% limits of agreement (dashed).

Significance

Our method of estimating gait and chair stand function remotely was found to be reliable, feasible, and acceptable, in this cohort of people with knee OA with moderate pain and disability. Wearable sensors could be used to remotely monitor gait and chair stand function in participant's natural environments at a lower cost, reduced participant and researcher burden, and greater ecological validity overcoming limitations of lab visits. Hence, our approach could be used in future clinical trials of people with knee OA.

Acknowledgments

This work was funded by Pfizer Inc. and Eli Lilly and Company.

References

[1] Olayiwola JN et al. JMIR Public Health Surveill 2020;6(2):e19045 [2] Dobson F et al. Osteoarthr. Cartil. 2013;21(8)

SUBJECT-SPECIFIC MODELLING OF MUSCLE FORCE DURING GAIT IN TOTAL KNEE ARTHROPLASTY

Erik Kowalski[1], Alexandre Pelegrinelli[1,2], Nicholas Ryan[1], and Mario Lamontagne[1*]
[1]Faculty of Health Sciences, University of Ottawa, Canada
[2]State University of Londrina, Brazil
email: *mlamon@uottawa.ca

Introduction

Pain, impaired mobility, and advanced progression of knee osteoarthritis require individuals to undergo a total knee arthroplasty (TKA)[1]. Although TKA is successful at reducing knee pain as early as one month after surgery, functional deficits persist in some patients[2]. These patients remain unsatisfied due to unresolved pain and mobility restrictions following surgery[3].

Patients often exhibit adaptations in their movement patterns during daily functional tasks, such as walking and climbing stairs[4]. These adaptations have been attributed to quadriceps strength deficits and altered muscle activation patterns required to stabilize the reconstructed knee[5]. Musculoskeletal modelling can evaluate how these adaptations effect knee contact and muscle forces in patients before and after undergoing TKA using patient-specific measurements and simulation.

The purpose of this study was to compare muscle forces and knee contact forces during gait in patients with knee osteoarthritis before and after TKA, and with healthy control participants.

Methods

Thirteen patients (female = 6, male =7; age = 63.9 ± 5.4 years; BMI = 28.4 ± 3.9 kg/m^2) with severe knee osteoarthritis completed a gait analysis pre-operatively and 12 months post-operatively after undergoing TKA. Patients were compared to 12 control participants (female = 6, male =6; age = 64.2 ± 6.1 years; BMI = 26.0 ± 2.6 kg/m^2). Full-body kinematics and kinetics were computed, and muscle forces and knee contact forces were estimated using a musculoskeletal model and static optimization. The knee model included medial and lateral compartment geometries that computed medial and lateral tibiofemoral contact forces. Muscles of interest included knee extensors (quadriceps) and flexors (hamstrings, gastrocnemius). Data was processed in Matlab where it was normalized to the gait cycle. Analyses were limited to the stance phase and were compared between the groups using statistical parametric mapping (SPM).

Results and Discussion

No significant differences in age, BMI or walking speed existed between the groups, therefore, walking speed was not used as a covariate.

No significant pre- versus post-operative, or pre-operative versus control differences existed in knee contact or muscle forces. Knee contact forces within this study were of similar magnitude to previous studies. Previous studies did not identify differences in knee contact forces between knee osteoarthritic and healthy individuals after adjusting for body weight and walking speed[6].

Gait may not be a difficult enough task to identify differences between groups. In vivo loading measured using instrumented implants identified that peak knee contact forces were 3.1 BW during gait, but during stair climbing it rose to over 5.4 BW[7]. Future studies should compare participants during more challenging tasks, which may identify differences between groups, including differences before and after TKA.

Compared to the control group, post-operatively, the TKA group had significantly lower biceps femoris (Figure 1A) and lateral gastrocnemius (Figure 1B) muscle forces. A previous study identified that TKA patients had reduced quadriceps force, but no differences in hamstrings or gastrocnemius muscles. They concluded their TKA participants walked with a ‘quadriceps avoidance’ gait pattern and compensated with a forward trunk lean[8]. Forward trunk lean was not evaluated in this study, but a ‘quadriceps avoidance’ gait pattern was not evident based on groups having similar quadriceps muscle forces.

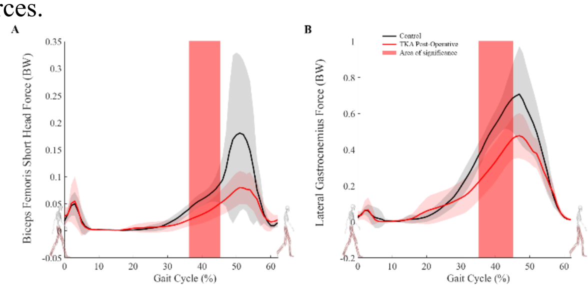

Figure 1: (A) Biceps femoris short head and (B) lateral gastrocnemius muscle force during gait for the TKA (red) and control (black) groups. Muscle forces were normalized by body weight (BW) and determined from static optimization. SPM results are highlighted in red and indicate significant ($p < .05$) differences between the TKA and control groups.

In this study, the lateral knee flexors (biceps femoris, lateral gastrocnemius) had reduced force during terminal stance (Figure 1). This may be indicative of a stiff knee gait pattern. Increased quadriceps/hamstrings co-contraction may be occurring within the TKA group, which may limit hip extension and force generation prior to toe-off. Further biomechanical and electromyographical analysis is warranted.

Significance

This study identified no differences in knee joint loading before or after a TKA during gait. However, biceps femoris and lateral gastrocnemius muscle force was lower post-operatively compared to the control group during terminal stance phase, which may be representative of a stiff knee gait pattern. Future studies should utilize for demanding activities of daily living for comparisons.

Acknowledgments

Institutional support for this research was provided by MicroPort Orthopedics.

References

[1] Guccione et al., 1994. *Am. J. Public Health.* 84:351-358. [2] Stevens-Lapsley et al., 2011. *PM&R*. 3:541-549 [3] Lin et al., 2020. *Orthopaedic Surgery.* 12:836-842 [4] Mizner et al., 2005. *Orthop Res*. 23:1083–1090 [5] Noble & Prentice 2006. *Exp Brain Res*. 169:482–495 [6] Kumar et al. 2013. *JOR*, 30(3):298-305 [7] Taylor et al. 2004. *JOR*, 22:625-632 [8] Li et al. 2013. *Gait Posture*, 38(1):79-85

IMPROVING MUSCLE CAPACITY UTILIZATION WITH A 12-WEEK STRENGTHENING PROGRAM FOR WOMEN WITH SYMPTOMATIC KNEE OSTEOARTHRITIS

Jacquelyn M. Maciukiewicz[1], Emma V. Tung[1], Elora C. Brenneman Wilson[2], Monica R. Maly[1]
[1]University of Waterloo, Department of Kinesiology and Health Sciences
[2]McMaster University, Department of Kinesiology
email: mrmaly@uwaterloo.ca

Introduction

Knee osteoarthritis (OA) often results in pain and mobility limitations [1]. Exercise is a cornerstone of treatment as it improves symptoms, comparably to pain medication [2]. However, because the knee adduction moment (KAM) is linked to OA worsening, exercise would ideally avoid repetitive exposures to elevated KAM [3]. This rationale underlined a previously completed biomechanically defined strengthening intervention [4].

Beyond KAM, a deficit in peak knee extensor torque (particularly in women) is a risk factor for the initiation of knee OA [5]. Due to lower absolute peak knee extensor torque, women may use a greater relative effort (proportion of maximal strength) during daily tasks, such as walking. The purpose of this secondary analysis was to determine if the 12-week biomechanically driven strengthening intervention also reduced muscle capacity utilization during level walking and lunge tasks.

Methods

Data from 25 women who met the American College of Rheumatology criteria of clinical knee OA were included in this secondary analysis. Exclusion criteria included other forms of arthritis, knee disease, knee surgery, physician-advised activity restrictions, and lower limb trauma in past three months.

Participants completed a 12-week strengthening exercise intervention, consisting of yoga postures focused on alignment [6]. Postures included static lunges and squats with varying foot, trunk, and arm positions; all postures activated lower limb musculature. Participants completed three, one-hour supervised groups classes a week. Assessments were completed on the most symptomatic knee at baseline and at conclusion of the program.

Peak extensor torque and the peak external knee flexion moment (KFM) during gait and a static lunge were measured. Peak extensor torque during a maximal isometric contraction was measured using a dynamometer (Biodex System 3, Shirley, MA, USA), with the knee angle set to 60°. Three maximal exertions were completed (5s each), with one minute of rest between. The peak of each trial was extracted and averaged for each participant. To calculate the KFM, three-dimensional kinematics were recorded with a three-camera bank (9 cameras) active-marker motion capture system (Optotrak Certus, Northern Digital Inc.) synchronized with ground reaction forces and moments collected with a floor-embedded force plate (OR6-7, AMTI) during barefoot walking (at a self-selected speed) and static lunges. Commercial software (Visual 3D, C-Motion Inc) was used to filter these data and calculate the KFM. Peak KFM was extracted from gait (5 trials) and lunge (3 trials) using a custom MatlabTM R2020a program (Mathworks Inc., USA).

Muscle capacity utilization was expressed as the ratio of peak KFM to peak extensor torque. This value models the proportion of maximal knee extensor torque required during tasks.

Paired t-tests were used to determine differences between peak extensor torque, peak KFM (gait/lunge) and muscle capacity utilization (gait/lunge) pre/post intervention ($p<0.05$).

Results and Discussion

Participants were 59.8 ± 6.3 years old, 81.0 ± 13.2 kg, 1.6 ± 0.05 m, and 30.5 ± 5.3 kg/m^2 at baseline.

Compared to baseline, peak extensor torque, peak KFM (gait) and muscle capacity utilization (gait) differed at follow-up (Table 1). Peak extensor torque increased at follow up, while both peak KFM and muscle capacity utilization during gait decreased (Table 1). Peak KFM and muscle capacity utilization during lunge remained unchanged from pre to post intervention.

A reduction in muscle capacity utilization during gait, through both increased extensor strength and decreased peak KFM may result in improvement of physical function in individuals with knee OA – and the ability to complete activities of daily living using less relative effort.

Significance

Muscle capacity utilization provides insight into the proportion of maximal strength required to complete a task. A reduction in this metric during gait indicates a decrease in relative effort for these individuals. Importantly, it is both an increased peak extensor torque and reduced peak KFM that results in an overall decreased muscular capacity utilization. Overall, this indicates that exercise may not only increase strength, but decrease relative effort during daily tasks in individuals with knee OA.

Acknowledgments

Project funding was received through a Canadian Institutes for Health Research Bridge Grant #137147 (MRM). MRM is supported by a STARS Mid-Career Award from The Arthritis Society/CIHR-IMHA. Funding for equipment used in this research was received through the Canada Foundation for Innovation and the Ontario Research Fund.

References

[1] Roos et al. (2003). *Health Qual. Life Outcomes*. 1(1), 1-10
[2] Fransen et al. (2015). *Cochrane Database Syst. Rev.* 49(24), 1554-1557.
[3] Robbins et al. (2011). *Arhritis Care Res.* 63(7), 991-97.
[4] Longpre et al. (2015). *Clin Biomech*. 30(8) 820-826
[5] Øiestad, et al. (2015). *Osteoarthr. Cartil*. 23(2), 171-177.
[6] Kuntz et al. (2018). *PloS one*, 13(4), e0195653.

Table 1: Mean ± SD data for peak extensor torque, KFM, and muscle capacity utilization (KFM/peak extensor torque), pre/post strengthening intervention during gait and lunge tasks. Significant data ($p>0.05$) are marked with an asterisk (*) and bolded.

	Peak Extensor Torque (Nm)	Peak KFM -Gait (Nm)	Peak KFM - Lunge (Nm)	Muscle Capacity Utilization – Gait (Unitless)	Muscle Capacity Utilization – Lunge (Unitless)
Pre-Intervention	**100.1 ± 29.6**	**41.0 ± 16.5**	27.9 ± 9.7	**0.43 ± 0.18**	0.31 ± 0.19
Post- Intervention	**108.6 ± 28.5**	**35.6 ± 13.9**	28.2 ± 4.3	**0.33 ± 0.12**	0.28 ± 0.09
p value	**0.02***	**0.04***	0.89	**0.003 ***	0.37

THE ROLE OF CUMULATIVE LOADING ON PREDICTING CHANGES IN KNEE CARTILAGE OUTCOMES: DATA FROM THE OSTEOARTHRITIS INITIATIVE

Natasha K. Ivanochko[1], Anthony A. Gatti[2,3], Paul W. Stratford[4], Monica R. Maly[1,4]
[1]Department of Kinesiology and Health Sciences, University of Waterloo, Waterloo, ON, Canada
email: mrmaly@uwaterloo.ca

Introduction

Exposure to high dynamic loading is associated with worsening knee cartilage morphology, in those with established knee osteoarthritis. Yet, running, an activity with high loading rates, is not associated with increased risk of developing osteoarthritis (OA).[1] The purpose of our work was to evaluate potential factors that influence the relationship between cumulative loading with knee cartilage outcomes. Our primary objective was to investigate the continuous relationship between cumulative loading and two-year changes in cartilage thickness and mean transverse relaxation time (T2). A secondary objective was to explore the relationship between tertiles of physical activity and body mass index with cartilage outcomes.

Methods

Data from the FNIH OA Biomarkers Consortium Project of the Osteoarthritis Initiative was used for our analysis (n=412 participants). Inclusion in the analysis was limited to participants with a Kellgren-Lawrence (KL) grading ≤ 3. Cartilage measures were calculated from scans acquired at the 24-month and 48-month visits using a validated convolutional neural network (NeuralSeg Ltd.). Dependent variables were change in cartilage thickness and T2 time in four regions of interest: lateral & medial weight-bearing femur, and lateral & medial tibia. Cumulative loading was defined by: Physical Activity Scale for the Elderly (PASE), and body mass index (BMI). An interaction term (PASE*BMI) was also used to represent cumulative loading. Multiple linear regression models (adjusted for baseline age, KL grade, cartilage measures, KOOS-Pain, and Charlson Comorbidity Index) were used to evaluate the relationship between cumulative loading and two-year changes in cartilage outcomes. Potential predictors were added in a forward fashion. For the secondary objective, the primary analysis was repeated stratified by PASE- and BMI-specific tertiles using ANOVA.

Results and Discussion

Mean (SD) age at baseline was 63.7 (8.7) years; 57% were female, KL grade 1 (n=42), KL grade 2 (n=204), KL grade 3 (n=166). Mean (SD) baseline values for predictors: PASE score 153 (78), and BMI 30.3 (4.5) kg/m^2. Cumulative loading was not associated with two-year changes in cartilage thickness in any region. Cumulative loading was associated with mean T2 time change, where PASE contributed to a model explaining medial femur T2 change ($F(7,401) = 9.042$, $R^2 = 0.121$, $p < 0.001$) and the PASE*BMI interaction term contributed to medial tibia T2 change ($F(9,398) = 7.148$, $R^2 = 0.120$, $p < 0.001$).

Two-year change in T2 values differed significantly between PASE tertiles only in the medial femur region ($p = 0.008$). The largest increase in T2 values occurred in the low PASE group 0.882 ms [95% CI 0.564, 1.200]. The low PASE group T2 values were greater compared to both the moderate (adjusted between group difference, 0.483 ms [95% CI 0.037, 0.929]) and high PASE group (adjusted between group difference, 0.712 ms [95% CI 0.250, 1.174]) (Figure 1).

When stratified by PASE and BMI, the highest cumulative loading group (high PASE/high BMI) had the greatest decreases in two-year change in T2 values in the medial tibia region compared to the other groups (-0.449 ms [95% CI -1.165, 0.267]), although differences between groups were not statistically significant.

Previous work found cumulative loading predicted loss of knee cartilage volume, but not cartilage thickness; we found no relationships with cartilage thickness.[2] Our analysis showed cumulative loading predicts T2 change over 2 years in knee OA. However, previous work in those without OA showed the greatest increases of T2 values occurred in participants in the highest and lowest 15% of PASE scores.[3] In an OA sample derived from another large cohort study, the highest and lowest cumulative loading groups (steps/day*BMI) also experienced worse knee cartilage morphology outcomes.[4] Future work should continue to explore the role of cumulative loading in cartilage quality and knee health.

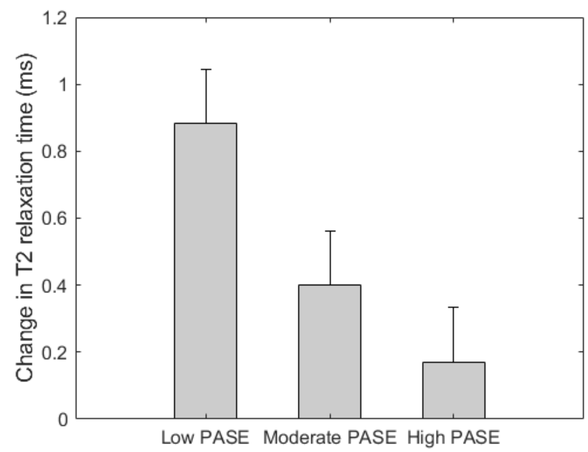

Figure 1: Two-year change in T2 relaxation time (ms) in the medial weight-bearing femur, stratified by tertiles of the Physical Activity Scale for the Elderly (PASE). Low PASE showed lengthened T2 times compared to moderate and high PASE.

Significance

Terms used to calculate cumulative loading, as well as the PASE*BMI interaction term were related with two-year change in T2 in the knee. Additionally, lower physical activity was related with worse cartilage quality.

Acknowledgments

NSERC Discovery (353715). MRM supported by STARS Mid-Career Award from The Arthritis Society/CIHR-IMHA.

References

[1] Timmins et al., 2017. *Am J. Sports Med* 45:6
[2] Brisson et al., 2017. *J. Orthop. Res.* 35:11
[3] Lin et al., 2013. *Osteoarthr. Cartil.* 21:10
[4] Voinier et al., 2020. *Arthritis Rheumatol.* 72:6

Impact of an Exercise Bout on Muscle Activation Patterns in Individuals with Knee Osteoarthritis

Skylar C. Holmes[1] and Katherine A. Boyer[1]
[1]University of Massachusetts, Amherst
email: scholmes@umass.edu

Introduction

Symptomatic knee osteoarthritis (KOA) leads to mobility deficits. Alterations in neuromuscular activation patterns and knee extensor weakness are thought to contribute to the reported mobility impairments in KOA [1]. Physical activity and exercise can have a beneficial effect for reducing impairment and improving function [2]. However, prolonged exertion may contribute to muscle fatigue and /or an exacerbation of pain [3]. Exertion and/or pain could contribute to alterations in muscle function including neuromuscular activation patterns and mobility on an acute basis. It is of interest to quantify if and how neuromuscular activation patterns may change in response to a prolonged walk and at varying speeds as increased muscle activation amplitude or prolonged activation may contribute greater joint loading [4]. We hypothesized that the magnitude of biceps femoris and gastrocnemius activation patterns would be greater with increased gait speed. We also hypothesized an increase in the magnitude and prolonged timing of muscle activation patterns in the vastus lateralis, biceps femoris and gastrocnemius in response to exercise in individuals with KOA.

Methods

Thirteen adults with symptomatic KOA (Age: 66±4.2 years, BMI: 25.3±3.8 kg/m^2, KOOS pain:69.9±16) participated in this study after completing informed consent approved by the University's IRB. Participants completed 5 overground walking trials at a preferred and 5 at a faster than preferred paces before and after a 20min treadmill walk (20MTW). Electrodes (Trigno Wireless, Delsys Natick MA) were placed on the vastus lateralis (VL), biceps femoris (BF), and medial gastrocnemius (MG).

Raw EMG data was band-pass filtered (20-500HZ), rectified, and filtered using a 4th order lowpass Butterworth filter. The average EMG from the stance phase of 5 overground walking trials at each pace was calculated for both pre and post 20MTW timepoints. PCA was used to determine the dominant patterns of muscle activation in each muscle We extracted the number of principal components (PC) needed to explain 90% of the variation in the original data for each muscle. Participant waveforms were projected onto each PC to calculate discrete PC scores. PCs were interpreted using a previously described technique of comparing the fifth and ninety fifth percentiles of PC scores. A 2 (time) x 2 (speed) ANOVA was used to compare PC scores between conditions (α= .05).

Results and Discussion

There was a significant main effect of time on the medial gastrocnemius for PC6 ($F(1,12)=4.99$, $p=.04$) and PC7 ($F(1,12)=6.19$, $p=.03$). Post hoc testing indicated scores were smaller for PC6 and larger for PC7 post 20MTW. PC6 represents the timing of the onset of MG activation in early stance. A decrease in PC6 suggests a delay in the onset of muscle activation post 20MTW. PC7 represents the location of peak amplitude in early stance. A larger PC7 score suggests increased MG activity during midstance post 20MTW. There were no significant main effects for speed for any PCs. However, there was a significant speed*time interaction for the biceps femoris for PC8 ($F(1,12)=18.3$, $p=.001$) and a significant main effect of time. PC8 represents the overall magnitude of the waveform for the duration of the stance phase. Post hoc testing indicated scores decreased for PC8 at preferred speed while PC8 scores increased at fast speed post 20MTW. This differential shift in PC8 suggests that fast speeds may require more effort to maintain than preferred speeds post exercise. Of note, there were no significant differences for any of the vastus lateralis PC.

The shift in timing of the medial gastrocnemius may be a strategy to help maintain load acceptance in early stance. The increase post treadmill of the BF could also be due to co-contraction which would be consistent with a pain response. This is further supported by participant self-reported pain data showing that all but one participant in this study developed pain post 20MTW, as measured by a verbal numeric rating scale throughout the 20MTW (Δpain: 2.62 ±2). The combined effects of exertion and pain may also be contributing to the alterations in muscle activation patterns post 20MTW.

Significance

Muscle activation patterns are altered in individuals with KOA after a prolonged walk. These neuromuscular alterations may be a compensatory strategy to maintain locomotion after exertion. Further research is needed to elucidate the respective influences of pain and exertion on muscle activation patterns in individuals with KOA.

Acknowledgments

Funding provided by a University of Massachusetts-Amherst hMRC Pilot Grant.

References

[1] Ling 2007.Osteoarthritis Cartilage.2007 Oct;15(10):1134-40.
[2] Henriksen et al., J Comp Eff Res. Jul 2016;5(4):417-31.
[3] Focht et al., Ann Behav Med. 2002;24(3):201-10.
[4] Rutherford et al., J Electromyogr Kinesiol. Jun 2013;23(3): 704-11.

Muscle	PC	Pre Score	Post Score	Eigenvalue (%)
MG	6	0.01	-0.13	4.46
MG	7	-0.17	0.10	2.96
BF	8	0.19	-0.20	3.64

Table 1: Mean PC Scores for the Preferred Pace and Eigenvalues for the biceps femoris (BF) and the medial gastrocnemius (MG). Eigenvalue represents the % of total variance explained by the PC.

KINEMATIC AND KINETIC ASYMMETRIES IN INDIVIDUALS WITH UNILATERAL, MILD-TO-MODERATE KNEE OSTEOARTHRITIS DURING GAIT

Carson Halliwell[1*], Derek Rutherford[1,2], Rebecca Moyer[1]
[1]School of Physiotherapy, Faculty of Health, Dalhousie University, Halifax, B3H 4R2, Canada
[2]School of Biomedical Engineering, Faculty of Engineering, Dalhousie University, Halifax, B3H 4R2, Canada
Email: carson.halliwell@dal.ca

Introduction

Knee osteoarthritis (OA) is a leading cause of functional disability worldwide. Functional decline and increased pain have been associated with asymmetrical lower limb movement patterns as a strategy to reduce joint symptoms[1,2]. These movement compensations in the affected limb have been shown to influence loading patterns in joints of the contralateral limb, which may contribute to accelerated cartilage degeneration in the knee and disease progresson[3,4]. Currently, the magnitude of kinematic and kinetic inter-limb asymmetry between the symptomatic and contralateral knees in individuals with unilateral mild-to-moderate knee OA during walking is not well understood. Therefore, the purpose of the proposed work is to examine sagittal and frontal plane kinematic and kinetic inter-limb asymmetry between symptomatic and contralateral knees in individuals with unilateral mild-to-moderate knee OA.

Methods

80 participants (37F, 43M) with unilateral mild-to-moderate knee OA underwent 3D gait analysis using a full-body passive reflective marker set during treadmill walking at a self-selected speed. Rigid plastic clusters containing four retroreflective markers were placed over the trunk, pelvis, and bilaterally over the lateral femur, lateral shank, and feet. Individual retroreflective markers were placed bilaterally over prominent bony landmarks. Participants walked for six-minutes and during the sixth minute a 20-second data collection was recorded. Sagittal and frontal plane knee joint angles were calculated using a Cardan rotations, and knee joint moments were calculated using an inverse dynamics model, with knee adduction moment (KAM) and vertical ground reaction force (VGRF) impulses calculated using trapezoidal integration. Symmetry indices (SI) were calculated for all metrics[5], where a positive SI indicates symptomatic > contralateral knee asymmetry and a negative SI indicates contralateral > symptomatic knee asymmetry. Paired t-tests were used to assess for differences in sagittal and frontal plane knee joint ranges of motion (ROM), moments and impulses between the symptomatic and contralateral limbs, and SI were used to assess the magnitude of inter-limb asymmetry. Due to the number of comparisons (7), a Bonferroni correction was applied, with $p<0.007$ being considered significant.

Results and Discussion

The symptomatic knee demonstrated significantly reduced ROM during early and late stance compared to the contralateral knee ($p<0.001$), with inter-limb asymmetry in the sagittal plane ranging from -15% to -23% (Figure 1). Total frontal plane ROM was not found to be statistically significant between the symptomatic and contralateral knees ($p>0.05$), with inter-limb asymmetry in frontal plane ROM being -4.5% (Figure 1). The symptomatic knee demonstrated significantly reduced sagittal plane knee moment range compared to the contralateral knee ($p<0.001$), with inter-limb asymmetry being -16.3% (Figure 1). No differences between peak KAM or KAM impulse were found between the symptomatic and contralateral knees ($p>0.05$), with inter-limb asymmetry ranging between 0.49% and 1.0% (Figure 1). The symptomatic knee demonstrated significantly reduced VGRF impulse compared to the contralateral knee ($p<0.001$), with inter-limb asymmetry being -2%.

Results indicate that sagittal plane motions and moments are the primary measures that differ between the symptomatic and contralateral knees in individuals with unilateral mild-to-moderate knee OA, demonstrating reduced dynamic ROM and loading in the symptomatic knee. In the frontal plane, minimal differences and a high amount of symmetry was noted between knees. This finding may have implications on contralateral knee OA development as elevated KAM values compared to asymptomatic knees have been found to be significantly associated with development and progression of knee OA[3].

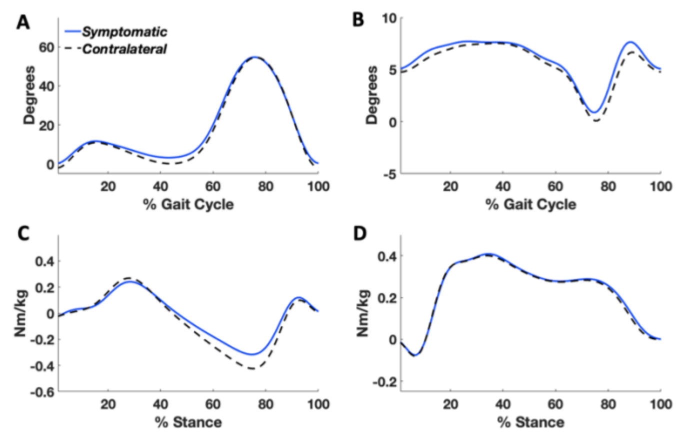

Figure 1. Ensemble average waveforms for sagittal (A) and frontal (B) plane knee ranges of motion, and sagittal (C) and frontal (D) plane knee moments.

Significance

To our knowledge, this is the first study to comprehensively examine kinematic and kinetic inter-limb asymmetry between symptomatic and contralateral knees in individuals with unilateral mild-to-moderate knee OA. This study represents a first step in assessing the importance of inter-limb asymmetry and its implications toward contralateral knee OA development. Future work should investigate inter-limb asymmetry in healthy controls to better interpret the clinical significance of current findings.

Acknowledgments

We would like to acknowledge the Nova Scotia Health Research Foundation for funding this project.

References

[1] Kim et al, 2021. *Phys Ther Korea*. 21(1); [2] Mills et al., 2013. *Arch Phys Med Rehab*. 94(11); [3] D'Souza et al., 2021. *Osteoarthr Cartil*; [4] Teoli et al., 2021. J Orth Res; [5] Herzog et al., 1989. *Med Sci Sports Exerc*. 21(1).

Effects of actuation timing and magnitude of a semi-rigid hip exoskeleton on metabolic cost

Arash Mohammadzadeh Gonabadi[1], Prokopios Antonellis[1,2], Sara Myers[1,3], Iraklis Pipinos[3], and Philippe Malcolm[1]
[1]Department of Biomechanics, University of Nebraska at Omaha, Omaha, NE USA
[2]Department of Neurology, Oregon Health & Science University, Portland, OR USA
[3]Department of Surgery, Veterans Affairs Medical Center and University of Nebraska Medical Center, Omaha, NE USA
Email: *amgonabadi@unomaha.edu

Introduction

Exciting developments in soft assistive robots - better known as exosuits - enabled devices that can assist different joints and activities [1,2]. Compared to rigid exoskeletons, soft exosuits provide greater freedom of movement. However, soft exosuits often cannot apply the same torque magnitudes as rigid exoskeletons [3] since they rely on friction with the skin to remain anchored. Semi-rigid exoskeletons could combine some advantages of rigid and soft approaches [4]. In a previous abstract, we describe the development of a semi-rigid approach for assisting the hip during walking. Although different groups have already investigated optimal actuation patterns for assisting the hip [2,5], we do not yet know the optimal assistance pattern for assisting with a semi-rigid device. The purpose of this study was to investigate the effects of timing and magnitude of assistance from a semi-rigid hip exoskeleton.

Methods

We recruited ten healthy young adults. We programmed (inspired from our previous study [6]) the semi-rigid hip exoskeleton to apply a sinusoidal force profile with extension moment starting from 90% of the stride cycle until the beginning of the next stride. A frontal spring also applied a small force to keep the thigh segments in place and assist hip flexion. We tested ten conditions that were combinations of 5 different end-timings, ranging from 21% to 49%, and 2 different moment magnitudes ranging from 0.06 to 0.12 Nm.kg^{-1} (Figure 1). The participants also walked in two reference conditions: a condition without actuation and a condition without the exoskeleton. We measured metabolic rate using indirect calorimetry and obtained steady-state values using an exponential fitting procedure [7].

Results and Discussion

In the highest magnitude setting, we found a U-shaped trend in metabolic cost versus end-timing. The greatest reduction in metabolic cost occurred in the condition with an end-timing of 42%. In the lower magnitude setting, however, metabolic cost showed a monotonic decreasing trend versus end-timing with the greatest reduction in the last timing condition. In further statistical analyses, we will evaluate if there is an interaction effect between magnitude and the second-order effect of timing. The majority of conditions resulted in a lower mean metabolic rate versus the unpowered condition. However, all conditions increased metabolic rate compared to walking without an exoskeleton. This is due to the device's current design (5.77 kg), which has not yet been optimized for minimizing weight.

Significance

The results show a semi-rigid hip exoskeleton can alter metabolic rate. However, to produce a net assistive effect, it will be necessary to design a lighter, more conforming device. In both actuation magnitude levels, the optimal end-timing was close to the maximum range, similar to findings from another study with human-in-the-loop optimization of a soft hip exosuit [2]. This could indicate that the optimal timing with a semi-rigid device is not very different from a fully-soft prototype.

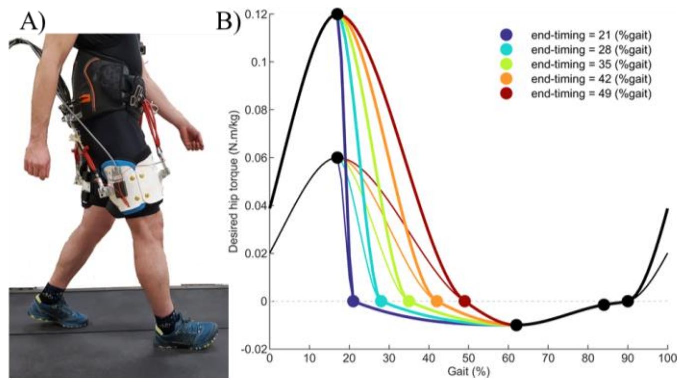

Figure 1: Methods. A) Device. B) Desired actuation profiles.

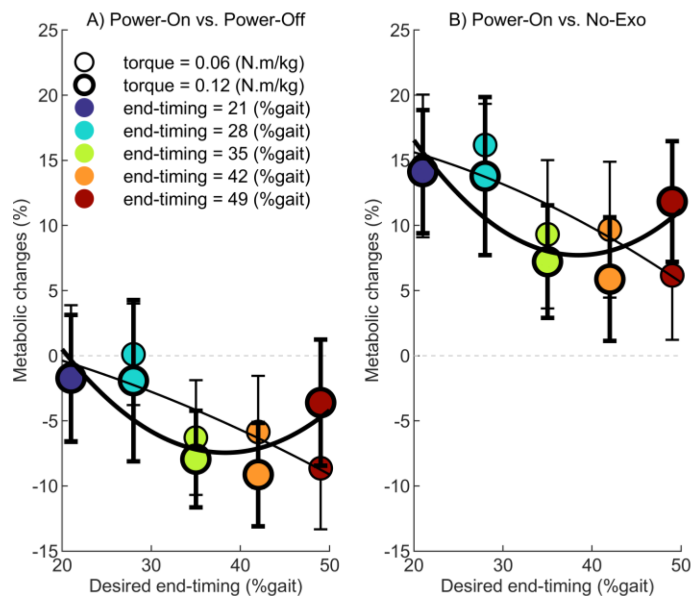

Figure 2: Metabolic changes in Power-on versus Power-off and No-Exo conditions.

Acknowledgments

NIH P20GM109090 and Graduate Research and Creative Activity Award (GRACA) for Arash Mohammadzadeh Gonabadi.

References

[1] Schmidt, K. *et al. Front. Neurorobot.* 11, (2017)
[2] Ding, Y. *et al. Sci. Robot.* 3, 1–9 (2018)
[3] Bryan, G. M. *et al. Int. J. Rob. Res.* 40, 722–746 (2021)
[4] Zhang, Y. *et al. IEEE Robot. Autom. Lett.* 6, 8514–8521 (2021)
[5] Young, A. J. *et al. Front. Bioeng. Biotechnol.* 5, 1–11 (2017)
[6] Gonabadi, A. M. *et al. IEEE Trans. Neural Syst. Rehabil. Eng.* 28, 1353–1362 (2020)
[7] Selinger, J. C. *et al. J. Appl. Physiol.* 117, 1406–1415 (2014)

CONTINUOUS TESTING OF SONOMYOGRAPHY AS A CONTROL PARADIGM FOR UPPER LIMB PROSTHESES

Erica L. King[1,2*], Susannah M. Engdahl[1,2], Samuel A. Acuña[1,2], Ahmed Bashatah[1,2], Siddhartha Sikdar[1,2]
[1]Department of Bioengineering, George Mason University, Fairfax, VA, USA
[2]Center for Adaptive Systems of Brain-Body Interactions, George Mason University, Fairfax, VA, USA
email: eking20@gmu.edu *corresponding author

Introduction

Sonomyography (SMG) is a novel ultrasound-based prosthesis control paradigm used for predicting grasps by mapping the different active muscle compartments to specific hand motions [1]. However, prior offline testing of classification performance has been conducted in laboratory settings, which do not involve real-world activities such as reaching. Arm movement may impact classification performance because the user can recruit different combinations of muscles in the residual limb as joint angles change, even if they are performing the same grasp [2]. The goal of this study was to determine whether performance of functional tasks degraded during continuous use of an SMG-controlled prosthesis.

Methods

A 30-year-old female with congenital bilateral limb absence wore thermoplastic test sockets connected to TASKA Hand. Ultrasound images were collected using a clinical transducer (Terason uSmart 3200T) mounted on the socket via a custom 3D printed bracket. Images were transferred to a PC in real-time using a USB-based video grabber.

To collect data for training a linear discriminant analysis classifier, the participant moved her arms through a pre-defined twenty second dynamic pattern the covered varying vertical heights and horizontal widths. While moving, she produced and maintained a set of muscle contractions at a comfortable level. Each contraction was mapped to a specific grasp that the TASKA hand then produced. *Tripod* was initiated by wrist flexion, index finger *point* was initiated by wrist extension, and *rest* was initiated by a relaxed muscle state.

After training, the participant wore the prosthesis for three hours without retraining the classifier. Three functional tests were performed in random order every thirty minutes. Box and Blocks (BBT) performance was measured by the number of blocks transferred over a barrier in one minute. Targeted Box and Blocks (tBBT) performance was measured by the time required to move 16 blocks over a barrier into predetermined positions. Rainbow task performance was measured by the time required to move blocks located at various heights from a white board to a box at waist height. During the breaks between functional testing, the subject performed pre-determined tasks that increased in intensity over time from light (e.g., typing) to strenuous (e.g., lifting 1.86 kg. bucket).

An additional outcome measure was used to characterize the efficiency of the classifier during each test. Transient classification bouts were defined as the prediction of the same grasp for less than five consecutive frames. Few transient bouts indicate high efficiency. A linear regression model was used to indicate any changes in outcomes measures over the testing period (α=0.05).

Results and Discussion

Socket wear time had few negative effects to functional task performance (Fig 1). The time of task completion significantly decreased for the Rainbow task on the left arm (p = 0.038) and tBBT on the right arm (p = 0.011). This decrease can be due to practice over the testing period. Additionally, the number of transient bouts significantly increased for the Rainbow task on the left arm (p = 0.027) which may be due to participant fatigue.

Significance

SMG can be used continuously as a prosthesis control paradigm without the need of retraining for several hours.

Acknowledgments

This study was supported by NIH grant number U01EB027601. Thanks to Brian Monroe for assisting with socket fabrication.

References

[1] Sikdar et al., 2014. *Neural Syst. Rehabil. Eng.* 22, 69–76.
[2] Fougner et al., 2011. *Neural Syst. Rehabil. Eng.* 19, 644-651

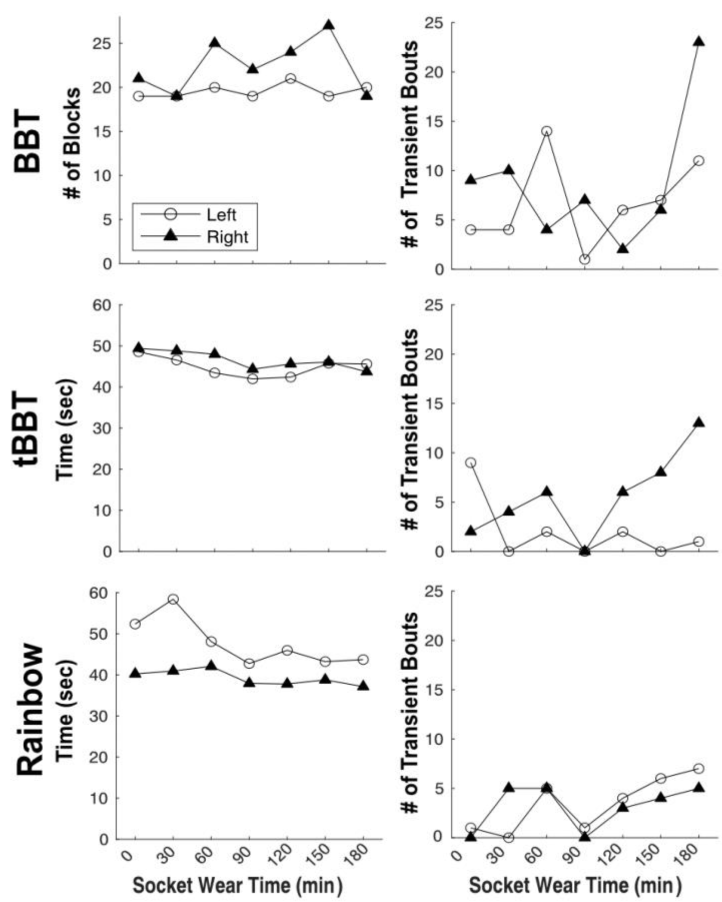

Figure 1: Trends in outcome measures for Box and Blocks (BBT), Targeted Box and Blocks (tBBT), and Rainbow tasks over time for both arms.

The Effect of Ankle Foot Orthoses on Ground Reaction Forces in Patients with Peripheral Artery Disease

Salamifar, Z[1*], Fallahrafti, F[1], Pipinos, I[2,3], Johanning, J[2,3], Rahman, H[1,2], Hassan, M[1,2], Myers, SA[1,2]
[1] Department of Biomechanics, University of Nebraska at Omaha, Omaha, NE US
[2] Department of Surgery and Research Service, Omaha Veterans' Affairs Medical Center, Omaha, NE USA
[3] Department of Surgery, University of Nebraska Medical Center, Omaha, NE USA
email: ssalamifar@unomaha.edu

Introduction

Peripheral arterial disease (PAD) is caused by atherosclerotic blockage of the arteries in the legs. Over 236 million people in the world live with PAD[1,2]. Intermittent claudication (IC) is the most common PAD symptom that includes muscle pain, cramping, and/or aching induced by physical activities and relieved with rest[3]. PAD impacts gait patterns and IC requires patients to stop and rest[4]. Patients with PAD have rapid ankle plantar flexion after heel contact which decreases optimal energy transfer[5]. An ankle-foot orthosis (AFO) is an assistive device made of carbon-composite material that improves gait in patients with neurological conditions. AFOs could help patients with PAD to improve ankle kinetics during walking[6]. The purpose of this study was to determine the impact of AFOs on ground reaction forces during walking in patients with PAD.

Methods

Fourteen patients with PAD were assessed before and after a three-month intervention with AFO (Age: 72.57±6.48 years, height: 172.46±8.29 cm, and body mass: 92.04±21.03 kg). Ground reaction forces data were recorded while participants walked with AFO (AFO) and without AFO (NAF) over the force platforms (Figure 1). Five successful trials (i.e., heel strike and toe-off events were located within the borders of the force platform) in each condition were completed. One minute of rest was required between each walking trial to prevent the onset of intermittent claudication. Peak values from anterior-posterior, medial-lateral, and vertical ground reaction forces were computed. Propulsion impulse and braking impulse were normalized based on the body weight. For the statistical analysis, independent 2×2-repeated-measure-ANOVAs ($p<0.05$) were used to determine significant differences due to intervention (pre- and post-3 months) and condition (AFO and NAF).

Figure 1. Participants walk overground with and without AFO until 5 successful heel strike and toe-off events were recorded.

Results and Discussion

Anterior/Posterior Ground Reaction Force

Anterior-posterior braking force was significantly reduced in the AFO condition compared to NAF (p=0.037). The 3-month intervention led to a significant reduction in the anterior-posterior normalized braking impulse when walking with AFO compared to NAF(p=0.032), however, there were no significant difference between the two conditions pre intervention. In a sub analysis of walking speed, we observed slower walking with AFO compared to NAF condition. Walking slower with AFO could be a potential reason for reducing braking impulse. Normalized propulsion impulse in walking with AFO was reduced compared to NAF, which could also be due to walking slower while wearing the AFO (p=0.006). The reduction in braking and propulsion impulses are consistent with the documented reductions in leg muscle strength[7]. Normalized propulsion impulse was significantly reduced during walking with AFO compared to NAF (p< 0.001). Patients with PAD have reduced propulsion force compared to healthy older adults, and the AFO led to further reduction.

Vertical Ground Reaction Force

There was a significant interaction between condition and intervention. Pre intervention, vertical ground reaction force in mid-stance with AFO was greater than NAF, however, post 3-months, the AFO condition had greater mid-stance force than the NAF condition (p=0.036). For vertical ground reaction force, initial and secondary peaks were significantly greater during AFO versus NAF condition (p=0.003 and p=0.002, respectively). Previous studies found patients with PAD have less fluctuation of the center of mass compared to healthy older adults[6]. Therefore, wearing AFOs improved vertical fluctuation.

Medial-Lateral Ground Reaction Force

Peak lateral ground reaction force after 3-month AFO intervention significantly increased (p=0.025). Increasing lateral ground reaction force by using AFOs is indicative of improved synchronization of hip adductors at heel contact during weight acceptance in patients with PAD[7].

Significance

AFOs enhanced vertical and lateral ground reaction forces, moving patients with PAD back towards the patterns of healthy older individuals without PAD. Additional studies of how AFOs and other assistive walking devices impact gait, are needed to understand the potential for assistive device interventions to help patients with PAD.

Acknowledgments

The National Institutes of Health (R01 HD090333) and Merit Award (I01RX003266) from the US Department of Veterans Affairs, Rehabilitation Research and Development Service funded this work.

References

1. Rosenbloom MS, et al.2000. Arch Surg 1988; 123:86770.
2. Kim, M, et al. 2021. Int. J. Environ *18*(20), 10941.
3. Koutakis, P, et al. 2010. *J. Vasc. Surg. Cases*, *51*(1),80.
4. Pietraszewski, et al. 2019. Biomed Res. Int, 2019, 1–9.
5. McCamley, et al. 2017*Gait & posture*, *57*, 258–264.
6. Scott-Pandorf,2007. J. Vasc. Surg. Cases. *46*(3), 491.
7. Schieber, M. N. et al *J. Vasc. Surg*, *71*(2), 575–583

EVALUATION OF HIGH DENSITY SURFACE ELECTROMYOGRAPHY FOR PROSTHESIS CONTROL

Fred Christensen, Corey A. Pew
Department of Mechanical and Industrial Engineering, Montana State University, Bozeman, MT
Email:*Corey.Pew@montana.edu

Introduction

To assist amputees in regaining the highest level of function and quality of life, surface electromyography (sEMG) is used for the control of advanced prosthetic devices [1]. However, skin impedance, motion artifacts, and sensor displacements can introduce error to standard sEMG measurements. Recently, high density surface electromyography (HDsEMG) has shown potential to mitigate barriers to using sEMG as a reliable control method [2]. This project seeks to evaluate what improvements HDsEMG might provide for advanced prosthesis control.

Methods

Three subjects (2 Male, mean age 35, SD +/-5 years) were recruited for an MSU IRB approved protocol. Standard, bipolar sEMG sensors (Delsys Avanti) were compared to 16-channel HDsEMG sensors (Delsys Maize) (Figure 1) over the knee extensors (Rectus Femoris, Vastus Laterallus) and flexors (Semitendinosus, Bicep Femoris). Sensor signals were evaluated in both optimal and displaced (1 cm distally from optimal placement) positions, to simulate prosthesis pistoning. Participants performed activities of daily living (straight walking, stair ascent/descent, ramp ascent/descent, left and right turns, sit to stand, stand to sit, and body weight squats). Each task was repeated three times for each sensor condition.

Figure 1: Standard bipolar sEMG sensor (Top) compared to HDsEMG array (Bottom).

Evaluation of signal quality utilized signal to noise ratio (SNR), a measure of signal strength where a greater SNR indicates a stronger signal in relation to the background noise [3]. The effect of sensor displacement (optimal vs displaced) was compared by percent change in the root mean square (RMS) of the rectified signal. RMS denotes the average amplitude of a signal. Thus, a smaller RMS denotes a signal with weaker strength. Three different sensor output modes were analysed: singular output signal from the Standard sEMG (Standard), the single channel of the HDsEMG with the highest calculated SNR of the 16 channels (Best), and a composite signal made from a time series average of all 16 HDsEMG signals (Composite). All collected signals were rectified and filtered using a 4th order Butterworth filter. The difference in SNR and RMS between optimal and displaced sensor conditions were determined for each activity and muscle combination. These initial results compared the variations between sensor outputs and positions with data from all muscles and activities combined.

Results and Discussion

When comparing SNR between the optimal and displaced conditions the Best signal outperformed the Standard signal ($p<0.01$) and Composite signal ($p<0.01$) and the Composite signal outperformed the Standard signal ($p<0.01$) (Figure 2, Top). No difference was found between optimal and displaced conditions within signal types.

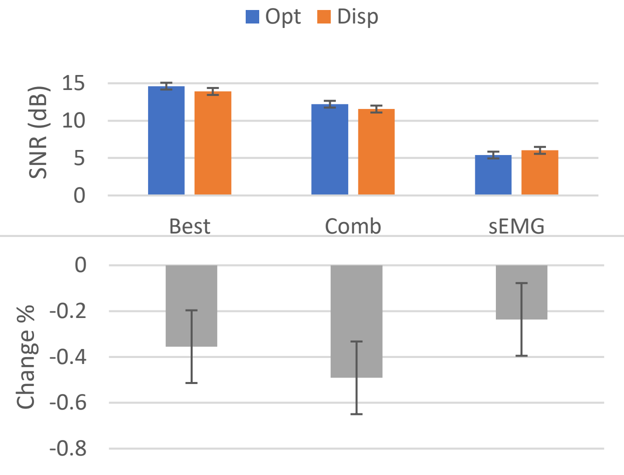

Figure 2: [Top] Mean +/- SD SNR values across all activities and muscles for Best, Combined (Comb) and sEMG signals (sEMG) in the optimal (Opt) and displaced (Disp) conditions. [Bottom] Percent change in RMS from optimal to displaced conditions.

No difference was found between the percent change in RMS values ($p=0.50$) (Figure 2, Bottom). All signal conditions showed a decrease in signal amplitude, meaning that the signals became weaker in the displaced condition. The trend of greater percent changes in Best and Combined signals could come from the processing methods. The Best Signal method did not account for change in electrode location due to condition change, and Composite methods did not consider the quality of individual electrode channels. Thus, both sensor types lose signal strength as the sensor becomes displaced, but improved processing methods could limit this effect for HDsEMG sensors.

Both Best and Combined Signals displayed higher SNR levels than the Standard signal across both sensor placements. However, more advanced processing methods are needed than those used on this data-set to achieve this technology's full potential and generate the best signal. Future work will investigate more measures of signal quality and advanced multi-channel signal processing to filter out noise and crosstalk.

Significance

Due to different sources of noise in EMG readings at different SNR levels, SNR levels above 10 dB can be considered clean of several common noise sources [4]. The HDsEMG sensors exhibited greater than 10 dB SNR values in all conditions. Thus, HDsEMG shows promises to provide improved signal quality for advanced prosthesis control.

Acknowledgments

Thank you to Kendall Larson Matthew Robinett.

References

1) Young et al,. *J. Neural Eng.,* 2014;
2) Martinez-Valdes et al, *Clinical Neurophysiology.,* 2016
3) Sinderby et al., *J Apl Phys*., 1995;
4) Fraser et al., *IEEE Trans on Inst and Meas.,* 2014

EFFECTS OF GAIT VELOCITY ON MECHANICAL COST-OF-TRANSPORT WHEN WEARING A CUSTOMIZED PASSIVE-DYNAMIC ANKLE-FOOT ORTHOSIS

Corey A. Koller[1,2], Luke Nigro[3], Jacob Skigen[4], Jason Wilken[5], Darcy S. Reisman[1,6], and Elisa A. Arch[1,2]
[1]Biomechanics and Movement Science Interdisciplinary Program, University of Delaware, Newark, DE, USA
[2]Department of Kinesiology and Applied Physiology, University of Delaware, Newark, DE, USA
email: ckoller@udel.edu

Introduction

Individuals post-stroke are commonly prescribed passive-dynamic ankle-foot orthoses (PD-AFOs) to aid in the control of shank forward rotation during mid-to-late stance due to plantar flexor (PF) weakness [1]. PD-AFO bending stiffness is a key orthotic characteristic that can assist the PFs [2] by providing the resistance needed to control shank forward rotation [3]. We developed a prescription model that can quantitatively prescribe PD-AFO bending stiffness based on an individual's level of PF weakness [3]. A baseline self-selected gait velocity, determined while walking without wearing an orthosis (No AFO velocity), is used in the PD-AFO prescription to calculate the targeted peak plantar flexion moment [3]. However, gait velocity has a direct effect on ankle stiffness [4] and individuals can walk at a variety of velocities throughout their daily lives. It is unknown how different velocities affect gait function, such as the mechanical cost-of-transport (COT), when walking with a PD-AFO stiffness-tuned for a specific velocity. This study aimed to quantify and compare post-stroke total mechanical COT while wearing a PD-AFO across three gait velocities: the No AFO velocity and the self-selected gait velocities determined while wearing the SOC AFO (SOC AFO velocity) and the PD-AFO (PD-AFO velocity). We hypothesized that 80% of individuals would significantly decrease total mechanical COT while wearing their PD-AFO at the No AFO velocity, which is the velocity used to tune PD-AFO stiffness, compared to at the SOC AFO and PD-AFO velocities.

Methods

Eight individuals greater than six months post-stroke underwent an instrumented gait analysis without wearing an orthosis at the No AFO velocity (male: 3, age: 65.1±6.9yrs, mass: 82.4±14.8kg, height: 1.72±0.1m). From these data, a PD-AFO was stiffness customized and manufactured for each participant [4]. After four-weeks of PD-AFO use, each participant underwent another gait analysis while wearing their PD-AFO at three self-selected gait velocities each determined via a 10 Meter Walk test under a different orthosis condition - No AFO, SOC AFO, and PD-AFO. From the gait analysis data, total mechanical COT was calculated in Visual 3D for each participant and condition. Simulation modelling analysis (SMA) was used to determine if a significant difference was seen in total mechanical COT while wearing the PD-AFO at the No AFO velocity compared to the SOC AFO and PD-AFO velocities for each participant [5].

Results and Discussion

Average gait velocities were 0.56±0.2m/s, 0.68±0.3m/s, and 0.80±0.3m/s at the No AFO, SOC AFO, and PD-AFO velocities, respectively. Minimal changes in COT were seen in all but one participant while wearing the PD-AFO at the No AFO velocity compared to at the SOC AFO velocity. Compared to at the PD-AFO velocity, significant, although sometimes conflicting, differences in COT were seen across participants (Fig. 1). Thus, both hypotheses were refuted.

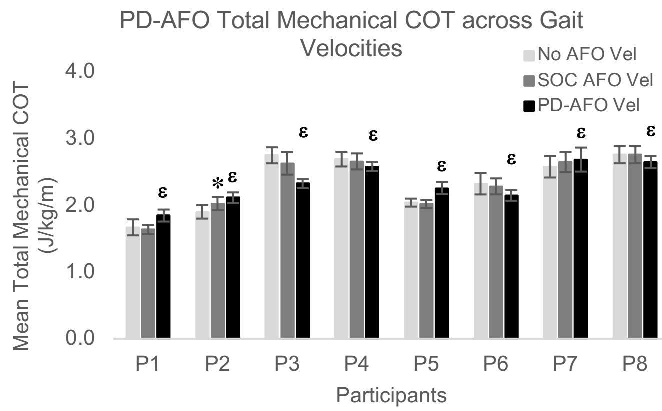

Figure 1: Total COT while wearing the PD-AFO at each gait velocity. Note: significant difference in COT at No AFO velocity compared to at SOC AFO velocity* and at PD-AFO velocity$^{\varepsilon}$ based on SMA ($p < 0.05$).

Significance

The minimal changes seen in COT while wearing the PD-AFO at the No AFO vs. SOC AFO velocities may be due to the small changes in velocity (averaged 0.12 m/s, less than one MDC) between conditions. Compared to at the PD-AFO velocity, four of the five participants (P3, P4, P6, & P8) whose No AFO velocity was < 0.6 m/s significantly increased COT and all three participants (P2, P5, & P7) whose No AFO velocity was > 0.6 m/s significantly decreased COT. We theorized that those who walked at slower No AFO velocities were prescribed a PD-AFO that was too stiff, thus inhibiting the initial dorsiflexion of the PD-AFO. When walking faster, they may have had greater angular momentum to initiate and then continue dorsiflexing the PD-AFO, thus utilizing the PD-AFO more and experiencing a reduced COT. In contrast, those who walked at a faster No AFO velocity may have been able to utilize the PD-AFO at the velocity for which it was prescribed and walking faster resulted in a higher COT. These results suggest there is an energetic optimal bending stiffness and/or gait velocity for individuals post-stroke and this interaction should be investigated further to optimize PD-AFO prescription.

Acknowledgments

UD CCM and IPO for helping manufacture and prepare the PD-AFOs. This work was supported by USAMRAA through the Orthotics & Prosthetics Outcomes Research Program under Award No. W81XWH-18-1-0502. Opinion, interpretations, conclusions, and recommendations are those of the author and not necessarily endorsed by USAMRAA.

References

[1] Perry J & Burnfield JM. (2010). *Gait Analysis: Normal & Pathological Function*; Slack Inc.
[2] Bregman DJJ et al. (2009). *Gait Posture*, **30**: 144-149.
[3] Koller et al. (2021). *Prosth Orthot Int*. **45**: 313-321.
[4] Collins et al. (2018). *Gait Posture*. **62**: 311-316.
[5] Borckardt et al. (2014). *Neuropsy Rehab*. **24:**492-506

Session 3

Tuesday August 23, 2022

1:30pm – 3:00pm

S5 - ASB Symposium: Running

O3.1 – Ergonomics & Occupational Biomechanics 2

O3.2 – Locomotion 1

O3.3 – Neuroscience and Motor Control

O3.4 – Tissue Mechanics 1

COMPARISON OF TYPE OF RUNNING SESSIONS FOR FEMALE HIGH SCHOOL CROSS-COUNTRY RUNNERS

Micah C. Garcia[1*] and David M. Bazett-Jones[1]
[1]The University of Toledo, Toledo, OH, USA
email: micah.garcia@rockets.utoledo.edu

Introduction

Running speed is typically manipulated to dictate the intensity of the running session. In the lab, running at faster speeds elicits an increase in cadence and step length [1]. While these lab-based studies have simulated different run types (e.g., easy, typical, hard), the running conditions are often short in duration and may not fully represent these different types of running sessions. Therefore, the primary purpose of this study was to compare running and physiologic parameters for different types of running sessions in the wild for high school cross-country runners during a competitive interscholastic season. Our secondary aim was to compare running parameters in the lab with running parameters during a typical running session in the wild.

Methods

We recruited adolescent runners during the fall 2020 cross-country season. Participants were loaned a GPS watch (Garmin Forerunner 45s) and recorded each running session during the season with the watch. Participants self-reported the type of run (recovery/easy, tempo/speed/fartlek, set distance, set time, hills, track workout, race) and session rating of perceived exertion (sRPE) [2] after each running session with an electronic journal.

We extracted speed, distance, cadence, step length, and average heart rate (HR) from the watch and matched with the self-reported run type and sRPE for all recorded running sessions during the season. Run types were collapsed into three groups: 1) *easy* (recovery/easy), 2) *typical* (set distance, set time), or 3) *hard* (tempo/speed/fartlek, track workout).

At the conclusion of the cross-country season, participants visited our motion analysis lab and underwent a 3-dimensional running analysis. Following a 5-minute self-selected treadmill warmup, participants ran over a 20 m runway with embedded force plates (sampling rate = 1800 Hz) at a comfortable speed that was "not too hard or too easy." We identified initial contact and toe-off events when the vertical force exceeded and dropped below 20 N, respectively, and calculated cadence and step length according to these events.

For our primary aim, we used repeated measures ANOVA to compare the different types of running sessions in the wild. We performed post-hoc pairwise comparisons with Bonferroni corrections when significant differences were found. For our secondary aim, we used paired t tests to compare running parameters between typical running sessions in the wild and the *lab* session. We set statistical significance at $p \leq .05$.

Results and Discussion

We included 13 female runners in our analysis (age = 15.8 ± 1.2 years, BMI = 19.7 ± 2.3) who completed at least one run for each type of running session and their lab visit. When comparing the different types of running sessions in the wild, we found significant differences in running speed ($p = .01$), distance ($p < .01$), step length ($p = .03$), average HR ($p < .01$), and sRPE ($p < .001$; Table 1). Pairwise comparisons showed that running speed was significantly slower for *easy* sessions compared to *typical* ($p = .03$) and *hard* sessions ($p = .01$); distance was significantly shorter for *hard* sessions compared to *easy* ($p < .01$) and *typical* sessions ($p < .001$) as well as *easy* sessions compared to *typical* sessions ($p < .01$); step length was significantly shorter for *easy* sessions compared to *hard* sessions ($p = .01$); average HR was significantly lower for *easy* sessions compared to *typical* ($p < .01$) and *hard* sessions ($p = .05$); and sRPE was significantly lower for *hard* sessions compared to *easy* ($p < .001$) and *typical* sessions ($p < .001$) as well as *easy* session compared to *typical* sessions ($p < .001$). When we compared *typical* sessions in the wild to the *lab* session, running speed and step length were significantly faster and longer for the *lab* session ($p \leq .02$; Table 1).

Significance

We found differences in running and physiologic parameters among the different types of running sessions in the wild. While *easy* runs were found to be less demanding than *typical* runs, there were fewer differences between *hard* runs and *typical* runs. Adolescent long-distance runners also appear to rely more on increasing step length than cadence for *hard* running sessions. Longer step lengths are associated with higher impact forces [3], which may place the runner at a higher risk of sustaining a running-related injury.

We also found that adolescent runners' self-selected speed in the lab was significantly faster than their *typical* running speed in the wild. This difference was due to longer step lengths as cadence was similar between the *lab* and *typical* running sessions. To improve the ecological validity of overground lab-based running studies, researchers should consider matching participant's running speed to a self-reported typical running speed.

References

[1] Fukuchi et al., 2018, *PeerJ.*
[2] Borg, 1998.
[3] Heiderscheit et al., 2011, *MSSE*.

Table 1. Comparisons for running parameters among running session types in the wild and in the lab.

Variable	Easy	Typical	Hard	Lab	p
Running speed [m/s]	3.25 ± 0.28	3.35 ± 0.34	3.45 ± 0.30	3.73 ± 0.45	.007 †‡
Distance [km]	7.4 ± 1.3	11.1 ± 3.8	5.1 ± 2.0	---	<.001 *†‡
Cadence [spm]	167 ± 7	169 ± 8	167 ± 8	166 ± 9	.21
Step length [m]	1.16 ± 0.12	1.18 ± 0.14	1.22 ± 0.13	1.36 ± 0.16	.001 †§
Average HR [bpm]	159 ± 11	167 ± 13	166 ± 10	---	.02 *
sRPE	2.7 ± 1.2	4.2 ± 1.2	6.1 ± 1.4	---	<.001 *†‡

Significance ($p \leq .05$): *easy vs typical, †easy vs hard, ‡typical vs hard, §typical vs lab

FOOT ARCH FUNCTION IN RUNNING: CHANGES DUE TO THE WINDLASS MECHANISM AND FOOT STRIKE PATTERN

Daniel J. Davis* and John H. Challis
The Biomechanics Laboratory, The Pennsylvania State University, University Park, PA
email: *djd426@psu.edu

Introduction

Arch stiffness has been proposed as an evolutionary advantage and driver of *Homo sapien* bipedalism. Since 1954, the concurrent raising of the foot's arch with metatarsophalangeal joint (MTPj) dorsiflexion in late stance (i.e., the windlass mechanism) has been touted as evidence that this mechanism further increases arch stiffness [1]. Recent evidence, however, has called into question this stiffening function of MTPj dorsiflexion [2]. When the foot was vertically loaded by Welte et al. (2018) it elongated more and had increased energy absorption and dissipation with the MTPj dorsiflexed compared with a plantarflexed position.

The purpose of the current study was to measure the influence of increased MTPj dorsiflexion in running for two different foot strike patterns. Should increased dorsiflexion stiffen the arch (as purported by the windlass mechanism), there should be less arch extension in midstance. Additionally, a relationship between the magnitude of MTPj dorsiflexion and arch joint stiffness would be expected.

Methods

Eleven participants completed running trials under four conditions at a velocity corresponding to a Froude number of 1.3. For all trials, participants wore a minimalist sandal on their right foot. In half of the trials, a small plastic wedge was adhered to the bottom of this sandal, dorsiflexing the MTPj an additional 10-15 degrees during stance. The bottom of this wedge was rounded to minimally perturb push-off. All participants ran with both rearfoot (RF) and non-rearfoot (NRF) strike patterns while motion and force plate data were collected.

The quasi-stiffness of the midtarsal joint equalled the slope of a linear least-squares fit of the curve describing midtarsal joint angle plotted against dimensionless resultant midtarsal joint moment. The midtarsal joint moment was assumed to be zero until the center of pressure crossed the joint.

Results and Discussion

The primary aim of the current experiment was to clarify the effect of increased MTPj dorsiflexion on the foot's arch in running. Using Statistical Parametric Mapping a time-series effect of the toe-wedge on MTPj dorsiflexion throughout stance was indeed found across both foot strike patterns, with the toe-wedge increasing the MTPj angle ($p = 0.001$). However, the sagittal plane midtarsal joint angle difference in the toe-wedge conditions did not reach the critical threshold to conclude a significant time-series effect. Further, there was not enough evidence to conclude statistically significant differences in midtarsal joint quasi-stiffness due to the toe-wedge (Figure 1a), or a correlation between MTPj angle and quasi-stiffness. Therefore, it does not appear that the windlass mechanism stiffens the foot's arch in the sagittal plane in running.

Previous authors have proposed that the MTPj could influence foot energetics [2,3]. McDonald et al. proposed that power absorbed at the MTPj during late stance could contribute to power generation at the midtarsal joint due to the joint's interrelation via the plantar aponeurosis. While the difference in midtarsal joint power when participants ran with the toe-wedge did not reach the critical threshold to conclude statistical significance, there was a strong correlation between peak negative MTPj power and peak positive midtarsal joint power across both strike patterns and toe-wedge conditions ($r = -0.71$, $p < 0.001$; Figure 1b). These results add support to the hypothesis of energy transfer between the midtarsal and MTP joints.

Lastly, the arch of the foot responded differently during the different running foot strike patterns. The RF strike trials resulted in greater midtarsal joint quasi-stiffness than NRF strike trials ($p < 0.001$; Figure 1a). This increase in quasi-stiffness was likely not due to increased MTPj dorsiflexion, as non-rearfoot strike trials demonstrated greater MTPj dorsiflexion in mid to late stance ($p = 0.001$). There was not enough evidence to conclude a difference in midtarsal joint total work between the foot strike patterns, however, positive work was ~1.6 times greater than negative work in NRF trials, versus ~2.3 times greater in RF trials. This suggests that more work in RF trials would need to be accomplished via active mechanisms, as opposed to the passive return of energy from the 'springy' arch of the foot. The increased quasi-stiffness together with the increase in positive relative to negative work in RF compared to NRF running suggests some contribution to arch stiffness from active mechanisms which differ between strike patterns.

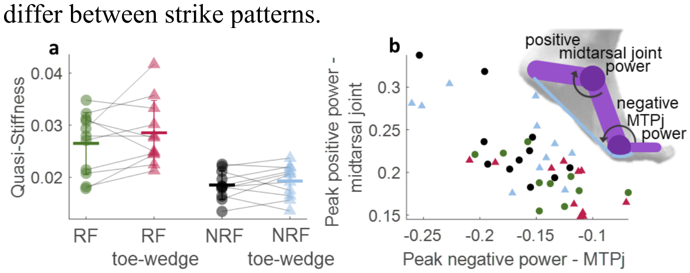

Figure 1: **a**) An increase in midtarsal joint sagittal plane quasi-stiffness when participants ran with increased MTPj dorsiflexion could not be concluded. However, quasi-stiffness was increased when running with a rearfoot versus non-rearfoot striking pattern. **b**) There was a strong negative correlation between peak negative MTPj power and peak positive midtarsal joint power.

Significance

Running with increased MTPj dorsiflexion and different foot strike patterns impacted foot joint behavior. The strong correlation between MTPj negative power and midtarsal joint positive power has implications when considering shoe designs which alter MTPj motion, especially considering that peak midtarsal joint power was approximately half of peak ankle joint power. Finally, the foot was more stiff and less 'springy' when RF striking, providing evidence that the foot could be serving different mechanical functions depending on the foot strike pattern.

References

[1] Hicks JH., 1954. *J Anat,* 88(1), 25-31.
[2] Welte et al., 2018. *J R Soc Interface*, 14(145), 20180270.
[3] McDonald et al., 2016. *PloS ONE,* 11(4): e014260.

CHANGING GROUND CONTACT TIME TO REDUCE ACHILLES TENDON FORCES DURING RUNNING OUTDOORS

Kevin G. Aubol* and Clare E. Milner
Department of Physical Therapy and Rehabilitation Sciences, Drexel University
email: *kga43@drexel.edu

Introduction

Achilles tendinopathy is a common overuse running injury that can be difficult to recover from. Excessive Achilles tendon loads are believed to contribute to the development of Achilles tendinopathy. Thus, interventions to decrease Achilles tendon loads may be helpful for preventing Achilles tendinopathy.

Increasing ground contact time may decrease peak Achilles tendon loads during running by allowing plantar flexor forces to be generated over a longer period of time [1]. However, it is unknown if runners can change their ground contact time enough to have a significant effect on Achilles tendon loads during running, or if any potential benefits may be offset by changes in cadence that may also occur while altering ground contact time.

The purpose of this study was to determine if changing ground contact time would affect Achilles tendon load during running with a fixed and/or free cadence. We hypothesized that increasing ground contact time would decrease peak Achilles tendon force and cumulative Achilles tendon damage compared to running with a preferred or decreased ground contact time, and that Achilles tendon impulse would be similar among conditions, with both a fixed and a free cadence.

Methods

As part of an ongoing study five runners completed a series of six one-minute runs on a concrete sidewalk at 3.0 ± 5% m/s. The conditions were combinations of preferred, low, and high ground contact times while running with either a fixed or a free cadence. During the fixed cadence conditions participants ran to the beat of a metronome set to their preferred cadence. During high/low ground contact time trials participants were instructed to "Increase/decrease the amount of time that your foot is in contact with the ground as much as possible" [2].

Instrumented Loadsol insoles were used to measure force under the foot. Loadsol data were used to calculate Achilles tendon force throughout stance [3]. Peak Achilles tendon force and Achilles tendon impulse were calculated. Cumulative Achilles tendon damage was calculated using a previously published approach [4]. Variables were averaged over ten strides from the middle of each trial.

A two-way repeated measures ANOVA was used to determine the effects of ground contact time condition and cadence condition on peak Achilles tendon force, Achilles tendon impulse, and cumulative Achilles tendon damage. Paired t-tests were used to compare conditions when significant differences were found. Alpha was set at 0.10 for this preliminary analysis.

Results and Discussion

There was no interaction effect for ground contact time and cadence on any Achilles tendon variables ($p = 0.499$-0.586). There was a main effect of ground contact time on peak Achilles tendon force ($p = 0.003$), Achilles tendon impulse ($p = 0.017$), and cumulative damage ($p = 0.002$). Peak Achilles tendon force was higher while running with a low ground contact time and free cadence than with a preferred ground contact time and free cadence ($p = 0.076$). Additionally, peak Achilles tendon force ($p = 0.050$) and cumulative Achilles tendon damage ($p = 0.073$) were lower while running with a high ground contact time and fixed cadence than with a preferred ground contact time and fixed cadence, but not with a free cadence. These preliminary findings were consistent with our hypotheses and suggest that interventions that increase ground contact time are beneficial for decreasing peak Achilles tendon force and cumulative Achilles tendon damage when cadence is fixed. However, there were no differences in peak Achilles tendon force or cumulative Achilles tendon damage with a free cadence. Therefore, interventions to reduce peak Achilles tendon force by increasing ground contact time should take care to control cadence in order to maximize any potential benefits.

Significance

This preliminary study demonstrates that increasing ground contact time while maintaining the same cadence may be a viable approach for decreasing peak Achilles tendon force and cumulative Achilles tendon damage during running. This finding may serve as the basis for future interventions to reduce the risk of Achilles tendinopathy in runners.

Acknowledgments

This study was funded by a Drexel University College of Nursing and Health Professions Dean's PhD Student Research Award.

References

[1] Beck et al., 2020. *Proc R Soc B*. 287(1933).
[2] Moore et al., 2019. *Front. Sports Act. Living*. 1(53).
[3] Hullfish & Baxter, 2020. *Gait Posture*. 79.
[4] Firminger et al. *Med Sci Sports Exerc*. 52(7).

Table 1. Means and standard deviations of Achilles tendon force variables while running with varying ground contact time and cadence conditions. GCT = ground contact time. **Statistically significantly different from preferred ground contact time (control) condition.*

Condition	Peak Achilles Tendon Force (BW)	Achilles Tendon Impulse (BW·s)	Cumulative Achilles Tendon Damage ($N \cdot [s/km]^{1/9}$)
Preferred GCT, Free Cadence (control)	6.9 ± 1.1	0.93 ± 0.14	6611 ± 1258
Low GCT, Free Cadence	7.1 ± 1.1*	0.92 ± 0.11	6771 ± 1093
High GCT, Free Cadence	6.3 ± 0.6	0.87 ± 0.07	6041 ± 881
Preferred GCT, Fixed Cadence	6.8 ± 0.8	0.92 ± 0.08	6498 ± 882
Low GCT, Fixed Cadence	7.1 ± 1.2	0.95 ± 0.15	6722 ± 813
High GCT, Fixed Cadence	5.9 ± 1.3*	0.78 ± 0.27	5501 ± 1291*

EFFECTS OF MILD DECLINES ON THE METABOLIC COST OF RUNNING

Montgomery Bertschy[1*], Michael Hester[1], Stephen Diefenderfer[1], Kristine L. Snyder[2], and Wouter Hoogkamer[1]
[1]Integrative Laboratory, Department of Kinesiology, University of Massachusetts, Amherst, Massachusetts, USA
[2]Stryd, Inc,, Boulder, Colorado, USA
email: mbertschy@umass.edu

Introduction

Typical major city marathons only contain relatively small grade fluctuations over the course of the race, but these grade fluctuations do exist and could influence the runners' optimal pacing. However, the effects of mild declines, specifically, on running energetics and performance have not been quantified precisely.

Most data on the metabolic cost of downhill running is focused on extreme slopes and/or relatively slow speeds, thereby having poor resolution and accuracy for slight to moderate grades at competitive marathon speeds [1]. We aimed to define a more precise estimation for the energetic cost of moderate declines typically found in major city marathons for runners at a 3-hour marathon pace. Further, we aimed to evaluate changes in running power during downhill running as provided by the Stryd Foot Pod, a wearable with an inertial measurement unit and environmental sensors.

Methods

14 healthy recreational runners who had recently run a sub 39 minute 10-km race (or equivalent 5-km race) participated in this study. Subjects ran a warm up to get accustomed to the treadmill (Treadmetrix, Park City, UT, USA) while wearing the mouthpiece of the expired-gas analysis system (True One 2400; Parvo Medics, Salt Lake City, UT, USA) and a standard shoe (Speed Sutamina, PUMA SE, Herzogenaurach, Germany) at the testing speed (14km/h). Next, subjects ran trials at 14km/h at grades of 0%, -1%, -2%, -3%, -4%, and -5% in a randomized order for 5 minutes each. We measured their oxygen uptake and carbon-dioxide production, and we calculated metabolic power for the final 2 minutes of the trial when aerobic steady state was achieved [2]. Subjects whose RER reached > 0.99 during any part of testing were excluded. Subjects (n=10) wore a Stryd Foot Pod (Stryd Inc., Boulder, CO, USA) on both feet to measure their running power at each decline. We expressed metabolic power in W, not normalized to body mass, to match Stryd Power units, even though scaling differs between power metrics.

A one-way repeated measures ANOVA was used to determine a significant effect of the slope. Additionally, we performed linear regression analyses for power across slopes and calculated Pearson's correlation coefficient r for the group and for each subject. We also performed linear regression analysis between Metabolic power and Stryd power at group level.

Results and Discussion

There was a significant effect of slope on Metabolic Power (W) ($p < 0.001$). Metabolic Power (% of level running) had a strong negative correlation with decreasing slope: $r = 0.928$ at a group level and $r = 0.970 \pm 0.055$ at an individual level. A change in decline of 1% was associated with a 4.00% decrease in Metabolic Power when normalized to the Metabolic Power of level running, which ranged from 3.16% to 5.26% between individuals.

Stryd Power had a very high correlation with Metabolic Power $r = 0.897$ at the group level and $r = 0.987 \pm 0.01$ at the individual level. For Metabolic Power (W) vs. slope, there was a low correlation of $r = 0.421$ at a group level and a very high correlation of $r = 0.986 \pm 0.011$ at an individual level. For Stryd Power vs. slope, there was a low correlation of $r = 0.265$ at a group level and a very high correlation of $r = 0.996 \pm 0.005$ at an individual level. Therefore, at an individual level, the Stryd Power measurements can be a strong proxy for measuring changes in metabolic energy cost due to moderate changes in declines. However, this relationship is best analysed at an individual, not group, level.

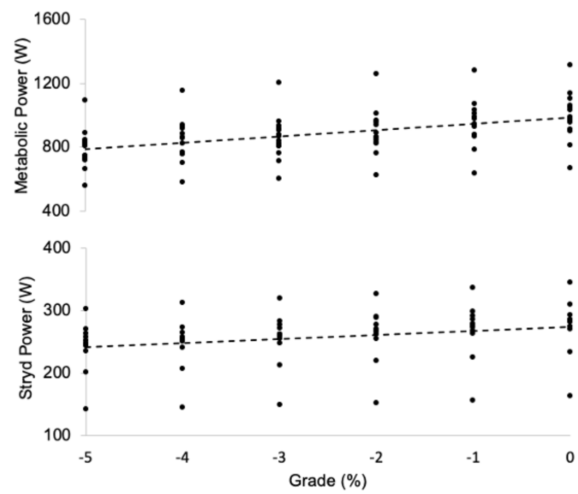

Figure 1: Individual values for Metabolic Power (W) and Stryd Power (W) across moderate declines.

Significance

Moderate decline running is abundant in major city marathons. Our findings show that declines as shallow as 5% can reduce metabolic cost by 20%, which can lead to major advantages for "point to point" marathons with a net downhill and should be considered for optimal pacing in courses with mildly rolling hills [3]. Metabolic Power's high correlation with slope suggests that it is fair to assume linearity at these moderate grades. Additionally, a running power device such as Stryd may be advantageous to monitoring energy consumption during marathon training and racing due to its considerable ability to represent metabolic power.

Acknowledgments

Stryd Foot Pods were provided by Stryd. MH was supported by a University of Massachusetts Honors College Research grant.

References

[1] Minetti et al. 2002. *Journal of Applied Pysiology.* 10.1152/japplphysiol.01177.2001
[2] Peronnet, F. and Massicotte 1991. *Can J Sport Sci.* 16(1), pp.23-29.
[3] Snyder et al. 2021. *Journal of Sports Sciences.* 10.1080/02640414.2020.1843820

MECHANICAL AND MORPHOLOGICAL PROPERTIES OF THE PLANTAR FASCIA IN RESPONSE TO IMPOSED RUNNING DEMANDS OVER THREE CONSECUTIVE DAYS

Lukas Krumpl[1*], Joshua P. Bailey[1]
[1]Department of Movement Sciences, University of Idaho, Moscow, ID, USA
email: *lkrumpl@uidaho.edu

Introduction

The plantar fascia (PF) is a band of connective tissue originating at the calcaneus and extending into the metatarsophalangeal joints. Injury, such as plantar fasciitis, often appears suddenly and unexpectedly, leaving its mechanism and timeline unknown. Research has suggested that the morphology of the tissue may play a role (Wang et al., 2009). The PF is a fibrous tissue sensitive to inflammation, which is quantifiable by assessing its thickness.

Fibrous structures display viscoelastic biomechanical properties, such as stress relaxation, hysteresis, and tissue creep. The proposed mechanical sequence of tissue creep (Frost, 1990) suggests that repetitive loading of a tissue, as during walking or running, would lead to a thinning and stiffening of the PF immediately post-exercise, followed by an inflammatory reparative process. However, this process has been scarcely investigated thus far, and the frequency and intensity of repetitive loading leading to potential injury remain unclear. Given the lack of understanding of how PF injuries develop, there is need for research investigating the effects of various intensities and volumes of repetitive loading in asymptomatic individuals.

Thus, the purpose of the present study was to evaluate the acute effects of three maximal effort 5k runs over three consecutive days on mechanical and morphological properties of the plantar fascia.

Methods

Six participants (age: 23.4 ± 4.5 yrs; mass: 61.5 ± 9.1 kg; height: 170.1 ± 8.0 cm) completed three 5 km runs on an outdoor track. Participants were instructed to perform the protocol with maximal perceived effort, and to avoid running, strenuous exercise, foot treatment or massages until the last data collection session was completed. PF properties were recorded with ultrasound imaging (LOGIQ S8, GE, Boston, MA, USA). Thickness was captured via B-mode and stiffness was measured via shear wave elastography before, immediately after, and 30 minutes after the run. Participants laid prone on a treatment table with their ankles and feet hanging off the edge to allow for relaxation of soft tissue and muscles surrounding the PF. The transducer was placed in line with the fibers of the PF. Three longitudinal live images for each property were taken at the calcaneal insertion after manually palpating and marking the site. Thickness of still images was measured in millimeters via ImageJ. Stiffness was analyzed with the ultrasound device and measured in m/s. Data were analyzed via two-way (session and measurement) repeated measures ANOVAs, and significant findings were explored with *post-hoc* t-tests. Alpha level was set at .05. Statistical analyses were completed via SPSS (v. 28.0).

Results and Discussion

Analyses showed a significant main effect of session ($p = 0.031$) and measurement ($p < 0.001$) for PF thickness. Further, analysis showed a significant main effect ($p = 0.008$) of measurement for PF stiffness. No significant interactions were found for neither thickness nor stiffness. *Post-hoc* t-tests further revealed a significant PF thickness decrease immediately following run 1 ($p = 0.026$; 3.6 ± 1.0mm) and run 3 ($p = 0.009$; 3.4 ± 1.1mm) compared to before (3.6 ± 1.0mm; 3.9 ± 1.1mm respectively). No significant change was found within run 2, or between the measurements pre- and 30 min post run, as well as immediately post and 30 min post-run for PF thickness. While stiffness displayed a similar pattern of decrease immediately post run, there was no significant change within each session. However, while not statistically significant, both thickness and stiffness followed an upward trend 30 minutes post-run. Figures 1 displays the change in mean PF thickness through all measurements and sessions.

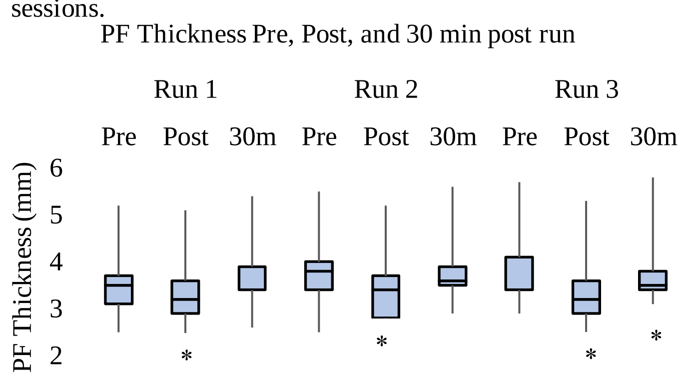

Figure 1. Boxplot and standard deviation whiskers depicting PF thickness for each measurement corresponding to the respective session. Significant difference compared to the first measurement taken is signaled by the * symbol.

The findings indicate that three maximal effort 5k runs have a significant effect on PF thickness. Mean thickness at the beginning (3.6 mm) was less than at the last measurement (3.92 mm). PF stiffness showed a similar pattern of decrease immediately post-run, indicating that repetitive mechanical loading may have an effect on the PF's ability to maintain proper arch support. However, after 30 minutes of recovery, both PF properties appear to approximate pre-exercise values, indicating that any detrimental effects to the tissue may only be acute. The timeline for PF injuries remains unclear.

Significance

To the knowledge of the authors, the present study is one of only two studies to investigate acute PF responses of asymptomatic individuals to exercise. The results provide essential information for understanding how healthy PF tissue reacts to mechanical loading, and open new avenues to evaluate PF injury prevention strategies. Future research should strive toward evaluating how varying intensities, distances, and durations of running may affect properties of the PF.

References

[1] Frost, H. M. (1990). Anatomical Record, 226(4), 433-439.
[2] Wang, H. Q (2009). BMC MK Disorders, 10(1), 105.

Data mining approach to determining gait abnormalities in runners with patellofemoral pain syndrome

Ross J. Brancati[1*], Katherine A. Boyer[1]
[1]Department of Kinesiology, University of Massachusetts Amherst, Amherst, MA
email: *rbrancati@umass.edu

Introduction

Patellofemoral Pain Syndrome (PFPS) is a common cause of anterior knee pain in recreational runners. Alterations in running mechanics may contribute to the onset of PFPS. However, pain may also contribute to additional changes in both gait mechanics and neuromuscular activation patterns. Previous research has found alterations in kinematic variables in runners with PFPS such as greater peak hip adduction angle.[1,2]

To date, most of the research with PFPS has focused on quantifying differences in discrete variables using a traditional hypothesis testing approach, which may miss important characteristics of biomechanical waveforms. With the recent advancements in machine learning, data mining has been applied to gait studies to determine important features for classifying pathological populations, which may have advantages over traditional parametric testing.[3] Shi et al. used machine learning approaches to diagnose[4] and determine biomechanical adaptations of[5] runners with PFPS. They reported hip, knee, and ankle flexion angle as well as electromyography (EMG) from multiple muscles as the most pertinent features for classifying these two groups. However, their approaches lack kinetic data and use the mean of the entire waveforms as features, omitting crucial aspects of waveform variables. This study's aim was to determine the biomechanical characteristics that are most influential on classifying runners with and without PFPS while considering entire waveforms. Identification of these key characteristics may support development of intervention and selection of critical outcomes for future research.

Methods

37 recreational runners - 19 symptomatic PFPS (10f, 22.6±4.3 years, speed: 2.88±0.53 m/s) and 18 who never experienced PFPS (10f, 22±3.5 years, speed: 2.80±0.32 m/s) participated in this study. Participants ran at self-selected pace for 21 minutes on an instrumented treadmill (Treadmetrix, Park City, UT, USA) while eight infrared motion capture cameras (Oqus-5 series, Qualysis, Inc. Gothenburg, Sweeden) and 11 wireless sensors (Delsys Trigno, Delsys, Inc., Natick, MA, USA) collected kinetic, kinematic, and EMG data. Ensemble averages of approximately ten strides at the first minute of the run were exported using Visual 3D (C-Motion Inc., Germantown, MD). Matrices for each kinetic, kinematic, and EMG variable were generated resulting in 27 total matrices (9 kinetic, 9 kinematic, and 11 EMG). A principal component analysis (PCA) was performed on each matrix, and the top two PC scores for each variable generated a data matrix, *[37x54]*, where each row represented the subject's stride, and each column represented the respective PC score.

A support vector machine (SVM) with a linear kernel was then trained on 80% of the data and tested with the remaining 20%. Metrics such as accuracy and F1 score were used to select the model with the best features. After training the model, the weights of each feature were calculated to determine feature importance and each pertinent feature was interpreted by plotting the 5th and 95th percentile of the principal component score, as previously described.[6] All data analyses were performed using Python 3.8.8 and multiple toolboxes such as scikit-learn.

Results and Discussion

An SVM model with eight features was selected to classify healthy and injured runners, resulting in high accuracy (85.7%), precision (90.5%), recall (85.7%), and F1 score (86.4%). The important features, their weights, and interpretations are listed in *Table 1*. The most heavily weighted kinetic features in the classification model were in the transverse plane. For all features, with the exception of the ankle and knee frontal plane moment, the PFPS group has smaller magnitudes and rates of change for the EMG, kinematic, kinetic selected features.

Significance

This analysis technique combining PCA to study entire waveforms with machine learning to mine important features uncovered variables that have not previously been outlined as important characteristics of runners with PFPS. Prior work on runners with PFPS highlights kinematic alterations in the frontal plane, whereas this approach found transverse plane kinetic variables to be essential to the classification procedure. Data mining approaches may be advantageous for determining variables to focus on when designing future studies and interventions to alleviate PFPS.

Acknowledgments

Funding: Deluca Foundation. Carl Jewel, for data collection.

References

[1] Barton et al., 2009. *Gait & Posture*. 30: 405-416
[2] Dierks et al., 2008. *J of Orth. & Sports PT*. 38(8): 448-456
[3] Halilaj et al., 2018. *J of Biomechanics*. 81: 1-11
[4] Shi et al., 2021. *Front. in Pub. Health*. 9: 643191
[5] Shi et al., 2020. *CSRSWTC*. 50769.2020.9372597
[6] Deluzio et al., 2007. *Gait & Posture*. 25: 86-9

Feature	Weight	Interpretation of Feature
Rectus Femoris PC 1	0.561	Healthy group showed greater peak activation during stance and in preparation for loading.
Hip Rotation Moment PC 1	0.283	Healthy group had faster rates of rotational loading change in the stance phase.
Ankle Rotation Moment PC 1	0.180	Healthy group presented a larger internal rotation moment at toe off.
Knee Rotation Moment PC 1	0.135	Healthy group had a larger peak knee flexion moment during stance.
Ankle Inversion Moment PC 1	0.063	Injured group showed a larger peak ankle inversion moment during stance.
Hip Rotation Moment PC 2	0.043	Healthy group had a larger peak internal rotation moment in early stance.
Hip Rotation Angle PC 1	0.034	Healthy group had greater hip external rotation at mid stance and in preparation for loading.
Knee Adduction Moment PC 1	0.001	Injured group presented greater peak knee adduction moment during stance phase.

Table 1: Interpretation of the most relevant features in the SVM-A classification task with the respective feature weights. Waveforms of the 5th and 95th percentiles of each of the features were plotted to interpret their meaning.

Lower Limb Kinetics During Curve Sprinting in Athletes with a Leg Amputation

Gabriela B. Diaz[1], Ryan S. Alcantara[2], and Alena M. Grabowski[1]
[1]Applied Biomechanics Lab, University of Colorado Boulder, Boulder, CO USA
[2]Department of Bioengineering, Stanford University, Stanford CA, USA
email: gabriela.diaz@colorado.edu

Introduction

People with and without unilateral transtibial amputation (TTA) run slower maximum velocities (v_{max}) on curves compared to straightaways, but the underlying biomechanical mechanisms that affect curve-sprinting v_{max} are not completely understood [1,2]. Determinants of curve-sprinting v_{max} are particularly relevant to athletic events such as the 200 m and 400 m sprint, where over half the race is along a curve. Curve-running v_{max} depends on the generation of vertical ground reaction force (vGRF) and centripetal GRF. The leg muscles generate moments about each joint that contribute to GRF production and sprinting velocity [3].

During curve-sprinting, athletes lean their upper body inward towards the center of the curve to generate centripetal force, which places the legs at different angles and leads to leg-specific differences in force production [1,4]. Athletes with TTA use a running-specific prosthesis (RSP) to sprint, which results in lower stance average vGRF in the affected leg (AL) compared to the unaffected leg (UL) when running on a straightaway [5]. Previous studies have found that the inside leg limits curve-sprinting v_{max} in non-amputees [1], RSPs limit GRF production on straightaways [5], and athletes run slower when their AL is on the inside versus the outside of the curve [2]. Due to competitive sprint races always being run in the counter-clockwise (CCW) direction, athletes with a right TTA will always run with their AL on the outside of the curve and athletes with a left TTA with their AL on the inside of the curve. Thus, we determined leg-specific joint moments during v_{max} curve-sprinting in people with a TTA on a curve used in competition to provide insight into the underlying differences in GRF production between the inside and outside legs during curve sprinting and determine if there are limitations from having the AL on the inside versus outside of the curve. We hypothesized that for athletes with TTA sprinting on a flat track curve, the hip and knee moments will: 1. be greater for the UL compared to the AL for trials when each leg is on the same side of the curve, 2. be smaller when the AL is on the inside compared to outside of the curve.

Methods

6 competitive sprinters (5 M; 1 F) with a right TTA completed a randomized series of 40 m sprints on a flat indoor track and were provided with ≥8-min rest between trials. Athletes sprinted along 40-m curves with a radius of 17.2 m (innermost lane of regulation 200 m track) in the CCW and CW directions so that data were collected with the AL on both the outside and inside of the curve. Athletes ran across mondo-covered adjacent force plates (AMTI; 1000 Hz) flush with the track surface. Lower body 3D kinematics were recorded using high-speed motion capture cameras (Vicon; 200 Hz). The force plates and capture volume (~2.5 x 5 m) were located halfway along the 40 m curve. We instructed athletes to run as fast as possible for each trial. Athletes adjusted their starting position to ensure they reached v_{max} within the capture volume. Trials were repeated until athletes successfully landed on the force plates at least once with the AL and with the UL. We calculated peak 3D joint moments for the knee and hip. We constructed linear mixed effects models to determine the effect of leg and curve side on joint moments.

Results and Discussion

Peak knee extension moment was 48% greater for the UL compared to the AL ($p < .001$), regardless of whether the leg was on the inside or outside of the curve. However, we detected no significant difference in peak knee flexion moment between the UL and AL. Peak hip extension moment was 99% greater for the UL compared to the AL ($p < .001$) and peak hip flexion moment was 36% greater for the UL compared to the AL, regardless of whether the leg was on the inside or outside of the curve. Our first hypothesis was partially supported, indicating that the use of an RSP results in lower sagittal plane peak joint moments when sprinting along a curve. These results suggest that while sprinting along curves, athletes with a TTA rely more on their UL to generate forces necessary to achieve v_{max}.

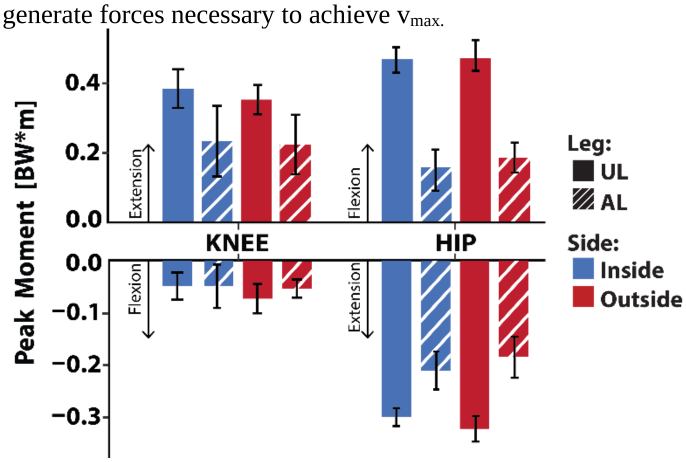

Figure 1. Peak extension and flexion moments for the knee and hip joints. Solid colors represent the unaffected leg (UL) and dashed lines represent the affected leg (AL). Blue represents when the leg was on the outside of the curve, and red represents when the leg was on the inside of the curve. Error bars represent SD.

We did not find any evidence supporting our second hypothesis. Differences between the peak moments generated by the AL when on the inside versus outside of the curve were not statistically different. Our findings suggest that use of an RSP may limit peak hip and knee moments, regardless of whether the AL is on the inside or outside of the curve. Future research is needed to determine why athletes with an amputation run slower along a curve compared to non-amputees.

Significance

Our results can be used to inform future RSP designs that improve sprinting along a curve. Additionally, our results can be used to inform the International Paralympic Committee on competition guidelines between athletes with leg amputations.

References

[1] Y.-H. Chang and R. Kram, *J. Exp. Biol.*, Mar. 2007
[2] P. Taboga, R. Kram, & A. M. Grabowski, *J. Exp. Biol.*, 2016
[3] S.R. Hamner & S.L. Delp, *J. Biomech.*, 2013
[4] S. M Churchill, *et al, J. Exp. Biol.,* Mar. 2015
[5] A. M. Grabowski, *et al*, *Biol. Lett.,* Apr. 2010

INFLUENCE OF SEX AND STRENGTH CAPACITY ON NORMALIZED LOW-BACK MOMENTS DURING BACKBOARD LIFTING

Justin B. Davidson[1*], David Clusiault[1], Daniel P. Armstrong[1] and Steven L. Fischer[1]
[1]Department of Kinesiology and Health Sciences, University of Waterloo
email: *jbdavids@uwaterloo.ca

Introduction

Backboard lifting has been identified as a high physically demanding job task for Canadian paramedics and can exceed both cumulative and acute injury risk thresholds [1]. While engineering interventions may provide effective solutions to mitigate injury risk for some lifting tasks, backboard lifting cannot be readily modified or eliminated. Therefore, it is important to investigate the potential that personal factors (e.g. strength capacity, sex) may have on the adopted movement strategies that lifters choose since it directly relates to resultant biomechanical exposures at the low-back.

An important personal factor that may influence injury related biomechanical exposures is sex. The influence of sex on biomechanical exposures in lifting has been previously investigated where females tend to use a more “leg-driven” approach while males tend to lift using a more “back-driven” strategy which leads to differences in low-back loading [2]. However, while sex may be one factor that can influence lifting strategies, it is important to investigate whether the difference is solely attributable to sex, or perhaps more specific to underlying differences in strength capacity.

The purpose of this study was to investigate if peak sagittal low-back extensor moments differed between participants based on sex and/or strength capacity when completing a backboard lifting task at relative loads of 25%, 50%, and 75% of their maximum backboard lift. It was hypothesized that individuals with a high strength capacity would have lower normalized low-back moments across all relative loads and no significant differences would exist between the sexes.

Methods

Two lab sessions were scheduled separated by a 24-hour period for 28 participants from a population of paramedics, paramedics trainees, and university students. In session one, participant’s one-repetition-maximum (1RM) backboard lift was determined using a sub-maximal testing protocol [3]. In session two, participants completed 10 backboard lifts at each of 25%, 50%, and 75% of their estimated 1RM.

Whole-body motion capture and ground reaction forces were collected from all lifts. Bottom-up inverse dynamics were computed to estimate peak sagittal plane low-back moments. Moments were normalized to the mass of the load lifted for the purposes of producing a relative biomechanical exposure variable as a dependent measure. Two sets of groups were dichotomized including a biological sex-based division (males, females), and a capacity-based division (low-capacity, high-capacity). The 14 participants with the lowest 1RM magnitudes were placed in the low-capacity group and the 14 with the highest were placed in the high-capacity group.

Two mixed model ANOVAs were used to test for differences in peak sagittal plane low-back moments with between factors either being the sex groups or the strength capacity groups, and the within factor being the three relative loads.

Results and Discussion

Individuals in the high-capacity group experienced significantly lower normalized peak sagittal low-back moments than low-capacity individuals at all relative load levels (Figure 1). When individuals were divided based on sex, no significant differences were detected between groups. An interaction effect was also found when groups were divided by strength capacity and showed that low-back exposure differences were greatest between strength capacity groups at lower relative loads.

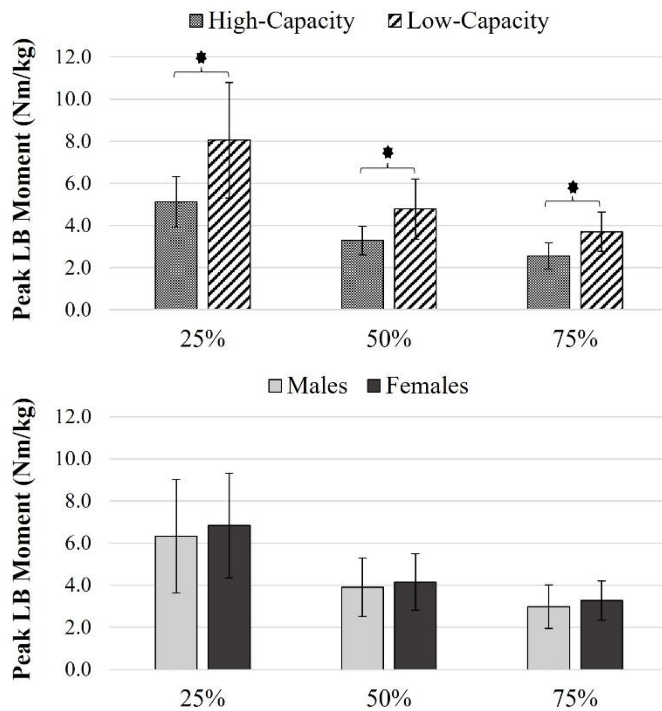

Figure 1: Normalized peak sagittal low-back (LB) extensor moment at three different relative loads between high-capacity and low-capacity groups (top), and females and males (bottom). Asterisk (*) indicates significant differences ($p < 0.05$).

Significance

This study showed that peak sagittal plane low-back extensor moments differed as a function of strength capacity, but not sex, in backboard lifting. The highest normalized low-back moments were found when participants were lifting lower normalized loads (25%) suggesting that minimizing exposures is less of a priority when the load is lighter. This study provides evidence that strength training interventions may be useful in mitigating low-back exposures during a backboard lifting task.

References

[1] Armstrong et al., 2020. IISE Trans. Occup. Ergon. Hum. Factors. 8(1), 9-19.
[2] Makhoul et al., 2017. J. Apple. Biomech. 33(2), 137-143.
[3] Wathan and Beachle, 1994. Human Kinetics.

SEX-SPECIFIC KINEMATIC ADAPTATIONS TO FATIGUE IN ASYMMETRICAL LIFTING

Daniel P. Armstrong[1], Michelle R. Cardoso[2*], Steven L. Fischer[1] and Wayne J. Albert[3]
[1]Department of Kinesiology and Health Sciences, Faculty of Health, University of Waterloo
[2]École de kinésiologie et de loisir, Université de Moncton
[3]Faculty of Kinesiology, University of New Brunswick
email: Michelle.cardoso@umoncton.ca

Introduction

When evaluating injury risk in manual materials handling work, it is important to consider sex-based differences. For example, females have a greater occupational injury rate than males in manufacturing work [1], as well as work closer to their spinal compression tolerance limits during lifting [2]. With the reported differences in both injury prevalence and biomechanical loading as a function of sex, a prudent research direction is to investigate underlying mechanisms that could influence these outcomes.

One such underlying mechanism that could explain differences in injury risk as a function of sex may be the influence of fatigue on kinematic strategy in physically demanding work. It has been shown that males and females have differing kinematic responses to fatigue in symmetrical lifting [3], but it is unclear whether similar differences exist in asymmetrical lifting. Asymmetric lifting is important to investigate as it has higher associated peak lateral shear joint reaction forces and muscle force than symmetrical lifting [4].

The purpose of this study was to investigate changes in trunk and upper body kinematics as a function of sex and fatigue in a prolonged asymmetric lifting protocol. It was hypothesized that significant interaction, in addition to main effects, of sex and fatigue on lifting kinematics would be observed. Such findings would support that males and females have differing kinematic adaptations to fatigue in asymmetrical lifting.

Methods

A sample of 33 participants (20 females, 13 males) completed a repeated asymmetric lifting protocol for 75 minutes while kinematics of the trunk and upper extremity were collected at 120 Hz. The lifting cycle consisted of lifting and lowering a crate with a mass of 10% of a participant's lift specific maximum voluntary isometric contraction (MVIC) 6 times per minute. On each lift the crate was lifted from the ground in front of the participant, deposited on a shelf at waist height 60º to the right of the participant, and then returned to its starting position. Lifting repetitions at the start, mid-point and end of the protocol were retained for analysis to represent non-fatigued, some fatigue and fatigued conditions. To confirm that fatigue had accumulated over the course of the protocol, differences in pre- and post-protocol low back and shoulder MVICs were compared using paired samples t-tests.

Principal component analysis (PCA) was used to detect modes of variance in trunk and upper extremity kinematic data [5]. Time-series *x, y,* and *z* coordinates of the L5/S1, C7 and shoulder, elbow and wrist joint were input to the PCA model to represent the trunk and upper extremity kinematics. Principal components explaining 95% of variance in the data set were retained for analysis and PC scores in all retained PCs were used as dependent measures of kinematic strategy. Two-way mixed ANOVAs were used to test for differences in lifting kinematics between sexes and across fatigue conditions. In PCs where there were significant effects, the modes of variance were interpreted using single component reconstruction [6], and gross differences in kinematics were visualized using aggregate component reconstruction [5].

Results and Discussion

Eleven PCs were retained for analysis explaining 95.4% of variance in the dataset. Significant main effects of sex and fatigue were seen for 4/11 and 6/11 PCs respectively, while there were significant interaction effects for 2/11 PCs. While both males and females utilized greater trunk extension to initiate the lift when fatigued, females did so to a greater extent (Figure 1). When fatigued females move their entire upper body to the right to deposit the load compared to males flexing the trunk. Both sexes had greater shoulder abduction, carried the load lower in the vertical and reduced the horizontal distance of the body to the load when fatigued.

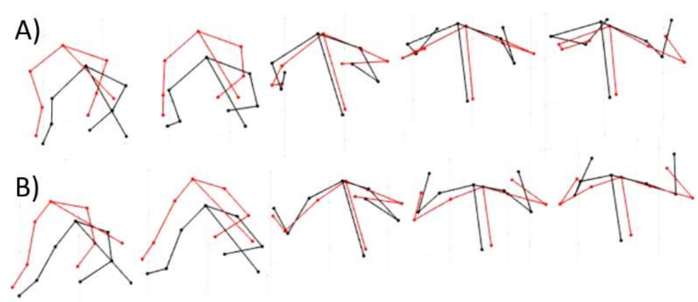

Figure 1: Aggregate component reconstructions visualizing kinematic differences in both A) males and B) females across non-fatigued (black) and fatigued (red) conditions.

Low back and shoulder MVICs were 19.2 and 17.0% lower respectively following the lifting protocol ($p < 0.001$), which supports that participants did fatigue.

With both main and interaction effects in PC scores for some retained PCs, our hypothesis that males and females have differences in fatigue-related kinematic adaptations was supported. These differences in kinematic adaptations may contribute to females having greater occupational injury rates and higher biomechanical exposures in lifting.

Significance

This study has implications when developing and implementing ergonomic interventions for asymmetrical lifting demands. Since the fatigue-related kinematic adaptations to fatigue differ between males and females it is important to explicitly consider sex differences in both risk assessment and job design as they relate to asymmetric lifting.

References

[1] Taiwo et al., 2009. *American J. of Epi.* 169:2, 161-166
[2] Marras et al., 2003. *The Spine Journal.* 3:2, 93-99.
[3] Eger & Stevenson, 2004. *Occ. Ergonomics.* 4:1, 27-39.
[4] Kim & Zhang, 2017. *Ergonomics.* 60:4, 563-576.
[5] Armstrong et al., 2021. *J. Occ. Rehab.* 31:1, 50-62.
[6] Brandon et al., 2013. *J. Electro. & Kin.* 23:6, 1304-1310.

BACK LOADING PREDICTION WITH INERTIAL MOTION CAPTURE DURING MANUAL MATERIAL HANDLING

Antoine Muller[1,*], Hakim Mecheri[2], Philippe Corbeil[3], André Plamondon[2] and Xavier Robert-Lachaine[2]

[1] Université Claude Bernard Lyon 1, Lyon, France. [2] Institut de recherche Robert-Sauvé en santé et en sécurité du travail, Montréal, QC, Canada. [3] Université Laval, Québec, QC, Canada. [*] corresponding author: antoine.muller@univ-lyon1.fr

Introduction

Magnetic and inertial measurement units (MIMUs) are portable, which allow ergonomic workplace assessment. MIMUs kinematics have been extensively validated in the laboratory. However, physical exposure indicators based on kinetic variables such as back loading represent valuable information during ergonomic assessment. A contact model for feet and hands during manual material handling (MMH) tasks could help to estimate kinetic variables from inertial motion capture system (IMC) on the basis of dynamics equations [1]. This approach has been evaluated on MMH tasks, but either using standardized tasks or optical motion capture (OMC) [2-4].

The aim of the current work was to estimate back loading during MMH tasks only with MIMUs. The evaluation consists in comparing L5/S1 joint moments estimated with IMC to those obtained with OMC and a force platform (OMC + FP).

Methods

Motion analysis was performed simultaneously with IMC and OMC on ten male subjects. The IMC system is composed of 17 XSens MIMUs sampled at 240 Hz. Eight cameras recorded at 40 Hz the 3-D coordinates of three-marker clusters rigidly fixed on each MIMU. 48 anatomical landmarks were identified. The ground reaction forces (GRF) were measured by a large homemade force platform. Four repetitions of various MMH conditions consisting in different objects (box sizes with and without handles and bags), masses (2, 10 and 20 kg), lift-deposit heights (16, 116 and 190 cm), distances (0.75 and 1.5 m), and technique (free and imposed) were achieved for a total of 176 transfers per subject.

The OMC biomechanical model was composed of 18 rigid segments linked by 17 joints corresponding to 43 degrees of freedom. The geometrical parameters were subject-specific calibrated using motion capture data and an optimization-based method. From the positions of the anatomical landmarks the joint coordinates were computed in an inverse kinematics step. An inverse dynamics step allowed to obtain L5/S1 joint moments. GRF were used in a recursive Newton-Euler algorithm with a bottom-up approach. The velocities and the accelerations were computed with a 2-order finite-difference method.

Data from MIMU were processed with MVN Analyze, which integrates a sensor fusion algorithm. The joint coordinates and the biomechanical model were extracted from this software. The IMC biomechanical model was composed of 23 rigid segments where each joint is assimilated to a spherical joint. For both models, body segment inertial parameters were estimated from an anthropometric table. The external forces were estimated by using a prediction method [1]. To map the contact area, 8 points under each foot and 8 points on each hand were defined.

The transfer phase was manually identified with video recordings. At each instant, prediction of the external forces and moments (GRF and hand contact forces) was performed through an optimization procedure that consisted of minimizing the sum of squared contact forces respecting the dynamics equations applied on the subject and applied on the load. Inverse dynamics for IMC+FP followed the approach described for OMC. Only the transfer phase (loaded phase) was analysed for GRF, and L5/S1 flexion and asymmetric moment (combination of the lateral flexion and twist components). OMC+FP and IMC were compared on the average of all trials with the RMSE, relative RMSE (rRMSE) and Pearson correlation coefficient (r).

Results and Discussion

Table 1: Average of trials for the comparison of OMC+FP and IMC on the vertical and transverse GRF, flexion and asymmetric L5/S1 moment.

Mean (SD)	RMSE	rRMSE	r
Vertical GRF	31.8 N (3.9 N)	11.5 % (1.3 %)	0.86 (0.05)
Transverse GRF	19.5 N (2.1 N)	14.6% (1.3 %)	0.75 (0.04)
L5/S1 flexion moment	18.6 Nm (4.0 Nm)	18.7 % (5.2 %)	0.82 (0.05)
L5/S1 asymmetric moment	13.0 Nm (2.2 Nm)	28.1 % (4.2 %)	0.41 (0.10)

The mean error in the flexion moment estimation is higher than for the asymmetric moment but since the amplitude of the moment is the most important along this axis, the relative error is lower (Table 1). On simpler tasks of trunk bending [3], the use of MIMU allowed to estimate L5/S1 joint flexion and symmetric moments with an error below 10 Nm. On similar tasks [2], errors of 14 Nm for flexion and 9 Nm for asymmetric moments were reported with OMC. Compared to literature, the observed level of error increased (Table 1) due to the complexity of the MMH tasks, the analysis of exclusively the transfer phase and that the IMC system is less accurate than the OMC system. Data should be interpreted cautiously especially for the L5/S1 asymmetric moment. Finally, it must be noted that MIMUs are sensitive to magnetic disturbances, which could occur in the workplace [5].

Significance

The proposed method seems promising since it allows the estimation of the L5/S1 joint moments with a limited error by using only IMC under a variety of experimental conditions. A complete ergonomic assessment of MMH tasks could be achieved outside the laboratory, directly in the workplace.

Acknowledgments

Funding for this project was obtained from IRSST [grant #2017-0019] and its scholarship programs, and Mitacs Acceleration program. The authors are grateful to Christian Larue for his help during the development of the protocol.

References

[1] Muller et al., 2020a. IEEE Trans Biomed Eng 67, 344-352.
[2] Muller et al., 2020b. Appl Ergon 82, 102935.
[3] Faber et al., 2016. J Biomech 49, 904-912.
[4] Larsen et al., 2020. Ann Biomed Eng 48, 805-821.
[5] Robert-Lachaine et al., 2020 Ergonomics 63(3), 283-292.

AN ELECTROMYOGRAPHY BASED MULTI-MUSCLE FATIGUE INDEX FORMULATIION AND VALIDATION

Leonardo H. Wei[1] and Suman K. Chowdhury[1*]
[1]Department of Industrial, Manufacturing, and Systems Engineering, Texas Tech University, Lubbock, Texas
email: *suman.chowdhury@ttu.edu

Introduction

Previous researchers used amplitude and/or frequency measures of surface electromyography (SEMG) signals to quantify muscle fatigue of individual muscles during a functional task. The efficacy of these measures has been tested using a few representative muscles (mostly one or two) in previous studies. Nevertheless, the successful completion of a task requires translation and rotation of a joint (or many joints) that is (are) controlled by various muscle groups with different anatomical characterizations (e.g., cross-sectional area, muscle fiber composition, etc.). To our knowledge, no multi-muscle fatigue index exists that combine both anatomical characterizations of muscles and their functional performances. Therefore, this study aimed to develop a multi-muscle fatigue index based on anatomical characteristics and functional performance to accurately measure the physiological strain of a joint during functional activities.

Methods

We formulated a SEMG based multi-muscle fatigue index (MMFI) by incorporating activation patterns (both amplitude and frequency of SEMG signals) of individual muscles during functional tasks, anatomical characterizations (muscle fiber compositions and physiological cross-sectional area), and number of activated and fatigued muscles. We used these criterion to develop this MMFI for any given fatiguing tasks: (1) muscles with a higher proportion of type II fibers fatigue faster; (2) an increase in the SEMG amplitude and a decrease in the SEMG frequency is the biomarker of localized muscle fatigue; (3) a decrease in both SEMG amplitude and frequency is the biomarker of cognitive fatigue, i.e., a decrease in brain effort to generate the required force; (4) tasks that engage a higher number of muscles have the ability to sustain longer, i.e., such task have the flexibility to engage alternate muscles if a group of muscles are fatigued; (5) muscles that fatigued faster contribute to a faster rate of physiological strain on the joint. By combining these five criteria, we formulated the following mathematical model of MMFI:

$$MMFI_i = \sum_{j=1}^{N}\left[\left\{[M_1]^{\frac{f_j}{s_j}} || [M_2]^{\frac{f_j}{s_j}}\right\} \times \frac{\frac{\sum_1^i \gamma_i}{t_i}}{\sqrt{t_i}}\right] \times \tanh\left(\frac{\frac{\eta}{N}}{\sqrt{N}}\right)$$

Where, i is an index for time step;
j is an index for the number of muscle;
N is the total number of muscles for a given task;
η is the number of fatigued muscles at any given time;
$t_i$is the total number of time steps (windows) at ith time step;
γ_i is a counter for the number of time steps (windows) a muscle experience both localized and cognitive fatigue by ith time step;
$\frac{\sum_1^i \gamma_i}{t_i}$ is a time domain multiplier to account the number of times a muscle experience fatigue by time step, i;
$tanh\left(\frac{\frac{\eta}{N}}{\sqrt{N}}\right)$ is a muscle fatigue multiplier;
$\frac{f_j}{s_j}$ is the ratio between fast (f_j) and slow twitch (s_j) fiber of muscle (j);
M_1 and M_2 respectively indicate localized muscle and cognitive fatigue of muscle (j) at time step (i);
$M_1 = M_2 = \sqrt{(A_i - \bar{A})^2 + (F_i - \bar{F})^2}$;
A_i and F_i are the amplitude and frequency at ith time step and ($\bar{F}, \bar{A}$) represents baseline frequency and amplitude, which are the average of the first three-time steps. We used the following decision criterion of two normalized reference values: $R_1 = \frac{A_i}{\bar{A}}$ and $R_2 = \frac{\bar{F}}{F_i}$ of to determine if a muscle undergoes localized or cognitive or no fatigue for any given time step, i.

- $R_1 \geq 1$ and $R_2 \geq 1$, then M_1 is considered;
- $R_1 \leq 1$ and $R_2 \geq 1$, then M_2 is considered;
- $R_2 < 1$, then $M_1 = M_2 = 0$.

We validated the proposed index by simulating three distinct dynamic shoulder exertion tasks (low-, medium-, and high-level tasks) using three different load conditions (2lb, 4lb, and 6lb) as discussed in a previous study [1]. Briefly, ten male subjects performed repetitive exertions at three shoulder heights: shoulder (high), elbow (medium), and trochanter (low) heights using 2lb, 4lb, and 6lb dumbbells for about three minutes. The duration of each repetition was about 8 s.

Results and Discussion

MMFI trends in Figure 1 showed comparatively a higher trend (both magnitude and slope) for high exertion task than medium and low exertion tasks; similarly, the MMFI trend in 6 lb task displayed comparatively a greater trend (both magnitude and slope) than 4 lb and 2 lb exertion tasks, validating the accuracy of our MMFI formulation.

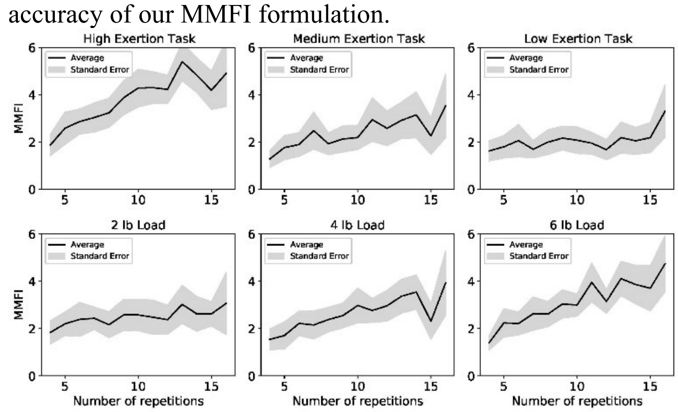

Figure 1: *Multi-muscle fatigue index (MMFI) trends for high, medium, and low exertion tasks using 6lb, 4lb, and 2lb weights.*

Significance

A multi-muscle fatigue index is expected to facilitate an accurate estimation of the physiological strain of a joint during functional activities and thus aid in designing the appropriate ergonomic interventions to reduce work-related injuries.

Acknowledgments

We want to thank Anindita Das to assist in data processing.

References

1. Chowdhury, S.K., et al., Ergonomics, 2018. **61**(12)

LOW BACK DISORDER RISK ASSESSMENT DURING MATERIAL HANDLING USING WEARABLE SENSORS: A FEASIBILITY STUDY

Cameron A. Nurse[1*], Laura, J. Elstub[1], Peter Volgyesi[1,2] and Karl E. Zelik[1]
[1]Department of Mechanical Engineering, Vanderbilt University, Nashville, Tennessee, United States
[2]Institute for Software Integrated Systems, Vanderbilt University, Nashville, Tennessee, United States
*Email: cameron.a.nurse@vanderbilt.edu

Introduction

Low back disorders (LBDs) are a major occupational health problem, accounting for 38.5% of work-related musculoskeletal disorders in the US [1]. LBDs often arise from the mechanical fatigue of tissues: an accumulation of microdamage from repetitive forces on the lower back.

Ergonomic assessment tools based on mechanical fatigue principles, such as the *Lifting Fatigue Failure Tool (LiFFT*) [2] can be used to assess LBD risks. To use LiFFT, a safety professional monitors an individual during their shift, manually records the weight of each object lifted, the distance of the object from the spine and the number of lift repetitions. Object weight and distance data are used to estimate the peak moment experienced by the lumbar spine. Moment and repetition data are then input into the LiFFT equation. The output of LiFFT is a numerical LBD risk score, which can be used to classify low vs. medium vs. high risk jobs. However, the observation and data collection period of this ergonomic assessment can be time-consuming and can introduce inaccuracies due to how different professionals measure spine-to-object distances.

Wearable sensor systems could improve ergonomic assessment by automating the time-consuming manual measurements. Sensors can also provide continuous data collection over longer durations than human observation, allowing for more representative and personalized analyses. Wearable systems using inertial measurement units (IMUs) primarily monitor high risk postures and are beginning to be adopted in industry to supplement ergonomic assessments. Recent studies suggest that combining pressure sensing insoles with a single IMU on the trunk can enhance monitoring capabilities (compared to a trunk IMU alone) by providing more accurate estimates of low back loading [3]. However, it remains unknown how accurate low back loading estimates need to be to provide reliable LBD risk scores and classifications.

Our objective was to characterize how accurately we can track and classify overexertion injury risk of the low back using only trunk motion (from a single IMU) versus using trunk motion and forces under the feet (from pressure insoles).

Methods

We re-analysed an existing dataset consisting of 3D motion capture data from 10 participants performing 40 different lifting tasks [3]. We estimated lumbar moment using idealized wearable signals, distilled from lab-based kinematic and force plate data and a Gradient Boosted Trees algorithm. Idealized wearable sensor signals provide a useful way to assess feasibility and relative performance of different sensor combinations. The target metric was the lumbar moment computed using inverse dynamics on lab-based 3D motion capture and force plate data. The algorithm was trained with previous methods [2] to estimate lumbar moment using data obtained from a single idealized trunk IMU versus an idealized trunk IMU and idealized pressure insoles under each foot. A minimum threshold of 100 Nm was used in the training data to improve estimates of peak lumbar moments during a lift.

We developed a simulation that used lumbar moment estimates to assess LBD risk of 1000 simulated workdays, consisting of 800 to 1500 random lifts each day. For each lift, the estimated peak moments were used as inputs in the LiFFT equation [2] to obtain three LBD risk scores (lab-based, from a single trunk IMU, from trunk IMU and pressure insoles).

We then plotted the LBD risk estimated by the idealized wearable systems vs. the LBD risk from the from the lab and computed the mean absolute percent error.

Results and Discussion

The addition of pressure insoles with the trunk IMU greatly improved the accuracy of LBD risk assessment and demonstrated strong potential to classify risks. The trunk IMU exhibited an average error of 32.5 ± 23.4% in LBD risk relative to the lab-based estimates, while adding pressure insoles with the IMU decreased the average error to 9.8 ± 5.7% (Figure 1).

The results suggest that since a single trunk IMU system lacks information about the weight of the object lifted the accuracy in LBD risk assessment is diminished. However, the weight of an object lifted can be estimated with pressure insoles. Therefore, algorithms developed from IMU and pressure insole data can leverage both kinematic and kinetic data to estimate lumbar moments more accurately which improves LBD risk assessment (Fig. 1).

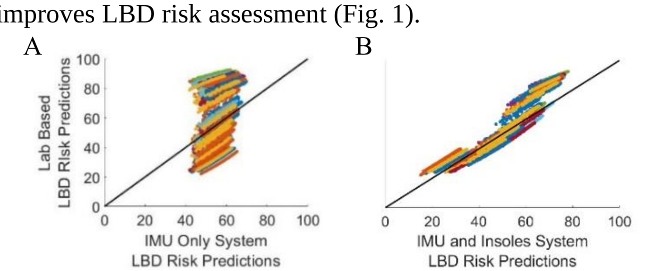

Figure 1: Lab based vs idealized wearable estimates of LBD risk (A) Idealized Trunk IMU Only and (B) Idealized Trunk IMU and pressure insoles. Each colour represents a participant, and each data point is a simulated workday.

Significance

These preliminary results suggest that combining a trunk IMU and pressure insoles with a trained algorithm has the potential to accurately assess and classify of LBD risk, which could help automate ergonomic evaluations, reduce workplace injuries, and deepen our scientific understanding of LBDs.

References

[1] US Department of Labor, 2016
[2] Gallagher et al., 2017 *Appl Ergon* 63,142-150
[3] Matijevich et al 2021 *Sensors* 21(2):340

THE INFLUENCE OF BACK MUSCLE FATIGUE ON TRAINING APPROACHES TO REDUCE LUMBAR SPINE MOTION DURING OCCUPATIONAL LIFTING TASKS

Kayla M. Fewster[1], Dennis J. Larson[2] and Stephen H.M. Brown[2]
[1]School of Kinesiology, The University of British Columbia, Vancouver BC, Canada
[2]Department of Health and Nutritional Sciences, University of Guelph, Guelph, ON, Canada
email: kayla.fewster@ubc.ca

Introduction

Repetitive lifting or repeated trunk flexion-extension movements during manual materials handing (MMH) tasks can result in low back muscle fatigue, which has been identified as a risk factor associated with low back pain (LBP) and low back disorder (LBD) reporting [1]. Low back muscle fatigue can result in a number of negative consequences, including decreased muscle force-generating capacity [2], changes in muscle activation patterns [3], changes in movement coordination [4] and changes in dynamic lumbar spine stability responses [5].

In terms of mitigating lifting-related LBD risk, MMH training may provide an effective supplement to traditional ergonomic controls. In this case, lifting movements can be trained using augmented feedback by directing attention to key movement features (i.e. avoid rounding your back, limit spine movement etc.). This permits the trainees the opportunity and flexibility to experiment with different movement solutions without being obliged to a one-size-fits all technique. This type of training approach has been successfully used in gait re-training investigations [6], real-time ergonomic feedback systems to improve industrial task performance [7] and has been shown to be an effective method to change lifting mechanics [8]. However, given the fatiguing nature of repetitive lifting type tasks, it is currently unknown how effective this type of training is in a fatigued state. Therefore, the purpose of this investigation was to compare the effectiveness of a training protocol, aimed at reducing lumbar spine motion during lifting tasks, in both fatigued and un-fatigued states.

Methods

Thirty participants with no history of LBP participated in this study. Thirteen participants served as the control group and moved directly into the training protocol. The remaining seventeen participants underwent a fatigue protocol prior to training. For the fatigue group, fatigue was induced in the back muscles by completing repetitive prone extensions, interspersed with maximum voluntary contractions, until max trunk extensor force output dropped to 60% of its original value.

Training consisted of 5 different sets of lifts and each set consisted of 10 lifts. Sets 1 and 2 were completed with tactile training cues applied to the skin of the low back. Set 3 consisted of no tactile training cues; however verbal performance feedback was provided at 5 different time points throughout the set. Set 4 consisted of performance feedback provided at 4 different time points and Set 5 consisted of performance feedback provided at 3 different time points. Throughout training 3D kinematic data were collected from two electromagnetic sensors positioned over the T12 and S1 vertebrae (Polhemus, Colchester, VT, USA). 3D lumbar spine angles (T12 relative to S1) were calculated and normalized to upright standing. Flexion-extension angular data were used to compute total lumbar spine range of motion (ROM) during each lift and peak lumbar flexion angle across each lift. ROM and peak flexion data were then averaged across each training set. Mean differences in lumbar ROM and peak flexion angle were evaluated between training groups (fatigue vs. control) and across training sets using a general linear model.

Results and Discussion

For total lumbar spine ROM there was a significant main effect of training group ($p = 0.038$). Overall, participants in the fatigue group lifted with significantly more lumbar spine motion in comparison to the control group (Figure 1A).

For peak lumbar spine angle flexion there was a significant main effect of training group ($p = 0.031$). Overall, participants in the fatigue group lifted with significantly more lumbar spine flexion in comparison to the control group (Figure 1A).

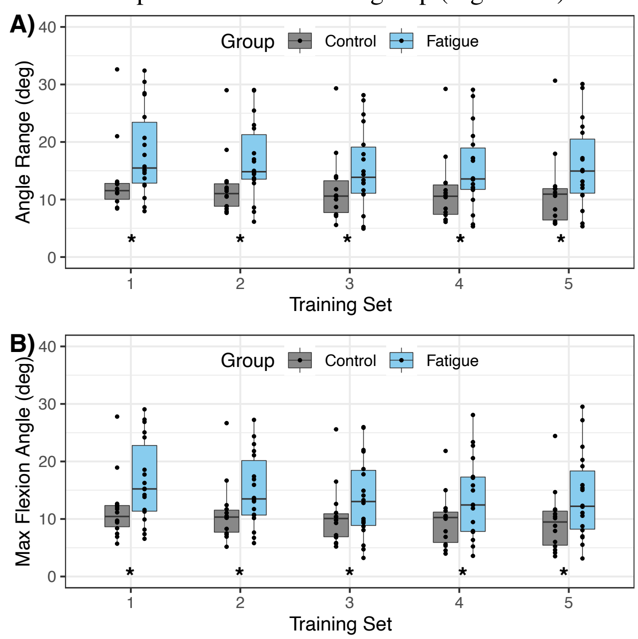

Figure 1: (A) Participant data for total lumbar spine flexion-extension ROM during lifting. (B) peak lumbar spine angle during lifting across training groups and lifting sets. Across both Figure (A) and (B) statistically significant differences are displayed across groups.

Significance

Overall, results suggest that low back muscle fatigue can influence the effectiveness of a lift training protocol. Participants who experienced a fatiguing protocol prior to training lifted with significantly more lumbar spine flexion as well as with approximately 27% more lumbar spine motion in comparison to non-fatigued controls. This suggests that the implemented training protocol was more successful in the non-fatigued group.

References

[1] Luoto et al., 1995. *Clin Biomech*., 10:323-324. [2] Taylor et al., 2000. *Euro J of App Phys.,* 83:106-115. [3] Potvin & O'Brien., 1998. *Spine*. 23:774-780 [4] Cowley & Gates., 2017. Hum. Mov. Sci. 56:109-118. [5] Larson & Brown., 2022. *J Biomech*. *In-press*. [6] Barton et al., 2016., *J Sports Med*. 50:513-526. [7] Vignais et al., 2013. *Appl. Ergon*. 44:566-574. [8] Pinto et al., 2018. *Hum. Mov. Sci*. 60:32-39.

IDENTIFYING THE BEST WINDOW SIZE AND LEAD TIME AND BEST SENSOR COMBINATION FOR CLASSIFICATION OF INJURIOUS VERSUS NON-INJURIOUS PATIENT TRANSFER FROM BED TO WHEELCHAIR

Kitaek Lim[1], Seyoung Lee[1], and Woochol Joseph Choi[1]
[1]Injury Prevention and Biomechanics Laboratory, Dept of Physical Therapy, Yonsei University, South Korea
email: wcjchoi@yonsei.ac.kr

Introduction

Low back pain is common in caregivers and frequent lifting and lowering tasks (i.e., patient transfer from bed to chair) are known to be risk factors. We determined a compressive force at a disc between L5/S1 (Fc) during patient transfers to define injurious versus non-injurious transfers using a NIOSH criterion (3,400 N) [1]. We then used the Support Vector Machine (SVM) with sensor data a. to create models for classification of injurious versus non-injurious transfers, and b. to find combination of window size and lead time and the number and location of sensors, offering the best classification performance. Details on the first part are provided in our companion abstract submitted to NACOB 2022, and here we describe details on the second part.

Methods

Fifteen individuals wore IMU sensors (Xsens Dot, Xsens Technologies, Enschede, The Netherlands) and simulated patient transfers from bed to wheelchair (Figure 1a). Trials were acquired with two patient body weights: 70 kg and 75 kg, with and without knee assist and a mobile lift. Kinematics of an upper body during transfers were recorded with a motion capture system, which were used to estimate the Fc.

Removing unanalysable trials, total 144 trials were categorized into injurious (31) versus non-injurious (113) transfers based on the NIOSH criterion (Fc greater or less than 3,400 N, respectively). Features (mean and variance of accelerations, velocities, and angular velocities in each axis) were extracted from the sensors placed on body segments. We then defined 5 different lead times (LT) and window sizes (WS) (from 0.1 s to 0.5 s with an increment of 0.1) (Figure 1b), and features from each combination of the lead time and window size acquired from ten sets of sensors (waist; both arms; both thighs; waist + both arms; waist + both thighs; both arms and forearms; both thighs and shins; waist + both arms and forearms; waist + both thighs and shins; waist + both arms and forearms + both thighs and shins) were used for data mining.

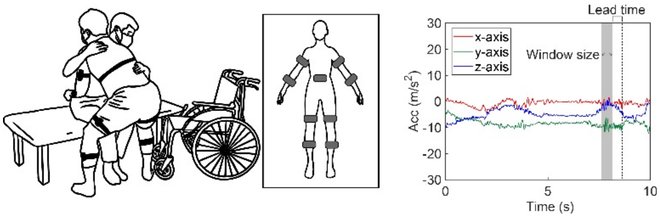

a b

Figure 1: Schematic of simulation with IMU sensors as shown in the inset (a) and sample data showing the LT and WS (b).

To create models, we first balanced injurious versus non-injurious data set by oversampling with average values of injurious data. We then used a radial basis function (RBF) kernel of SVM in LIBSVM [2] to classify injurious versus non-injurious transfers. The training and testing data sets were split into equal size. A grid-search with exponential growing sequences was conducted to determine the best combination of cost and gamma. A five-fold cross-validation was conducted for each combination of every combination of window size and lead time to determine the best combination.

The accuracy, sensitivity, and specificity were compared to assess the classification performance. All data analyses were conducted with MATLAB routines (R2021B, MathWorks Inc.).

Results and Discussion

All models created with IMU sensor data provided good sensitivity and specificity for classification of injurious versus non-injurious patient transfers (over 92%) (Table 1), informing the best combination of window size, lead time and the number and location of sensors, which offers the best classification performance. The best performance (98.2% of accuracy) was achieved with sensors at the waist, both arms and forearms with the window size of 0.2 s and the lead time of 0.1 s, and at both arms with the window size of 0.2 s and the lead time of 0.3 s.

Location of sensors	WS/LT combination	Acc (%)	Sen (%)	Spe (%)
Waist + both arms and forearms + both thighs and shins	0.3 s/0.1 s	95.6	96.8	94
Waist + both arms and forearms	0.2 s/0.1 s	98.2	100	96.1
Waist + both thighs and shins	0.3 s/0.1 s	94.7	94.5	94.8
Waist + both forearms	0.5 s/0.2 s	96.5	95.2	98
Waist + both thighs	0.4 s/0.1 s	95.6	94.9	96.3
Both arms and forearms	0.5 s/0.4 s	95.6	95.2	96
Both thighs and shins	0.1 s/0.2 s	93.8	92.3	95.1
Both thighs	0.4 s/0.5 s	95.6	100	91.9
Both arms	0.2 s/0.3 s	98.2	96.6	100
Waist	0.4 s/0.4 s	96.5	94.4	98.3

Table 1: Performance of classification models. Acc: accuracy; Sen: sensitivity; Spe: specificity.

Significance

Our study presents high-performance risk detection models for low back injuries during patient transfers from bed to wheelchair, informing the development of application to help address musculoskeletal injuries in caregivers.

Acknowledgments

This research was supported by the Transitional Research Program for Care Robots funded by the Ministry of Health & Welfare, Republic of Korea (HK21C0008).

References

[1] Waters et al., 1993. *Ergonomics*, 36: 749-776
[2] Chang and Lin, 2011. *ACM trans. Intell. Syst. Technol.*, 2(3):27

EFFECT OF ANKLE QUASI-STIFFNESS ON BALANCE CONTROL DURING WALKING AT DIFFERENT SPEEDS

Stephanie L. Molitor[1*], Nicholas P. Fey[1], Glenn K. Klute[2] and Richard R. Neptune[1]
[1]Walker Department of Mechanical Engineering, The University of Texas at Austin, Austin, TX
[2]VA Center for Limb Loss and MoBility and Department of Mechanical Engineering, University of Washington, Seattle, WA
email: *stephanie.molitor@utexas.edu

Introduction

The role of ankle stiffness during gait has been explored in the context of foot energy storage and return, and in prosthetic designs that aim to reduce the metabolic cost of walking [1]. However, the role of ankle stiffness in relation to other biomechanical objectives, such as maintaining dynamic balance in various gait conditions, is unclear.

Previous studies have found that the shape of the ankle's moment-angle curve (quasi-stiffness) changes with speed [2], and that the range and rate of change of whole-body angular momentum are similarly influenced by walking speed [3-4]. However, the relationship between ankle quasi-stiffness and balance control across walking speeds has not been identified.

Thus, the objective of this study was to determine whether ankle quasi-stiffness during slow, natural, and fast walking is correlated with changes in balance control in able-bodied individuals. Since ankle quasi-stiffness is dominated by the ankle dorsi-plantar flexion angle and moment, we focused on sagittal-plane balance control. We hypothesized that when accounting for speed, there would exist a correlation between ankle quasi-stiffness and balance control. Further, we hypothesized that individuals who modulate ankle quasi-stiffness more across speeds would demonstrate better balance control.

Methods

Full-body kinematic and kinetic data during overground walking from a previously recorded dataset [5] were analysed for 50 healthy subjects (age range: 6-72 years, 25 females) at three self-selected speeds (slow, natural and fast).

Ankle quasi-stiffness was evaluated during the braking and propulsive phases of the gait cycle by the shape of the moment-angle curve, fitted using a second-order polynomial [6]. Dynamic balance was quantified by the time rate of change of whole-body angular momentum ($\dot{H}$, equal to the net external moment acting on the center of mass) normalized by body weight, in which greater magnitudes of $\dot{H}$ indicate poorer balance control [4].

To determine if quasi-stiffness was correlated with $\dot{H}$, a linear mixed-effects model was generated for each of the two phases of gait (braking and propulsion). For each, $\dot{H}$ was the dependent variable, the fixed factors were walking speed, quasi-stiffness and their interaction, and the random factor was each subject.

To test the second hypothesis, we calculated the mean quasi-stiffness at each speed and its coefficient of variance (CV), with higher CV representing more modulation of ankle stiffness between speeds. Pearson correlation analyses were performed between the CV and peak magnitude of $\dot{H}$ within both the braking and propulsion phases.

Results and Discussion

The linear mixed-effects models confirmed there exists a correlation between balance control and walking speed for both braking and propulsion (Fig. 1); however, ankle quasi-stiffness was not found to have a significant relationship with $\dot{H}$.

In the analysis of quasi-stiffness modulation, CV appeared to be weakly correlated to peak $\dot{H}$ during braking (Fig. 2) but this relationship was not significant ($R^2 = 0.09$, $p = 0.22$), and there was no correlation during propulsion. Contrary to our hypothesis, these results suggest it is unlikely that able-bodied individuals modulate ankle quasi-stiffness when walking at different speeds to control sagittal-plane balance. Since deviations in dynamic balance in the sagittal plane can be passively corrected [7], modulating ankle quasi-stiffness may not be necessary. However, ankle quasi-stiffness modulation may be a more effective strategy in the frontal plane where balance is more actively regulated [7].

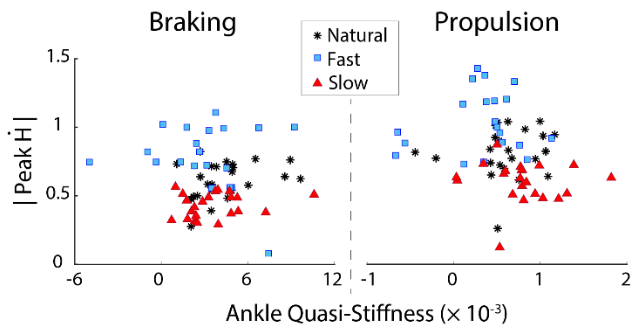

Figure 1: Ankle quasi-stiffness (Nm/deg^2/kg) and magnitude of peak $\dot{H}$ across walking speeds during braking and propulsion.

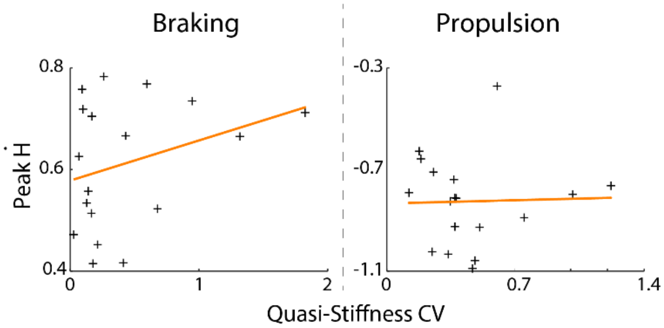

Figure 2: Correlations between ankle quasi-stiffness coefficient of variance (CV) and peak $\dot{H}$ during braking and propulsion.

Significance

Although ankle quasi-stiffness does not appear to play a significant role in sagittal-plane balance control during steady-state walking for healthy able-bodied individuals, this study provides a baseline for comparing stiffness-balance control relationships in other gait tasks (e.g., turning) and in populations with increased fall risk.

Acknowledgments

The authors are thankful for the data provided in [4]. This work was supported in part by VA award RX002974.

References

[1] Clites et al., 2021. *J. Neuroeng. Rehabilitation. 8*(1), 1-16.
[2] Hansen et al., 2004. *J. Biomech. 37*(10), 1467-1474.
[3] Silverman et al., 2011. *J Biomech. 44* (3), 379-385.
[4] Nott et al., 2014. *Gait Posture. 39*(1), 129-134.
[5] Lencioni et al., 2019. *Sci. Data. 6*(1), 1-10.
[6] Rouse et al., 2014. IEEE *Trans. Neural Syst. Rehabil. Eng.*
[7] Bauby and Kuo., 2000. *J. Biomech.33(11):1433-40.*

THE EFFECT OF DUAL-TASKS ON COGNITIVE PERFORMANCE AND BALANCE CONTROL DURING WALKING WITH ALTERED STEP WIDTHS

Gabriella H. Small*, Lindsey K. Lewallen and Richard R. Neptune
Walker Department of Mechanical Engineering, The University of Texas at Austin, Austin, TX
email: *gsmall@utexas.edu

Introduction

Dual-task studies often combine walking with an additional cognitive load to determine their influence on gait performance [1]. Performing a challenging cognitive task during steady-state walking has been shown to negatively affect frontal plane balance [2]. Frontal plane balance during walking is partially mediated by foot placement, with clinical populations often walking with a wider step width [3]. Wider steps lead to an increase in peak-to-peak whole-body angular momentum (*H*), which is associated with poorer balance control [4]. Therefore, the purpose of this study was to determine the effect of an additional cognitive load when walking over a range of step widths. We hypothesized that cognitive performance would be optimal at an individual's self-selected (SS) step width and would decrease at wider and narrower step widths. We further hypothesized that the addition of a cognitive load would have a greater effect on balance control at the SS step width as we expect individuals would focus more on the challenging motor task than their cognitive performance when walking at non-SS step widths.

Methods

A 10 camera system (VICON, Los Angeles, USA) recorded 3D full body kinematics for 15 young healthy adults (age: 25.3 ± 4 years, 8 females) during normal treadmill walking (no step width targets), and with step width targets projected onto the treadmill at each subject's SS width, 25% narrower (narrow), 50% wider (wide) and 100% wider (extra wide). All walking conditions were performed with and without an additional cognitive load (spelling 5-letter words backwards [2]) at their SS speed. All trial conditions were randomized. Motion data was then analyzed in Visual3D (C-Motion, Germantown, MD) and MATLAB (Mathworks Inc., Natick, MA, USA) to determine changes in dynamic balance across conditions. Dynamic balance was quantified using the range of *H*, where a higher range correlates with lower clinical balance scores and thus poorer balance control [5]. Cognitive performance was evaluated by correct response rate for the spelling task.

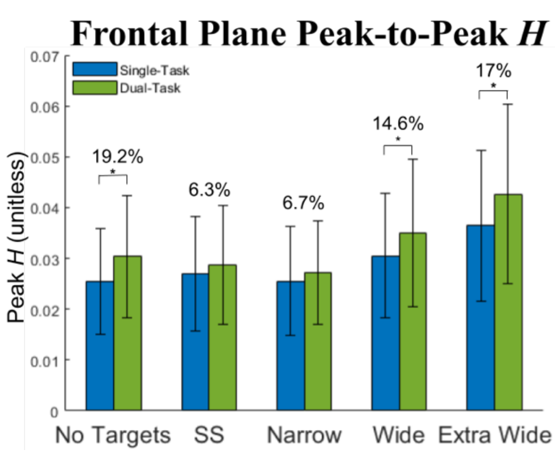

Figure 1: Normalized peak-to-peak difference in whole-body angular momentum (*H*, normalized by height, mass and speed of each individual) in the frontal plane for the different walking conditions. * indicates significance of $p < 0.05$.

Results and Discussion

There was a trend of a decrease in cognitive performance with the correct response rate decreasing from SS width (2.4 ± 0.6 letters/s) to narrow (2.1 ± 0.6 letters/s) and wide conditions (2.2 ± 0.6 letters/s). However, the difference only reached significance at the extra wide condition (2.0 ± 0.5 letters/s, $p < 0.01$). The cognitive performance decrease as one moved away from their SS width supported our hypothesis at the widest steps.

The addition of the cognitive load caused an increase in the range of *H* between the single- and dual-task across all conditions, which was significant at the wide and extra wide steps ($p < 0.01$ for both). Contrary to our hypothesis, the percent difference in the range of *H* between the single- and dual-tasks increased as step width increased. We did not see an increase in range of *H* at the narrow step width, likely because a smaller step width would decrease the range of *H*. The lack of significant change at the SS width was likely due to the easier and more natural walking task. There was a difference in the range of *H* between the control (no targets) and the SS condition, even with no change in step width, likely due to the targets causing participants to focus more on the motor task as others have shown that instructed focus can change task prioritization [6]. However, even with more attention on foot placement, the wide and extra wide conditions were challenging enough to see a significant decrease in balance control. The wider step widths coupled with the challenging cognitive task required enough attentional resources to see a decrease in both motor and cognitive performance.

Significance

This study showed that balance control during dual-tasks decreases with wider step widths. Given that decreased balance control while walking may increase the risk of falling, our results could have implications for clinical populations (e.g., the elderly or individuals post-stroke) who often walk with wider step widths [3]. When walking at non-SS conditions, our results suggest there is a threshold at wider steps where attentional resources become insufficient and balance control and cognitive performance decrease. These results also provide insight into the automaticity of walking [7] and task prioritization in healthy individuals, which provides a basis for future studies to determine differences in neurologically impaired populations.

Acknowledgments

This project was supported in part by the National Science Foundation Graduate Research Fellowship Program.

References

[1] Ebersbach G., et al., *Percept Mot Skills* 81(1), 1995.
[2] Small, G., et al., *J Biomech* 122, 2021.
[3] Bruijn, S. & van Dieen, J. *J. R. Soc. Interface* 15, 2018.
[4] Neptune, R. & Vistamehr, A., *J. Biomech. Eng.* 141(7), 2018.
[5] Nott, C., et al., *Gait Posture* 39(1), 2014.
[6] Yogev-Seligmann, G., et al., *Phys Ther* 90(2), 2010.
[7] Clark, D., *Front. Hum. Neurosci.* 9(1), 246, 2015.

KNEE JOINT QUASI STIFFNESS DURING MID-STANCE IN ADULTS WITH AND WITHOUT OBESITY

Derek N. Pamukoff[1*], Steven A. Garcia, Skylar C. Holmes, and Michael N. Vakula
[1]Western University, School of Kinesiology, London ON
*email: dpamukof@uwo.ca

Introduction

Individuals with obesity are at greater risk for knee osteoarthritis partially due to altered gait biomechanics. Studies focusing on the effects of obesity on gait biomechanics have generally investigated features that correspond with loading during heel strike (i.e., early stance) or propulsion (i.e., late stance).[1,2,3] However, few data are available on the mid-portions of stance phase, which may have important implications for knee joint loading and unloading during the gait cycle.

The purpose of this study was to examine sagittal plane knee biomechanics during mid-stance in adults with and without obesity. We hypothesized that adults with obesity would have greater absolute sagittal plane knee joint quasi-stiffness (KJS) during mid-stance than those without obesity that is explained by less knee extension excursion, and a larger change in the internal knee extension moment during mid-stance.

Methods

48 individuals with obesity (24 males/24 females; Age: 22.9 years (22.0-23.8); BMI: 33.0 kg/m^2 (32.1-33.9); Body Fat: 37.9 % (35.9-39.9)) and 48 without obesity (24 males/24 females; Age: 21.9 years (21.0-22.8); BMI: 21.36 kg/m^2 (20.7-22.5); Body Fat: 19.9 % (17.9-21.9)) participated and matched on age and sex. Participants were grouped based on BMI (Normal Weight: 18.5-24.9 kg/m^2; Obesity: 30.0-40.0 kg/m^2), and the presence of obesity was verified via air displacement plethysmography. Participants wore form-fitting clothing, laboratory standard footwear and retroreflective markers to complete an overground gait analysis at a self-selected speed on a 10m walkway. Kinetic data were recorded using 2 force plates (2400Hz) located at the centre of the walkway, and marker trajectories were recorded using a 9-camera Qualisys motion capture system (240Hz). Data were exported to Visual 3D for model construction and analyses were completed in MATLAB.

The mid-stance phase was identified as the period from peak knee flexion following heel contact to peak knee extension. Knee joint quasi-stiffness during mid-stance was quantified using the linear slope of moment/angle plot during mid-stance (Fig 1). One-way MANOVA was used to compare the absolute and normalized (BWxHeight) KJS values (α=0.05). The changes in knee flexion angle and internal knee extensor moment during mid-stance were also included to elucidate the source of group differences in KJS. Pairwise comparisons were made using a Bonferroni adjustment. Finally, we completed an exploratory analysis on the role of gait speed on group comparisons of KJS using one-way ANCOVAs.

Results and Discussion

There was a significant effect of group on mid-stance biomechanics (Pillai's trace = 0.962, $p<0.001$). Adults with obesity had greater absolute (4.77 vs. 5.83 Nm/°, p=0.02), but lower normalized (0.0037 vs. 0.0046 Nm/°/BWxHeight, p=0.01) mid stance KJS compared with adults without obesity. The change in knee flexion angle during mid-stance was not different between groups (12.99° vs. 12.51°, p=0.71). The change in absolute knee extensor moment during mid-stance was greater in those with compared to those without obesity 82.12Nm vs. 64.06Nm, p=0.01), but the change in normalized knee extensor moment was greater in those without compared to those with obesity (0.0046 vs. 0.0037 BWxHeight, p=0.04).

Results were similar when adjusted for gait speed; and adults with obesity had greater absolute (4.82 vs. 5.78 Nm/°, p=0.04), but lower normalized (0.0037 vs. 0.0047 Nm/°/BWxHeight, p=0.01) mid-stance KJS compared with adults without obesity.

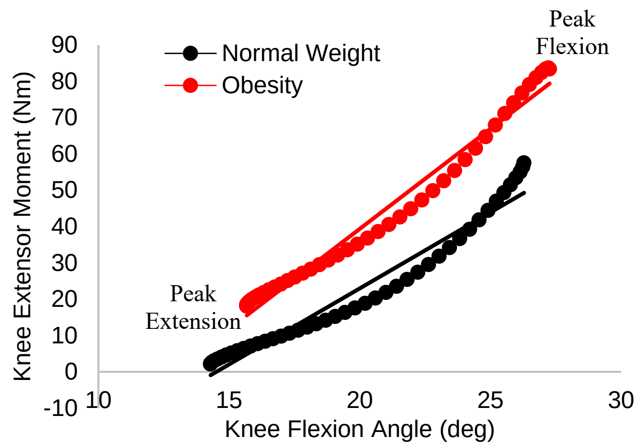

Figure 1: Linear slopes of moment-angle plot from group ensemble averages during mid-stance in normal weight (black) and obesity (red) groups.

Significance

Typical gait patterns include a period of knee unloading during mid-stance. However, greater absolute KJS in adults with obesity suggests a resistance to knee unloading during the mid-stance. As such, the knee joint may experience prolonged and concentrated mechanical stress, which can be attributed to a larger change in absolute joint moments. These features may contribute to a larger cumulative knee load during each step.

Conversely, we also observed lower normalized KJS in adults with compared to those without obesity, which may indicate joint instability during mid-stance. Finally, we found that group differences persisted after adjusting for speed, which suggests that body size provides a unique contribution to mid stance KJS. Future studies are needed that evaluate the contribution of mid-stance gait characteristics to knee osteoarthritis development in adults with obesity.

Acknowledgments

This study was supported by the California State University Fullerton Junior Intramural Grant Program.

References

[1] Vakula et al., 2019. *MSSE*. May;51(5):951-961.
[2] Garcia et al., 2021. *Gait and Posture*. Jan;83:217-222.
[3] Pamukoff et al., 2020. *MSSE.* Oct;52(10):2189-2197.

A BIOMECHANICAL ASSESSMENT OF A SERVICE MEMBER WITH TRANSTIBIAL AMPUTATION ACROSS THE UTILIZATION OF DIFFERENT PROSTHETIC FEET

Tyler C. Cardinale[1], Shannon E. Isley[1], Tatiana E. Djafar[1], and Trevor D. Kingsbury[1]
Clinical Biomechanics Laboratory, Navy Medicine Readiness and Training Command San Diego, San Diego, CA, USA
Email: tyler.c.cardinale.ctr@mail.mil

Introduction

Many service members who undergo transtibial amputation (TTA) have the potential to achieve high function and the desire to continue performing the physically demanding requirements of their occupation and desired recreational activities. In order to meet these requirements, service members need to utilize prosthetic feet that optimize both performance and functionality. However, there is currently little research comparing different prosthetic feet during higher level tasks. One of the most distinguishing aspects of prosthetic feet is stiffness [1]. Decreased stiffness in prosthetic feet tends to increase overall energy absorption. Yet, some of these advantages can be offset by the increased muscle activation needed to maintain overall stability [2]. The purpose of this study was to assess the biomechanics of a service member with TTA while utilizing different prosthetic feet during both ballistic and maximal strength tasks.

Methods

A male service member with a left unilateral TTA (age: 45yr height: 187cm mass: 84.7kg) underwent biomechanical assessments during 3 different sessions while utilizing 3 different prosthetic feet, the Össur Pro-Flex XC (an energy storage and return (ESAR) foot), BioDapt Versa Foot 2 (a non-ESAR foot with a metal frame and shock absorber typically used for weight lifting and higher level activities), and the Össur Flex-Run (a C-shaped running-specific prosthesis). We compared and categorized the stiffness of each foot through their manufacturers' websites and then validated their measures by comparing them to the limb active stiffness computed in ForceDecks (VALD performance, Newstead, AU). Each biomechanical assessment included one lower body ballistic movement, the Countermovement Jump (CMJ), and one whole body strength measurement, the isometric mid-thigh pull (IMTP). The subject performed the assessment on two forceplates (Kistler Instrument Corp, Novi, MI, USA) while using ForceDecks software to collect and process the assessment protocol. The assessment protocol consisted of the subject performing five cued maximal CMJ with approximately two seconds between each jump and hands on hips throughout the movement to control the effect of arm swing. The IMTP consisted of three, five second maximal pulls on a 45lb bar anchored to a squat rack. Variables of interest for the CMJ included peak takeoff force, peak takeoff force asymmetry, and jump height. Variables of interest for the IMTP included peak vertical force and peak vertical force asymmetry.

Results and Discussion

During the CMJ, the subject's peak takeoff force was highest with the Flex-Run and lowest with the Versa Foot 2, suggesting a more elastic device could promote higher force production in ballistic tasks (Table 1). The subject's CMJ was more symmetrical during peak takeoff force using the Flex Run, while use of the stiffer devices resulted in more lower limb asymmetry. Overall jumping performance was improved in the Flex-Run as well in terms of jump height (Table 1). This implies that less stiffness in prosthetic feet could improve both performance and peak force symmetry while performing ballistic tasks. The elastic properties of the Flex-Run might have aided in lower limb symmetry and improved performance because the subject was able to load the device more efficiently and better utilize energy return.

During the IMTP, the subject achieved his maximum peak vertical force while wearing the stiffest foot, the Versa Foot 2, and produced the least amount of force wearing the Flex-Run (Table 1). This suggests utilizing a stiffer prosthetic foot could help one achieve greater force production in maximal strength tasks. However, the subject's peak force asymmetry was higher in the stiffer devices, the Versa Foot 2 and Pro-Flex XC, whereas the Flex-Run proved to be the most symmetrical. This indicates a springier device could again be useful in maintaining lower limb symmetry during a maximal strength task despite not optimizing peak vertical force.

Significance

It is important to take into consideration the trade-off between peak force generation and symmetry when trying to optimize prosthetic feet during high level activity. Ideally, a prosthetic foot should be able to adequately meet the physical demands of a task while also minimizing lower limb asymmetries. However, this study further establishes the benefits and consequences of different stiffness levels depending on the physical demands of a task, which can help drive the decision making process when prescribing prosthetic feet to service members.

Acknowledgments and Disclaimer

Thanks to General Dynamics Information Technology for support. The views expressed herein do not necessarily reflect those of the Department of the Navy, Department of Defense, DHA, or U.S. Government.

References

[1] Shephard, 2019. Northwestern University dissertation.
[2] R. Neptune et al., 2013. *J Biomech* vol. 46.

Device	CMJ Peak Takeoff Force (N)	CMJ Peak Takeoff Force Asymmetry (%)	CMJ Jump Height (in)	IMTP Peak Vertical Force (N)	IMTP Peak Vertical Force Asymmetry (%)
Flex-Run	1442	23.9	7.0	2598	13.1
Pro-Flex XC	1441	29.9	6.8	2736	23.9
Versa Foot 2	1425	33.5	6.2	2810	23.1

Table 1. Descriptive statistics of each prosthetic foot

INFLUENCE OF CONTEXT ON HUMAN WALKING IN THE REAL WORLD

Loubna Baroudi[1*], Xinghui Yan[1], Mark W. Newman[1], Kira Barton[1], Stephen M. Cain[2], and K. Alex Shorter[1],
[1]University of Michigan, Ann Arbor, MI, USA and [2]West Virginia University, Morgantown, WV, USA
email: *lbaroudi@umich.edu

Introduction

Humans navigate the world using walking as a principal mode of locomotion. Walking strategy can be defined by the choice of stride length for a given stride speed. Researchers have explored the factors (e.g., energetics) that influence this relationship in the lab, both on a treadmill and overground [1]. Measurements of unconstrained overground walking outside of a supervised experimental setting are an essential complement to lab-based investigations of walking. However, there are multifarious contextual factors that can affect walking strategy in the real world. Here, we use wearable sensors and a mobile phone to collect real-world walking data, location, and self-reported behavioural context to investigate the interaction between context and gait.

Methods

We collected unconstrained movement data over 14 days using a foot-worn inertial measurement unit (IMU), a thigh-worn accelerometer (activPAL), and a phone for a single participant. The built-in activPAL activity classification algorithm was used to identify bouts of walking. A walking period started when walking was detected and ended when standing (>1min) or the transition to another state (e.g., sitting) was detected. Thus, a period contains both walking and pauses between bouts (<1min) to capture the discontinuous nature of real-world walking. Only walking periods longer than a minute and with at least five strides were kept for analysis. Using the foot-worn IMU, we implemented the zero-velocity update algorithm to obtain estimates of stride speed (SS) and stride length (SL) [2]. A model, $SL = a \times SS^b$ [3], was fit to the data using non-linear least squares to obtain parameters a and b. Finally, we labelled each walking period with the location (phone GPS) and self-reported context.

Results and Discussion

We collected 108 walking periods over 14 days of data collection, with a range of 6 to 864 strides per walking period. The fitted model had an R^2 value of 0.84 and an RMSE of 0.08 m (Figure 1). The good model fit suggests the individual maintained a consistent walking strategy despite diverse contextual factors. Seven common behaviors that spanned the observed stride speed range were used to label the data; walks tend to cluster according to their labels. For example, unconstrained walks in open space (e.g., between work and parking lot, outdoor stroll, and walk with a friend) all have larger stride lengths and faster speeds. On the other hand, walks while shopping and at home – with space constraints – span a larger range of moderate stride length and stride speed. Spatially constrained and unconstrained walks also present different variabilities. Larger standard deviations were observed for constrained walks (0.5-1.3 m/s) compared to the unconstrained walks at the extremes. These observations indicate that context has a meaningful and varied effect on daily movement patterns and suggest that an extended measurement period is needed to capture the range of speeds required for a well-fitted model.

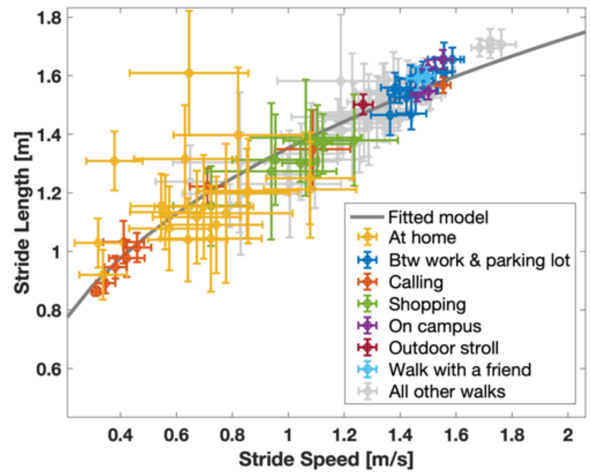

Figure 1: Each data point corresponds to average stride speed and stride length for a walking period with error bars for standard deviation. The line corresponds to the least-squares best fit for the power model.

Stride speed is of particular interest for clinical stakeholders as it is a strong predictor of overall health [4]. The subject adopted a large range of stride speeds that cluster based on context. The distribution of stride speeds is negatively skewed (*Sk* = -1.69) with a peak around 1.5m/s. This shape is explained by a concentration of strides (57% of all strides) during the outdoor walks (e.g., between work and parking lot, on campus, outdoor stroll, and walk with a friend). If we isolate these walks, we obtain a bimodal distribution between the purposeful walks and the outdoor stroll. The outdoor stroll presents a slower stride speed of 1.3 m/s (N = 864 strides) compared to 1.5 m/s (N = 4401 strides) for the other outdoor walks. Observation of behaviour in the real world with elements of context offers nuances to the analysis of stride speed and suggests that an individual's speed profile may be better represented by a range of stride speeds as opposed to one value of preferred walking speed.

Significance

In-lab data offer a snapshot of someone's walking whereas real-world data open a large window into an individual's daily behaviour. This work demonstrates how knowledge of context is important for interpreting free-movement data. These results represent a step towards a framework for the analysis of the large amount of movement data that can be collected using wearable sensors in the real world. Future research will explore how key features in the data streams can be used to classify context.

Acknowledgments

Funding: Precision Health Initiative (University of Michigan).

References

1. Ojeda L, et al. *Med Eng and Physics,* Pages 929-936, 2015.
2. Ojeda L, et al. *J of Navigation,* Pages 391-407, 2007.
3. Kuo A, et al. *J Biomech Eng,* Pages 264-269, 2001.
4. Fritz S, et al. *J of Geriatric and PT,* Pages 2-5, 2009.

RELIABILITY OF HIP AND KNEE KINEMATICS DURING LEVEL AND INCLINE TREADMILL WALKING

Aleksandra R. Budarick[1*], Carson J. Halliwell[1], Derek J. Rutherford[1,2], and Rebecca F. Moyer[1]
[1]School of Physiotherapy, Faculty of Health, Dalhousie University, Halifax, NS, Canada
[2]School of Biomedical Engineering, Faculty of Engineering, Dalhousie University, Halifax, NS, Canada
email: *abudarick@dal.ca

Introduction

Walking is a common form of physical activity across many populations. Walking on an incline can augment health benefits by challenging the cardiovascular and musculoskeletal systems. Laboratory-based gait analyses may investigate incline treadmill walking to challenge the lower extremity joints and assess changes over time; thus, it is important to evaluate the reliability of these assessments to discern true change from error. Although level treadmill and over-ground walking elicit similar kinematic outcomes [1,2], incline walking on a treadmill, compared to a ramp, elicits different kinematic and spatiotemporal parameters [3]. Level treadmill walking demonstrates reliable kinematic measurements [4]; however, the reliability of incline treadmill walking remains unknown. Therefore, the purpose of this study was to quantify the test-retest reliability of hip and knee kinematics during level and incline treadmill walking.

Methods

Twelve asymptomatic, healthy participants (29.7 ± 7.0 years) underwent two standardized data collections approximately one-week apart (range: 3-14 days). Each participant was instrumented with a full-body passive-reflective marker set, and kinematic data were collected at 100Hz using an eight-camera Qualisys motion capture system. Participants walked barefoot at a self-selected speed on a dual belt instrumented treadmill for 6-minutes at a level grade (to achieve a sufficient familiarization and warm-up period) and 3-minutes at an incline (+10°). A 20-s data collection was recorded during the final minute of each walking condition. All kinematic data were averaged across all strides within the 20-s collection and time-normalized to 100% of the gait cycle. One leg was randomly selected for analysis and matched between visits. Sagittal and frontal plane hip kinematics and sagittal plane knee kinematics were calculated using Cardan rotations. Test-retest reliability was assessed using Intraclass-Correlation Coefficients (ICC) and 95% confidence intervals (CI) based on a mean-rating, absolute-agreement, two-way mixed-effects model. ICC values were interpreted using cut-points: ≥0.8 (excellent), 0.60-0.79 (high), 0.40-0.59 (fair), and ≤0.39 (poor).

Results and Discussion

Kinematic waveforms for both walking conditions and data collection days are shown in Figure 1. Test-retest reliability was excellent for sagittal and frontal plane hip, and sagittal plane knee, kinematics with few exceptions (Table 1). ICC values were similar across the level and incline walking conditions, indicating more challenging walking tasks do not exhibit lower test-retest reliability. Absolute angles were less reliable than ranges of motion, particularly at the hip joint. Absolute angles are more prone to measurement error, including marker placement variations, thus decreasing their reliability.

These results indicate that this standardized gait assessment protocol in healthy adults obtains reliable hip and knee kinematic measures during level and incline walking conditions. Further, challenged walking conditions (i.e., incline) are similarly reliable to level walking in controlled laboratory environments.

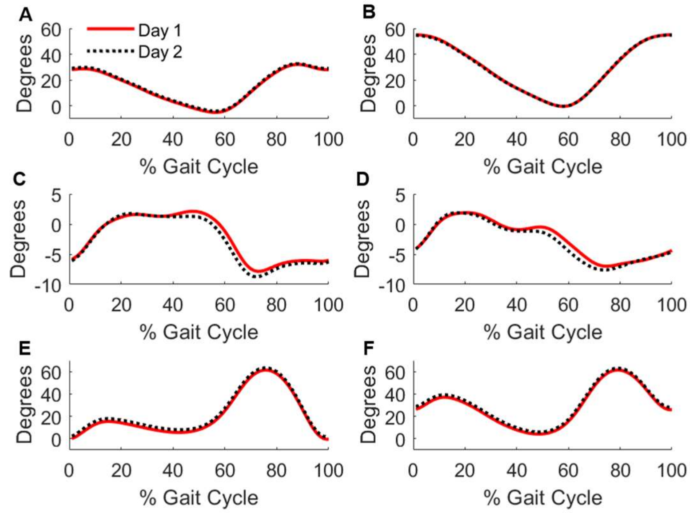

Figure 1. Ensemble average kinematic waveforms during walking for hip sagittal plane at (A) level and (B) incline, hip frontal plane at (C) level and (D) incline, and knee sagittal plane at (E) level and (F) incline.

Table 1. Intraclass-Correlation Coefficients (ICC) and 95% Confidence Intervals (95% CI) for kinematic outcomes.

	Level	Incline
	ICC [95% CI]	
Hip Sagittal Plane		
Max St	0.76 [0.16, 0.93]	0.71 [-0.09, 0.92]
Min St	0.86 [0.52, 0.96]	0.87 [0.54, 0.96]
Max St to Min St	0.85 [0.47, 0.96]	0.93 [0.74, 0.98]
Hip Frontal Plane		
Heel-strike	0.86 [0.51, 0.96]	0.84 [0.43, 0.95]
Max St	0.44 [-1.24, 0.84]	0.69 [-0.17, 0.91]
Heel-strike to Max St	0.87 [0.53, 0.96]	0.87 [0.55, 0.96]
Knee Sagittal Plane		
Heel-strike	0.80 [0.35, 0.94]	0.88 [0.52, 0.97]
Max St	0.84 [0.47, 0.96]	0.84 [0.47, 0.95]
Min Late St	0.78 [0.28, 0.94]	0.91 [0.68, 0.97]
Heel-strike to Max St	0.97 [0.88, 0.99]	0.87 [0.55, 0.96]
Max St to Min Late St	0.96 [0.85, 0.99]	0.96 [0.88, 0.99]
Max Swing	0.87 [0.52, 0.96]	0.85 [0.51, 0.96]

Note: Max = maximum. Min = minimum. St = stance.

Significance

To our knowledge, this is the first study to quantify test-retest reliability of hip and knee kinematics during incline walking. These results suggest this standardized gait assessment protocol produces reliable kinematic measures during level and incline walking; therefore, incline walking can be deemed a reliable assessment tool for lower extremity joint function. Future work should confirm these findings with clinical populations for whom incline walking may present a larger locomotor challenge.

References

[1] Riley et al., 2007. *Gait Posture.* 26(1):17-24. [2] Parvataneni et al., 2009. *Clin Biomech.* 24(1):95-100. [3] Strutzenberger et al., 2022. *Gait Posture.* 91:73-78. [4] Rutherford et al., 2020. *J Electromyogr Kines.* 51:102401.

HOW DOES MOTOR COMPLEXITY ALTER GAIT QUALITY? DATA-DRIVEN ANALYSIS OF SIMULATED MOTOR IMPAIRMENTS.

Michael C. Rosenberg[1*], Taniel S. Winner[1], Gordon J. Berman[2], Trisha M. Kesar[3] and Lena H. Ting[1,3]
[1]W.H. Coulter Dept. Biomedical Engineering, Emory University and Georgia Institute of Technology, Atlanta, GA, USA
[2]Department of Biology, Emory University, Atlanta, GA USA
[3]Department of Rehabilitation Medicine, Division of Physical Therapy, Emory University, Atlanta, GA, USA
email: *mcrose3@emory.edu

Introduction

Motor complexity, defined as the number of muscle synergies needed to explain most variance in muscle activity, is often impaired following neurological injury, such as in stroke and cerebral palsy [1, 2]. Lower (*i.e.,* more impaired) motor complexity is associated with slower walking speeds. However, it is challenging to determine how motor complexity directly impacts walking speed and quality (*e.g.,* holistic similarity to able-bodied gait) of the resulting gait dynamics [3].

Neuromusculoskeletal simulations enable the effects of motor complexity and walking speed on gait dynamics and kinematics to be decoupled. Reducing motor complexity in simulations reduces the ability to achieve able-bodied (AB) gait dynamics [4]. As such, simulations can be used to assess the effects of motor complexity on dynamics. Interactions between walking speed and motor complexity may also affect gait quality, with direct implications for optimizing rehabilitation.

We developed a novel, data-driven technique to holistically evaluate gait dynamics. We encode individualized dynamical *gait signatures* using a recurrent neural network (RNN) model of gait dynamics and dimensionality reduction. This approach enables a compact representation of the net effect of neural and biomechanical constraints on gait dynamics, and can be compared between normative AB and post-stroke gait dynamics [5]. Gait quality is defined as the multidimensional distance between gait signatures, and captures individual differences in post-stroke gait that are associated with motor function level.

Here, we combine neuromusculoskeletal simulation and our data-driven approach to holistically evaluate the potential effects of motor complexity on gait quality. We predicted that, across three speeds, gait quality worsens with lower motor complexity.

Methods

We simulated walking using a sagittal-plane, 7 degree-of-freedom, 8 musculotendon actuator neuromusculoskeletal model that could be constrained to activate muscles in synergistic patterns [4]. We used a direct collocation framework with a cost function minimizing the sum of squared muscle activations and lightly penalizing deviations from baseline gait.

We simulated 15 gait cycles of walking with “unconstrained” motor complexity (8 synergies), and 5, 4, 3, and 2 synergies [4], each at 0.8, 1.0, and 1.4 m/s. Small random perturbations to the initial condition introduced inter-stride variability.

Sagittal-plane hip, knee, and ankle kinematics from all simulations were used to train a sequence-to-sequence RNN [3] . The model had 3 layers with a 500-unit hidden long short-term memory layer and was trained for 3000 iterations. We reduced the RNN’s internal parameters to 6 dominant principal components (PCs), whose weights defined *gait signatures* for each trial. *Gait quality* was defined as the Euclidean distance between each gait signature and the centroidal signature of the *unconstrained* simulations (a normative reference) [3]. *Smaller* distances to the reference centroid imply better gait quality. We evaluated gait quality as a function of speed and motor complexity.

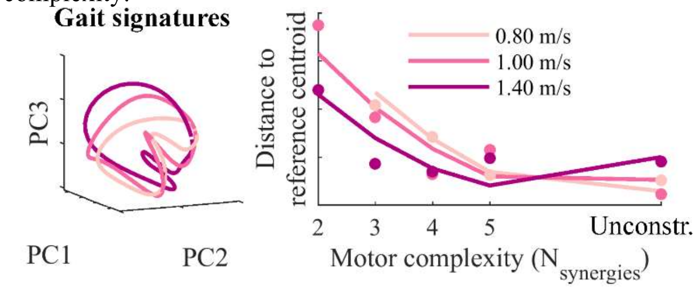

Figure 1: Left: The first 3 PCs showing exemplary “unconstrained” RNN gait dynamics over the gait cycle (one stride) at three speeds. Right: Gait quality (*i.e.,* multidimensional distance to the reference centroid) decreased with motor complexity across speeds (colors).

Results and Discussion

Gait signatures (Fig. 1, left) illustrate changes in gait dynamics with speed. Consistent with experimental associations between motor complexity and walking function (*e.g.,* [2]), the distance of the gait signatures from the unconstrained gait dynamics was greatest when motor complexity was low. Gait quality quadratically was related ($r^2 = 0.77$) to motor complexity ($p = 0.003$; Fig 1, right). Poorer gait quality with lower motor complexity suggests that altered neural constraints can *drive* measurable differences in gait quality. Consistent with findings in stroke survivors, gait quality improved as gait speed increased ($p = 0.030$), (Fig. 1, right) demonstrating that speed can improve gait quality within a level of motor complexity [3, 5]. However, the speed-motor complexity interaction ($p = 0.051$) suggests that motor complexity may constrain changes in gait quality with speed and may explain differences in responses treadmill training in high- vs. low-functioning stroke survivors [6].

Significance

Combining neuromusculoskeletal simulation and data-driven models that encode the generative processes underlying gait, we gained novel insight into how neural constraints impact holistic gait quality. Our approach enables novel characterization of gait whether in patient populations, with assistive devices, or even differences between simulations and reality.

Acknowledgments

Supported by an Emory University Synergy II/Nexus award and the National Institute for Child Health and Human Development of the National Institutes of Health under award numbers R01HD095975 and R21HD095138.

References

1. Steele K. M., et al. *DMCN*, 57, 1176-1182, 2015.
2. Clark D. J., et al. *J of Neurophysiol*, 103, 844-857, 2010.
3. Winner T. S., et al. *American Physical Society*, 2021.
4. Mehrabi N., et al. *J Biomech*, 90, 84-91, 2019.
5. Lamontagne A., et al. *Stroke*, 35, 2543-2548, 2004.
6. Jonkers I., et al. *Gait & posture*, 29, 129-137, 2009.

EFFECT OF FIBER TRACTS AND DEPOLARIZED BRAIN VOLUME ON RESTING MOTOR THRESHOLDS DURING TRANSCRANIAL MAGNETIC STIMULATION

Neil Mittal [1], Connor Lewis [1], Yeajin Cho [1], Ravi L. Hadimani [2] Carrie L. Peterson [1]
[1]Department of Biomedical Engineering, Virginia Commonwealth University, Richmond, VA 23220, USA
[2]Department of Mechanical and Nuclear Engineering, Virginia Commonwealth University, Richmond, VA 23220, USA
email: clpeterson@vcu.edu

Introduction

Finite element modeling simulations of transcranial magnetic stimulation (TMS) using complex head models and coils have been used to better understand neuromodulation strategies. TMS is a promising neuromodulation paradigm for brain mapping, diagnostics, and treatment of neurological and psychiatric disorders [1]. However, TMS is limited by high intra- and inter-subject variability in its effects [1]. The purpose of this study was to investigate the effect of neuroanatomy on response to TMS. We investigated the dependence of resting motor threshold (RMT) on neuroanatomy including fiber tracts which is related to functional connectivity in the motor pathway network. We hypothesized that RMT would negatively correlate with depolarized volume of grey matter (DVG), indicating greater TMS response with more brain volume depolarization.

Methods

Ten healthy individuals (7 females, 3 males, 23.5 ± 5 years) participated after screening to ensure safety of the TMS and MRI protocols. Participants underwent TMS sessions targeting the motor hotspot of the first dorsal interosseous. Each participant had 2 RMT measurements in their session, to account for intra-subject variability. Structural T1- and T2-weighted images and whole brain diffusion weighted images were acquired for head model generation and fiber tractography from diffusion tensor imaging (DTI) respectively. Extracted T1- and T2-weighted images passed a SimNIBS pipeline to create individual segments. Sim4Life finite element analysis software was used to compute magnetic field, B, and induced electric field, E on the generated head models from peak intensity stimulation of the primary motor cortex. Fiber tracts were extracted from DTI using DSI Studio based on the anatomical landmarks (superior frontal sulcus, precentral sulcus, central sulcus, and precentral gyrus) to the “knob” of the primary motor cortex. Spearman’s correlation tested for associations between either DVG or fiber tract surface area and RMT. Linear mixed effects models tested for associations between DVG and fiber tract surface area and their effects on RMT.

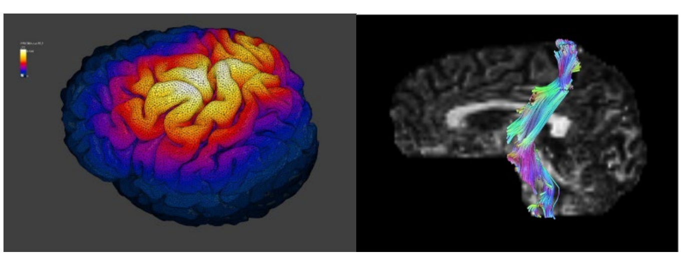

Figure 1: Left) Simulated magnetic field on cortex. Right) Corticospinal fiber tracts were extracted from DTI beginning from a region of interest that encompassed upper limb motor control in the primary motor cortex.

Results and Discussion

A linear mixed effects model including the interactions between DVG and fiber tract surface area revealed an association between RMT and DVG ($p < 0.001$). RMT negatively correlated with DVG, but only at high fiber tract surface area. The correlation became less negative as fiber tract surface area decreased, until a positive correlation was observed at the lowest fiber tract surface area range. DVG and fiber tract surface area were positively correlated ($p = 0.013$). Thus, our hypothesis that RMT would correlate negatively with DVG was partially supported; this relationship was found with a negative correlation between RMT and DVG, but only when accounting for fiber tract geometry, with larger fiber tracts (high fiber tract surface area).

The interaction between DVG and fiber tract geometry suggests that the expected relationship between brain depolarization and TMS evoked motor response is dependent on the connectivity within the cortex and overall neuroanatomy. Previous studies also support that the relationship between brain depolarization and TMS evoked motor response is dependent on the connectivity within the cortex and neuroanatomy. Rossi, et al., discussed age-related influences on TMS intensity variation between individuals, with neuroanatomical differences between children and older individuals being one driver in the intensity variation [2]. Cantone, et al., showed that individual physiological differences affect the amplitudes of motor evoked potentials elicited by TMS, further highlighting the impact of individual neuroanatomy [3]. TMS studies paired with electroencephalography have shown that induced activity spreads along motor networks [4], and cortical connectivity and hemodynamics can be modulated by repetitive TMS paradigms [5]. That is, it would be expected that more depolarized brain results in a motor response with less required stimulation as the brain is more sensitive to stimulation as a whole. This did occur in the present study in the presence of higher fiber tract surface area, as fiber tract surface area was a metric of cortical connectivity.

Significance

Our results show that the effects of TMS are governed by cortical organization due to anatomy and fiber tract geometry. Further investigation is needed to understand the mechanistic drivers of the relationship between depolarized brain volume and RMT at different fiber tract sizes.

Acknowledgments

This study was supported by the Virginia Commonwealth University Center for Rehabilitation Science and Engineering, and the Commonwealth Cyber Initiative.

References

[1] A. Herrold *et al.*, 2020 *J. Head Trauma Rehabil.*, v35.
[2] S. Rossi *et al.*, 2009 *Clin Neurophy*, v120.
[3] M. Cantone *et al.*, 2019 *Front. Hum. Neurosci.*, v13.
[4] M. Bortoletto, et al., 2015 *Neurosci. Biobehav. Rev.*, v49.
[5] R. Li *et al.*, 2019 *Front. Hum. Neurosci.*, v13.

EFFECTS OF INCREASING SKIN TEMPERATURE ON FOOT SENSITIVITY AND POSTURAL CONTROL IN DURING AGING

Mathias S Machado[1]*, Álvaro S Machado[1], Eliane C Guadagnin[1], Daniel Schmidt[2], Andresa M C Germano[2], Felipe P Carpes[1]
[1]Applied Neuromechanics Research Group, Federal University of Pampa, Uruguaiana, RS, Brazil
[2] Motor Control, Cognition and Neurophysiology, Institute of Human Movement Science and Health, Chemnitz University of Technology, Chemnitz, Germany
email*: sosamathiasun@hotmail.com

Introduction

Aging is accompanied by impaired capacity of motor control associated with reduced proprioceptive functions and lower foot skin sensitivity [1, 2]. Increased foot temperature can be utilized to alter both skin sensitivity and postural control responses in young adults [3-5]. Here, we hypothesize that foot warming can also be advantageous for older adults, resulting in better foot sensitivity and postural responses.

Methods

Two protocols for foot warming were applied in 18 older adults (14 ♀) (age mean ± SD: 65.8 ± 6.2 years) aiming to increase foot temperature by 5–6°C compared to the baseline using infrared radiation at plantar aspects and the whole foot and ankle region (Figure 1). Before and after warming the foot, skin sensitivity (Semmes Weinstein filaments) was measured at 10 anatomical locations (Figure 2). Furthermore, the upright postural control with open and closed eyes was assessed before and after the warming protocols. The Center of pressure (CoP) parameters were: the 95% ellipse area (cm²), mean displacement velocity (cm/s), and range in the anteroposterior and mediolateral directions (cm). Inferential statistical analyses were performed for skin sensitivity and CoP data (α=0.05) to compare pre and post warming effects and the protocols.

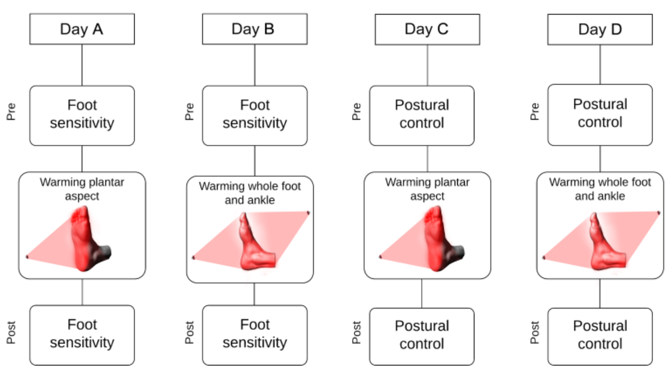

Figure 1: Experimental design. Participants visited the laboratory on four days (A, B, C, and day D) to assess foot sensitivity and postural control before and after two warm-up protocols (plantar aspect and whole foot and ankle) in randomized order.

Results and Discussion

Both protocols successfully induced foot warming, with no differences between the evaluation days (average increase of 5.7ºC). When the whole foot and ankle region were warmed, sensitivity increased in the plantar forefoot and midfoot regions of both feet (Figure 2). Surprisingly, when warming the plantar aspects only, no change in sensitivity was observed. This finding does not agree with previous studies [4, 5], but may be explained by the participants' characteristics or different methodological aspects (e.g., mechanical stimuli, warming protocol). A similar protocol conducted on young participants showed improved sensitivity after plantar warming [3]. However, the effects were higher following warming of the whole foot and ankle region. Here, similar to the sensitivity results, the mediolateral amplitude of the CoP data (in closed eyes condition) decreased only when the whole foot and ankle region was warmed ($F_{(1)}=10.405$; $p=0.005$). No changes in postural control were evident after warming only the plantar aspect. These results can be explained by the lack of changes in foot sensitivity following this protocol. However, in a recent study [3], we investigated a similar protocol in young adults and found improved balance performance using both warming procedures. It appears that older adults require an enlarged area to be warmed to improve skin sensitivity and, consequently, to impact postural capacity. Further studies are planned to examine this issue further.

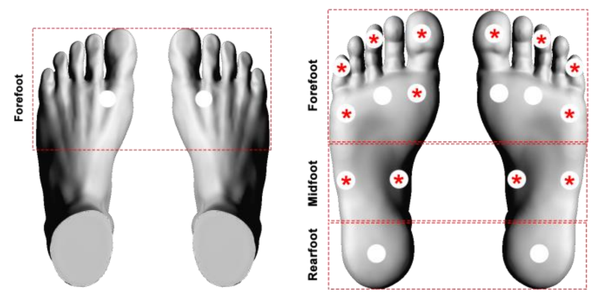

Figure 2: White circles indicate anatomical locations: forefoot; lateral and medial midfoot and rearfoot. Significant improvements of sensitivity after plantar and dorsal warming are highlighted with red asterisks (* p≤0.05).

Significance

Passive warming of the whole foot and ankle promoted increased skin sensitivity. Furthermore, mediolateral postural control with eyes closed improved in the elderly subjects. Acute sensitivity gain can be useful for older adults to improve balance during everyday tasks and can be a tool for clinical interventions, e.g., for patients in rehabilitation treatment programs.

Acknowledgments

This research is funded by the PROBRAL/PPP program from Coordenação de Aperfeiçoamento de Pessoal de Nível Superior (CAPES)/DAAD granted to FPC, and AMCG (grant number 88881.371321/2019-01). Fundação de Amparo à Pesquisa do Estado do Rio Grande do Sul, Brazil funded ECG (18/2551-0000525-8) and MSM (young investigator fellowship). A research fellowship from CNPq-Brazil supports FPC.

References

[1] Peterka, 2002. *J. Neurophysiol.* 88: 1097–1118.
[2] Machado et al., 2017 *Rev. Bras. Reumatol.* 57: 30–36.
[3] Machado et al., 2021. *Foot.* 101887.
[4] Schlee et al., *Clin. Neurophysiol*. 120: 1548–1551.
[5] Schmidt et al., 2016. *Clin. Neurophysiol. Pract.* 2: 38–43.

DO HUMANS REGULATE MEDIOLATERAL STABILITY FROM STEP-TO-STEP?

Meghan E. Kazanski[1*], Joseph P. Cusumano[2], Jonathan B. Dingwell[1]
[1] Department of Kinesiology, Pennsylvania State University, University Park, PA 16802, USA
[2] Department of Engineering Science & Mechanics, Pennsylvania State University, University Park, PA 16802, USA
*email: mek79@psu.edu

Introduction

Maintaining frontal-plane stability is a major objective of human walking. Humans overcome mediolateral instability by adjusting center-of-mass (CoM) dynamics and foot placement [1].

Several simulated and empirical walking studies have proposed that humans adjust these dynamics to achieve a constant mediolateral Margin-of-Stability (MoS_{ML}) [2]. However, we still lack a coherent theoretical framework to develop and test hypotheses regarding how walking humans regulate CoM state fluctuations to achieve stability, defined here by MoS_{ML}.

Here, we unify the well-established inverted-pendulum model with analyses based on the goal-equivalent manifold (GEM) concept [3]. We use this framework to test our hypothesis that humans regulate their CoM dynamics from step-to-step to maintain a constant MoS_{ML}.

Methods

We identified a linear candidate stability GEM in the inverted pendulum model phase plane (Fig. 1A). All CoM dynamics along this line achieve a constant MoS_{ML}. To test our hypothesis that humans adopt a constant MoS_{ML} stability strategy, we evaluated whether humans exploit CoM state redundancy along this GEM.

We extracted time series of CoM state (z_n, $\dot{z}_n$), lateral support boundary $(u_{max})_n$, and minimum mediolateral MoS $(MoS_{ML})_n$ at each step n from walking trials of 17 older (ages 60+) and 17 young (ages 18-31) healthy adults in the presence of visual and platform perturbations [4]. We converted $[(z-u_{max})_n, (\dot{z}/\omega_0)_n]$ coordinates into perpendicular, 'goal-relevant' (δ_P) and tangent, 'goal-equivalent' (δ_T) deviations from the candidate stability GEM. We quantified variability (σ) and statistical persistence (DFA-α) of δ_P and δ_T.

To characterize the extent to which participants exploited kinematic redundancy to achieve constant MoS_{ML} at each step, we evaluated whether CoM variability aligned with the GEM, *and* how readily deviations off of the GEM were corrected. A constant MoS_{ML} stability strategy would be indicated by reduced variability of CoM dynamics perpendicular to the GEM ($\sigma(\delta_P) << \sigma(\delta_T)$), as well as readily corrected deviations perpendicular to but not along the GEM ($\alpha(\delta_P) \approx 0.5 << \alpha(\delta_T)$).

Results and Discussion

Participants' variability of CoM states were aligned along the constant-MoS_{ML} GEM, indicated by δ_P deviations off of the constant-MoS_{ML} GEM that were far less-variable than δ_T deviations along the GEM (Fig. 1B).

However, while participants readily corrected δ_P deviations off of the GEM (i.e., $\alpha(\delta_P) \approx 0.5$), they *also* readily corrected δ_T deviations along the GEM (i.e., $\alpha(\delta_P) < \alpha(\delta_T) << 1$) (Fig. 1C). Since participants readily corrected δ_T deviations tangent to the GEM, they did not exploit equifinality along the GEM in ways consistent with a constant-MoS_{ML} stabilizing strategy.

Despite how CoM variability was structured along the GEM, the isotropy of deviation corrections supports the hypothesis that participants tightly regulate CoM dynamics from step-to-step, just not as part of the proposed stability strategy.

Furthermore, the extent to which participants regulated foot placement variables of step width (w) and mediolateral body position (z_B), strongly predicted the extent to which they regulated CoM deviations δ_P and δ_T (not shown). Thus, how people regulated w (and to a lesser-extent z_B) predicted their regulation of CoM state. Since walking humans cannot directly actuate their CoM itself, this suggests that regulation of mediolateral CoM state occurs as a biomechanical consequence of regulating foot placement.

Significance

Identifying what control variables humans regulate to achieve locomotor stability is a major focus in biomechanics. While MoS_{ML} has been widely-implemented to quantify gait stability, and constant MoS_{ML} control schemes have been posed, our findings demonstrate that humans do not regulate their CoM dynamics to enact such a scheme. Our finding that CoM states and foot placement variables are regulated in mutually consistent ways *across* steps complement the *within* step mapping between foot placement deviations and CoM states identified in other studies [5].

Acknowledgments

NIH / NIA Grant #: R01-AG049735.

References

[1] Bruijn et al., 2018. *J. R. Soc. Interface.* 15: 20170816.
[2] Hof et al., 2005. *J. Biomech.* 38(1), 1-8.
[3] Cusumano et al., 2006. *Biol. Cybern.* 94, 367-369.
[4] Kazanski et al., 2020. *J. Biomech*. 104: 109714.
[5] Wang et al., 2014. *Biol. Let.* 10(9): 20140405.

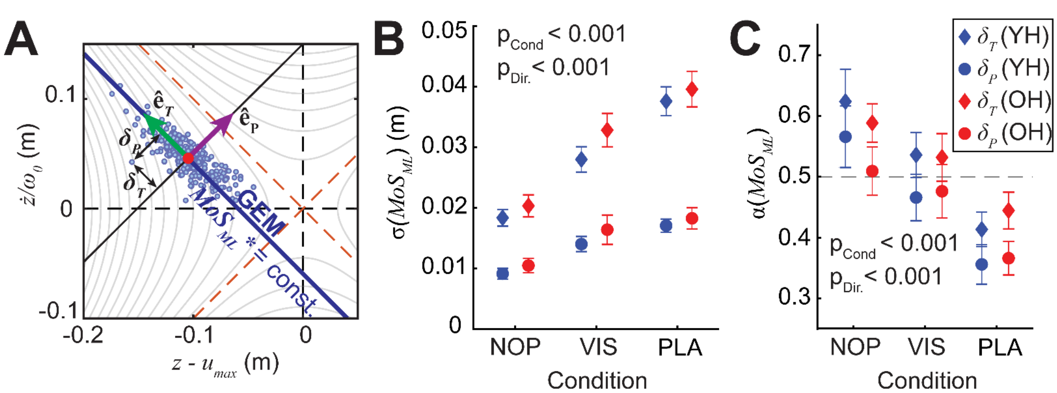

Figure 1: (A) Schematic of the candidate stability GEM for human walking. The solid line defines a MoS-based GEM, containing all combinations of mediolateral CoM state components achieving the task goal to maintain MoS_{ML}^* = const. For each trial $MoS_{ML}^* = \overline{(MoS_{ML})_n}$. CoM states were decomposed into tangent $(\delta_T)_n$ and perpendicular $(\delta_P)_n$ deviations from the GEM in $[\hat{e}_P, \hat{e}_T]$. **(B)** Variability and **(C)** statistical persistence of deviations (DFA exponent: α) for δ_P and δ_T time series.

NEUROMECHANICAL LOCOMOTOR AFTER-EFFECTS AS A FUNCTION OF GRAVITY LEVEL

Chase G. Rock[1], Angela Luo[1], Xiao Yang[1], and Young-Hui Chang[1,2]
[1]School of Biological Sciences, Georgia Institute of Technology, Atlanta, GA, USA
[2] BioEngineering Program, Georgia Institute of Technology, Atlanta, GA, USA
email: crock@gatech.edu

Introduction

When landing from a jump, muscles of the lower limb are activated prior to ground contact to mitigate the risk of injurious muscle stretch[1,2]. This ‘preactivation’ in preparation for landing indicates a prediction of the effects of gravity on the body, as the timing of preactivation is tightly controlled to occur at a set time prior to landing[3]. In fact, manipulating gravitational acceleration leads to a delay in preactivation timing[4]. Recently, we have discovered that this delay in preactivation timing persists upon returning to normal gravity[5]. However, the gravity-dependence of this adaptive after-effect is not fully understood. In the current study, we simulated a range of reduced gravity levels to promote adaptation of preactivation timing and then tested for the presence of a subsequent after-effect. We hypothesized that a critical gravity level exists below which adaptive after-effects would occur but above which after-effects would not occur.

Methods

In this retrospective analysis, data from two cohorts of participants were investigated for adaptive after-effects following exposure to varying levels of simulated reduced gravity. The first cohort (n = 10) engaged in one-legged jumping on the dominant limb before (PRE), during, and after (POST) exposure to a simulated gravity level targeted at 0.5 g. The second cohort (n = 7) followed the same protocol, but each participant in the second cohort went through the protocol twice, with a different gravity level targeted in the first and second exposure. The one-legged jumping task required participants to perform a countermovement jump targeted at 75% of their maximum one-legged jump height. This target was used for all 70 jumps (10 PRE at 1g; 50 in simulated reduced gravity, <1g; 10 POST at 1g). Electromyographic activity was recorded from the medial gastrocnemius (MG) and soleus (SOL) muscles of the dominant limb and ground reaction forces were measured via a force plate to determine the time of landing. To assess for the presence of an after-effect, the preactivation timing on the first POST jump was compared to baseline preactivation timing (i.e., mean of the final 3 PRE trials) via a paired t-test. Participants were grouped according to actual simulated reduced gravity level experienced, resulting in three groups of 8 participants each: Lower G (0.42 ± 0.08 g), Middle G (0.54 ± 0.04 g), and Higher G (0.65 ± 0.02 g).

Results and Discussion

Of the three different gravity groups, only those in the Lower and Middle G groups exhibited significant aftereffects in either MG or SOL. Upon returning to normal gravity, the Lower G group showed significant delays in preactivation timing in MG (p = .007; Fig. 1) and in SOL (p = .037). This delay was also experienced by the Middle G group in MG (p = .021) but not in SOL (p = .256). The Higher G group did not have a significant aftereffect for either muscle (MG: p = .422; SOL: p = .210). The existence of an aftereffect in lower levels of simulated gravity but not at the higher gravity level is consistent with our hypothesis that a critical gravity level exists below which adaptation leads to after-effects. The results of the current study point to that critical gravity level being between 0.54 – 0.65 g for MG and between 0.42 – 0.54 g for SOL. While the effect of different gravity levels on preactivation timing is known[4], the current study is the first to show the after-effect upon returning to normal gravity also depends on the simulated gravity level.

Jumping in simulated reduced gravity leads to neuromuscular adaptation in the form of delayed preactivation times upon return to 1g. This effect seems to arise only when the simulated gravity is low enough to cross a critical sensory threshold that exists between 0.42 and 0.65 g.

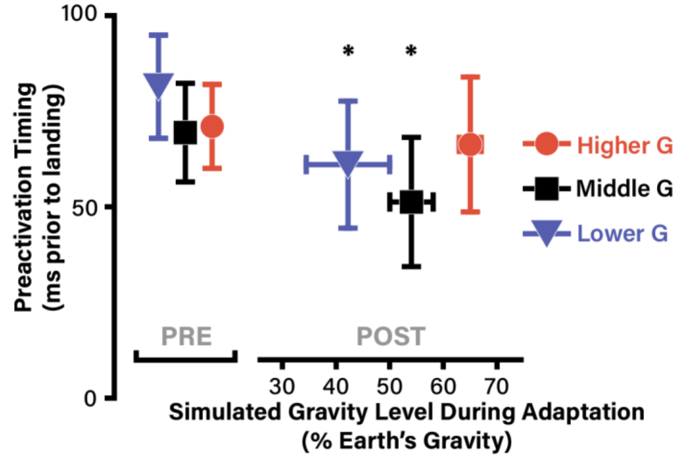

Figure 1: Preactivation timing of the medial gastrocnemius muscle at 1g is delayed following hypogravity adaptation in groups that experienced a simulated gravity level less than ~65% of Earth’s gravity. The groups that experienced the lowest (Lower G: blue triangle) and middle (Middle G: black square) levels of simulated gravity saw significant differences between POST (left) and PRE (right), but this difference did not exist for the group that adapted to the highest simulated gravity (Higher G: red circle). * indicates significant difference from PRE (p < .05)

Significance

Humans can adapt to many novel and challenging environmental constraints. When it comes to the novel task of adapting to a new gravity level, it appears that there may be a critical sensory threshold where difference from Earth gravity is large enough to prompt significant changes to the motor strategy. Understanding which changes in the physical environment require sensorimotor adaptation will help elucidate the neuromuscular strategies for accommodating an ever-changing environment.

Acknowledgments

This work is supported by the HEERF-III program and NSF GRFP to CGR (DGE-1650044). Any opinions, findings, and conclusions or recommendations expressed are those of the authors and do not necessarily reflect the views of the NSF.

References

1. Azizi, E. & Abbott, E. M. *Biol. Lett.* **9**, 8–11 (2013).
2. Greenwood, R., et al. *Physiol.* **254**, 507–518 (1976).
3. Santello, M., et al. *Exp. Physiol.* **83**, 857–874 (1998).
4. Gollhofer, A., et al. *Int. J. Sports Med.* **12**, 34–40 (1991).
5. Rock, C., Yun, K., Luo, A. & Chang, Y. In review.

ADAPTATIONS OF GROUND REACTION FORCES IN ABRUPT VS GRADUAL SPLIT BELT TREADMILL WALKING

Olivia S. Elie[1], Montgomery Bertschy[2], Maia Schlechter[2] , Daniel Gregory[2,3] , Wouter Hoogkamer[2] , Brian P. Selgrade[1]*
1 – Department of Sports Medicine & Human Performance, Westfield State University, United States
2 – Department of Kinesiology, University of Massachusetts Amherst, United States
3 – Shriners Children's New England, Springfield, MA, United States
Email bselgrade@westfield.ma.edu

Introduction

Split-belt treadmill walking involves two treadmill belts moving at different speeds and has previously been used to correct gait asymmetry in stroke survivors. Motor adaptation is defined as trial-to-trial modification of a movement based on sensory feedback [1]. Abrupt onset split-belt walking has induced aftereffects in braking but not propulsive ground reaction forces when the split-belt condition is removed [2], suggesting predictive control of braking and reactive control of propulsion. However, prior work with gradual onset split-belt walking under different conditions found aftereffects in braking *and* propulsive force, suggesting predictive control for both.

The purpose of this study was to compare locomotor adaptation of ground reaction forces during abrupt and gradual onset split-belt walking using similar conditions. We hypothesized that there would be aftereffects in braking force and propulsive force after both abrupt and gradual onset adaptation, indicating predictive control of braking and propulsion (alpha=0.05).

Methods

Twenty subjects were randomly assigned to either gradual or abrupt acceleration of one treadmill belt. Each experiment began with a 2-minute slow baseline (0.7m/s) and 2-minute fast baseline (1.4m/s), followed by a 1-minute slow baseline trial (Fig. 1). For the gradual group, fast belt speed slowly accelerated to 1.4m/s over 350s. For the abrupt group, fast belt speed increased immediately to 1.4m/s. After 15 minutes of adaptation to the split-belt condition, the fast belt immediately decelerated back to the same speed as the slow belt. This post-adaptation continued for 10 minutes. We calculated step length symmetry, peak braking and propulsive forces and braking and propulsive impulse, then conducted one-way, repeated measures ANOVA for each group, using post hoc Tukey HSD tests for pairwise comparisons when there were significant main effects.

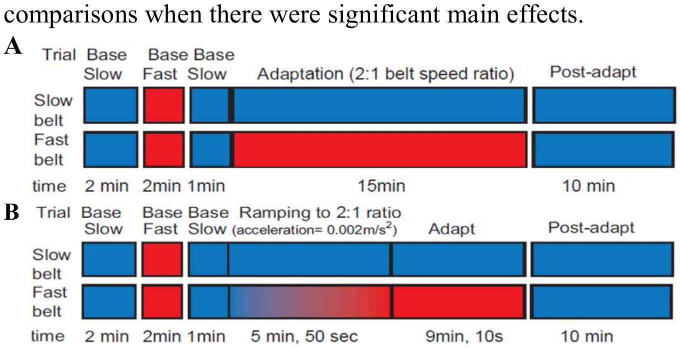

Figure 1: Experimental protocol for abrupt (A) and gradual (B).

Results and Discussion

There were significant aftereffects in the fast leg's peak propulsive forces for both the gradual ($p=0.019$) and abrupt groups ($p<0.001$). Peak braking forces showed significant aftereffects for both legs and both gradual and abrupt groups ($p\leq0.001$ for both groups and both legs). We observed significant aftereffects in step length symmetry ($p=<0.001$ for both groups). We also found significant aftereffects for propulsive impulse for the fast leg ($p<0.001$ for abrupt, $p=0.012$ for gradual) and braking impulse for the slow leg ($p\leq0.001$ for both abrupt and gradual). Lastly, the abrupt split-belt condition caused significant aftereffects in slow leg peak propulsive force ($p=0.025$).

These data support our hypothesis that in both gradual and abrupt split-belt conditions, propulsive and braking forces would have aftereffects, indicating predictive control of anterior-posterior leg forces, in which the motor control system gradually changes limb forces in response to sensory feedback over many strides rather than reacting immediately to feedback from the same stride. These results are consistent with previous research [3], which found aftereffects in propulsive and braking forces in people with amputations. The study that found no aftereffects for propulsive force used relatively slow belt speeds (1.0m/s for the fast belt), which could explain the discrepancies between studies. A slower belt speed may have caused propulsive forces effect sizes that were too low to yield statistical significance.

These findings indicated that gradual and abrupt onset split-belt walking induce similar kinetic aftereffects. Prior work showed similar aftereffects in step length symmetry whether the split-belt condition was introduced gradually or abruptly [4]. The present study supports this finding and extends it to anterior-posterior forces and impulses. Overall, this indicates that not just step length symmetry adapts via predictive control but that the forces that drive changes in step length are controlled predictively as well.

Significance

Split-belt treadmill walking has potential to correct gait asymmetry in clinical populations. Our results show similar aftereffects for both conditions. The patients most likely to benefit from split-belt walking (e.g. stroke survivors) also tend to have poor balance. Gradual onset challenges balance less than abrupt onset, making it potentially useful for gait rehabilitation in clinical populations. However, most studies of locomotor adaptation focus on abrupt onset. Aftereffects provide a glimpse at what could be a more permanent result of repeated split-belt therapy, so similar aftereffects between gradual and abrupt conditions suggest that gradual onset could produce similar benefits to sudden onset with less of a challenge to balance.

Acknowledgments

This research was supported by Priscilla M. Clarkson Endowment Scholarship from the University of Massachusetts Amherst.

References

[1] Bastian et al.; 2008. *Curr Opin Neur.* 21:628–33
[2] Ogawa et al.; 2014. *J. Neurophysiol*. 111, 722–732.
[3] Selgrade & Chang. 2020. Am Soc Biomechanics Conference.
[4] Torres-Oviedo & Bastian. 2012. *J. Neurophysiol*. 107, 346-56.

A LINK TO NEURAL OSCILLATIONS THROUGH WAVELET TRANSFORMS: EFFECT OF DUAL TASK STANDING ON CENTER OF PRESSURE TRAJECTORIES IN MULTIPLE SCLEROSIS

Brittany N. Sommers*[1], Brian L. Davis[1], Douglas A. Wajda[2]
[1]Cleveland State University Mechanical Engineering Department – Center for Human Machine Systems, Cleveland, OH, USA
[2]Cleveland State University Health and Human Performance Department – Center for Human Machine Systems, Cleveland, OH, USA
*email: b.n.sommers@vikes.csuohio.edu

Introduction

Neural oscillations (NOs) of the brain are categorized in five ranges: gamma, beta, alpha, theta, and delta, each corresponding to a frequency range [1]. These NOs represent activity of the central nervous system (CNS) during daily living. In conditions such as Multiple Sclerosis (MS), a condition caused by degeneration and demyelination of white matter of the brain, the connection between NOs and motor outputs such as center of pressure (COP) trajectories may be impaired.

This study uses discrete wavelet transforms (DWT) to decompose COP trajectories during dual task standing into frequency ranges analogous to NOs associated with visual and balance tasks. Alpha NOs are widely reported to increase activity when the eyes are closed [1]. Due to the disruption of neuromuscular signaling caused by demyelination, it was hypothesized that (1) Patterns seen in alpha NOs will be reflected in the motor outputs of COP and (2) For COP amplitudes in frequency ranges corresponding to alpha NOs (8 – 12 Hz), MS individuals will have higher COP amplitudes compared to able-bodied controls.

Methods

Thirty-three (33) able-bodied controls and sixteen (16) MS participants volunteered for the study. Ages for controls and MS were 62.6 ± 9.1 and 55.3 ± 11.1 years, respectively. Participants completed four postural tasks within one testing session. Postural tasks were (1) eyes-open quiet standing (EO), (2) eyes-closed quiet standing (EC), (3) EO standing while responding to an auditory cue (STA), and (4) EO standing while responding to an auditory cue and leaning to their limits of stability (LOS). COP signals were analyzed at 100 Hz, with a focus on the anterior-posterior (AP) sway directions. The AP COP signals were decomposed with a level 12, Symlet 2 (sym2) wavelet decomposition. The number of levels and type of wavelet were chosen based on previous work by the authors [2].

The DWT technique allows for analysis of specific frequency bands. At each decomposition level, a set of wavelet coefficients are produced. The average wavelet coefficients (AWC) can be estimated at each decomposition level, representing the COP amplitude. Decomposition level 4 (L4) was used for analysis in this study as it contains frequencies analogous with the alpha NO band (L4 = 6.25 – 12.5 Hz, alpha NO = 8 – 12 Hz).

Results and Discussion

AWC were calculated for MS (AWC_{MS}) and able-bodied controls (AWC_C) at L4 for the four tasks (EO, EC, STA, LOS). *Within* each group, three AWC comparisons were made: EO vs. EC, EC vs. STA, and EC vs. LOS. These comparisons were made to test if, for visual constraints, the COP amplitudes have similar activity patterns to those reported for alpha NOs. *Between* groups, comparisons were made for the AWC magnitude difference between the task comparisons (i.e., difference in AWC between EO vs. EC, between EC vs. STA, etc.) (Table 1).

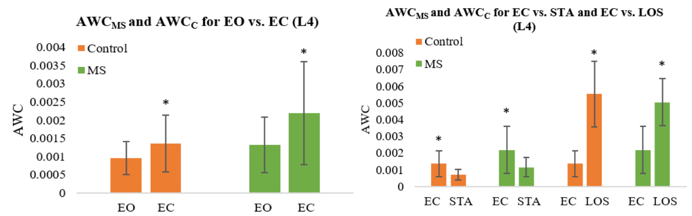

Fig. 1: AWC_{MS} and AWC_C at L4 (6.25 – 12.5 Hz) for MS (green) and controls (orange) for task comparisons EO vs. EC (left), EC vs. STA (right) and EC vs. LOS (right). * Indicated statistical significance *within* the MS or control group for the tasks being compared.

Table 1: Difference in AWC magnitude between task comparisons for control and MS. *Indicates that the difference in AWC between tasks is significantly different between MS and controls.

Task Comparison	AWC_C Task Difference	AWC_{MS} Task Difference	Significance (p-val) Between Groups
EO vs. EC	0.00040	0.00087	0.049*
EC vs. STA	0.00066	0.0010	0.127
EC vs. LOS	0.00418	0.0029	0.0040*

For controls, L4 COP amplitudes (AWC_C) were significantly greater in the EC task compared to EO ($p = 0.002$). Additionally, AWC_C were significantly greater in the EC task compared to STA ($p < 0.0001$). Interestingly, the AWC_C were significantly greater in the LOS task compared to EC ($p < 0.0001$).

For MS, L4 COP amplitudes (AWC_{MS}) displayed similar patterns to controls, with significantly greater AWC_{MS} for EC versus EO ($p = 0.002$) and STA ($p < 0.0001$) and significantly greater AWC_{MS} for LOS compared to EC ($p < 0.0001$). From Table 1, the MS group exhibited a significantly greater increase in AWC magnitude for EC vs. EO and EC vs. LOS than control.

Previous research has shown that the activity in the alpha neural band increases when the eyes are closed. Similarly, this study showed that COP amplitudes corresponding to the neural alpha range increased significantly when the eyes were closed (EC), and also increased for dual tasks (LOS) for both controls and MS. Additionally, COP amplitudes were almost always greater for the MS group than control group among the tasks, likely due to the disruption of neural signaling caused by the MS condition.

Significance

This study tested the hypothesis that decomposed COP trajectories will exhibit similar activity patterns to neural oscillations. The results suggest that there is a connection, thus future would should extend to (1) examining other decomposition levels corresponding to other neural oscillation bands and (2) collecting EEG and COP data in the same study to validate these relationships.

References

[1] Wittenberg E. Front Hum Neurosci. 2017; 11: 170.
[2] Sommers B. Gait & Posture. 2021; 88.

HAIR CONSIDERATIONS FOR EQUITABLE SUBJECT REPRESENTATION IN NEUROMECHANICS

Lietsel Richardson, M.S.[1], Nina Woodley, A.A.S.[2], Jennifer Sandoval., Ph.D.[3], Lindsay Neuberger, Ph.D.[3] and Helen J. Huang, Ph.D.[4]
[1]Burnett School of Biomedical Sciences, University of Central Florida
email: lietsrichardson@knights.ucf.edu

Introduction

More researchers in neuromechanics are beginning to measure brain activity to understand neural control more comprehensively for a variety of tasks such as grasping, arm reaching, standing, cycling, walking, and running. The primary accessible technique to investigate brain activity is electroencephalography (EEG), which has provided insight into the neural control of movement. Despite its utility, the methods and hardware upon which EEG was developed is inherently exclusive such that EEG findings are not representative of the entire population.

EEG requires a solid connection between the electrode and scalp, either with dry electrodes that fit tightly, or wet electrodes that use a conductive gel as a conduit to connect the electrodes with the scalp. As such, incompatibility with different hair types, primarily curly and tightly coiled hair, could hinder the ability to record viable EEG signals. The largest part of the global population with curly and tightly coiled hair types identifies as African, African American, or Caribbean and are at risk of being declined from taking part or excluded from EEG research [1]. A few groups have worked on hardware approaches, developing electrodes such as the Sevo electrodes that work specifically with curly and tightly coiled hair types [2].

With the growing concern that EEG findings do not represent all individuals, we created and shared a working document with guidelines to provide EEG researchers options for preparing different hair types for EEG recordings (UCF BRaIN Lab EEG Hair Project, https://hellobrainlab.com/research/eeg-hair-project/). Knowing that we, and likely most other EEG researchers, have limited experience with preparing different hair types, we launched a survey to gather researcher and participant experiences with hair and EEG preparations and to examine potential roots of the exclusion problem in EEG research. Here, we present preliminary results from our survey for current or new researchers using EEG for neuromechanics studies to consider to conduct more inclusive brain research.

Methods

An online survey hosted on Qualtrics was made available on the UCF BRaIN Lab's website and distributed primarily through the team's professional network, social media, and organizations like Black in Neuro that shared survey information with their membership. The University of Central Florida's Institutional Review Board approved the online survey. For this abstract, we analyzed responses collected from August to December 2021 with a total of 230 respondents of primarily EEG researchers (academia and healthcare) and some past participants. Our analyses here focus on responses from researchers. We used statistical analyses in Qualtrics to examine the strength of relationships between survey responses related to EEG preparation experience, subject recruitment, and subject exclusion.

Results and Discussion

When researchers were asked to identify potential community barriers that would prevent equitable recruitment and retention, the most frequently used words were research, participant, people, community, and time (Fig. 1).

Figure 1: Generated word cloud shows how often key words were mentioned in survey responses of survey respondents who have conducted EEG preparations and data collections to the prompt to share what they think are barriers that limit their ability to have a diverse pool of participants. Larger and darker words were mentioned more frequently.

Researchers were also asked to report the total number of EEG preparations (data collections) performed in their role, Black or African American subjects recruited, and an estimate of those participants declined or excluded from their dataset. A one-way ANOVA revealed a strong statistical relationship ($p=0.001$) between the total number of Black/African American subjects recruited and the number of those participants declined from participating or excluded from the study. A ranked correlation analysis ($p = 0.000549$) showed that as the total number of EEG preparations increases, the potential for disproportionate exclusion increases as well. These results highlight the role that race, ethnicity, and hair play in the recruitment and retention of Black/African American subjects in EEG research.

Significance

These findings unveil an unsettling truth that some participants are denied or excluded from brain research on hair type, a factor that is highly influenced due to race and ethnic origins. If this issue is indeed prevalent in all EEG studies, then these results further motivate the brain research community to consider additional mechanisms in their respective fields that might contribute to inadvertent participant exclusion. Would you and your students benefit from cultural competency training or a collaboration with a hair specialist to improve subject interaction? Are your preparation techniques comprehensive of all hair types? What modifications would you apply to your hardware to improve hair compatibility? These are all considerations researchers should make when implementing EEG and other electrophysiological techniques in their work.

Acknowledgments

This work was supported by NIH R01AG054621 to HJH.

References

[1] Choy, T. et al., 2021. *Affective Science*. doi:10.1007/s42761-021-00050-0
[2] Etienne, A. et al., 2020. *bioRxiv* 2020.02.26.965202.

INTRINSIC MODULUS OF COLLAGEN FIBRES IN CARTILAGE DID NOT CHANGE AT DIFFERENT STAGES OF OSTEOARTHRITIS

Eng Kuan Moo[1,2*], Mohammad Ebrahimi[1], Petri Tanska[1], and Rami K. Korhonen[1]
[1]Department of Applied Physics, University of Eastern Finland, Kuopio, Finland
[2]Faculty of Kinesiology, University of Calgary, Calgary, Canada
Email: *engkuan.moo@uef.fi

Introduction

Osteoarthritis (OA) is a painful and debilitating joint disease that affects articular cartilage. Cartilage consists of collagen fibres, proteoglycans (PGs), interstitial fluid and ions. The load bearing capacity of a healthy tissue results from a balanced interaction between swollen PG matrix and tension-resistant collagen fibres. Such balance is lost in diseased tissue due to the degradation of PGs and collagens. Decrease of collagen content, disorganisation of collagenous structure and softening of individual collagen fibrils may each contribute to the degradation of the collagen fibrous network. Previous studies found that collagen content remains unchanged until very late OA [1]. This brings the question as to whether collagen–related deterioration of cartilage during OA results solely from collagenous disorganisation. We previously found that depth-dependent collagenous organisation alone dictates the mechanics of cracked cartilage [2]. However, it is technically difficult to tease out the individual effects of intrinsic mechanical properties of individual fibres, collagen content and organisations.

The purpose of this study was to estimate the intrinsic modulus of collagen fibre in cartilages at different OA stages using a geometrically, structurally and compositionally realistic computational model. We hypothesize that the load-bearing ability of collagen fibres degrades with OA progression, which is reflected in a decrease in fibre modulus as a function of OA stage.

Methods

Cartilage is modelled as a multi-phasic material containing solid (collagen fibres and proteoglycans), water, and monovalent counterions (Na^+, Cl^-) [3]. Collagen fibres are represented by a continuous ellipsoidal distribution, with an individual fibre modelled with a power law that can only sustain tensile loads. Compressive modulus of the tissue results from the electrostatic fixed charge density (FCD) and the non-electrostatic configurational entropy of the PGs. Fluid flow is assumed to obey Darcy's law with an exponential isotropic permeability.

Depthwise composition and structure of the cartilage are defined based on previously collected experimental data [4]. Briefly, 18 cartilage-bone specimens were harvested from tibias of 7 patients aged 68 – 79 years. Based on OARSI scoring of the histological sections, the specimens were divided into healthy (score of 0 – 1, n =5), early OA (score of 2 – 3, n=6), and late OA (score of 4 – 4.5, n=7) groups. The ellipsoidal distribution of collagen fibres is defined by the orientation and anisotropy data obtained from polarised light microscopy. Collagen content measured from infrared spectroscopic images are fitted by a sigmoidal function and used as a multiplicative factor for the fibre modulus, ξ. Optical densities of Safranin-O stained sections were converted into FCD by an empirical equation [5].

All simulations were performed using the open source finite element software FEBio. Cartilage is assumed to be axisymmetric and represented as a 3° wedge model. The tissues went through a four-step incremental indentation protocol with 5% nominal tissue strain at each step, but only the indentation curves from the second and third steps were used for curve-fitting. Five material parameters, which include fibre modulus (ξ), weight for FCD (w_f), weight for configurational entropy (φ), initial permeability (k_0) and strain-dependent coefficient for permeability (M), are optimised for each specimen using a genetic algorithm.

Results and Discussion

The optimization procedure produced a good fit to the experimental indentation data, with r^2 ranging from 0.87 – 0.95. OA progression substantially affected the interstitial fluid flow (i.e., decrease of M factor) and the functional behavior of proteoglycans (i.e., decrease of w_f and φ values, Fig 1). However, the moduli of individual fibres were unaffected by the progression of OA, with mean values ranging from 223 – 377 MPa for healthy, early OA and late OA tissues (Fig 1). These values are in good agreement with experimentally measured fibril modulus of 200 – 800 MPa under aqueous condition [6].

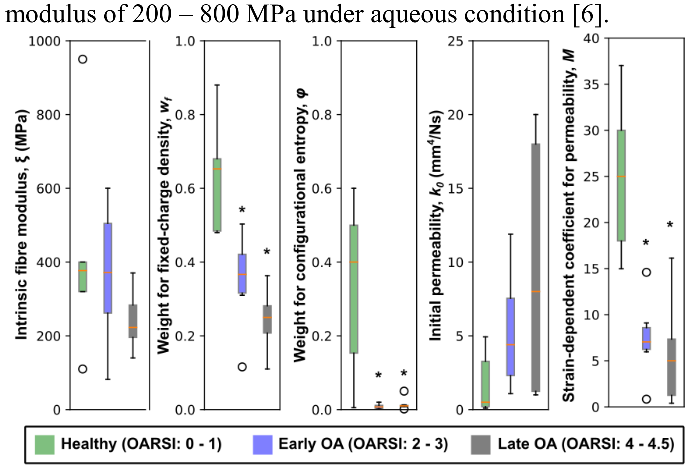

Fig. 1. Fitted material properties of cartilage at different OA stages. * indicates statistical difference from healthy group.

Significance

We found that the collagen quality in cartilage, measured in intrinsic fibre modulus, remains unchanged during OA progression. This suggests that the degradation of collagen in OA cartilage involves primarily disorganisation of the collagen network, resulting in an overall reduction of stiffness of the collagen network [4]. These findings provide valuable insights into the pathogenesis of OA and may be used to shape future treatment strategies into regaining the collagenous organisation across tissue depths.

Acknowledgments

Marie Sklodowska-Curie postdoctoral fellowship (890936)

References

[1] Saarakkala et al. 2010 Osteoarthrits Cartilage 18 (1).
[2] Moo et al. 2020 Acta Biomaterialia 126.
[3] Ateshian et al. 2013. J Biomech Eng 135 (11).
[4] Ebrahimi et al. 2019 Ann Biomed Eng 47 (4).
[5] Kiraly et al. 1996 Histochem J 28 (8).
[6] Van der Rijt et al. 2006 Macromol Biosci 6 (9).

COLLAGEN-BASED CONTRIBUTIONS TO FEMORAL STRENGTH IN FALL-REALTED HIP FRACTURES

Daniel R. Martel*[1], Daniel Y. Dapaah[2], Taylor B. Winberg[1], Thomas Willett[2], and Andrew C. Laing[1]
[1]Department of Kinesiology and Health Sciences, [2]Department of Systems Design Engineering, University of Waterloo, Waterloo, ON
email: *dmartel@uwaterloo.ca

Introduction

Fall-related hip fractures in the older adult population are costly and deadly injuries[1-3]. Though much research has been dedicated to understanding the underlying mechanics of these injuries, previous investigations of femoral bone strength have not directly considered the role of collagen. While the relationship between bone fracture toughness and the quality of the collagen network has been established[4-5], the influence of bone collagen on bone strength has yet to be investigated in the context of fall-related hip fractures. The goal of this study was to quantify metrics of bone collagen quality towards relating them to measures of femoral bone strength in the context of fall-related hip fractures.

Methods

Twelve pairs of fresh-frozen cadaveric femurs (mean[SD] age = 76.2[16.8] years, femoral neck areal bone mineral density [*BMD*] = 0.669[0.105] g/cm^2, 3 female/9 male) were split between two experiments to quantify bone strength (F_x) and collagen-quality metrics (fracture toughness [K_{max},J_{max}], collagen network connectivity, [*Max Slope*], and denaturation temperature [T_d]). One femur from each pair was subjected to simulated lateral hip impact experiments (4 m/s impact velocity, 40 kg mass, 45 kN/m stiffness) using a CSA standard aligned vertical drop tower to quantify F_x. Single Edge Notch Bending (SENB) specimens of the inferior femoral neck were extracted from the other femur of each pair and subjected to high-rate (12 mm/s) 3-point bending tests to extract elastic and elastic-plastic fracture toughness (K_{max}, J_{max}). Demineralized portions of the SENB were used in hydrothermal isometric tension (HIT) tests to quantify the rate of isometric tension generated as a function of temperature (*Max Slope*), as well as the temperature at which isometric tension began increasing (denaturation temperature, T_d). Regression analyses were conducted to quantify the additional variance explained by collagen-related metrics when compared to models predicting F_x from *Sex* and *BMD*.

Results and Discussion

While *Max Slope* was significantly related to both K_{max} and J_{max} (Table 1), *Max Slope* and the fracture toughness metrics were not significantly associated with F_x ($p > 0.05$). However, T_d was significantly related to F_x (adj R^2 0.395, $p = 0.017$). *BMD* and *Sex* (1 for female, 2 for male) were significantly related to F_x, and together had an adjusted R^2 of 0.910 ($p < 0.001$) (Table 2). Adding T_d to this model resulted in an additional 3.2% of variance explained (adj. $R^2 = 0.942$, $p < 0.001$). Finally, when using *BMD* and T_d alone, comparing standardized coefficients revealed that T_d explained 22% of the variance compared to the 77% explained by *BMD*.

Table 1: Linear regression results of fracture toughness metrics versus Max Slope

Linear Models		Adj-R^2 (p)
K_{max}	Max Slope $\beta = 0.57$	0.299 ($p = 0.002$)
J_{max}	Max Slope $\beta = 0.44$	0.163 ($p = 0.021$)

Table 2: Linear model results of multiple combinations of *Sex*, *BMD*, and T_d to predict F_x.

Linear Models				Adj-R^2 (p)
F_x	Sex ($\beta = 0.35$, $p = 0.001$)	BMD ($\beta = 0.76$, $p < 0.001$)	T_d ($\beta = 0.22$, $p = 0.039$)	0.942 ($p < 0.001$)
	Sex ($\beta = 0.35$, $p = 0.004$)	BMD ($\beta = 0.88$, $p < 0.001$)		0.910 ($p < 0.001$)
		BMD ($\beta = 0.77$, $p = 0.001$)	T_d ($\beta = 0.22$, $p = 0.212$)	0.802 ($p < 0.001$)
			T_d ($\beta = 0.67$, $p = 0.017$)	0.395 ($p = 0.017$)

Though T_d was a significant predictor of F_x, it's addition only resulted in a small increase in the strength of an already strong model without collagen-related metrics. However, when compared to *BMD* alone (the most common factor used to predict femoral bone strength), it explained a sizeable amount of unique variance. As T_d is a collagen-related metric that captures information about the crosslinking of the collagen network[6], as well as the relative organization of the collagen network[7], these findings support the notion that collagen quality contributes to femoral bone strength.

Significance

These results provide some of the first direct evidence that collagen is an important contributor to proximal femur bone strength. Further research into this relationship may result in significant improvements in our ability to predict bone strength, and ultimately prevent fall-related hip fractures.

Acknowledgments

This research support through NSERC (RGPIN-2015-03636), CIHR (RN # 350903), and the Alexander Graham Bell Canada Graduate Scholarship – Doctoral program.

References

[1] Jean et al, 2013. *J Bone & Mineral Research*. 28(6): 1283-89; [2] Ioannidis et al., 2009. *CMAJ*. 181(5): 265-71; [3] Burge et al., 2007. *J Bone & Mineral Research*. 22(3): 465-75; [4] Burton et al., 2014. *Bone*. 61: 71-81; [5] Willett et al., 2019. *Bone*. 120: 187-93; [6] Wang et al., 2002. *Bone*. 31(1): 1-7; [7] Arakawa et al., 2020. *Scientific Reports*. 10(1): 1-12

MECHANICAL UNCOILING OF COLLAGEN AS A TOUGHENING MECHANISM OF CORTICAL BONE

Corin Seelemann, MASc; Thomas L. Willett, PhD
Waterloo Composite Biomaterial Systems Laboratory, University of Waterloo, Ontario, Canada
email: thomas.willett@uwaterloo.ca

Introduction

Bone, as a tissue, serves a variety of physiological functions including protection of organs and the nervous system, allowing locomotion, and as a weapon. Despite this versatility of function, bone has a well conserved nanostructure of mineralized collagen fibrils [1]. Bone has rising R curve behaviour, during fracture such that the energy needed to propagate a fracture through the bone increases as the crack starts to grow [2]. Toughening mechanisms (such as diffuse microcracking) absorb energy away from the crack front. One toughening mechanism, which has been widely accepted and predicted in silico, but never directly observed, is the unravelling or denaturation of collagen molecules during cortical bone fracture[3].

Methods

To produce bone fracture surfaces with clear stable tearing bovine (tibia) and human (femur) cortical bone beams were chevron notched and broken under 4-point bending with a quasi-static displacement rate. The WFx (mJ/mm^2) was calculated for each beam. This displacement rate, and notch geometry were selected to promote stable fracture [4]. Bovine bone was tested hydrated and dehydrated (six beams each). Prior research has suggested that water is needed to allow the unravelling of the collagen triple helix [3].

To investigate the state of collagen molecules after bone fracture, a new biotechnology, Fluorescently-labelled Collagen Hybridizing Peptides (F-CHPs), was used to selectively stain denatured collagen on bone fracture surfaces. After fracture, the fracture surface, along with a damaged and undamaged control were taken from each beam. Each surface was demineralized, stained with F-CHP, and imaged using laser confocal microscopy, in accordance with published methods[5].

Comparison of staining intensity between damaged and undamaged controls was used to establish efficacy of F-CHP staining of cortical bone. Undamaged controls were also used to determine a threshold brightness level indicative of mechanical damage. Hydrated fracture surfaces were analysed by identifying a rough textured region of interest (ROI) similar to what has been observed via SEM as a result of stable tearing [4]. The threshold was applied to fracture surfaces, and the staining above that level within the ROI was used to evaluate denaturation produced by fracture. Human bone beams were used qualitatively; only two beams were prepared for confirmation.

To verify the co-localization of staining and stable tearing, a bovine tibia beam was prepared with one fracture surface imaged via SEM and the other stained and imaged with confocal microscopy.

Results and Discussion

Denatured collagen resulting from fracture was detected via confocal imaging of F-CHP stained cortical bone. This denaturation was consistently within a rough textured ROI associated with stable tearing. Figure 1 below shows the results of SEM and confocal imaging from opposite sides of a bovine bone fracture.

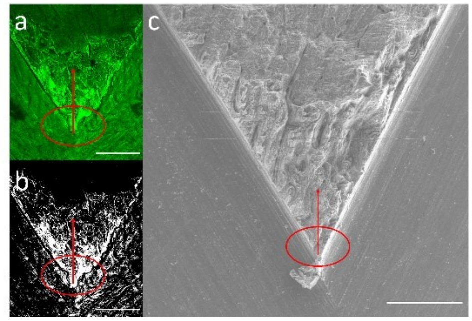

Figure 1: a) Fracture surface stained with F-CHP and imaged with laser confocal microscopy, b) Thresholded image of F-CHP stained fracture surface, c) SEM image of fracture surface. All scale bars: 500 microns. Red circle and arrow indicates origin and direction of fracture.

This staining correlated with the WFx of the notched beam in hydrated specimens. Dehydrated beams showed no correlation between work done and staining. See Figure 2 below.

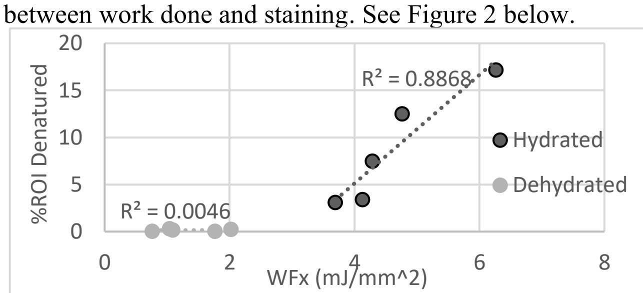

Figure 2:Relationship between staining within ROI for hydrated and dehydrated bovine bone beams. Only relationship between WFx and staining in hydrated samples is significant (P<0.05) from two tailed students' t-distribution.

Human bone also showed staining associated with fracture, corroborating the cross species impact of this mechanism.

Significance

This research provides the first empirical evidence of collagen denaturation as a toughening mechanism in cortical bone. Previously the quality of collagen was understood as an important predictor of bone fragility. This research is a contribution to the understanding of *how* bone resists fracture and leads to hypotheses related to mechanisms of bone fragility.

Acknowledgments

The authors thank the Canadian Institutes of Health Research, the Canadian Foundation for Innovation and Ontario Research Funds for funding, and Dr. Michaela Strüder-Kypke (University of Guelph) for assistance with laser confocal microscopy.

References

[1] N. Reznikov, et al., *Acta Biomater.* **2014**, *10*, 3815.
[2] J. Yan, et al., *Bone* **2007**, *40*, 479.
[3] A. Gautieri, et al., *J. Mech. Behav. Biomed. Mater.* **2009**, *2*, 130.
[4] J. Yan, et al., *J. Biomech.* **2006**, *39*, 1066.
[5] J. Hwang, et al., *Acta Biomater.* **2017**, *53*, 268.

CAN CARTILAGE SUSTAIN FLUID LOAD SUPPORT AS CONTACT FORCES INCREASE DURING MOVEMENT?

Steven Voinier*, David Burris[1]
[1]The University of Delaware Mechanical Engineering
email: *voinier@udel.edu

Introduction

Cartilage degeneration is associated with chronic overstressing or under-stressing of the articular joint. During movement, joint contact stresses hydrostatically pressurize fluid within cartilage, reducing solid matrix stress and friction. This stress also drives fluid exudation, which defeats the protective fluid pressure.

Fortunately, many articular joints do not experience consistent contact stresses as contact areas are intermittently exposed. These migrating contact areas (MCA) reduce the magnitude of fluid lost while allowing the tissue to regularly rehydrate during synovial fluid bath exposure[1]. With joint articulation, the migrating contact can maintain high levels of fluid load support (FLS), a metric representing the percent of load bore by the fluid constituent. However, many articular contacts (e.g. medial tibial plateau) cannot leverage the MCA as they remain unexposed during normal movement. Fortunately, recent research from our group has demonstrated that the joint sliding mechanism triggers a hydrodynamic pressurization that rehydrates stationary contact areas (SCA) [2]

While the MCA may sustain FLS >90%, the FLS of buried contacts is unknown, especially for varying levels of contact force. In this study, we establish the FLS for the SCA and hypothesize a decrease in FLS with increased contact loads.

Methods

Theoretical framework—According to biphasic theory, FLS = $P_F/(P_F+P_S)$, where P_F represents the fluid pressure, P_S represents the solid stress, and (P_F+P_S) represents the total contact stress (σ_c) (see Fig 1). If cartilage deformation (δ) is maintained while allowing the total contact stress to subside, fluid pressure will diminish to ~0 resulting in $\sigma_{eq} = P_S$. The FLS can then be calculated for a given cartilage strain as: FLS = $1 - \sigma_{eq} / \sigma_c$.

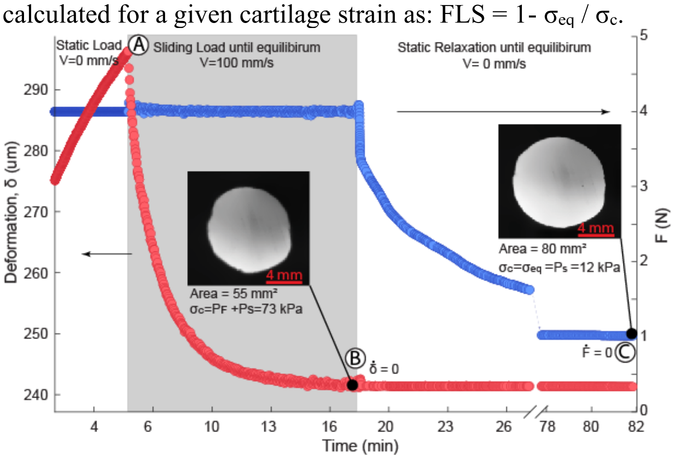

Figure 1: The deformation and force response of cartilage from exudation(A) to sliding-equilibrium(B) to force relaxation equilibrium(C). We calculated the FLS for cartilage at the point where rehydration and exudation rates equated ($\dot{\delta} = 0$) as it represents the deformation where cartilage regularly operates during movement[3].

Testing and Data Analysis—We experimentally measured the contact pressures for bovine osteochondral cores (n = 5 samples, 19 mm dia.) on a pin-on-disk tribometer. Samples submerged in PBS (0.15 M) and 5 ml of India Ink were statically loaded at 4N for 5 minutes to exude fluid (Fig. 1A). Loaded samples were then slid at 100 mm/s to recover to "sliding equilibrium" deformation (Fig. 1B). Holding the equilibrium deformation constant, the sliding speed was set to 0 mm/s, while allowing the force on the cartilage to subside to an equilibrium value (Fig. 1C). A camera captured contact area images at sliding-equilibrium and force-relaxation-equilibrium to quantify the contact pressures. This process was repeated for 1,2,3,5 N for each sample. A linear mixed effects model was fit to FLS as a function of load to compare load dependency among samples ($\alpha = 0.05$ for significance).

Results and Discussion

Our hypothesis was rejected as the linear mixed model demonstrates that force does not significantly affect the FLS ($p=0.59$), which is visualized in Figure 2. Intuitively, a higher contact load would increase the exudation rate. However, the hydrodynamic pressurization developed during sliding seems to compensate for the increased exudation rate.

A one-way ANOVA performed on the average FLS per sample demonstrated a significant sample dependency to develop FLS during sliding ($p<0.001$). The average FLS within a sample ranges from 71.0-83.8%, which is comparable in magnitude and variance shown in MCA experiments[4]. The variance can likely be attributed to the difference in material properties of the tissue and the conformability of the contact[4]

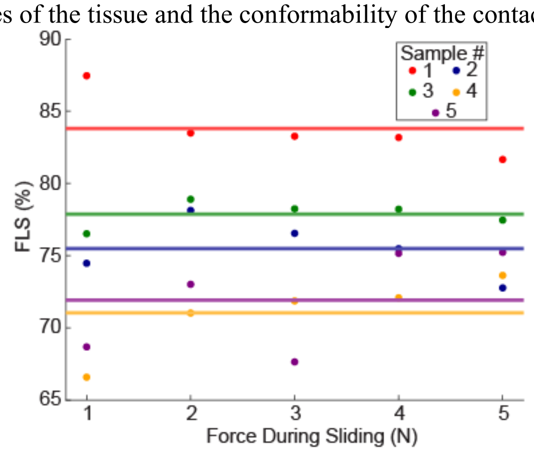

Figure 2: The FLS vs. contact force for n=5 samples. The mean for all loads is displayed for each sample.

Significance

While the MCA requires unloading and exposure to develop FLS, results from this study demonstrate the SCA is also a significant contributor to developing FLS in the articular joint. More importantly, healthy cartilage seems primed to develop fluid pressurization to help protect the tissue, regardless of the contact load.

Acknowledgements

N/A

References

[1]Benson, J. M. *et al.*, 2021 *Osteoarthr. Cartil.* 29: doi:15229653.[2] Moore, A. C. & Burris, D. L., 2017 *Osteoarthr. Cartil.* 25: doi:1063-4584.[3]Eckstein, F., Hudelmaier, M. & Putz, R., 2006 *J. Anat.* 208: doi:0021-8782. [4]Moore, A. C. & Burris, D. L., 2015 *Osteoarthr. Cartil.* 23:

SITE-SPECIFIC MECHANICAL PROPERTIES OF PORCINE KNEE CARTILAGE DETERMINED WITH INDENTATION MAPS AND MACHINE LEARNING

Erfan Hamsayeh Abbasi Niasar, and LePing Li *
Department of Mechanical and Manufacturing Engineering, University of Calgary, Alberta, Canada
* Leping.Li@ucalgary.ca

Introduction

Cartilage biomechanics is of great importance as osteoarthritis and joint injuries are associated with the mechanical environment of the joint. The geometry and tissue properties of articular cartilage are of 3D variations in the joint. The zonal differences of cartilage, i.e., the tissue property variation with the tissue depth, are well established [1]. However, the tissue property variation across the joint has been less investigated. It may be necessary to understand the site-specific mechanical properties of the whole cartilage in order to understand the site-specific gene expression and onset of osteoarthritis [2]. It may also be essential to implement site-specific cartilage properties in the 3D finite element models of joints, e.g., knee joints, to better understand the contact pressure distributions in the joint [3], a necessary step to a full understanding in the pathomechanics of the joint. The objectives of the present study were to determine the number of regions required to characterize the tissue property variation in a porcine tibiofemoral joint and determine the site-specific mechanical properties of cartilages using indentation maps and finite element modeling.

Methods

Porcine cartilages from each knee joint were dissected into 4 cartilage-bone blocks to facilitate indentation tests with Mach-1 (Biomomentum, Laval, Quebec, Canada): lateral and medial femoral specimens, and lateral and medial tibial specimens. Six complete sets, or 24 specimens from 6 fresh porcine knees, were collected from which 22 specimens were successfully tested. A 2-mm spherical indenter was used to map the tissue response of each specimen with ~30 indentation points. A relaxation testing of 100s was measured at each point with 0.2mm-compression applied at 0.2 or 0.4 mm/s (Fig. 1). Cartilage thickness was then mapped with needle probing. K-means clustering algorithm in coupling with differential evolution was used to optimize the number of regions or clusters required to quantify the site-specific tissue properties for each specimen, which was determined from the indentation data with the Elbow method based on the evaluations of 2-8 clusters (Fig. 2).

The average load response from the data points in each region was then curve-fit (Fig. 1) to extract the mechanical properties of cartilage using a finite element model of indentation in ABAQUS. A previously developed fibril-reinforced constitutive model was used for the simulation of the load response at the rather high compressive rates used in the tests. Mechanical properties of cartilage include the elastic modulus, E_m, and Poisson's ratio of the proteoglycan matrix, the nonlinear modulus of the collagen fibrillar matrix, $E_f = E_0 + E_\varepsilon \varepsilon$, and tissue permeability k. Tissue orthotropy was modeled.

Results and Discussion

Based on the results from 6 sets of porcine knee cartilage specimens, 4 distinct regions would best represent the site-specific tissue properties for the medial tibial cartilage, while 3 regions would be sufficient for the lateral tibial cartilage, lateral or medial femoral cartilage (Fig. 2). Therefore, 13 distinct regions in total are needed to fairly describe the site-specific cartilage properties for the tibiofemoral joint.

There was a good agreement between the relaxation data and the finite element results with an error < 10%. A deviation in the range of 25-40% was seen when comparing the material properties extracted for distinct regions to the average over the whole specimen, e.g., lateral femoral cartilage. For instance, the material properties for lateral tibial cartilage were in the following range: E_m = 0.15-0.28 MPa; E_{0x} = 1.06-1.85 MPa; $E_{\varepsilon x}$ = 443-725 MPa; k_x = 1.7-2.5($\times 10^{-3}$) mm^4/Ns.

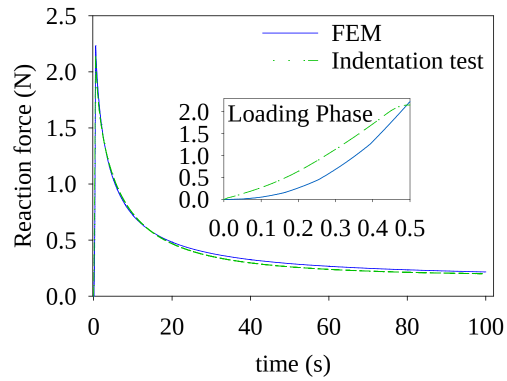

Figure 1: Relaxation for indentation of lateral femoral cartilage

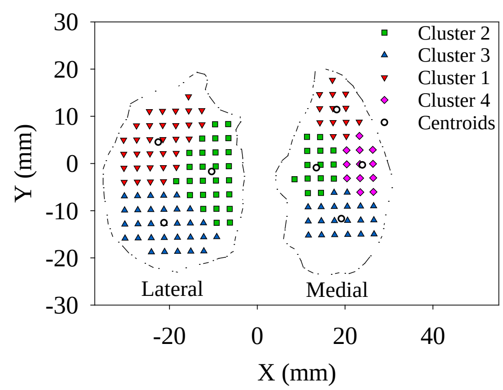

Figure 2: K-means clustering results for tibial cartilages of joint #3

Significance

The methodology developed in this study can be used to characterize the site-specific cartilage properties of human knee cartilages. Dividing cartilages in the joint into a limited number of regions, 13 in the study, rather than using continuous domains, will simplify lab tests and implementation of material properties in a finite element model of the joint. The study may pave the way, e.g., for understanding site-specific cartilage gene expressions and degenerations under *in-vivo* joint loadings [2].

Acknowledgments

We would like to thank Dr. Brent Edwards for providing access to lab tests. This study was supported by NSERC, Canada.

References

[1] Schinagl et al, *J Orthop Res* **15**, 499; [2] Otoo et al, *J Biomech Eng* **144**: 024502; [3] Dabiri & Li, *Med Eng Phys* **35**, 1591

THE PROBABILITY OF WHOLE-BONE FATIGUE FRACTURE CAN BE ACCURATELY PREDICTED USING SPECIMEN-SPECIFIC FINITE ELEMENT ANALYSIS INCORPORATING A STOCHASTIC FAILURE MODEL

Ifaz T. Haider[1,2], Andrew J. Pohl[1], W. Brent Edwards[1,2]
[1]Human Performance Laboratory, [2]McCaig Institute for Bone and Joint Health, University of Calgary
*email: ifaz.haider@ucalgary.ca

Introduction

Stress fractures are associated with mechanical fatigue, where repetitive submaximal loading causes progressive material degradation leading to eventual failure of the bone structure. Studies on small material samples of bone have identified a nonlinear relationship between load magnitude (stress or strain) and fatigue life [1]. Specimen size or stress/strained volume also plays a role, due to the stochastic nature of fatigue crack propagation around existing voids/damage [2]. However, it is unclear how to extend these principles, which were established on small specimens under uniform load, to predict fatigue life of whole bones which experience complex (compression + torsion) loading and non-uniform stress/strain. The purpose of this investigation was to use specimen-specific finite element (FE) analysis incorporating a stochastic model based on strain magnitude and volume, to predict fatigue failure of whole bones under complex loading.

Methods

12 rabbit tibiae were loaded to failure under cyclic axial compression with peak loads ranging from 925-2450 N, while another 22 tibiae were loaded biaxially (compression + torsion). Biaxial specimens were loaded to 50% compressive strength and 0% (n=10), 25% (n=6) or 50% (n=6) torsional strength. Computed tomography was performed prior to testing and specimen-specific FE models with heterogeneous material properties were generated with loads and boundary conditions that mimicked the experimental test. A stochastic model based on the Weibull distribution [3] was used to calculate the probability that each model would fail at $\leq N$ cycles, where N is a trial number specified by the user. Using parameters selected *a-priori* [3], the model computed the probability of failure for each element as a function of element strain, volume, and N; the probability of whole-bone failure was the cumulative probability that any 1 element would fail. This model was solved iteratively to identify the number of cycles (N) associated with a 25%, 50%, 75% and 95% probability of whole bone failure. The model was assessed by comparing the percentage of bones where the experimental fatigue life was ≤ model predicted N. To further quantify strength of the model, we used a Brier scoring rule [4] to generate a score between 0 and 1, where 0 represents a perfect model. For comparison, we scored two null models that always predict 0% and 100% chance of failure independent of strained volume.

Results and Discussion

Figure 1 compares experimentally measured number of cycles to failure against the model predicted cycles to failure. Respectively, for the 25%, 50%, 75%, and 95% probabilistic predictions, we observed experimental failure ≤ model predicted values in 41%, 53%, 76%, and 80% of the tested specimens. Our model generated an average Brier score of 0.22, which was superior to the scores of 0.63 and 0.67 from models that always assign probability of 0% or 100%, respectively.

In this work, we used information from the apparent/material level, only. However, previous studies have shown that bone microarchitecture plays an important role in fatigue fracture [4]. We speculate that differences in bone microarchitecture could explain samples #26 and #27, which were both from the same animal and survived much longer than the model predictions. In the future, modifying our model to include microstructure information could help improve predictions.

In summary, we validated a specimen-specific FE model incorporating a stochastic failure model to predict the fatigue life of whole bones. Experimental observations confirmed a close match between model predicted failure probability and the proportion of specimens observed to fail experimentally. Furthermore, a Brier scoring rule demonstrated that this model was superior to null models agnostic to strain or volume.

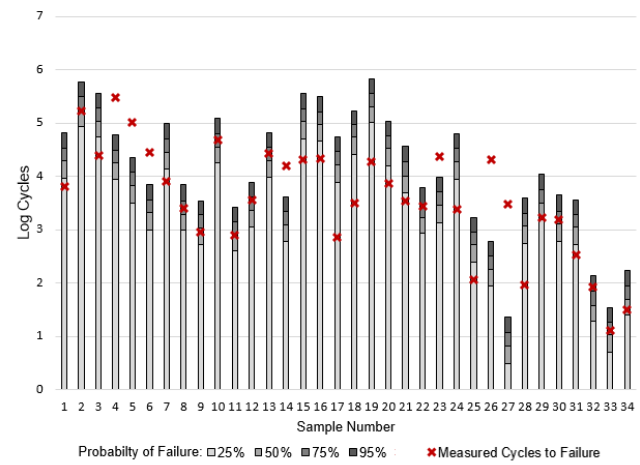

Figure 1: Experimental (red X) vs model predicted cycles to failure. Gray bars indicate predicted regions associated with 25% (lightest gray), 50%, 75% and 95% (darkest gray) probability of failure.

Significance

The etiology of stress fractures in humans are still not fully understood. Combined with musculoskeletal modelling, the model presented here may be a powerful tool to assess how differences in movement biomechanics and bone health (density, geometry) influence stress fracture risk at the population level.

Acknowledgments

This work was supported in part by the Natural Science and Engineering Research Council of Canada (RGPIN 01029– 2015 and RTI 00013–2016) and the Canadian Foundation for Innovation John R. Evans Leaders Fund (Project #37134).

References

[1] Carter et al. 1981. Acta Orthop 52, 481-490; [2] Bigley et al. 2007, J. Biomech 40, 3548-3554; [3] Taylor and Kuiper. 2001. JOR 19, 919-926; [4] Benedetti 2009. Mon. Weather Rev. 138, 203-211. [5] Loundagin and Edwards. 2020 J Mech Behav Biomed Mater 111, 10400

THE EFFECT BONE GEOMETRY ON CONTACT STRESS IN 3D-FINITE ELEMTN HINDFOOT MODEL

Jinhyuk Kim[1], Sebastian Y. Bawab[1], Matt B. Mccullough[2] Stacie I. Ringleb[1],
[1]Old Dominion University, Norfolk, VA, USA
[2]North Carolina Agricultural & Technical State University, Greensboro, NC, USA
email: sringleb@odu.edu

Introduction

Computational modelling of foot and ankle is conducted to understand the effect of foot injuries and pathologies and to plan foot surgeries [1,2,3]. Anatomical bone morphology can be affected by age, sex, and foot disease and foot use (e.g., athletes that load their feet) [4,5,6], and the thickness of ankle articular cartilage varies across people [7]. Finite element (FE) foot models can be also affected by the degree of curvature to the facet of the talus and tibia, and the thickness of cartilage [8,9]. As the biomechanics community moves toward patient specific models, it's critical to understand which parts of models should be patient specific and what can be generic. Therefore, the aim of this study was to determine how changes in the bone morphology and cartilages thickness effect the stress distribution in the talocrural joint.

Methods

3D finite element (FE) models including tibia, talus, and cartilage were developed using Hypermesh (Altair, Troy, MI) and FEBio (FEBio, Salt Lake City, UT) segmented from CT images obtained from one cadaver, BodyParts3D (lifesciencedb.jp), a patient before a total ankle replacement, and a patient before an ankle fusion (Figure 1). The models were axially loaded with 600N on the top surface of tibia [3]. Cartilage thicknesses of 0.5mm, 1mm, and 1.7mm were included in the models. The sliding contact method was applied between tibia and talus and one spring as ligament was conducted between tibia and talus at middle of two cartilages.

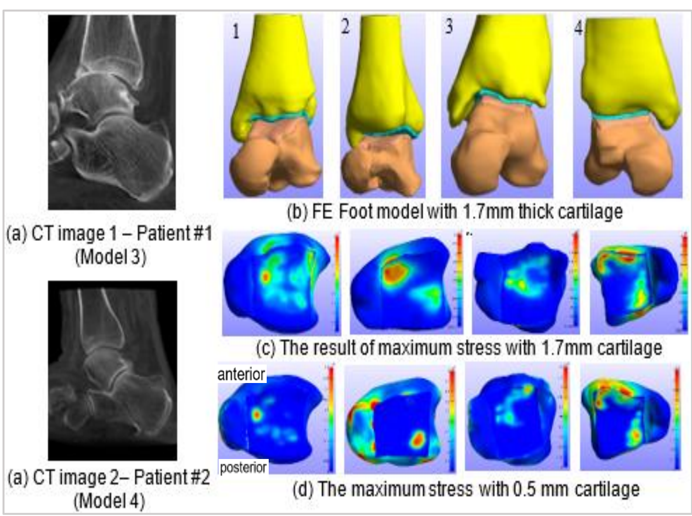

Figure 1: 3D FE models and the peak stress with 1.7mm and 0.5mm thickness of cartilage at neutral position. (a) Two CT images for patient #1 (model 3) and patient #2 (model 4). (b) Four 3D FE models; 1. From cadaver; 2. From lifesciencedb.jp; 3. From patient #1 (replace ankle joint); 4. From. Patient #2 (right, fuse the ankle joint) (c) the maximum stress at 1.7mm thick cartilage of tibia, (d) the maximum stress with 0.5mm thick cartilage of tibia.

Results and Discussion

The peak talocrural contact stress ranged in healthy group was similar between model 1 and model 2 (Figure 2). In the healthy models (model 1 and 2) as well as the ankle before total ankle replacement (model 3) the peak stress increased as cartilage thickness decreased (Figure 2). However, in model 3, the peak contact stress did not increase as much as it did in the healthy models. Further, in model 4, the peak contact stress decreased when the cartilage was more thin (Figure 2). The differences between the peak stress trends in the healthy vs. injured models may be explained by contact area and the stress distribution across the joint contact surface. Specifically, in models 1 and 2, contact areas decreased from 491mm^2 to 263mm^2 and from 318mm^2 to 72mm^2, respectively, as the cartilage got thinner. While the contact area in models 3 and 4 did not decrease as much (from 454 mm^2 to 302mm^2 and from 490mm^2 to 421mm^2, respectively). Additionally, in model 4, the stress distribution showed more area of high stress across the joint surface, suggesting more a change in stress distribution, which wasn't visible in other models. According to the study, the peak stress, contact area, and stress distribution were affected by the bone morphology and thickness of cartilage.

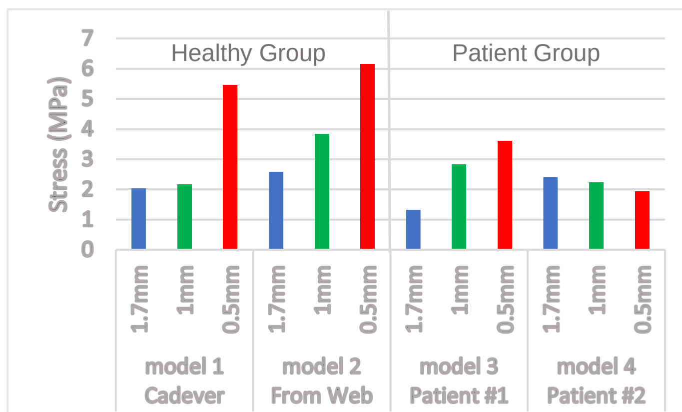

Figure 2: The peak contact stress results based on four different foot models including two patient models and three different thickness of cartilage with 600N axial load.

Significance

Stress distributions at the talocrural joint vary based on cartilage thickness and bony morphology. Therefore, when creating patient specific models including the hindfoot these parameters should not be generalized.

References

[1] A. Chitsazan et al., 2015. *IJECB.067681*
[2] Bouguecha et al., 2011. *Biomed. Eng. Online.1186*
[3] Anderson et al., 2007. *J. Biomech.2007*
[4] Shiota et al., 2020. *Orthop. J. Sports Med.1177*
[5] Tumer et al., 2019. *J. Anat.* 234;111
[6] Abellan et al., 2014. *Ergonomics*.1080
[7] Shepherd et al., 1999. *Ann. Rheum Dis*.1999
[8] Siegler et al., 2014 Clin Biomech.2013
[9] Anderson et al., 2010. J Bone Joint Surg Am. 00431

Session 4

Tuesday August 23, 2022

3:30pm – 5:00pm

O4.1 – Imaging 2 – Soft Tissue

O4.2 – Locomotion 2 – Prostheses & Orthoses

O4.3 – Trunk & Spine 1

Thematic Poster Session 2 – Knee joint loading/Osteoarthritis

HIGH-FIELD MRI ANALYSIS OF THE 3D GEOMETRY OF THE TRIPLE-BUNDLE ACHILLES TENDON

Stephanie G. Cone[1*], Hoon Kim[2], Jason R. Franz[2], and Darryl G. Thelen[1]
[1]Department of Mechanical Engineering, University of Wisconsin, Madison, WI
[2]Department of Biomedical Engineering, University of North Carolina and North Carolina State University, Chapel Hill, NC
email: *sgcone@wisc.edu

Introduction

The Achilles tendon is a triple-bundle structure that enables the triceps surae to actuate the ankle [1]. Highly variable subject-specific bundle anatomy has been identified in cadavers, with individual differences described based on calcaneal insertion patterns [2,3]. However, characterizing the structure of the bundles of the Achilles tendon *in vivo* is challenging due to limitations in 3D resolution and contrast between similar tissue types typical of clinical imaging modalities. High-field magnetic resonance imaging (MRI) has previously been used to identify bundles of the ACL, with the sheath between bundles and the predominant fiber directions within bundles visible due to variations in bound water across these tissue components [4]. Leveraging these innovations in research imaging, high-field MRI was used in this study to delineate the 3D bundles of the Achilles tendon. Our objective was to validate this imaging approach and to explore routes for characterizing relative bundle size and twist *in vivo*.

Methods

MRIs were collected in duplicate for the right ankle of 10 subjects (5F/5M, 27±5 years, height: 1.8±0.1 m, mass: 70±11 kg) in an IRB-approved study. Images were collected with a 7T MRI (Siemens Magnetom) and a double echo steady state scan sequence [4]. Leveraging the contrast in signals between the bundle sheaths and the fiber tracks in addition to standard techniques of identifying outer boundaries of a tissue, 3D masks were developed of the three Achilles tendon bundles (Fig. 1).

Individual bundle models were analysed using a custom Matlab code summarized in Figure 1. Briefly, models were aligned to the dominant axis of the Achilles tendon and divided into 2D slices at 1mm increments. The cross-sectional area was measured for each slice along the tendon, the position of the bundle centroid was recorded along the free tendon as a measure of bundle rotation, and two independent reviewers paired each tendon to Type I, II, or III keeping with descriptions in prior literature [2,3]. Statistical analysis consisted of multi-way ANOVA testing with subjects as repeated measures, and intraclass correlation assessments for repeatability testing.

Results and Discussion

Analysis of the bundles revealed significant variation in the cross-sectional area of each bundle along the length of the tendon in a subject-specific manner ($p<0.01$), and significant variation in the relative size of the three bundles between subjects ($p<0.01$). Rotation analysis revealed significant twist along the length of the tendon in some, but not all ankles. Of the 20 scans, 80% were identified as Type I, 12% as Type II, and 8% as Type III. This fits well with prior estimates of twist type frequency in adults [2,3] where most Achilles tendons are Type I or "least twisted". On average, areas of the medial gastrocnemius (25.1±9.0 mm^2) and the lateral gastrocnemius (23.5±9.4 mm^2) bundles were greater than the soleus bundle (12.4±5.8 mm^2).

Repeatability within subjects was high across metrics of interest, with lower standard deviation between scans for any individual (averages in the mid-tendon of MG: 6.3 mm^2, LG: 5.2 mm^2, S: 4.0 mm^2) compared to standard deviation across subjects. Additionally, the differences in size between scans were approximately 4-fold lower within each individual compared to the range across subjects. Further, our methods had primarily good to high repeatability across metrics (ICC>0.75).

Significance

Subject-specific variations in the Achilles tendon bundles were repeatably characterized *in vivo*. This extension of prior cadaveric analyses of the bony insertions has great potential to improve our understanding of the spatial mechanics of the Achilles tendon. With the ability to better assess tendon structure, we can investigate the relationship between tendon twist and injury risk, plantarflexion strength, and ankle stability [3]. Future work will address implications of the variations in the structure the bundles on clinical planning and human performance.

Acknowledgments

Funding from the NIH (F32 AR076267, R01 AG051748).

References

[1] Stenroth+, 2018. *TSM*.; [2] Pekala+, 2017, *SJMSS*.; [3]Edama+, 2014, *SJMSS*.; [4] Cone+, 2021, *JOR*.

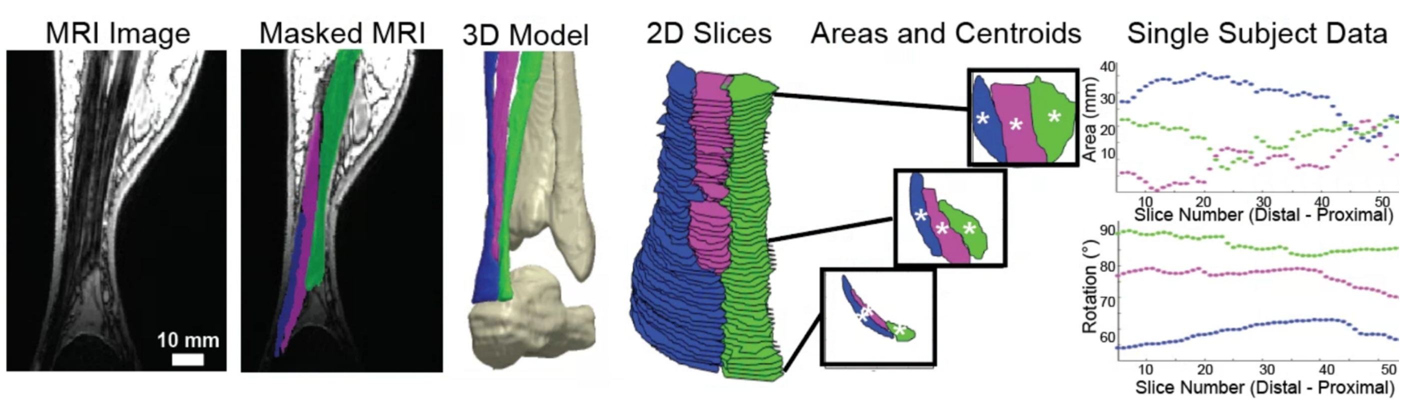

Figure 1: Process illustrating the translation of MRI images into 3D tissue models and further processing based on stacked 2D slices. Data shown are cross-sectional areas and bundle rotations for a single subject.

HOW DO MUSCLE FORM AND FUNCTION RELATE IN SPINAL MUSCULAR ATROPHY AND DUCHENNE MUSCULAR DYSTROPHY?

Allison N. McCrady[1*], Robert J. Gutierrez[2], Chelsea D. Masterson[3], Medhi O. Boukhechba, PhD[2], Laura E. Barnes, PhD[2], Rebecca J. Scharf, MD, MPH[3], and Silvia S. Blemker, PhD[1]
[1]Department of Biomedical Engineering, University of Virginia, Charlottesville, VA, USA
[2]Systems and Environmental Engineering Department, University of Virginia, Charlottesville, VA, USA
[3]University of Virginia Children's Hospital, Charlottesville, VA, USA

email: *anm9xd@virginia.edu

Introduction

Spinal muscular atrophy (SMA) and Duchenne muscular dystrophy (DMD) are progressive neuromuscular disorders characterized by severe muscle weakness and functional declines [1]. Although recent pharmaceutical advances have extended patient life expectancy and improved motor function, current clinical function assessments remain subjective and are not sensitive to functional changes in patients. To improve treatment of patients with SMA or DMD, an objective, sensitive, and clinically accessible muscle assessment method is needed.

Ultrasound is a common imaging modality to measure skeletal muscle architecture and quality due to its non-invasive nature and low cost. Previous studies have demonstrated the use of ultrasound to measure quality of skeletal muscle in neuromuscular disease based on the echogenicity or brightness to estimate disease progression [2]. However, no correlation between muscle force per unit area (specific tension) and echogenicity has been reported [3]. <u>The goal of this study was to examine the relationship between an estimated muscle specific tension and ultrasound measurements of echogenicity across a range of individuals with SMA and DMD, as well as age-matched controls.</u>

Methods

Ultrasound and dynamometry were used to measure biceps brachii structure and function in children with SMA and DMD and age/sex matched healthy controls. A linear array transducer (H9.0/40, Telemed LS 128 CEXT, Italy) was used with settings held constant across subjects. The dominant arm biceps brachii muscle of 40 subjects (patients with SMA: n = 9, patients with DMD: n = 18, healthy controls: n = 13) were imaged in the midsection in the longitudinal (**Fig. 1A**) and transverse (**Fig. 1B**) planes. An image processing algorithm was developed in MATLAB (Mathworks) to measure the cross-sectional area (CSA) and average echogenicity of the muscle. Five images of the same region were measured and averaged. The average echogenicity was measured in both planes and then averaged to minimize transducer orientation effects. Maximum voluntary elbow flexor moment was measured using a handheld dynamometer (Chatillon DFS II) placed on the forearm with the elbow positioned at 90 degrees (**Fig. 1C**). Estimated specific tension was calculated by dividing the elbow flexor moment (Nm) by the CSA (cm^2). To compare CSA across populations, CSA was normalized by forearm length to mitigate effects of subject size. All statistics were calculated in R (α=0.05). Statistic tests used were a single factor ANOVA with Tukey's HSD post-hoc test.

Results and Discussion

The normalized biceps brachii CSA was significantly lower in the SMA cohort as compared with the healthy cohort in (p=0.007). Average echogenicity was significantly higher in subjects with SMA and DMD relative to healthy controls (DMD v healthy: p=0.00008, SMA v healthy: p=0.00002). We found that a power law best fit the data relating estimated specific tension and muscle echogenicity (R^2=0.58, **Fig. 1D**). This relationship indicates that as echogenicity increases, the estimated specific tension and therefore the muscle tissue contractile capacity decreases.

Significance

Current clinical assessments of patient motor function are subjective and lack sensitivity. By relating ultrasound measurements to functional capacity, we can observe and track functional changes objectively and easily in the clinic. Our future work will track subject measurements over time to develop a novel imaging based functional assessment. This innovative assessment will help improve the clinical care of patients with SMA and DMD.

Acknowledgments

Research funded by NIH Award T32GM136615 and University of Virginia Center for Engineering in Medicine.

References

[1] Pillen et al., 2008. *Muscle Nerve.* 37(6): 679 [2] Jansen et al., 2012. *Neuromuscul Disord.* 22(4): 306. [3] Mota et al., 2017. *Physiol. Meas.* 38(8): 1529.

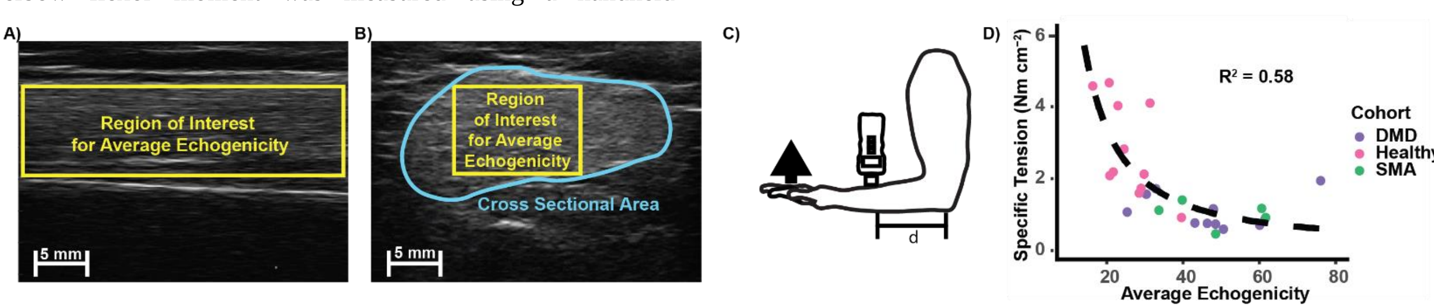

Figure 1: A) Measurement in longitudinal plane, B) measurement in transverse plane, C) elbow torque measurement setup, and D) hyperbolic relationship between estimated specific tension and average echogenicity.

MULTI-SWEEP 3-DIMENSIONAL ULTRASOUND IS ACCURATE FOR *IN VIVO* MUSCLE VOLUME QUANTIFICATION, EXPANDING USE TO LARGER MUSCLES

Jorie D. Budzikowski[1,2,3*] and Wendy M. Murray[1,2,3]
[1]Northwestern University, [2]Shirley Ryan AbilityLab, [3]Edward Hines, Jr. Veterans Affairs Hospital
email: JorieBudzikowski@u.northwestern.edu

Introduction

Three-dimensional ultrasound (3DUS) reconstructs 3D anatomy from 2D images acquired during dynamic scans while motion of the ultrasound probe is tracked. 3DUS has enabled successful quantification of organ volume,[1] tendon length,[2] and muscle volume.[3-5] Accuracy of 3DUS is excellent (<1.5% error)[4] when the entire anatomical structure can be acquired via a single sweep of the transducer. However, more than one sweep is often necessary to reconstruct muscle anatomy. Previous studies describe confounding image registration errors between multiple sweeps for the soleus[6] and extensor carpi radialis brevis;[7] tissue deformation differed substantially between sweeps, yielding a discontinuity in the composite images. Uncertainty about the resulting error limits use of 3DUS for measuring muscle volume.

We have developed an image acquisition protocol for measurement of muscle volume via 3DUS that mitigates the image registration error introduced by variable muscle deformation among repeated sweeps. Here, we detail imaging phantom studies used to (1) define an acquisition protocol that reduces the misalignment in the 3D reconstruction caused by muscle deformation, and (2) quantify accuracy of 3DUS for measures of volume when the phantom is too large to be fully imaged via a single transducer sweep. Finally, we establish the feasibility of our protocol for *in vivo* measures by comparing muscle volumes of the biceps brachii using 3DUS and MRI.

Methods

Images were acquired with an Acuson 2000 (Siemens Medical Solutions). A rigid body was attached to a 14L5 probe; an Optitrak 6-camera system tracked probe position. Open-source software (Stradwin) integrated image and position data.

We evaluated how acquisition protocols affected the composite images produced during multiple sweeps using water balloons. We qualitatively evaluated image misalignment, varying sweep direction (parallel/antiparallel) and operator intention for the applied pressure difference between sweeps (variable/constant). We calculated accuracy for each protocol by comparing volumes calculated from image reconstruction to the known phantom volumes. We also quantified the best possible outcome for multiple sweeps using non-deformable (PVC) phantoms, imaged through a water bath without contact. To evaluate *in vivo* performance, multi-sweep 3DUS was applied to image biceps brachii in both limbs of a single participant (Fig. 1). Biceps volume calculated from reconstructions of three sweeps was compared to a previous measure from MRI.[8]

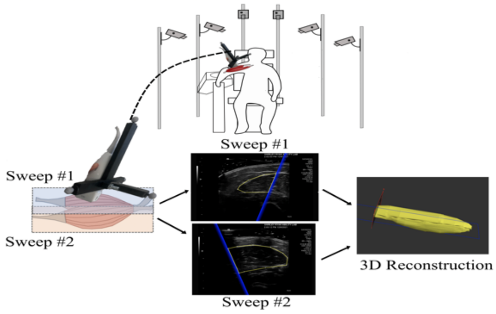

Figure 1: 3DUS setup; corresponding images and 3D reconstruction.

Results and Discussion

The constant pressure, parallel direction, multiple sweep protocol effectively mitigated image misalignment (Fig. 2) yielding minimal volume error (1.70 ± 1.30%). Variable pressure, anti-parallel sweeps replicated the discontinuity observed previously[6,7], leading to larger errors (5.30 ± 0.94%). While accuracy could be improved by eliminating contact (error from PVC phantom, water bath: 1.50 ± 0.24%), this method is not practical for all muscles.

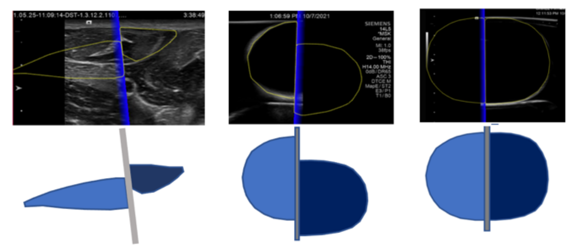

Figure 2: Composite image cross-sections (top row) and schematic representation (bottom row) displaying misalignment for ECRB[7] (left) and flexible phantom (anti-parallel, variable pressure; middle). Operator intent to apply constant pressure between sweeps mitigated this issue for the phantom when sweep direction was parallel (right).

Based on these findings, we adopted a gel bag standoff pad and acquired multiple sweeps in the parallel direction for *in vivo* biceps imaging. Biceps volumes for this participant were reported as 246 mL (dominant arm) and 241 mL (non-dominant arm) in a previous study.[8] 3DUS underestimated the previously reported volumes in both limbs by 2.4 and 3.7 %, respectively. These results indicate a more robust evaluation of 3DUS volume measures relative to MRI data obtained at the same time point is worth pursuing. Interlimb difference in muscle volume detected by 3DUS (3.8%) was comparable to the previous study (2.1%), and the error observed in our deformable phantom using the optimal acquisition protocol (1.7%).

Significance

Accuracy of 3DUS is sufficient for comparisons among muscles. The lower cost and greater accessibility of US versus MRI would benefit research and clinical settings. In this study, we resolve a critical obstacle for the adoption of 3DUS, establish accuracy for multiple sweeps, and show feasibility of volume measurement in large muscles.

Acknowledgments

Research has been funded by the National Science Foundation Graduate Research Fellowship Program, and the Rehab R&D Service of the VA (I01 RX001990, I21 RX003610)

References

[1]Treece et al., 2001. *Medical image analysis* [2]Obst et al., 2013. *Ultrasound in Med. & Biol*. [3]MacGillivray et al., 2008. *Ultrasound in Med. & Biol*. [4]Barber et. al., 2016. *Developmental Medicine & Child Neurology* [5]Noorkoiv et al., 2019. *Clinical Anatomy* [6] Barber et al., 2018. *Journal of Anatomy* [7] Adkins, AN. *PhD Dissertation,* 2021. [8] Adkins et al., 2020. *PNAS*

MUSCLE DENSITY ANALYSIS USING COMPUTED TOMOGRAPHY: AN INTERNAL CALIBRATION APPROACH

Ainsley C.J. Smith[1,2,3*], Justin J. Tse[2,3], Tadiwa H. Waungana[1,2,3], Michael T. Kuczynski[1,2,3], Steven K. Boyd[1,2,3], and Sarah L. Manske[1,2,3]
[1]Biomedical Engineering Graduate Program, University of Calgary, Alberta, Canada
[2]Department of Radiology, Cumming School of Medicine, University of Calgary, Alberta, Canada
[3]McCaig Institute for Bone and Joint Health, University of Calgary, Alberta, Canada
email: ainsley.smith@ucalgary.ca

Introduction

Muscle density and cross-sectional area (CSA) loss can result in muscle weakness and ultimately lead to physical impairment, lack of independence, and reduced quality of life [1,2]. Muscle CSA can be measured using opportunistic computed tomography (CT) imaging, which is inexpensive and non-invasive [3]. However, the use of opportunistic CT scans to evaluate muscle density is limited because a density calibration phantom is required within the field of view to convert Hounsfield Units (HU), linear attenuation coefficients, into density values (g/cm^3). Recently, Michalski and colleagues developed an "internal calibration technique" that utilizes regions-of-interest (ROIs) of internal tissues (i.e., air, blood, bone, muscle, adipose) within the scan to derive the relationship between HU and bone density, obviating the need for an external calibration phantom [4] (https://github.com/Bonelab/Ogo). However, this technique has only been validated for bone, not muscle. The objective of this study was to modify and validate the CT internal calibration method developed by Michalski and colleagues for muscle density analysis [4]. We hypothesized that this modified internal calibration method would be comparable to the gold-standard phantom calibration method and would be more reliable than no calibration method, which reports HU as a surrogate for density and is the current standard in muscle research.

Methods

We scanned 10 bovine muscle samples with a custom-made sucrose phantom. Internal calibration ROIs were selected from various regions within bovine tissue samples to represent air, adipose, bone, blood, and muscle (Figure 1). To assess reliability of the internal calibration method, samples were scanned at five different scan positions and with two different scan protocols. The 10 scans were each calibrated using a modification of the Michalski [4] internal calibration method and the traditional phantom calibration method. To accurately compare the calibration methods, we used image registration to ensure that muscle density was measured at the same location in each scan. Image analysis was conducted using ITK-SNAP V3.8.0 and Python 3.8.8.

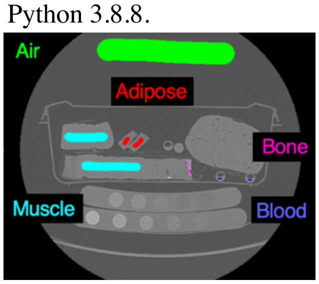

Figure 1: Internal calibration regions of interest (ROIs).

Results and Discussion

We found that the muscle density values derived from the internal and phantom calibration methods were highly correlated ($R^2 > 0.99$). When testing different ROIs, we found that the inclusion of bone as a ROI increased the error associated with the internal calibration derived muscle density values when compared to the phantom calibration derived muscle density values (Figure 2). This error may have been due to tissue inhomogeneity with the bone ROIs. We found that adipose and air ROIs were sufficient to yield accurate muscle density values with the internal calibration method. Our modified internal calibration method slightly underestimated muscle density, but the error was low (< 0.006 g/cm^3). The mean coefficient of variation (CV) for density of muscle samples across different scan protocols and positioning was statistically lower for the modified internal calibration method (mean CV = 0.33%) when compared to the phantom calibration method (mean CV = 0.52%) (p-value < 0.001) and no calibration as reported using HU as a surrogate for density (mean CV = 6.52%) (p-value < 0.001). This indicates that the internal calibration method is more reliable across scan conditions and less sensitive to scan protocol and positioning. These results support our hypothesis that the internal and phantom calibration methods are comparable, and that internal calibration derived muscle density values are more reliable than HU across scan conditions. We conclude that the internal calibration method allows accurate assessment of muscle density in opportunistic CT scans and therefore, can facilitate the study of muscle weakness with CT scans that do not include a phantom, e.g., clinically acquired scans.

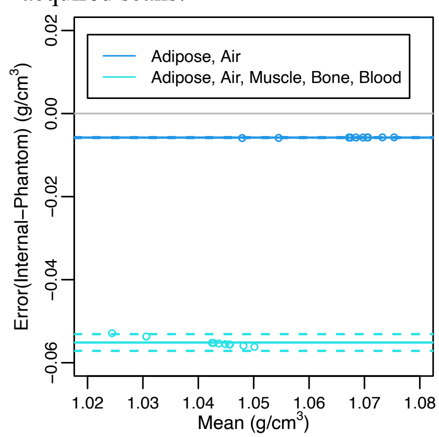

Figure 2: The difference between muscle density values derived from the phantom and internal calibration methods were reduced when bone, muscle, and blood were excluded as internal calibration ROIs.

Significance

We have developed an internal calibration method to produce accurate and reliable muscle density measures from CT images without calibration phantoms. This will enable the use of opportunistic CT image analysis to assess muscle density, a surrogate for muscle weakness, in a non-invasive and inexpensive method. This work will help improve our understanding of muscle weakness, especially in patients with severely limited mobility where traditional methods of strength testing are not feasible. Internal calibration may also prove useful for the screening and diagnosis of muscle density loss in other musculoskeletal disorders.

Acknowledgments

NSERC; University of Calgary Biomedical Engineering.

References

1. Appleton et al., 2014. *Journal of the Intensive Care Society;* 2. Vanhorebeek et al., 2020. *Intensive Care Med;* 3. Rasch et al., 2009. *Acta Orthopaedica;* 4. Michalski et al., 2020. *Medical Engineering & Physics*

CAN WE RELIABILY MEASURE STRAIN IN THE ITB VIA ULTRASOUND DURING ISOLATED CONTRACTIONS?

Laura A. Hutchinson[1*], Glen A. Lichtwark[1], Luke A. Kelly[1]
[1]The University of Queensland, St. Lucia, QLD, Australia
email: *laura.hutchinson@uq.edu.au

Introduction

The iliotibial band (ITB) is a unique anatomical structure in humans, believed to be important for bipedal locomotion. One curious feature of the band is that it transmits force across the lateral knee from two seemingly antagonist muscles: gluteus maximus (GM) and tensor fascia latae (TFL). We have been developing techniques to understand how these muscles transmit tension through the ITB using ultrasound imaging. Here we explore the validity, reliability, and feasibility of using a Kanade-Lucas-Tomasi (KLT) [1,2] algorithm to track ITB length changes during isolated contractions of GM and TFL.

Methods

Fifteen healthy participants (9m/6f, a:29±7years, h:175±7cm, w:78±11kg) gave informed consent. To test the validity of our tracking algorithm (MATLAB, vision.PointTracker) we compared the displacement of an ultrasound transducer measured using traditional motion capture (Qualisys, 200Hz) to the displacement measured by our algorithm (Telemed, 110Hz). Participants were seated and instructed to relax. An ultrasound probe with 3 reflective markers was placed on the distal lateral thigh and moved along the axis of the ITB a distance of ~10mm for 10 seconds. In MATLAB, the RF-data was filtered and up-sampled and the displacement of the ITB tissue was tracked across the entire trial. One hundred randomly selected frames of ultrasound and motion capture displacement were compared and the average R^2, slope, and intercept was found.

We imaged the ITB in a similar location to described above, and assessed joint movement by a string potentiometer attached between the transducer and Gerdy's tubercle. A constant current electrical stimulator (Digitimer) was programmed to deliver trains of electrical stimulation (60 rectangular pulses, 110Hz) through fine wires inserted into the TFL. The ultrasound probe and string potentiometer were then removed and replaced, and the stimulations were repeated to test the between-session reliability. In MATLAB, the ITB region was manually selected by an operator and the points were tracked using our algorithm as above. Combining the string potentiometer and the ultrasound tracking displacements, the average, maximal ITB strain during stimulation was calculated. Bland-Altman plots were created to compare within session, between session, and between operator reliability.

Finally, to test the feasibility of this method, participants also received a "low" level stimulation that was ~50% lower than the high-level stimulation above. We compared the average maximum strain during stimulation across participants and between sessions using a 2-way repeated measures ANOVA with Bonferroni pairwise corrections.

Results and Discussion

The ultrasound and motion capture displacements had an average R^2 of 0.96, slope of 1.02, and intercept of -0.57, indicating good agreement between motion capture and ultrasound displacements. Therefore, we concluded our method is valid for measuring ITB displacement.

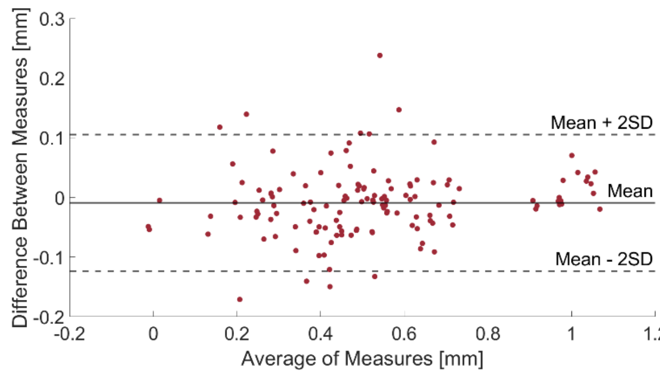

Figure 1: Bland-Altman plot between single-session measures repeatedly tracked by a single operator (within session reliability).

Bland-Altman comparisons within operator (Figure 1), between operators, and between sessions were conducted and found little to no bias indicating the reliability of our method.

Finally, our method found significant differences between stim level and visit ($P<0.05$) but only found pairwise differences between the low stim during visit 2 and both of the high stim conditions (Figure 2). This indicates that our method is able to quantify changes in ITB strain as they relate to muscular activation.

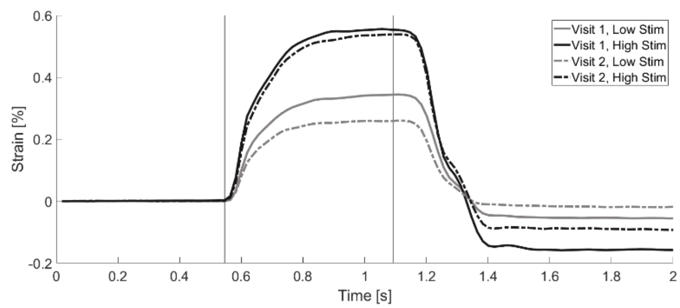

Figure 2: Ultrasound-based strain measures averaged across 15 participants during high (solid line) and low (dashed line) level stimulations during two visits (light and dark lines). The vertical lines indicate the timing of the applied stimulation.

Significance

Our novel method for measuring *in vivo* ITB strain shows promising results for validity, reliability, and feasibility in tracking and comparing isolated muscular contractions that strain the ITB. We aim to use this method to explore regional variation in strain during isolated contractions of the two in-series muscles: GM and TFL.

References

[1] Lucas & Kanade, *7th Int. Jt. Conf. Artif. Intell.* 1981.
[2] Tomasi & Kanade, *Carnegie Mellon Univ. Tech. Rep.*, 1991.

TEST-RETEST RELIABILITY OF T1ρ AND T2* IN SMALL AND LARGE TUBE PHANTOMS AND LEFT-RIGHT OF ISOCENTER POSITIONAL DEPENDENCE

Niccolo M. Fiorentino[1,*], Mack Gardner-Morse[2], Andrew Borah[2], John Ramsdell, Jiming Zhang, Pamela Vacek, Mickey Krug[2], Matthew Geeslin, Timothy Tourville[2], Mathew Failla[2], and Bruce Beynnon[2]
Departments of [1]Mechanical Engineering and [2]Orthopaedics and Rehabilitation, University of Vermont, USA
email: niccolo.fiorentino@uvm.edu

Introduction

Identifying changes in cartilage composition prior to cartilage loss may allow novel therapeutic interventions to prevent osteoarthritis onset and progress. Recent imaging advancements aim to capture changes in tissue composition using quantitative magnetic resonance imaging (qMRI) techniques [1], with qMRI metrics demonstrating a difference between healthy knees and those at increased risk of osteoarthritis [2]. Establishing the reliability of qMRI metrics is an ongoing challenge due to research-based acquisitions and newer metrics such as T2*.

The reliability of qMRI metrics is frequently assessed with an imaging phantom composed of liquid or gel placed at the center of the magnet (i.e. isocenter). Imaging phantoms consist of either an array of smaller tubes, usually arranged in a circular pattern, or one larger container. While the smaller phantoms permit simultaneous imaging of an array of qMRI values, the tube size is small compared to diarthrodial joints. Furthermore, phantoms imaged at isocenter may generate misrepresentative results, as diarthrodial joints in the extremities are located to the side (left and right) of isocenter during imaging.

Therefore, the purposes of this study were to quantify the variance in qMRI metrics T1ρ and T2* in small and large imaging phantoms relative to:

- Test-retest (day-to-day variability)
- Image location (slice)
- Phantom position (left and right relative to magnet isocenter)

Methods

We conducted a test-retest reliability study of T1ρ and T2* using two imaging phantoms. The 'small tubes' phantom consisted of three pairs of tubes (six total) of agarose gel (2, 3 and 4%) for T1ρ imaging (The Phantom Laboratory, Inc.) [3], and six different tubes with three concentrations of $MnCl_2$ for T2* imaging (Fig. 1). The 'large tube' phantom was a single tube (Nalgene™) of 89 mm diameter and 285 mm length. Both phantoms were imaged 100 mm to the right of isocenter and 100 mm to the left on five separate days using a T1ρ sequence (TSL = 0, 10, 40 and 80 ms, 500 Hz) [4] and a T2* sequence (TE = 0.42, 1, 5, 15 and 30 ms). Images were acquired on a Philips Achieva 3T MR Scanner with a 16-channel transmit-receive RF coil.

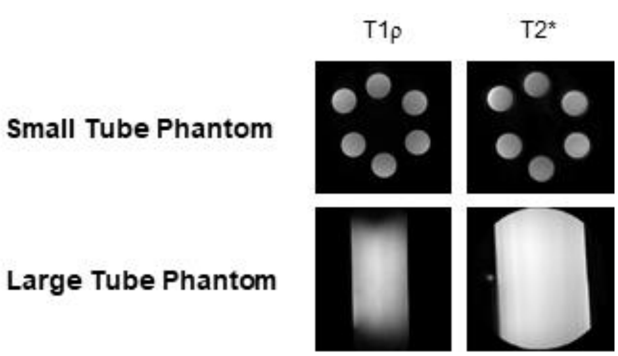

Figure 1: Representative phantom images used to calculate T1ρ (images on the left, TSL = 0 ms) and T2* (images on the right, TE = 0.42 ms).

Each pixel was fit with a mono-exponential function using custom MATLAB software (The Mathworks Inc., Natick, MA). Variance component analysis estimated the amount of measurement error attributable to day, slice and side for the large phantom. For the smaller phantoms the variability between vials was also estimated. Paired t-tests tested for systematic differences between the right and left imaging locations relative to isocenter from the same slice and day ($p<.05$). Averaged data reported as mean +/- STD.

Results and Discussion

T1ρ small tubes phantom: The average (total variance) across all days and both imaging positions relative to isocenter for T1ρ was 34.1 ms (0.6), 66.0 ms (1.9), and 44.8 ms (0.6), for the three pairs of small tubes with different concentrations. Percentage variance was highest for 'side' at all concentrations (38%, 49%, 41%). All vials demonstrated a difference between the left and right imaging locations relative to isocenter (0.9 +/- 0.4 ms).

T2* small tubes phantom: The average (total variance) across all days and right and left imaging locations for T2* was 23.4 ms (7.0), 11.7 ms (1.1), and 3.1 ms (0.1), for the three pairs of small tubes with different concentrations. Percentage variance was highest for 'slice' (57%), 'vial' (93%) and 'vial' (71%), resp. Five of six vials demonstrated a difference between the left and right imaging locations (0.1 +/- 2.0 ms).

T1ρ large tube phantom: The average (total variance) across all days and both scanning positions for T1ρ was 42.6 ms (0.4). Percentage variance was highest for 'day' (97%). Measurements were different on the left vs. right locations (0.1 +/- 0.1 ms).

T2* large tube phantom: The average (total variance) across all days and both sides for T2* was 24.3 ms (0.9). Percentage variance was highest for 'day' (62%). Measurements were different on the left vs. right imaging locations (0.8 +/- 0.3 ms).

Our variance estimates were similar to previously reported T1ρ values using the same small tubes phantom; however, our results showed a position dependence that was not observed previously [3].

Significance

To our knowledge our study was the first to quantify:

- Source of variability in T1ρ and T2*
- T1ρ and T2* variability in small and large phantoms
- Effect of phantom size on left-right position dependence

Acknowledgments

We acknowledge technical support from the UVM MRI Center for Biomedical Imaging and statistical analysis by the UVM Biomedical Statistics Research Core.

References

[1] Guermazi et al., 2015. *Osteoarthritis Cartilage.* 23(10): 1636.
[2] MacKay et al., 2018. *Osteoarthritis Cartilage.* 26(9): 1140.
[3] Kim et al., 2020. *Osteoarthritis Cartilage.* 28(12): 1539.
[4] Li et al., 2008. *Magn Reson Med*, 59(2): 298.

RELIABILITY OF T1ρ AND T2* MEASUREMENTS OF CARTILAGE IN HEALTHY KNEES UNDER LOAD

John Ramsdell[1, *], Bruce Beynnon, Mack Gardner-Morse, Jiming Zhang, Matthew Geeslin, Tim Tourville, Mathew Failla, Andrew Borah, Mickey Krug, and Niccolo M. Fiorentino[1]
[1] Department of Electrical and Biomedical Engineering, University of Vermont, USA
email: john.ramsdell@uvm.edu

Introduction

Compositional magnetic resonance imaging (MRI) techniques such as T1ρ and T2* have generated much interest as potential biomarkers for detecting pre-arthritic changes in populations at-risk for developing osteoarthritis (OA). Traditionally, MR images are acquired while the knee is in a non-weight bearing state. However, a custom MRI-compatible knee loading device developed at the University of Vermont permits applying physiological loads to the knee while simultaneously imaging the joint.

The purpose of this study was to test the effect of load, visit, and limb, on the T1ρ and T2* relaxation times of a healthy population within a central ROI in the tibiofemoral joint's articulating cartilage.

Methods

A total of 10 healthy subjects (4 male, 6 female, age: 23±2.4 years) with no history of lower limb injuries participated in this study. The effect of visit was tested by scanning subjects at two timepoints 7±3 days apart on a 3T Phillips MR system with a 16 channel RF coil. A scanning session included T1ρ and T2* image acquisitions of each knee in two separate knee loading conditions:1) supine in a traditional unloaded state, and 2) supine while supporting a load of 40% bodyweight as applied by the MRI loading device.

T1ρ and T2* relaxation times were calculated by curve fitting the signal intensity of the pixels within a ROI and finding the average relaxation time. A 12mm diameter plug was defined with the intent of examining the area of contact between the two cartilage surfaces in each compartment (Fig. 1). The position of the plugs in the ML direction was placed at 20% and 80% of the width of the tibial plateau. The AP positions of the plugs were centered about the AP length of the tibia within the plug. Cartilage pixels within the plug on both bones were further split into a deep and superficial layer, ultimately defining each ROI.

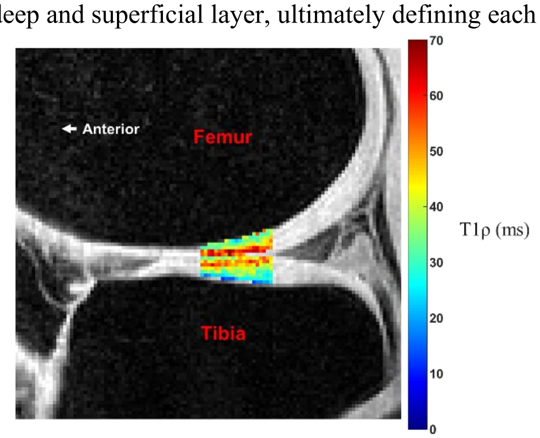

Figure 1: Sagittal T1ρ map of the most center slice within the lateral plug is represented.

T1ρ and T2* relaxation times from each subject were grouped into their ROI by bone, compartment, and layer. Three-way analysis of variance tested if T1ρ and T2* relaxation times within each ROI were significantly different with respect to load, visit, and limb. P values of less than 0.05 were considered significant.

Results and Discussion

No Significant differences were found with respect to visit. Significant differences with respect to limb were found in four of the 16 ROIs: for T2*, Tib_Lat_Sup(p=0.002); for T1ρ, Fem_Lat_Deep(p=0.031), Fem_Lat_Sup(p<0.001), and Tib_Lat_Sup(p<0.001). Significant difference with respect to load were found in 11 of the 16 ROIs (Fig. 2).

The results from this study suggest that our T1ρ and T2* measurements were reliable between visits, but only partially reliable between sides. The results also suggest that loading the knee with our loading device significantly effects the T1ρ and T2* relaxation times. In general, loading caused a decrease in relaxation times.

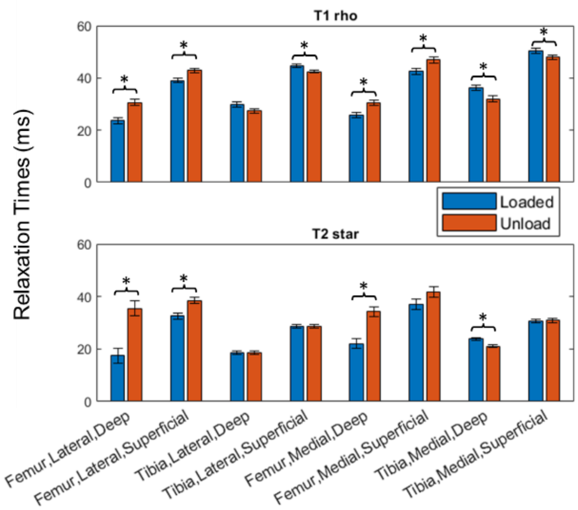

Figure 2: Analysis of multiple comparisons shows the effect of load on both T1ρ and T2* within each ROI. The vertical axis represents the estimated value of mean relaxation times. Error bars represent the standard errors, and '*' represents a significant difference.

Significance

Early abnormalities to the articular cartilage content (in the form of T1ρ and T2* relaxation times) following ACL injuries have been linked to the accelerated degeneration of cartilage surfaces[1]. Detection of these abnormalities are key to developing therapeutic interventions that can take place prior to irreversible changes. We hypothesized that studying cartilage content under loaded conditions will provide a novel understanding of the disease progression. This study provided an understanding of how our T1ρ and T2* calculations change in a healthy population when utilizing our MR knee loading device. These results will ultimately yield more powerful conclusions in future studies regarding post traumatic OA onset and/or progression.

Acknowledgments

We acknowledge technical support from the UVM MRI CI enter for Biomedical Imaging.

References

[1] Atkinson et al. *BMC musculoskeletal disorders* 2019

EVALUATION OF A NOVEL ROBOTIC ANKLE PROSTHESIS: STIFFNESS EMULATION AND ACTIVE PUSH-OFF

Anthony J. Anderson[1,2], Yuri Hudak[1,2], Kira Gauthier[1,2], Brittney Muir[1,2], and Patrick M. Aubin[1]
[1]Department of Mechanical Engineering, University of Washington, Seattle, WA
[2]Center for Limb Loss and Mobility (CLiMB), VA Puget Sound Health Care System, Seattle, WA
email: ajanders@uw.edu

Introduction

Robotic prosthetic ankles have the potential to improve mobility-related quality of life in individuals with transtibial amputation. Currently, only one ankle prosthesis is commercially available that can deliver active push-off in late stance (Empower, Ottobock). Clinical evaluations of this device show mixed outcomes [1], and further research is required to understand optimal robotic prosthesis behaviour.

We designed and built a novel high-performance robotic ankle that allows us to explore optimal prosthesis behaviour in a laboratory environment. This abstract describes the first walking tests of our robotic ankle prosthesis with one transtibial amputee. We evaluated our device in terms of its ability to 1) emulate virtual passive stiffness profiles and 2) provide peak push-off power in late stance comparable to that of the healthy human ankle. Our outcomes and analysis focus on the biomechanical capabilities of the device rather than its effects on gait.

Methods

In our novel robotic ankle prosthesis, ankle plantarflexion moments are provided by an offboard motor and Bowden cable transmission, while dorsiflexion moments are provided with a parallel torsion spring. Ankle torque and angle are measured with sensors on the prosthesis, and foot-ground contact is measured via an instrumented treadmill. Prosthesis behaviour is determined by an offboard controller that communicates with a desktop PC for experimenter input.

We evaluated the prosthesis in two modes. In the first mode, the prosthesis emulated an idealized passive prosthesis by enforcing a linear torque-angle relationship during mid and late stance. Both the stiffness and neutral angle were configured in software. In the second mode, the prosthesis emulated the biological ankle by providing a large burst of push-off work in late stance. The prosthesis was spring-like in midstance, and the amount of push-off work in late stance was modulated with a single ‘push-off’ parameter, similar to the device in [1].

One person with transtibial amputation (114.2 kg) was recruited to this IRB-approved research study. A certified prosthetist fit the prosthesis to the participant and set the digital neutral angle of the ankle joint. For all walking conditions, the participant walked on a split-belt treadmill at a non-dimensionalized Froude speed of 0.16 (1.22 m/s).

Three walking bouts were performed. The first bout gave the participant time to adapt to the novel device with static stiffness parameters. The second bout of walking contained a sweep of three stiffnesses (10.6 Nm/deg, 13.3 Nm/deg, and 15.9 Nm/deg). The final walking bout evaluated the powered push-off controller with ‘low’, ‘medium’ and ‘high’ push-off parameters that were determined in prior pilot tests. Each bout consisted of 10-20 minutes of walking. All outcomes were computed with signals measured by the prosthesis.

Results and Discussion

The participant successfully completed all walking bouts. The greatest average peak plantarflexion torque was 96.4 Nm and occurred during the stiffest prosthesis setting. Stance phase RMS torque tracking errors were 2.23 Nm, 2.54 Nm, and 1.91 Nm for the 10.6 Nm/deg, 13.3 Nm/deg, and 15.9 Nm/deg stiffness settings, respectively. For context, the error in the 13.3 Nm/deg stiffness condition represents less than 3% of the peak torque. The low torque tracking errors indicate that the prosthesis can emulate idealized passive devices with high fidelity.

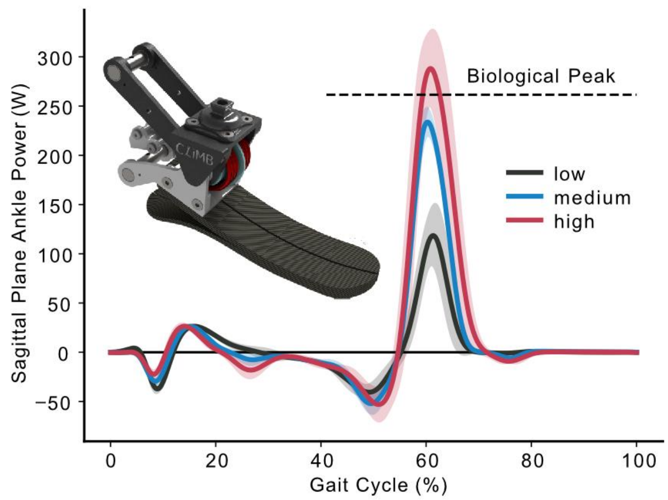

Figure 1: Robotic prosthesis sagittal plane ankle power over the gait cycle. Biological peak power (dashed line) was taken from [2] and scaled to our participant’s body mass. Inset shows rendering of prosthesis.

Figure 1 shows the prosthetic ankle power for the three active push-off settings. Average peak push-off power ranged from 118.9 W to 288.4 W. The latter peak push-off power exceeds the peak power of the biological ankle at the same Froude speed [2]. These findings indicate that our device is mechanically capable of emulating the biological ankle and other robotic prostheses in terms of sagittal plane gait biomechanics.

Significance

This work represents a major milestone in the development of a novel robotic ankle prosthesis that will be used to conduct research at the interface of active prosthesis control and amputee biomechanics. Active prostheses are becoming more prevalent in research and clinical care, and improved tools are needed to answer scientific questions surrounding optimal prosthesis behaviour, amputee biomechanics, and clinical outcomes. Our new prosthesis allows for the broad exploration of potential prosthesis behaviours that may improve amputee gait outcomes and can help inform the design and control of future devices.

Acknowledgments

This work was funded in part by VA RR&D grants A9243C, RX002357, and RX002130.

References

[1] Gardinier et al., 2020. *Clin Rehabil.* 10.1177/0269215517723054
[2] Russell-Esposito et al., 2016. *ISPO.* 10.1177/0309364614564021.

Effect of prosthetic ankle push-off power and foot stiffness on individual leg work during walking in people with transtibial amputation

Joshua R. Tacca[1], Zane A. Colvin[2], and Alena M. Grabowski[2,3]
[1]Department of Mechanical Engineering & [2]Department of Integrative Physiology, University of Colorado Boulder, Boulder, CO
[3]Department of Veterans Affairs, Eastern Colorado Healthcare System, Denver, CO
email: Joshua.tacca@colorado.edu

Introduction

Many people with unilateral transtibial amputation (TTA) use passive-elastic prosthetic feet to walk. Such prostheses cannot provide the peak mechanical power typically generated by the biological calf muscles during walking [1] resulting in reduced positive affected leg (AL) work during push-off compared to non-amputees. Reduced positive AL work can lead to greater collision forces on the unaffected leg (UL) and may increase the risk of knee osteoarthritis for people with unilateral TTA [2].

Powered ankle-foot prostheses such as the BiOM (Ottobock, Duderstadt, Germany) provide stance-phase, battery-powered ankle torque. People with TTA using the BiOM normalize biomechanics during walking compared to non-amputees by increasing positive AL work of the trailing leg and decreasing negative UL work of the leading leg [3]. However, the relationship between the power generated by the BiOM and AL and UL work is unknown. Moreover, the BiOM attaches in-series with a passive-elastic prosthetic foot with manufacturer-recommended stiffness that may affect AL and UL work. A previous study found that less stiff prostheses are associated with greater positive AL work during push-off [4]; however, the effect of prosthetic stiffness may also depend on the power generated by the BiOM. We hypothesized that increasing prosthetic power and reducing stiffness would increase positive trailing AL work and decrease negative leading UL work.

Methods

6 subjects (3M, 3F; mean±SD: 38±10 yrs.; 69.1±15 kg; 1.70±0.06 m) with TTA walked at 0.75–1.75 m/s on a dual-belt force treadmill (Bertec, Columbus, OH) using the low-profile (LP) Variflex (Össur, Reykjavik, Iceland) prosthetic foot at the recommended stiffness category (Rec Cat), one Cat more stiff (+1), one Cat less stiff (-1), and two Cat less stiff (-2). Then, subjects walked at 1.25 m/s using the BiOM that was tuned so that their net positive prosthetic ankle work was within 2 SD of average non-amputee net positive ankle work [3]. Subjects walked at 0.75–1.75 m/s using the BiOM at the recommended power (Rec Pow) from tuning, 10% greater power (+10%), and 20% greater power (+20%) with each prosthetic Cat.

We measured vertical ground reaction forces (vGRFs) at 1000 Hz, filtered them using a 4th-order low-pass Butterworth filter with a 30 Hz cut-off and used a 20 N vGRF threshold to determine the contact phase. We calculated individual leg external mechanical work during the step-to-step transition, defined as the double support phase, when the AL was the trailing leg and UL was the leading leg from 6 strides (MATLAB, Mathworks, Natick, MA) [5]. We constructed linear mixed effects models to determine the effects of prosthetic power, stiffness Cat, speed, and their interactions on positive external mechanical work of the trailing AL (W_{pos}) and negative external mechanical work of the leading UL (W_{neg}). We set subject as a random effect and used $p < 0.05$ to determine significance.

Results and Discussion

At 0.75 m/s, use of the BiOM at Rec, +10%, and +20% power increased AL W_{pos} by 2.1, 5.3, and 7.1 J, respectively, compared to use of the passive prosthesis ($p < 0.01$; Fig. 1a). At 1.75 m/s, use of the BiOM at Rec, +10%, and +20% power increased AL W_{pos} by 9.9, 12.0, and 13.4 J, respectively, compared to use of the passive prosthesis ($p < 0.01$; Fig. 1a). Across all speeds, use of the -1, Rec, and +1 Cat increased AL W_{pos} by 0.7, 1.0, and 0.8 J, respectively, compared to use of the -2 Cat ($p < 0.01$; Fig. 1b).

At 0.75 m/s, use of the BiOM at +10% and +20% power decreased the magnitude of UL W_{neg} by 1.5 and 2.4 J, respectively, compared to use of the passive prosthesis ($p < 0.02$; Fig. 1c). In contrast, at 1.75 m/s use of the BiOM at +10% and +20% power increased the magnitude of UL W_{neg} by 3.3 and 2.5 J, respectively, compared to use of the passive prosthesis ($p < 0.02$; Fig. 1c). We did not detect an effect of stiffness Cat on UL W_{neg} (Fig. 1d).

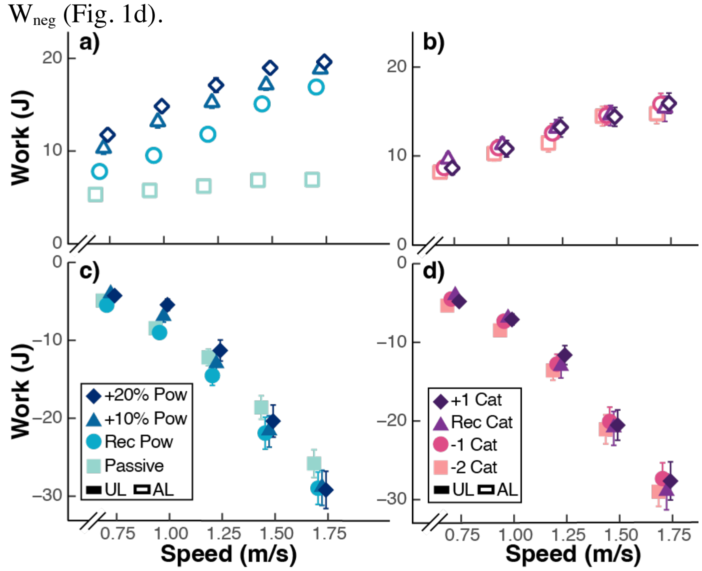

Figure 1: W_{pos} (a, b) and W_{neg} (c, d) across walking speeds. Left panels (a, c) are averaged across stiffness categories (Cat) for each prosthetic power setting (Pow) and right panels (b, d) are averaged across Pow for each Cat. Filled symbols refer to the UL and open symbols to the AL. Error bars are SEM. Symbols are offset for clarity.

Significance

Increasing prosthetic power increased AL W_{pos} but did not reduce the magnitude of UL W_{neg} at faster walking speeds. Prosthetic stiffness category had little to no effect on individual leg work. Our results inform prosthetic prescription and design, which could reduce injury for people with TTA.

Acknowledgments

This study was funded by the Department of Veterans Affairs 1IO1RX002941-01A2.

References

[1] Zmitrewicz et al. (2007). *J. Biomech,* **40:** 1824-1831
[2] Morgenroth et al. (2011). *Gait Posture,* **34:** 502-507
[3] Herr & Grabowski (2012). *Proc. Royal Soc. B,* **279:** 457-464
[4] Halsne et al. (2020). *Clin. Biomech,* **80:** 105141
[5] Donelan et al. (2002). *J. Biomech,* **35:** 117-124

HIP BIOMECHANICS IN PEOPLE WITH UNILATERAL ABOVE-KNEE AND THROUGH-KNEE AMPUTATIONS

Brieuc Panhelleux[1*], Alison McGregor[1] and Anne K. Silverman[2]
[1] Department of Surgery and Cancer, Imperial College London, London, UK
[2] Department of Mechanical Engineering, Colorado School of Mines, Golden, CO, USA
email: *b.panhelleux19@imperial.ac.uk

Introduction

In through-knee amputation (TKA), a longer residual femur and greater thigh muscle volume are retained compared to above-knee amputation (AKA). TKA may thus have biomechanical advantages compared to AKA, such as better hip muscle control and function [1]. Direct comparisons of walking biomechanics between people with TKA and AKA remain unclear because they are often grouped together in scientific studies [2]. Thus, the purpose of this study was to compare hip angles and moments during gait between TKA and AKA, providing insight into walking biomechanics with potential to guide surgical practice.

Methods

Three participants with a unilateral AKA (2F/1M, 60 (±10.1) yrs, 173.6 (±4) cm, 66.3 (±11.5) kg) and two with a unilateral TKA following the classical surgical technique [1] (2M, 47 (±8.5) yrs, 178.5 (±3.5) cm, 76.5 (±2.12) kg) walked at a self-selected walking speed (SSWS) on a level walkway with four embedded force plates (Kistler, 2000Hz). Kinematics (Vicon, 200Hz) were collected using a full-body marker set with 107 markers. Marker trajectory data was filtered with a fifth order spline interpolating function through Vicon's built-in Woltring filter with a smoothing factor of 15. Sagittal-plane hip angles and moments were calculated for each participant from the kinematic marker data, ground reaction forces, and a whole-body kinematic model using Cole et al.'s joint coordinate systems definitions [3]. At least 10 trials with two consecutive force plate hits, were analysed for each participant. Cohen's d effect size was computed to compare hip angle range of motion and hip flexion/extension moment peaks between each leg of AKA and TKA using the pooled standard deviation.

Results and Discussion

The participants with AKA and TKA had a mean SSWS of 1.03 (±0.07SD) m/s and 1.18 (±0.02SD) m/s, respectively. The hip range of motion (ROM) of AKA and TKA had a large effect size (d=1.7) on the amputated side and a medium effect size on the intact side (d=0.7), with TKA having a larger ROM. Participants with TKA had a greater peak hip extension moment during stance phase compared to AKA (Figure 1). Peak extension moment had a large effect size on the intact side (d=1.3) and a medium effect size on the amputated side (d=0.6). Peak flexion moment had a large effect size on the amputated and intact sides (d=0.9 and d=1, respectively) The higher peak moments can be partially attributed to a higher SSWS in TKA compared to AKA, suggesting that greater retained muscle volume in this group may enable larger moments and therefore faster walking speeds. This result supports retaining a greater residual leg length that is characteristic of TKA. A prior study of AKA and TKA found that when residual femur length was between 57% and 100% of intact femur length, there was no correlation between femur length and kinematic or kinetic parameters [2]. However, this study did not compare TKA to AKA directly, and thus there may be important differences between groups. Another study found no differences in SSWS between matched unilateral TKA and AKA, contrary to our results and highlighting the wide variation in walking speed in the AKA population [4]. Our preliminary data suggest hip kinematic and kinetic differences between TKA and AKA during walking. Further research is needed with additional participants and investigating non-sagittal planes of the hip and other joints.

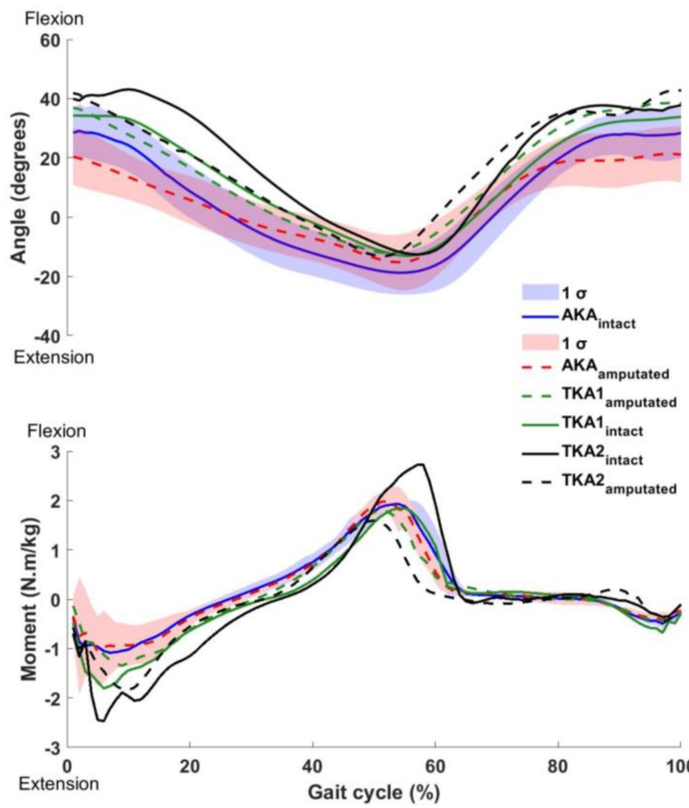

Figure 1: Hip flexion/extension angles and moments. The mean ± 1σ are presented for the three AKA participants. Data are time-normalised over a gait cycle from heel strike to ipsilateral heel strike.

Significance

This work suggests that people with unilateral TKA may have greater hip range of motion and higher peak hip flexion/extension moments during gait compared to unilateral AKA, although additional participants are needed to generalize the results. Biomechanical differences between unilateral TKA and AKA indicate that these groups should be separately considered in scientific studies. Additional exploration of the relationship between gait biomechanics and functional mobility can provide evidence to inform surgical decision making.

Acknowledgments

We acknowledge the Royal British Legion Centre for Blast Injury Studies at Imperial College London.

References

[1] Panhelleux et al., 2021. *Vascular.* (in press)
[2] Baum et al., 2008 *Injury.*39:728
[3] Cole et al., 1993. *J. of Biomech.Engineering*. 115:344
[4] Schuett et al., 2019 *Clin. Ortho. and Related Res.* 477:821

MUSCLE-DRIVEN, IMPLANTED FOOT-ANKLE PROSTHESIS: PRELIMINARY *IN VIVO* BIOMECHANICS

Katrina L. Easton[1*], Caleb Stubbs[1], Caroline Billings[2], Kristin Bowers[2], Stacy M. Stephenson[3], Cheryl B. Greenacre[2], David E. Anderson[2], and Dustin L. Crouch[1]

[1]College of Engineering, [2]College of Veterinary Medicine, [3]Graduate School of Medicine; University of Tennessee-Knoxville

email: *keaston@utk.edu

Introduction

Limb amputation causes severe disability and affects about 2 million people in the US[1]. Most patients reject limb prostheses, partly because even state-of-the-art devices fail to restore natural sensorimotor function[2]. One potential approach to achieve this "holy grail" is to physically attach prostheses to muscles in the residual limb to leverage their innate sensorimotor capabilities. Since all existing prostheses must be worn externally, muscle forces had to be externalized by cineplasty surgery[3], which has not been widely adopted due to limitations in function, comfort, and appearance. Rather than externalize muscle forces, we propose to *internalize* the prosthesis to facilitate more functional and anatomically realistic muscle-prosthesis attachment. In a previous *in vivo* study, we showed that it is feasible to completely implant a prosthesis within living skin at the distal end of a residual limb[4]. In an ongoing *in vivo* study, we are testing a prototype of a muscle-driven, articulated, foot-ankle implanted prosthesis in a rabbit model of hindlimb below-knee amputation. In this abstract, we present preliminary biomechanics data during hopping gait as a quantitative indicator of prosthetic limb use.

Methods

The custom foot-ankle prosthesis prototypes included 3D-printed 316 stainless-steel foot and shank segments. The segments were joined by a polyethylene hinge pin and overmolded in medical-grade silicone (BIO M360, Elkem Silicones). The *in vivo* study was approved by our Institutional Animal Care and Use Committee. Two 18-week-old female New Zealand White rabbits underwent surgical amputation of the left hindlimb under general anesthesia. Briefly, the skin surrounding the foot and ankle was retracted proximally. The musculoskeletal tissues were amputated approximately 2 cm proximal to the distal end of the tibia. After amputation, the prosthesis was anchored in the intramedullary canal of the tibia and immobilized using bone cement. The tibialis cranialis and triceps surae muscles were attached to eyelets on the foot segment using polyester-based artificial tendons in Rabbit 1 and the native tendons in Rabbit 2. The skin was replaced and sutured over the prosthesis (Fig. 1).

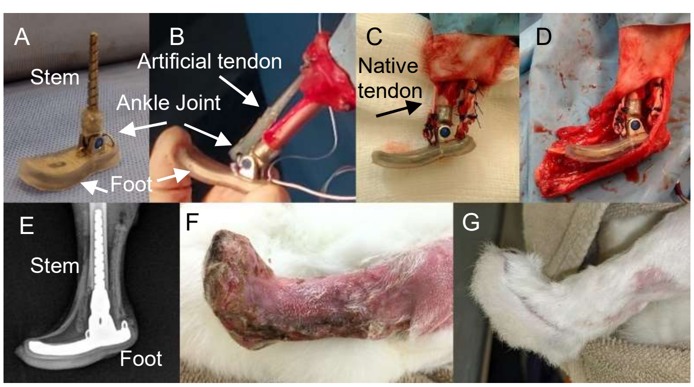

Figure 1*:* A) Jointed prosthesis B) Intra-op prosthesis with artificial tendons C) Intra-op prosthesis with native tendons D) Intra-op just prior to skin closure E) Lateral radiograph post-surgery with artificial tendons F) Eight days post-op G) Thirty days post-op.

Once bandages were removed (3 weeks post-surgery), we recorded ground contact pressures (HR Strideway System, Tekscan, Inc.) and kinematics during hopping gait. We used off-the-shelf software (Strideway Research 7.80, Tekscan, Inc.) to process the pressure data.

Results and Discussion

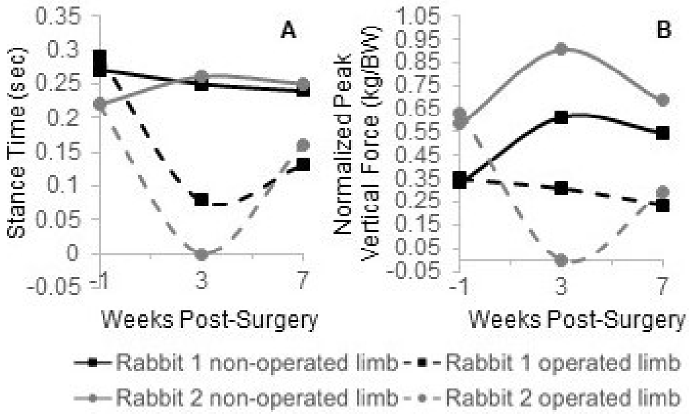

Figure 2*:* A) Stance time and B) Normalized peak vertical force, averaged across 9 - 11 gait cycles at each timepoint.

Stance time on the operated limb initially decreased from pre-surgery (-1 week) to 3 weeks post-surgery, but then improved from 3 to 7 weeks post-surgery in both rabbits (Fig. 2A). The normalized peak vertical force gradually decreased in the operated limb from pre-surgery to 7 weeks post-surgery in Rabbit 1 (artificial tendons); conversely, in Rabbit 2 (native tendons), force sharply declined initially but improved from 3 to 7 weeks post-surgery. In both rabbits, normalized peak force in the non-operated limb initially increased but returned towards baseline by 7 weeks post-surgery. The lower force at post-surgery week 3 in Rabbit 2 may have been due to high stiffness and low range of motion in the ankle joint during the first 4-6 weeks post-surgery.

Pressure quantified limb use but did not reveal whether the prosthesis ankle was moving or being actively controlled by the attached muscles. To determine this, the anticipated kinematic data and electromyography will be needed.

Significance

Biomechanics data are critical for determining the potential sensorimotor function restored by muscle-driven prostheses.

Acknowledgments

Funding from NIH (R61AR078096) and NSF (1944001). Thanks to Kaitlyn Stephens, Sarah Clabo, Victoria Theobald, and Nicholas Ray for help with data collection; and to Ivy Milligan, Dylan Marler, and Carter Hatch for help with data processing.

References

[1] Ziegler-Graham, 2008. *Arch Phys Med Rehabil.* 89(3):422.
[2] Biddiss, 2007. *Am J Phys Med Rehabil.* 86(12):977.
[3] Blaschke, 1952. *J Appl Physiol.* 5(5):195.
[4] Hall, 2021. *Ann Biomed Eng*. 49(3):1012.

ANKLE MECHANICS OF TYPICAL INDIVIDUALS WALKING WITH A BI-LINEAR STIFFNESS ANKLE-FOOT ORTHOSIS

Luke Nigro[1*], Elisa S. Arch, PhD[2]
[1]Department of Mechanical Engineering, University of Delaware, Newark, DE, USA
[2]Department of Kinesiology & Applied Physiology, University of Delaware, Newark, DE, USA
email: *lnigro@udel.edu

Introduction

Natural ankle quasi-stiffness (NAS), defined as a linear regression of the sagittal ankle moment vs. ankle angle during the loading (second rocker) phase of stance, can be used as a design parameter to customize passive-dynamic AFO bending stiffness. This spring-like stiffness can substitute for lost plantar flexor function for individuals [1]. Historically, a single NAS value was defined over the entire loading phase of stance [2]. However, NAS increases during the loading phase of healthy gait [3], often with two distinct stiffness regions – a lower stiffness early in loading (EL) and higher stiffness later in loading (LL). We designed an AFO with two stiffness elements – termed a bi-linear AFO (BL-AFO, Fig. 1) – which exhibits this bilinear EL/LL stiffness profile. The BL-AFO works by only having an anterior strut of one stiffness engaged at low dorsiflexion (DF) angles. Then, after a specific DF angle, a catching mechanism grabs and engages a second posterior strut, adding to the initial stiffness (Fig. 1). The purpose of this study was to test how this BL-AFO affects typical individuals' ankle mechanics during walking. Our hypotheses were that peak plantarflexion moment would stay the same across AFO conditions – which subsequently means that peak DF angle would decrease with higher BL-AFO stiffness, EL-NAS would stay the same across AFO conditions, and LL-NAS would increase with increased posterior strut stiffness.

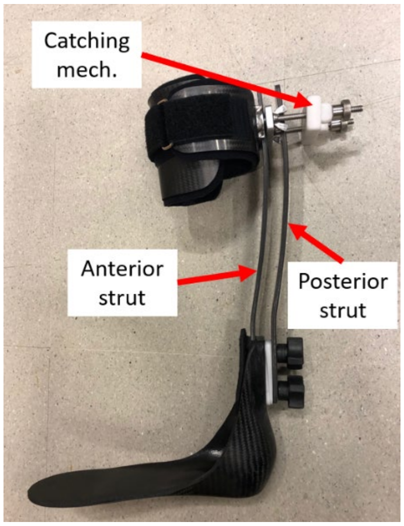

Figure 1: BL-AFO with interchangeable anterior and posterior struts.

Methods

Four healthy subjects (avg ±std) (2M/2F, 25 ±2.4 yrs, 175 ±10.1 cm, 67 ±6 kg) walked on an instrumented split-belt treadmill at 0.8 statures/s while a motion capture camera system tracked bilateral pelvic and lower extremity kinematics. Subjects walked for five conditions: No AFO, single strut AFO ('Single'), BL-AFO with low late stiffness ('Low'), medium late stiffness ('Med'), and high late stiffness struts ('High'). The strut used in the single condition was the same anterior strut used in the BL-AFO conditions. Sagittal plane ankle joint angles and moments were calculated using a standard inverse dynamics approach. EL and LL stiffness were computed as best-fit lines on the sagittal ankle moment vs. sagittal ankle angle curve during the EL and LL phases. EL and LL phases were defined using the same method as Shamaei et al. [4] for the No AFO and single conditions. For the BL-AFO conditions, the EL phase was defined from initial minimum sagittal ankle angle during stance to the angle at which the second strut engaged (6.5deg DF past the subject's neutral ankle position during quiet standing). Repeated-measure ANOVAs were used to compare EL and LL stiffness, ankle angles, and ankle moments on a subject-by-subject basis across conditions. Reported *p*-values apply to all individuals.

Results and Discussion

The following results were consistent across all subjects. Peak DF angles for all AFO conditions (single or bi-linear) compared to No AFO was lower by 2-4 degrees ($p<0.025$). Among AFO conditions, subjects had their highest peak DF angle during the Single condition and the lowest peak during the High condition. Subjects did not exhibit significantly different peak ankle moments across all conditions ($p>0.284$). All subjects exhibited increased EL and LL stiffness compared to No AFO ($p<0.010$). Among the BL-AFO conditions, EL stiffness did not change ($p>0.601$). This was expected, since the anterior strut was kept the same for all conditions. Among the AFO conditions, LL stiffness generally increased with stiffer posterior struts. This increase was significant when comparing the Single and Low conditions ($p<0.034$), and the Med and High conditions ($p<0.042$), but not between the Low and Med conditions ($p>0.192$). This increase in net stiffness was approximately the same as the increase in posterior strut stiffness of the BL-AFO on its own. This study confirms our hypotheses. Future work will include more healthy subject recruitment, and ultimately testing on individuals with lower limb impairments.

Significance

This work represents a step forward in passive-dynamic AFO design. The typical individuals part of this study appeared to use the BL-AFO in a way that allowed it to substitute for the biological ankle's moment-generating function, but altered ankle kinematics in a tunable way. The substitution of function may mean that a BL-AFO could enhance the function of individuals with impairments, such as individuals who have had a stroke. The ability to tune different portions of the stiffness profile of the BL-AFO could allow further customization for patients, who might have difficulty initiating DF with an AFO that might be too stiff at the beginning of loading.

Acknowledgments

Luke Nigro acknowledges the National Science Foundation's Graduate Research Fellowship no. 1940700 for funding. The authors also acknowledge Custom Composites, Inc. (Cranston, RI, USA) for BL-AFO fabrication.

References

[1] Arch & Reisman (2016), *J.Prosthet.Orthot.*, 28(2):60-67.
[2] Davis & DeLuca (1995), *Gait & Posture,* 4:224-231.
[3] Nigro et al. (2021), *Gait & Posture*, 84:58-65.
[4] Shamaei et al. (2013), PLOS One, 8(3).

A BIOMECHANICAL ASSESSMENT OF A SERVICE MEMBER WITH TRANSTIBIAL AMPUTATION ACROSS THE UTILIZATION OF DIFFERENT PROSTHETIC FEET

Tyler C. Cardinale[1], Shannon E. Isley[1], Tatiana E. Djafar[1], and Trevor D. Kingsbury[1]
Clinical Biomechanics Laboratory, Navy Medicine Readiness and Training Command San Diego, San Diego, CA, USA
Email: tyler.c.cardinale.ctr@mail.mil

Introduction

Many service members who undergo transtibial amputation (TTA) have the potential to achieve high function and the desire to continue performing the physically demanding requirements of their occupation and desired recreational activities. In order to meet these requirements, service members need to utilize prosthetic feet that optimize both performance and functionality. However, there is currently little research comparing different prosthetic feet during higher level tasks. One of the most distinguishing aspects of prosthetic feet is stiffness [1]. Decreased stiffness in prosthetic feet tends to increase overall energy absorption. Yet, some of these advantages can be offset by the increased muscle activation needed to maintain overall stability [2]. The purpose of this study was to assess the biomechanics of a service member with TTA while utilizing different prosthetic feet during both ballistic and maximal strength tasks.

Methods

A male service member with a left unilateral TTA (age: 45yr height: 187cm mass: 84.7kg) underwent biomechanical assessments during 3 different sessions while utilizing 3 different prosthetic feet, the Össur Pro-Flex XC (an energy storage and return (ESAR) foot), BioDapt Versa Foot 2 (a non-ESAR foot with a metal frame and shock absorber typically used for weight lifting and higher level activities), and the Össur Flex-Run (a C-shaped running-specific prosthesis). We compared and categorized the stiffness of each foot through their manufacturers' websites and then validated their measures by comparing them to the limb active stiffness computed in ForceDecks (VALD performance, Newstead, AU). Each biomechanical assessment included one lower body ballistic movement, the Countermovement Jump (CMJ), and one whole body strength measurement, the isometric mid-thigh pull (IMTP). The subject performed the assessment on two forceplates (Kistler Instrument Corp, Novi, MI, USA) while using ForceDecks software to collect and process the assessment protocol. The assessment protocol consisted of the subject performing five cued maximal CMJ with approximately two seconds between each jump and hands on hips throughout the movement to control the effect of arm swing. The IMTP consisted of three, five second maximal pulls on a 45lb bar anchored to a squat rack. Variables of interest for the CMJ included peak takeoff force, peak takeoff force asymmetry, and jump height. Variables of interest for the IMTP included peak vertical force and peak vertical force asymmetry.

Results and Discussion

During the CMJ, the subject's peak takeoff force was highest with the Flex-Run and lowest with the Versa Foot 2, suggesting a more elastic device could promote higher force production in ballistic tasks (Table 1). The subject's CMJ was more symmetrical during peak takeoff force using the Flex Run, while use of the stiffer devices resulted in more lower limb asymmetry. Overall jumping performance was improved in the Flex-Run as well in terms of jump height (Table 1). This implies that less stiffness in prosthetic feet could improve both performance and peak force symmetry while performing ballistic tasks. The elastic properties of the Flex-Run might have aided in lower limb symmetry and improved performance because the subject was able to load the device more efficiently and better utilize energy return.

During the IMTP, the subject achieved his maximum peak vertical force while wearing the stiffest foot, the Versa Foot 2, and produced the least amount of force wearing the Flex-Run (Table 1). This suggests utilizing a stiffer prosthetic foot could help one achieve greater force production in maximal strength tasks. However, the subject's peak force asymmetry was higher in the stiffer devices, the Versa Foot 2 and Pro-Flex XC, whereas the Flex-Run proved to be the most symmetrical. This indicates a springier device could again be useful in maintaining lower limb symmetry during a maximal strength task despite not optimizing peak vertical force.

Significance

It is important to take into consideration the trade-off between peak force generation and symmetry when trying to optimize prosthetic feet during high level activity. Ideally, a prosthetic foot should be able to adequately meet the physical demands of a task while also minimizing lower limb asymmetries. However, this study further establishes the benefits and consequences of different stiffness levels depending on the physical demands of a task, which can help drive the decision making process when prescribing prosthetic feet to service members.

Acknowledgments and Disclaimer

Thanks to General Dynamics Information Technology for support. The views expressed herein do not necessarily reflect those of the Department of the Navy, Department of Defense, DHA, or U.S. Government.

References

[1] Shephard, 2019. Northwestern University dissertation.
[2] R. Neptune et al., 2013. *J Biomech* vol. 46.

Device	CMJ Peak Takeoff Force (N)	CMJ Peak Takeoff Force Asymmetry (%)	CMJ Jump Height (in)	IMTP Peak Vertical Force (N)	IMTP Peak Vertical Force Asymmetry (%)
Flex-Run	1442	23.9	7.0	2598	13.1
Pro-Flex XC	1441	29.9	6.8	2736	23.9
Versa Foot 2	1425	33.5	6.2	2810	23.1

Table 1. Descriptive statistics of each prosthetic foot

IDEALIZED ASSISTIVE KNEE BRACE PREDICTIVE MODELING FRAMEWORK

Alexa J. Boyer[1*], Scott C. E. Brandon[1]
[1]School of Engineering, University of Guelph, Canada
email: *aboyer01@uoguelph.ca

Introduction

Knee braces are commonly used to prevent injury, improve function, and alleviate pain. Braces that unload the tibiofemoral joint are often prescribed for individuals with osteoarthritis who can experience pain from the degradation of the articular cartilage in the knee, which is partially caused by excessive loading over time [1]. Many knee brace offloading designs have been implemented with varying effectiveness, including passive valgus moment braces and both passive and motorized knee extension assist (KEA) braces [2]. While experimental prototyping and testing of novel devices is costly and time-consuming, innovation in brace mechanism design might be accelerated via *in silico* simulations of brace effectiveness using musculoskeletal models.

Thus, the objectives of this study were: i) to develop a framework for computer-informed design and evaluation of knee unloading braces, and ii) to validate this approach relative to experimental data from participants using a physical KEA brace.

Methods

This preliminary study reports results from one of eighteen subjects who completed walking trials under three conditions: unbraced, braced "low", and braced "high", where braced conditions used bilateral passive nonlinear spring KEA braces (Levitation® Tri-Compartmental Unloader™, Spring Loaded Technology, Halifax, NS) adjusted to "low" or "high" assistance modes (7.5Nm and 25Nm, respectively, at 140º knee flexion).

Lower limb motion capture was recorded along with ground reaction forces (GRF). Experimental kinematics were computed for each of the three conditions using Inverse Kinematics (IK) with a published 2D sagittal plane gait model (10 DOF, 18 muscles and 4 contact spheres) [3] in OpenSim [4].

The biomechanical effect of the KEA brace was simulated using the OpenSim Moco [3]. First, an unbraced "Tracking" simulation solved for dynamically consistent kinematics, muscle activations and ground reaction forces, while minimizing the weighted sum of error versus unbraced IK results, error versus experimental vertical GRF, and metabolic cost. Half of the gait cycle was simulated, then reflected into a complete gait cycle via symmetry constraints. Second, a "Predictive" simulation used the unbraced tracking simulation as an initial guess, then estimated an optimal walking motion to minimize metabolic cost ("effort"). Third, a virtual KEA brace was added, bilaterally, to the musculoskeletal model as an expression-based knee extension coordinate force as a nonlinear function of knee flexion angle; the nonlinear exponential function was fitted to experimental moment-angle data from "Low" and "High" braces. Finally, the simulated effect of the KEA brace was compared to the experimental IK results.

Results and Discussion

The predictive modelling framework generated a physiologically-plausible walking motion in the unbraced and braced "high" and "low" modes; however, relative to experimental data, the predicted decrease in knee flexion angles is less. Averaged across right and left knees, the difference in peak knee flexion angles between unbraced and braced "high" conditions was 5.13º for predicted states and 9.63º for IK states. The difference between unbraced and braced "low" conditions was 0.59º and 3.71º for predictions and IK results, respectively (Figure 1). Predicted walking motions exhibited both a lack of knee flexion angles during stance and diminished magnitudes during swing.

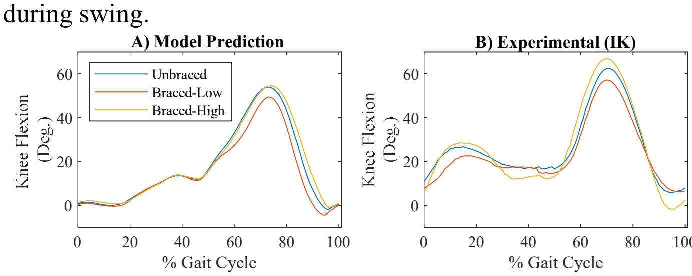

Figure 1: Knee Angles for unbraced (yellow), braced "high" (orange) and braced "low" (blue) conditions. A) Model Prediction. B) Experimental Results (IK).

Recognizing that experimental data are currently from a single subject, agreement between experimental and prediction results should be interpreted cautiously. Nevertheless, it appears that the proposed simulation framework can predict the correct direction, if not magnitude, of kinematic changes due to the addition of an energy storage and return knee brace to a human leg.

The low knee flexion angles predicted throughout the gait cycle, contrary to experimental observations, imply a quadriceps-avoidance gait strategy that may be resulting from excessive penalization of metabolic effort. Future work will expand the sample size and investigate modelling modifications to encourage more realistic knee motion by adjusting the model structure (DOF and number of muscles) or to develop a more physiologically-realistic objective function. Additionally, future work will validate the model predictions across all kinematic states, and against experimental electromyography (EMG) data.

Significance

In silico prototyping of novel assistive devices could lead to innovated designs and enhanced effectiveness. Once validated, the proposed predictive modelling framework could be helpful for examining the effects of knee bracing in either a research and development or clinical setting.

Acknowledgment

Thank you to Spring Loaded Technology for providing the braces for the study at cost and Samuel Salemi for guidance and assistance with data collection.

References

[1] Arazpour M et al. (2013). Prosthet Orthot Int [2] A. R. Budarick, B. E. MacKeil, S. Fitzgerald, and C. D. Cowper-Smith. (2020). J. Biomech. Eng., vol. 142, no. 1, pp. 1–8.
[3]Dembia CL, Bianco NA, Falisse A, Hicks JL, Delp SL. OpenSim Moco. *PLOS Comput. Biol.* 2020;**16**(12):e1008493.
[4]Delp SL, et al. OpenSim. *IEEE Trans. Biomed. Eng.* 2007;**54**(11):1940–1950.

LOADING HISTORY ALTERS COMPRESSION TOLERANCE AND MECHANICAL PROPERTIES IN SPINE TISSUES

Jackie D. Zehr, Jeff M. Barrett, Fasih A. Rahman, Joe Quadrilatero, Jack P. Callaghan
Department of Kinesiology & Health Sciences, University of Waterloo, Waterloo, Ontario, Canada
email: jackie.zehr@uwaterloo.ca

Introduction

The alleged cause of many low back injuries, specifically to the cartilage endplate (CEP), is the performance of lifting tasks described as "high demand" [1]. Despite the internal compression (4.5-6 kN) exceeding that of habitual and recommended (3.4 kN) exposures [2], it is less than estimates of ultimate compression tolerance (UCT) (~10.5 kN) [3]. Fundamentally, overuse injuries are caused by physiological and mechanical changes that occur in response to repeated loading. As such, compression loading history, even if low-moderate demand, may alter tissue properties overtime and thus the ability for spinal joints to withstand abrupt high-demand exposures. The documented effects of posture [4], peak loading variation [5], and loading duration [4] on the joint fatigue lifespan and vertebral joint mechanics motivated the study objective to quantify the effect of these factors on the joint UCT, regional CEP microindentation responses, and the amount of mechanically induced constitutive damage in the CEP.

Methods

108 spinal units were assigned to 18 groups that differed by posture (flexed, neutral), peak compression variation (10%, 20%, 40%), and loading duration (1000, 3000, 5000 cycles). Six additional spinal units were included as a control group. Scaled waveforms represented the *in vivo* L4L5 joint forces during lifting. All waveforms had a loading frequency of 1 Hz, an average peak compression normalized to 30% of the predicted tolerance, and a cumulative load that was equalized after each 5-cycle block. After the conditioning tests, spinal units were transected and the endplates (one from each vertebra) randomly underwent subsequent UCT or microindentation protocols.

Destructive ultimate testing was performed by compressing a single vertebra at a rate of 3 kN/s [3]. A custom machined tissue interfacing steel indenter was fabricated to a representative shape and validated against the intact spinal unit. Force and actuator displacement data were sampled at 100 Hz.

The CEP was dissected from the vertebra and suspended from a custom-built apparatus. Non-destructive uniaxial indentation was performed at five size-normalized surface locations (central, anterior, posterior, right, left) using a Motoman robot (Yaskawa) equipped with a load cell and aluminum indenter (3mm hemisphere). Surface microindentation was performed with custom multi-mode control: i) loaded at 0.1 mm/s until a 10 N load was reached; ii) 10 N load was maintained for 30 seconds; iii) unloaded at 0.1 mm/s [6]. Vertical force and end-effector position were sampled at 10 Hz. From the force-displacement data, the stiffness was quantified from the linear loading region. Immunofluorescence staining of the central CEP region was subsequently performed with primary antibodies against Type I (COL I) and Type II (COL II) collagen. A general linear model (α = 0.05) was used to evaluate group differences in UCT, indentation loading stiffness, and mean fluorescence of each antibody (i.e., collagen content).

Results and Discussion

There was a significant posture × variation × duration interaction effect observed for UCT ($p = 0.043$). Pairwise comparisons of group means are demonstrated in Figure 1.

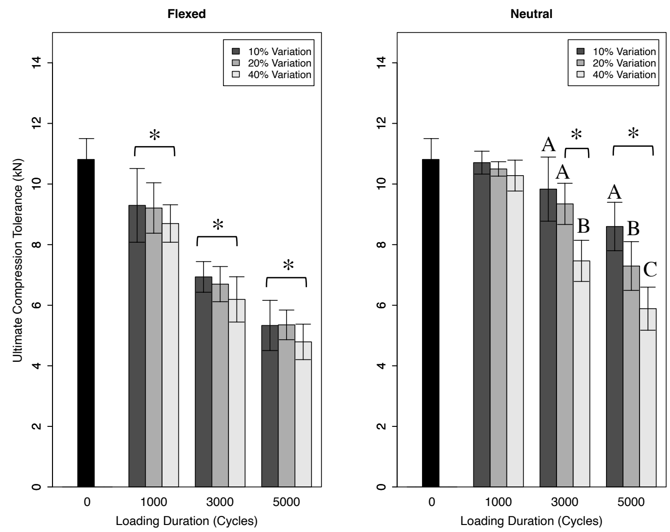

Figure 1: Significant differences from 0 are indicated by *. Within a duration, bars marked with different letters achieved significance.

Loading stiffness in the central region mimicked the UCT response ($p = 0.019$). This finding was supported by significant reductions in COL II (CEP) and COL I (subchondral bone) as a function of posture and duration. In the posterior and lateral regions, the stiffness was, on average, 13% less when flexed compared to neutral after 5000 cycles ($p < 0.007$). Additional duration × variation interactions were observed in the lateral regions ($p < 0.011$). Compared to 10% variation, 7% and 10% reductions in stiffness were found after 5000 cycles for 20% and 40% variation groups, respectively.

Significance

Using an accelerated injury model, the effect of low back posture on the potential for load management strategies to influence injury risk was highlighted. That is, control of peak compression exposures (via variation in this study) became particularly relevant only when a neutral posture was maintained during an average low-moderate risk exposure [2]. Mechanical changes to the joint UCT and central CEP stiffness are attributed to the development of microstructural constitutive damage, which was evidenced by the reduction in COL I and COL II content. Ongoing research will investigate the radial propagation of histochemical and microstructural damage across the endplate surface. These findings also motivate applied biomechanics research that aims to establish the emergence and persistence of key movement features during lifting performed in occupational and/or training contexts.

Acknowledgments

The authors acknowledge funding received from NSERC.

References

[1] Videman et al., 1990. *Spine*. 15: 728-740.
[2] NIOSH. 1981. Technical Report No 81-122.
[3] Gunning et al., 2001. *Clin Biomech*. 16: 471-480.
[4] Gooyers & Callaghan. 2015. *JBiomech*. 48: 3701-3708.
[5] Zehr et al., 2019. *JBiomech*. 88: 48-54.
[6] Patel et al., 2018. J Biomech Eng. 140: 111-119.

SEDENTARY PROFILE IS A POTENTIAL PREDICTOR OF TRANSIENT LOW BACK PAIN

Graham Mayberry[1*], Jack P. Callaghan[1] and Janessa D.M. Drake[2]
[1]University of Waterloo, Waterloo, ON, Canada
[2]York University, Toronto, ON, Canada
email: * graham.mayberry@uwaterloo.ca

Introduction

Low back pain (LBP) continues to malign society by affecting between 70-85% of the adults at some point in their lives.[1] The economic and social impacts of LBP are likely to increase given the rise in sedentary lifestyles and the reported link between the two.[2,3] Predicting whom will suffer from LBP is difficult given that between 40-65% of individuals develop it doing common, functional tasks despite no history of LBP.[4,5] Identifying this cohort of the population is difficult however the emergence of screening tools like the Active Hip Abduction (AHAbd) Test provide hope.[6] This test has greatly improved the odds of correctly identifying these LBP sufferers yet its uptake has not been as widespread as expected, perhaps due to the impediment of rater training. Capturing activity data may provide insight into this segment of the population and may provide an alternative methodological identification approach. The purpose of this study was to determine whether alternative measures could be useful in characterizing AHAbd score groups and therefore help predict who might be a transient LBP sufferer.

Methods

One hundred participants from a university population (mean age = 21.4yrs) were recruited for this study. Anthropometric information was taken in addition to measuring their lumbar and thoracic spine range of motion. Pelvic control was classified using the AHAbd Test (see Figure 1 for scoring criteria used). Participants in this study were also requested to wear an activity monitor for one week in order to gather their MVPA (moderate to vigorous physical activity) and sedentary information. AHAbd tests were videotaped and scored by 4 trained undergraduate students who had achieved a high degree of consistency (ICC = 0.725, CI = 0.55,0.832).

Score	Cues for Examiner
0, Able to maintain position of pelvis in the frontal plane	Smoothly and easily performs movement; lower extremities, pelvis, trunk, and shoulders remain aligned in frontal plane.
1, Minimal loss of pelvis position in the frontal plane	Slight wobble at initiation or throughout movement; may show noticeable effort or "ratcheting" of moving limb.
2, Moderate loss of pelvis position in the frontal plane	Has at least 2 of the following: noticeable wobble through movement; tipping of pelvis, trunk, or shoulder rotation; increased hip flexion and/or rotation of the moving limb; rapid or uncontrolled movement.
3, Severe loss of pelvis position in the frontal plane	Has more than 3 of the above characteristics and/or unable to regain control of movement once lost or may lose balance (has to place hand on table)

Figure 1: Scoring Criteria Examiners used for the Active Hip Abduction (AHAbd) Test as Provided by Raters.[6]

Results and Discussion

Two distinct populations were identified using the AHAbd scores by grouping individuals above and below one standard deviation (0.468) from the mean (1.161): < 0.693 (Low) and > 1.629 (High). The mean and SD of the Low (n=18) and High (n=11) AHAbd score groups were 0.529±0.099 and 1.909±0.159. Percent sedentary (% wear time), MVPA (min/day), and Lumbar ROM (degrees) of the two groups is illustrated in Figure 2. Percent Sedentary time was significantly different (p = 0.028) between the two groups.

No significant difference (p = 0.307) was found between the two groups in terms MVPA per day, as the Low group engaged in 34.2 minutes per day while the High group was at least moderately active for 26.2 minutes per day. Activity level may not be significantly different between groups, however with a larger sample size the current trend may be borne out. It was surprising not to see MVPA exhibit the same effect as sedentary time on AHAbd scores, given that previous research has linked LBP reporting with a sedentary lifestyle.[2,3] Our Lumbar ROM is consistent with magnitudes reported in the literature and there does not appear to be a consistent relationship between ROM and LBP developers and non-developers. As such, it was not expected that a significant difference between AHAbd score groups would exist.

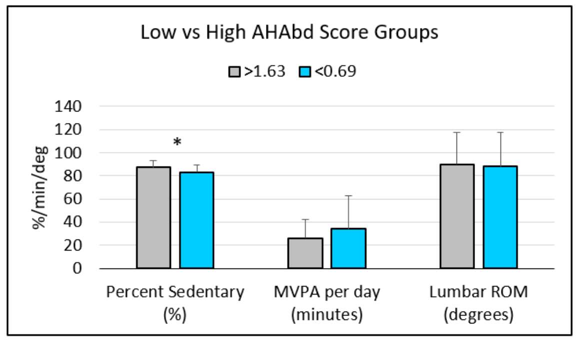

Figure 2: The Percent Sedentary time (% of time worn as measured by the activity monitor), MVPA per day (average minutes of moderate to vigorous minutes of physical activity per day as measured by the activity monitor), and Lumbar Range of Motion (measured in lab) of the Low (< 0.69) and High (>1.63) AHAbd groups were compared. The * denotes significance below p <0.05. Figures or tables may be included.

Significance

This study provides evidence for a potential alternate and less invasive screening tool to identify LBP developers, in much the same way as the AHAbd test currently is used for predicting whether an individual may be a low back pain developer. From a research perspective, this is particularly relevant to labs researching low back pain or clinicians who screen for transient LBP sufferers. Screening for LBP developers often necessitates all participants coming into the lab for a bout of prolonged standing – which can be a deterrent in participation. Activity monitors offer the potential to improve the screening process for LBP sufferers during occupation standing in much the same way that the AHAbd test currently does.

References

[1] Giesecke et al., 2004. *Arthritis Rheum.* 50: 613-23.
[2] Gardiner, et al. 2011. *JAGS.* 59: 788-96.
[3] Nourbakhsh et al., 2001. *J Spinal Discord*. 14:283-92.
[4] Nelson-Wong & Callaghan. 2009. *J Electromyogr Kinesiol.*
[5] Nelson-Wong et al. 2008. *Clin Biomech*. 23: 545-53.
[6] Nelson-Wong et al. 2009. *J Ortho Sports.* 39(9): 649-5

THE IMPACT OF COMBINED FLEXION AND COMPRESSION ON THE MECHANICAL INTEGRITY OF THE ANNULUS FIBROSUS

K. Josh Briar [1]*, Diane E. Gregory [1,2,]
[1] Department of Kinesiology and Physical Education, [2] Department of Health Sciences, Wilfrid Laurier University, Waterloo, Ontario, Canada
*Email: Bria6330@mylaurier.ca

Introduction

Intervertebral disc (IVD) herniation is characterized by an expulsion of nucleus pulposus (NP) material through the annulus fibrosus (AF). The AF contains two major adhesive structures, the intralamellar matrix and the interlamellar matrix, which act to maintain the strength of the AF and prevent NP material migration. As a herniation occurs, clefts form within the intralamellar matrix, pushing the NP between adjacent collagen fibres; meanwhile delamination of the interlamellar matrix causes the NP to pool between layers of the AF [1]. Further, herniation more readily occurs in a combined loading scenario of both compression and flexion [2]. Flexion, and in particular end range flexion, induces tissue creep, where the elongation of fibres within the AF reduces its capacity for tensile resistance, thereby providing a potential mechanism for why flexion is needed to induce herniation [1,3]. While previous research has examined the effect of combined flexion and compression on the mechanical properties of the AF, the isolated effect of flexion has not been ascertained [2]. The purpose of the current work was to observe the effect of static flexion, in combination with compression, on the intralamellar and interlamellar adhesive properties of the AF.

Methods

For this study, the C3/C4 cervical functional spinal units (FSU) of porcine specimens were selected due to their anatomical and biomechanical similarity to human spines [4]. Following 300N of preloading for 15 minutes, all specimens were loaded under 1200N axial compression and one of the following posture conditions: neutral or static end range flexion for 2-hours.

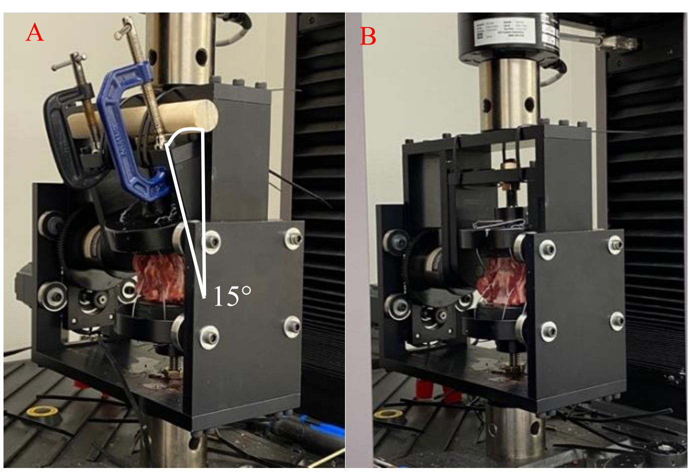

Figure 1: (A) a specimen mounted into the 15º flexed posture condition in the uniaxial material testing system. (B) a specimen mounted into the neutral posture condition in the uniaxial material testing system.

Following loading, six AF samples were dissected from each IVD: four single-layer samples and two multilayer samples. The multi-layer samples underwent peel tests to quantify the mechanical properties of the interlamellar matrix while the single layer samples underwent tensile tests to quantify the mechanical properties of the intralamellar matrix. Statistical comparisons between mechanical properties were performed to determine if there was a difference between extraction location (anterior vs posterior), extraction depth (inner vs outer AF) and postural condition.

Results and Discussion

Flexion was found to impact both matrices of the AF. Specifically, flexion elicited a significant decrease in lamellar adhesive strength ($p=0.045$) and a decrease in single layer failure strain ($p=0.03$) when compared to a neutral posture. Flexion further had extraction depth-specific effects namely increased intralamellar matrix stiffness in the inner AF following flexion when compared to neutral ($p=0019$). Flexion also resulted in a significant decrease in toe region strain for the inner region of the AF ($p=0.035$). The inner region of the AF was also shown to have a significant increase in stress at 30% strain when compared to the outer region of the AF when undergoing flexion ($p=0.041$). The current findings suggest that the mechanical properties of the interlamellar and intralamellar matrices are sensitive to flexion, creating an environment that promotes an increased potential for damage to occur.

Significance

The results of the current work provide evidence to support the link between flexion and risk of herniation. As a herniation originates from the inner portions of the AF and progresses outwards; a weaker inner region intralamellar matrix following flexion could result in an environment within the AF that supports easier clef formation and accelerated IVD herniation progression. Future work should focus on expanding the current findings and tracking the progression of sub-failure mechanics and their influence on failure mechanics.

Acknowledgments

Funding for this study was provided by the Natural Sciences and Engineering Research Council of Canada

References

[1] Gregory et al., 2011, *Spine (Phila Pa 1976),* 36(4):225-31

[2] Callaghan et al., 2001, *Clin Biomech*, 16(1):28-37

[3] Calvo-Echenique et al., 2018, *Med Biol Eng Comput,* 56(5):865-77

[4] Oxland et al., 1991. *J Orthop Res.* 9(3):4

MEASURING SARCOMERE DYNAMICS FOLLOWING IMMUNOFLUORESCENT LABELLING OF α-ACTININ AND MYOMESIN STRUCTURAL PROTEINS

Armaan S. Sekhon[1*] and Walter Herzog[1]
[1]Human Performance Laboratory, Faculty of Kinesiology, University of Calgary, 2500 University Drive NW, Calgary, Alberta, Canada, T2N 1N4
*email: armaan.sekhon@ucalgary.ca

Introduction

Myofibrils are the organelles responsible for contraction in muscles. Myofibril filaments contain sarcomere subdivisions repeating in series. Mechanical and kinetic characterization of these molecular structures rationalize many macroscopic muscle properties and contractile mechanisms.

Measurement of sarcomere dynamics is conventionally accomplished through bright field and phase contrast light microscopy, reaching accuracies marginally below the resolution limit of light microscopy by semiautomatic analysis of sarcomere striation patterns (A-band, I-band) at approximately 50 nm. However, during experiments bands become distorted, striations become asymmetric, and pattern intensities fluctuate [1]. To compensate, sarcomere striations have been further delineated by placing immunofluorescent markers on structural proteins like α-actinin for localization of Z-line boundaries and myomesin for localization of M-line boundaries [2]. How the introduction of these molecular markers might compromise sarcomere dynamics has not been well established. Replicate experiments with comparable protocols, tissues, or antibodies have produced contradictory results. Sarcomeres can behave identically to unlabeled controls or have constrained dynamics [2, 3].

Thus, in this research we investigated the dynamics of sarcomeres following immunofluorescent labelling of α-actinin and myomesin structural proteins. We hypothesized that, as markers would not interact directly with proteins involved in contraction, sarcomere properties including length, passive stretch force, active force and rate constants of calcium-induced force development or decline would be comparable to controls.

Methods

New Zealand White rabbits were euthanized by an intravenous injection of sodium pentobarbital. Psoas muscle tissue was dissected and stored in rigor-glycerol solution. For experiments, tissue was purified of connective tissue and fractionated to isolate myofibril threads. Samples were incubated in rigor solution with monoclonal IgG1 anti-α-actinin (A7811, Sigma-Aldrich) and monoclonal IgG1 anti-myomesin (mMaC myomesin B4, Developmental Studies Hybridoma Bank). Subsequently, they were incubated with polyclonal IgG (H+L) AlexaFluor488 antibodies (A32723, Fisher Scientific). Incubations were moved onto a chamber mounted on an Olympus IX83 microscope (Olympus). Samples were flushed with relaxing solution before image capturing and analysis on CellSens software (Olympus).

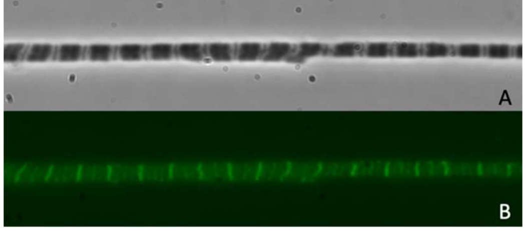

Figure 1: Labelled myofibril observed under phase contrast (A) and FITC-filtered fluorescent microscopy (B) on an Olympus IX83 microscope under 200x magnification. Optical resolution is 32 nm/pixel.

Results and Discussion

	SARS	MEAN LENGTH (μm)	SD	REPLICATE MEASUREMENT SD
CONTROL	47	2.40	0.16	0.05
LABEL	115	2.23	0.29	0.03

Table 1: Sarcomere (SARS) length analysis as means and standard deviations between unlabelled control myofibrils (CONTROL) and fluorescently labelled myofibrils (LABEL) observed under phase contrast or FITC-filtered microscopy on an Olympus IX83 microscope.

Sarcomere lengths (SLs) in controlled and labelled myofibril samples remained consistent with literature. SLs in labelled myofibrils were 0.17 μm below control myofibrils, indicating introduction of antibodies may have stiffened Z-line and M-line lattice structures, compromising ability of adjacent sarcomeres to interact fluidly, and inducing subtle contraction. This behaviour contrasts with some published research [2] but was not as significant as observed by other researchers [3], indicating a potential concentration-dependent and antibody-identity-dependent modularity of this phenomenon.

Labelled myofibrils had SLs ranging from 1.83 μm to 3.04 μm. The standard deviation increased from 0.16 to 0.29 following the labelling protocol, demonstrating antibody markers interacted with myofibrils to induce compression with inconsistency.

Labelled myofibrils demonstrated resolution and precision advantages over controls as the standard deviation of replicate SL measurements was 0.03 compared to 0.05. Obscurity related to striation asymmetricity, pattern intensity, or band distortion were noticeably mitigated because of experimental protocols.

Significance

Whether increasing throughput or tracking asymmetric (half-) sarcomere displacements with higher precision, enhanced signal-to-noise ratio in fluorescently labelled myofibril samples benefits traditional investigations into sarcomere mechanics. Quantifying, regulating, and mitigating the influence of antibodies during this process ensures the consistency of results obtained with in vivo systems. Controlled marker-induced interference with sarcomere proteins, both structural as α-actinin and myomesin or functional as titin, will allow researchers to systematically study the mechanistic roles of these proteins in sarcomere mechanics. Towards that objective, more invasive variables including SLs during myofibril contraction are being collected and used to inform our understanding of how factors including phototoxicity, immunological compatibility, or incubation conditions influence the functional integrity of myofibrils following labelling.

Acknowledgments

NSERC of Canada.

References

[1] Schmidt et al., 2021. *Journal of Biomechanics.* 126: 110628.
[2] Telley et al., 2006. *Biophysical Journal.* 90 (2): 514-530.
[3] Shimamoto et al., 2008. *PNAS.* 106 (29): 11954-11959.

THE EFFECTS OF A DYNAMIC CORE STABILITY GROUP EXERCISE INTERVENTION ON TRUNK MUSCLE ACTIVITY, STRENGTH, AND ENDURANCE IN PEOPLE WITH AND WITHOUT A HISTORY OF LOW BACK PAIN: A RANDOMIZED CONTROLLED TRIAL

Gillian L. Hatfield[1]
[1]School of Kinesiology, University of the Fraser Valley, Chilliwack, BC, Canada
email: gillian.hatfield@ufv.ca

Introduction

Low back pain (LBP) is a common problem, with many going on to have recurrent episodes. Contributing to the recurrence could be alterations in trunk muscle activity. Individuals in the sub-acute phase of healing show higher muscle activation amplitudes [1,2] and higher abdominal and back extensor co-activity [1] compared to participants with no history of LBP.

A recent network meta-analysis found all forms of exercise are effective for improving pain and function in people with LBP, relative to no/minimal treatment interventions, but some exercise interventions are more effective than others, including core exercises [3]. While core exercises are commonly used in LBP rehabilitation, no studies have looked at the effect of these exercises on altered trunk muscle activity observed in those with a history of LBP.

This study determined if an 8-week group exercise intervention focusing on dynamic core stability would alter trunk muscle activity, strength, and endurance in people with a history of LBP, and whether the effects would differ from those in people without a history of LBP. It was hypothesized that in both groups, trunk muscle activity would decrease (as strength and endurance increased), co-activation of abdominals and back extensors would decrease, and that decreases would be larger in participants with a history of LBP.

Methods

17 participants with a history of LBP (LBPEx) and 19 participants with no history of LBP (NoLBP) completed an 8-week group exercise intervention focusing on dynamic core stability. 19 participants with a history of LBP were randomized to a control group (LBPCon) who did not do the exercise intervention.

The exercise intervention was Core™, created by Les Mills International (Auckland, NZ). The 30-minute classes consisted of exercises using body weight, resistance bands, and free weights to challenge coordination, balance, and strength. Participants completed two classes per week, on non-consecutive days.

Pre-and post-intervention data collection included measurement of bilateral abdominal (upper and lower rectus abdominus, anterior, lateral, and posterior external obliques) and back extensor (erector spinae and multifidus) surface electromyograms (EMG) during a trunk stability task designed to assess lumbar-pelvic stability. This task required participants to use an abdominal hollowing maneuver and maintain the lumbar spine in the neutral position while leg movements were performed in the sagittal plane [2]. After the trunk stability task, ten maximum voluntary isometric contraction (MVIC) exercises were performed to elicit maximum activity from each muscle for amplitude-normalization of the EMG. Abdominal and back extensor strength and endurance were also measured.

EMG data were analyzed using Principal Component Analysis (PCA) to extract the main patterns in the data corresponding to overall amplitude (PC1) and co-activation (PC2) [2]. Two-factor (group, time) analysis of variance (ANOVA) models were run, with repeated measures on time. For PC scores, an ANOVA was run for each muscle. Significance was $\propto = 0.05$. Main effects and interactions were explored using pairwise comparisons with a Bonferonni correction.

Results and Discussion

Consistent with the hypothesis, abdominal muscle activity (PC1) decreased in most muscles for both groups that completed the intervention, reaching significance for upper rectus abdominus, lateral and posterior external obliques for the NoLBP group and lower rectus abdominus and all external obliques for the LBPEx group. Decreases in activity are consistent with significant increases in abdominal muscle strength and endurance in both groups; the muscles would not have to activate to as high a percentage of maximum in order to generate the force required to complete the trunk stability task. While there were no significant time by group interactions, effect sizes were generally larger for the NoLBP group, indicating more of a decrease in this group, which is inconsistent with the hypothesis. Likewise, changes in strength and endurance had larger effect sizes in the NoLBP group. This is likely because participants without a history of LBP were able to push themselves more in the exercise classes.

Decreases in co-activation (PC2) were seen in all abdominal muscles for the NoLBP group, but not the LBPEx group. This indicates that the LBPEx group still relied on co-activation of the abdominals in order to complete the task, and were unable to adjust their muscle activation to the task demands.

No changes in back extensor overall activation (PC1) and co-activation (PC2) were seen for either group, and there were no changes in trunk muscle activity, strength, or endurance in the LBPCon group.

Significance

The intervention resulted in increased abdominal and back extensor strength and endurance in people with and without a history of LBP. There were decreases in abdominal muscle activity during tasks designed to challenge trunk stability for all participants who completed the intervention, and decreases in abdominal muscle co-activation for people without a history of LBP. This intervention, CORE™ by Les Mills International, is readily available online, and in gyms and fitness studios internationally, and may be recommended as a safe, accessible, and effective intervention to increase trunk strength and endurance, even for people with a history of LBP.

Acknowledgments

Les Mills International for funding.

References

[1] Butler et al., 2013. *J Electromyogr Kinesiol*. 23:369-77. [2] Moreside et al., 2014. *Arch Phys Med Rehabil*. 95:686-98. [3] Hayden et al., 2021. *J Physiother*. 67(4):252-62.

USING MUSCLE FATIGUE AND MOVEMENT TRAINING TO EXPLORE THE RELATIONSHIP BETWEEN DYNAMIC STABILITY AND COORDINATION VARIABILITY OF THE LUMBAR SPINE

Dennis J. Larson* and Stephen H.M. Brown
Department of Human Health and Nutritional Sciences, University of Guelph, Guelph, Ontario, Canada
email: larsond@uoguelph.ca

Introduction

Traditionally, increased movement variability has been associated with decreased stability, while more stable movements are viewed as less variable [1]; however, these views are based on the concept of 'end-point variability' (e.g., range of motion standard deviation) and not 'coordination variability' (e.g., segment interaction variability) [2]. Although it may be counterintuitive at first, previous work has suggested that less variable coordination patterns between segments is associated with decreased dynamic stability, specifically when experiencing lumbar muscle fatigue [3]. While this relationship has been suggested previously, to the authors' knowledge, this relationship has yet to be examined for the lumbar spine during repetitive flexion-extension movements and lifting.

Therefore, we examined this relationship between dynamic stability and coordination variability using muscle fatigue and movement training to manipulate movement coordination. We hypothesized that movements with more dynamic stability (lower λ_{max}) would be associated with greater coordination variability, while movements with less dynamic stability (higher λ_{max}) would be associated with lower coordination variability.

Methods

In study 1, 30 participants repetitively touched two targets, one at shoulder height and one at knee height, with their hands together, arms fully extended, and hips constrained with a belt [4]. Participants performed these repetitive trunk flexion-extension movements before and after the induction of back muscle fatigue. In study 2, 28 participants repetitively lifted a box between shelves at shoulder and knee height before, immediately after, and 1-week after learning a spine sparing lifting technique using an augmented feedback training paradigm with a tactile cue [5]. 14 randomly selected participants performed this training paradigm with their back muscles fatigued.

For each trial, flexion-extension lumbar spine data from 30 continuous movement repetitions were analyzed to determine local dynamic stability and coordination variability of the lumbar spine. Local dynamic stability was determined using maximum finite-cycle Lyapunov exponents (λ_{max}) [4], while coordination variability was quantified using a vector coding analysis technique and is representative of the mean cycle-to-cycle variation of coupling angles between T_{12} and S_1 segments [6].

Results and Discussion

Overall, our results support our hypotheses across both studies. In study 1, when experiencing muscle fatigue, ~30% of individuals displayed more stable (lower λ_{max}) flexion-extension movements with greater coordination variability, ~17% became less stable (higher λ_{max}) with lower coordination variability, and ~53% expressed no change in both outcome measures (Figure 1A). In study 2, both fatigued and control groups demonstrated more stable (lower λ_{max}) spine movements both immediately and 1-week after learning a spine sparing lifting technique, which coincided with observed increases in coordination variability (Figure 1B).

Previous work has suggested that as coordination variability decreases, the available movement pattern repertoire is also reduced, resulting in decreased system flexibility [2]. As such, the system may be unable to quickly respond to local perturbations (i.e., neuromuscular control errors), and greater divergence away from the target movement trajectory, or decreased dynamic stability (higher λ_{max}). In contrast, greater coordination variability may increase the available movement repertoire, resulting in more dynamically stable movements.

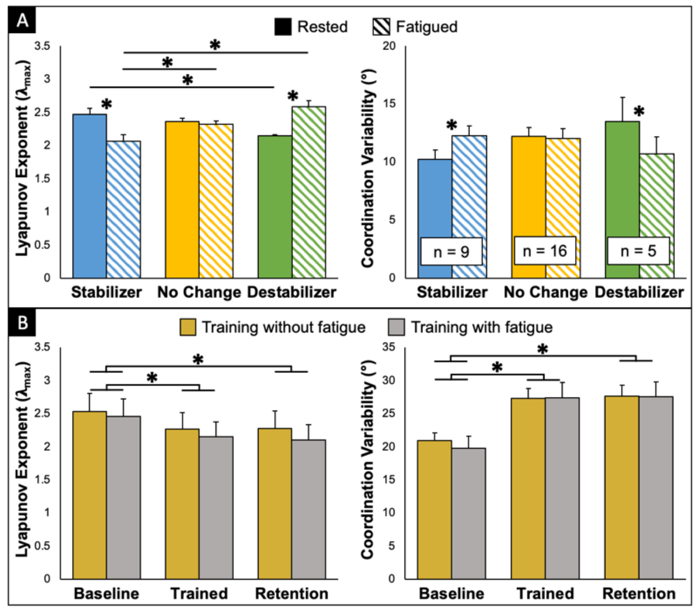

Figure 1: Lumbar spine maximum Lyapunov exponents (λ_{max}) and coordination variability (degrees °), (A) during repetitive flexion-extension movements before (Rested) and after (Fatigued) back muscle fatigue and (B) during repetitive lifting before (Baseline), immediately after (Trained), and 1-week after (Retention) training of a spine sparing lifting technique with and without back muscle fatigue.

Significance

Reductions in coordination variability have been previously associated with injury, frailty, or pathology [2]. Using the current results, future work can exploit the relationship between decreased variability and dynamic stability to determine if they are a cause, or result of, low back pain or injury.

Acknowledgments

This combined work was funded by the Natural Sciences and Engineering Council of Canada (NSERC).

References

[1] Stergiou & Decker, 2011. *Hum Mov Sci*. 30(5): 869-888.
[2] Hamill et al., 2012. *Sports Med Arthrosc Rehabil Ther Technol*. 4: 45.
[3] Hu & Ning, 2015. *Ergonomics*. 58, 1424-1432.
[4] Granata & England, 2006. *Spine*. 3: E271-E276.
[5] Chan et al., 2022. *Appl Ergon*. 99: 103612.
[6] Needham et al., 2014. *J Biomech*. 47: 1020-1026.

A MORPHABLE LUMBAR SPINE MODEL CONTROLLED BY ANATOMICAL MEASUREMENTS

Allison L. Clouthier[1*], Jessica Wenghofer[1], Eugene Wai[2], Ryan B. Graham[1]
[1]School of Human Kinetics, Faculty of Health Sciences, University of Ottawa, Ottawa, ON
[2] Division of Orthopaedic Surgery, The Ottawa Hospital, Ottawa, ON

*email: allison.clouthier@uottawa.ca

Introduction

Geometry of the lumbar spine has been found to be associated with function and pathology [1]; however, causal relationships can be difficult to establish. While computational simulation can be used to investigate the effect of geometry on function, a method to modify geometry in a coherent and realistic way is needed. Statistical shape models generated using partial least squares (PLS) regression provide a means to quantify sources of geometric variability associated with a selected parameter, such as an anatomical measurement. The aims of this work were 1) to generate morphable models of the lumbar spine that are controlled by anatomical measurements, and 2) determine the accuracy of generating the desired anatomical measurement using the morphable models.

Methods

CT images of the lumbar spine were obtained for 87 patients at The Ottawa Hospital (44 female, age 61±15 years). Images were manually segmented to produce 3D meshes of bone geometry and correspondence was established among the meshes using Coherent Point Drift [2]. A variety of anatomical measurements were automated based on fitting planes to surfaces, including facet joint angles, vertebral body dimensions, vertebral body wedge angle, spinal canal dimensions, disc height, disc wedge angle, and vertebral body slip (spondylolisthesis). Partial least squares (PLS) regression was used to generate statistical shape models capturing variation associated with each anatomical measure. The number of latent variables that explained 90% of the variation in the anatomical measure were retained. This enabled the generation of a lumbar spine model with a specified anatomical measurement. The root mean square error (RMSE) between desired measurements and the measurement for the geometry generated by the morphable model was calculated across 50 points spanning the range of values observed in the dataset for various measures.

Results and Discussion

PLS regression extracted shape features capturing the greatest sources of variability and a vector that can be used to morph the model through this feature space according to the chosen anatomical measurement (Figure 1). This procedure can be used to generate geometry with a specified anatomical measurement with a high degree of accuracy (RMSE <0.8° and <0.2 mm; Table 1). The overall geometry of the resulting model is consistent with the selected measurement based on the patients included in the dataset. For example, increasing the vertebral body wedge angle increases lordosis (Figure 1).

Significance

The ability to coherently manipulate specific anatomical measurements on 3D models could enable further computational simulation studies into the effects of anatomy on lumbar spine function and on the cause and treatment of pathology. This method could also be used in biomedical device design or the generation of patient specific models based on more easily obtained measurements.

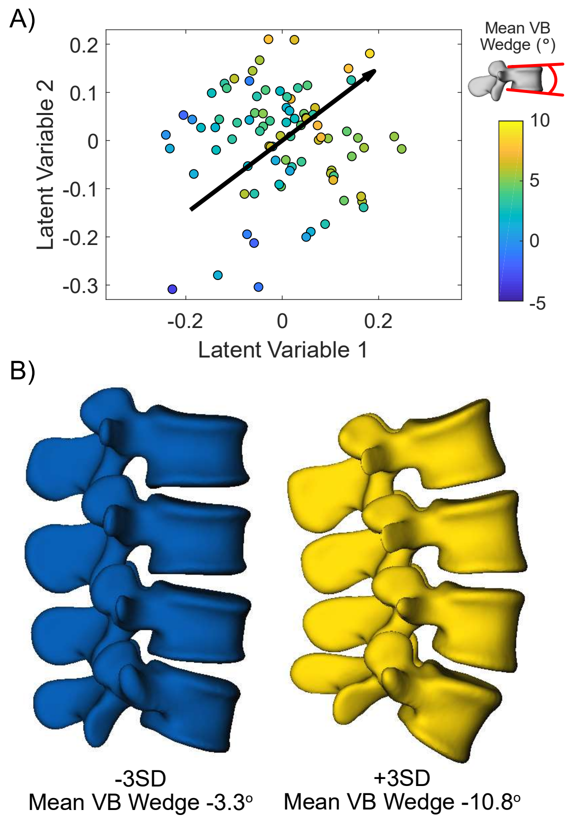

Figure 1: A morphable model controlled by the mean sagittal plane vertebral body (VB) wedge angle across L2-L5. A) Scatterplot of scores for the first two latent variables resulting from PLS regression. The vector used to morph the model through the space is shown. B) The models generated at the endpoints of the vector in A).

Table 1: Root mean square error (RMSE) between the desired and resulting anatomical measure when generating models across the range observed in the dataset used to generate the statistical shape model.

Measure	Range	RMSE
Mean disc height (mm)	3.1 – 11.4	0.03
Mean VB height (mm)	23.5 – 32.4	0.07
Mean VB wedge angle (°)	-3.5 – 8.7	0.08
Mean axial facet angle (°)	27.6 – 85.8	0.75
Mean canal depth (mm)	13.0 – 20.4	0.12
L4/L5 VB slip (%)	0.2 – 27.8	1.2

Acknowledgments

This work was supported by NSERC.

References

[1] Deane et al., 2020. *BMC Musculoskelet Disord.* 21: 433.
[2] Myronenko et al., 2010. *IEEE PAMI.* 32(12): 2262-75

THE INFLUENCE OF KNEE POSITION ON ULTRASOUND IMAGING OF FEMORAL CARTILAGE IN INDIVIDUALS WITH ANTERIOR CRUCIATE LIGAMENT RECONSTRUCTION

Harry S. Battersby[1*], Skylar C. Holmes, Eric J. Shumski, Caitlyn E. Heredia, Steven A. Garcia, and Derek N. Pamukoff[1]
[1]Western University, London ON, Canada
email: hbatters@uwo.ca

Introduction

Articular cartilage is important for knee function [1], and can be imaged using ultrasound. However, knee position during imaging may influence cartilage measurements. Knee loading during gait is inconsistent due to variation in joint contact patterns, which may contribute to regional differences in cartilage thickness. Echo-intensity (EI) represents the gray-scale of an ultrasound image, and may provide a surrogate of cartilage composition [2]. The purpose was to compare femoral cartilage thickness and EI when measured at 90° and 140° of knee flexion, and between limbs in a cohort with unilateral ACL reconstruction (ACLR). We hypothesized cartilage would be thicker when measured at 90° than at 140° of knee flexion, and thicker in the uninjured compared to the injured limb. We also hypothesized EI would be greater in the ACLR limb compared with the contralateral limb. We examined the associations between gait biomechanics and cartilage outcomes from both positions. We hypothesized a larger knee flexion angle (KFA) and external moment (KFM) would be associated with thicker cartilage and lower cartilage EI.

Methods

Twenty-seven individuals with primary unilateral ACLR participated (12 males, 15 females; Age = 22.3 ± 3.8 years; BMI = 25.8 ± 6 kg/m^2; Time since ACLR = 71.2 ± 47.2 months). While supine, participants were positioned at 90° and 140° of knee flexion following a 45-minute non-weightbearing period. Ultrasound was used to obtain femoral cartilage thickness and EI. The superior and inferior borders of the femoral cartilage were manually segmented. The Euclidian distance between 300 evenly spaced data points on the superior and inferior borders was used to measure thickness, and the average thickness from data points 1-100, 101-200, and 201-300 represented thickness of the medial, central, and lateral regions of the femur. Echo-intensity was assessed via tracing the cartilage cross-sectional area from the same portions of cartilage. Each pixel in the traced image received a value based on brightness on a scale of 0 (darkest) to 255 (brightest), with the average representing EI.

Gait biomechanics were assesed over 5 gait trials along a 10m walkway. Marker trajectories were sampled at 240 Hz and force plate measurements were sampled at 2400hz. Gait outcomes included the peak KFA and peak external KFM. Cartilage outcomes were compared between imaging positions and limbs using 2(position) by 2(limb) repeated measures ANOVA. Gait and cartilage association outcomes were assessed using Pearson and Spearmon correlations.

Results and Discussion

There were no position by limb interactions for any cartilage outcome (all $p>0.05$). There was a main effect of position on medial cartilage thickness ($p=0.038$), central cartilage thickness ($p<0.001$), central EI ($p=0.029$) and lateral EI ($p=0.003$). Medial and central cartilage were thicker when measured at 90°compared at 140° whilst central and lateral EI were lower at 90° compared to 140° (Table 1). There was significant main effect of limb for medial cartilage thickness where cartilage was thicker on the ACLR compared with contralateral limb ($p=0.016$). A larger KFM was associated with thicker medial cartilage ($r=0.413$, $p=0.030$) and central cartilage ($r=0.386$, $p=0.047$) measured at 140° of knee flexion. No additional associations were found between gait and other cartilage outcomes (all $p>0.05$).

Significance

Medial and central cartilage thickness were greater when measured at 90° than 140° of knee flexion. Ultrasound imaging of the knee joint at 90° of knee flexion may provide a view of femoral cartilage that is loaded to a different extent during gait than when viewed in 140°of knee flexion. Alternatively, 90° and 140°of knee flexion may provide unique vantage points of the femoral articulation with the patella, respectively. Greater EI within cartilage measured at 140° may indicate that portions of femur also vary in cartilage composition.

Medial cartilage was thicker in the ACLR compared with contralateral limb. These findings disagreed with our hypothesis but may be due to the sample having, on average, overweight BMI, which also contributes to cartilage damage. Early-stage knee osteoarthritis may involve an increase cartilage thickness due to inflammation or swelling [3]. A higher knee flexion moment was associated with thicker medial and central cartilage when measured at 140° but not at 90° of knee flexion. As such, imaging at 90° of knee flexion may expose regions of cartilage that are affected by other gait factors (e.g. second KFM peak) [4].

Acknowledgments

This study was supported by the California State University Program for Education and Research in Biotechnology New Investigator Grant (PI: Pamukoff).

References

1. Hunter, *Best Pract Res Clin Rheumatol*, 28(1), 61–71.
2. Freedman, *Knee*, 22(5), 405–410.
3. Frobell, *Osteoarthritis Cartilage*, 17(2), 161–167.
4. Schmitz, *J Athl Train*, 52(6), 560–566.

	Contralateral Limb		ACLR Limb	
	90°	140°	90°	140°
Medial Thickness (mm) [a,b]	2.15 ± 0.43	1.92 ± 0.32	2.01 ± 3.8	2.00 ± 0.4
Central Thickness (mm) [a]	2.99 ± 0.64	2.22 ± 0.45	2.93 ± 0.69	2.22 ± 0.4
Lateral thickness (mm)	2.10 ± 0.43	1.96 ± 0.31	2.05 ± 0.36	1.98 ± 0.3
Medial EI (0-255)	20.98 ± 20.22	32.72 ± 20.49	24.52 ± 18	23.61 ± 18.54
Central EI (0-255) [a]	45.63 ± 12.16	47.67 ± 12.93	43.9 ± 10.92	50.27 ± 12.7
Lateral EI (0-255) [a]	35.04 ± 23.18	39.36 ± 25.32	30.04 ± 20.01	41.84 ± 23.23

Table 1: Comparison of cartilage and EI characteristics (Mean ± SD; [a] indicates main effect of position, [b] indicates main effect of limb

DOMINANT VS. NONDOMINANT KNEE JOINT LOADS DURING LOAD CARRIAGE

Blake W. Jones[1*], Paul DeVita[1], John. D. Willson[2], and Ryan D. Wedge[2]
[1]Department of Kinesiology, East Carolina University, Greenville, NC, USA
[2] Department of Physical Therapy, East Carolina University, Greenville, NC, USA

email: *Jonesbl20@students.ecu.edu

Introduction

Load carriage induces an increase in peak total (TFJF), medial (MTFJF), and lateral (LTFJF) tibiofemoral joint contact forces[1]. Since muscle forces, especially the quadriceps, are the dominant source of joint loads[1] and since dominant limbs exhibits greater extensor strength than the nondominant limb[2], we hypothesized that knee joint loads will increase with load carriage, but increase to greater extent in the dominant limb (D) as compared to the non-dominant limb (ND). The purpose of this study was to investigate differences between D and ND total, medial and lateral tibiofemoral joint contact forces with and without load carriage.

Methods

Twenty-four young healthy adults, (12 females, 22 yrs.; BMI < 25; 3 left leg dominant determined via self-report), with no history of major lower extremity injuries, walked at 1.4 m·s^{-1} on an instrumented split belt treadmill while carrying vest-borne loads of 0%, 15%, and 30% body weight for 5 minutes per condition. 10 seconds of 3D motion capture and ground reaction force data were recorded in each condition for inverse dynamics calculations. Hip, knee, and ankle joint angles, moments, and reaction forces were input to a musculoskeletal model of axial TFJ contact force[3,4] that were parsed to medial and lateral compartments as a function of knee joint width and frontal plane knee joint moment. Comparisons between load conditions and limbs were made using 2 x 3 repeated measures ANOVAs and follow up paired T-tests, alpha at $p < 0.05$.

Results and Discussion

There were no interactions between load and limb dominance for peak TFJF ($p = 0.059$), or peak MTFJF and LTFJF as seen in **Figure 1**, which does not support our hypothesis. From 0% to 15% to 30% load, first peak TFJF increased ($p < 0.001$), with D contact forces being greater than ND ($p = 0.035$) (D 3.22 vs ND 3.11 BW, 3.73 vs 3.54, 4.29 vs 4.10). Peak MTFJF and LTFJF both increased with load; ND MTFJF was greater than D, while D LTFJF was greater than ND as seen in **Figure 1**. There was no difference between D and ND maximum vertical ground reaction force or D and ND sagittal and frontal plane kinematics.

The medial and lateral contact force distribution difference among the loading conditions may be attributed to a 20% greater peak internal knee abduction moment acting on the ND knee as compared to the D knee ($p = 0.007$). The greater ND internal abduction moment is potentially due to a 7.5% greater peak medial ground reaction force (GRF) acting on the ND limb ($p = 0.004$), which increases the external knee moment arm. The D limb did not exhibit the increased peak medial GRF. Therefore, a smaller internal abduction moment acted on the D knee reducing the proportion of the total load that acts through the medial compartment, thus increasing the lateral proportion.

The abductors are the largest contributor to peak medial GRF, while the quadriceps attenuate the abductors' effect on peak medial ground GRF[5]. The D limb exhibited 15% greater estimated peak quadriceps force ($p = 0.011$) than the ND limb, potentially counterbalancing the D limb's abductor force, and attenuating the peak medial GRF to a greater extent than the ND limb. This provides an explanation as to why the dominant limb experienced less peak MTFJF than the ND limb. However, the MTFJF differences did not exceeded the minimum detectable difference with this model (0.246 BW)[6]. Therefore, it also fair to describe the effects as within the range of measurement error.

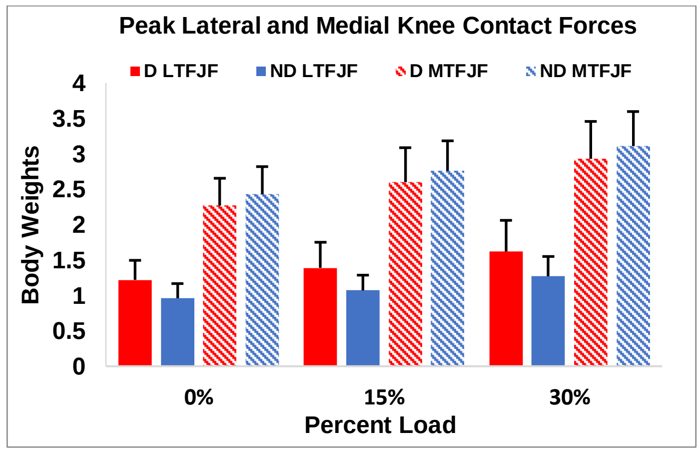

Figure 1: Peak lateral and medial D and ND knee contact forces across all loading conditions. Significance*
LTFJF: D vs ND $p = 0.009$*, Load $p < 0.001$*, Interaction $p = 0.159$
MTFJF: D vs ND $p = 0.009$*, Load $p < 0.001$*, Interaction $p = 0.627$

Significance

There were no interactions between load and D vs. ND knee contact forces, but load did increase contact forces, and peak D TFJF and LTFJF were greater than ND, while peak ND MTFJF was greater than D. These results are a basis for considering leg dominance when investigating knee contact forces. To better understand this compartmental force distribution shift, more work should be conducted on the contributing muscle forces. Furthermore, chronic increases in TFJF can contribute to OA onset and progression[7]. Investigating the prevalence of medial vs lateral compartment knee OA in D vs ND limbs in general and military populations could provide valuable information on pathological patterns.

Acknowledgments

Kinesiology and Physical Therapy departments for funding and lab resources. Research assistants Alex Clark and Brian McGill.

References

1. Lenton et al., *PLoS One San Franc*. 2018;13(11):e0206859.
2. Kong & Burns. *Phys Ther Sport* 2010;11(1):12-17.
3. DeVita & Hortobágyi. *J Appl Biomech*. 2001;17(4):297-311.
4. Willy et al,. *J Biomech.* 2016;49(16):4028-4033.
5. John et al,. *J Biomech*. 2012;45(14):2438-2443.
6. Barrios & Willson. *J Appl Biomech*. 2017;33(2):171-175.
7. Sun. *Ann N Y Acad Sci*. 2010;1211(1):37-50.

PREDICTIONS OF KNEE JOINT CONTACT FORCES USING ONLY KINEMATIC INPUTS WITH A RECURRENT NEURAL NETWORK

Kaileigh E. Estler[1*], Hunter J. Bennett[2]
[1]Biomechanics/Sports Medicine Lab, The University of Tennessee, Knoxville, TN, USA
[2]Neuromechanics Lab, Old Dominion University, Norfolk, VA, USA
email: kestler1@vols.utk.edu

Introduction

Measures of knee joint contact (bone on bone) forces (KJCF) are commonly used as indicative measures for estimating joint healthy. However, true KJCF can only be attained with invasive implantation of instrumented total knee replacements. Estimations of KJCF are currently attained via surrogate measures such as internal knee adduction moments (with limited success) or musculoskeletal modeling (with more successful). Therefore, the purpose of this study was to design a novel prediction method of KJCF measurements that is equal to musculoskeletal modeling accuracy but more simplistic in terms of inputs.

Methods

A recurrent neural network with a long-short term memory (LSTM) was created using MATLAB (R2019B, The Mathworks, Inc., Natick, MA) to predict medial and lateral KJCF waveforms using combinations of kinematic inputs.

Participant Data

This study included motion capture and in-vivo instrumented knee prosthesis data (e.g. true knee joint contact forces) from the opensource "Grand Challenge" (simtk.org) and "CAMS" (CAMS-Knee.orthoload.com) datasets. Musculoskeletal modeling was performed using OpenSim (v3.3, SimTK, Stanford, CA) and the Lai 201 model. Inverse kinematics were used to derive the stance phase hip (sagittal, frontal, transverse), knee (sagittal, frontal), ankle (sagittal), and trunk (frontal) kinematic inputs for the network.

Network Validation Normal Gait

Six datasets of "normal" level ground walking trials (34 trials) were used to train the neural network. Validation of the network was performed using two datasets of normal walking trials (5 trials), separate from the training data for generalizability purposes. Combinations of the kinematic variables with at least one knee kinematic element were used, resulting in 96 input models. Network validation was determined by the proportion of variance (R^2) and root mean square error (*RMSE*) between network predictions and in-vivo data waveforms.

Network Test Medial Thrust and Trunk Sway Gait

The network then performed predictions of medial and lateral KJCF for medial thrust (MT) and trunk-sway (TS) gait. Four datasets were used for both conditions with 15 and 14 trials, respectively. Predictions of medial and lateral KJCF for both conditions were assessed for accuracy against the respective in-vivo data using R^2 and *RMSE*.

Results and Discussion

The overall best network contained frontal hip and knee, and sagittal hip and ankle input variables and presented the finest visual waveform agreement with the in-vivo data for medial KJCF (R^2=0.77, RMSE=0.27) for normal walking. These results outperform most reports of medial KJCF attained by musculoskeletal modeling and knee adduction moments [1-3]. However, predictions of medial KJCF by the network for MT and TS were not as successful (Table 1). These poor results may be due to the specific kinematic variables that were apart of the network. Therefore, further work should implement the kinematic parameter that includes the trunk for predicting KJCF in "non-normal" gait conditions.

The designed LSTM network presented itself to be proficient at predicting KJCF during normal walking conditions. The successful output predictions on waveforms demonstrates generalizability across subjects (but not conditions), unlike its counter method of musculoskeletal modeling.

Table 1. Network prediction agreements of KJCF with the respective in-vivo data

	Medial		Lateral	
Condition	***RMSE***	***R²***	***RMSE***	***R²***
NORM	0.24	0.84	0.26	0.06
MT	0.74	0.08	0.71	0.002
TS	0.67	0.04	0.61	0.004

Notes. Normal walking gait (NORM), medial thrust (MT), trunk sway (TS)

Significance

True in-vivo KJCF can only be measured via implantation technology in patients with total knee replacements yet are extremely scarce. Focus has shifted towards musculoskeletal modeling to estimate KJCF, however, that methodology presents limitations in its complexity. The design of the LSTM network allows for generalizability and real-life application of time series data. These results highlight the non-linear relationship of kinematics that drive joint kinetics and provide a prospective mechanism for predicting bone-on-bone forces. This methodology is a beneficial alternative method for estimating joint contact forces among clinicians and researchers as it requires less time, and computations compared to it's counter of musculoskeletal modeling/simulation.

References

[1] Zhao et al., 2007. *J Ortho Res*. 25: 1121-1127.
[2] Jung et al., 2016. *J Biomech Eng*. 138(2): 1-9.
[3] Ding et al., 2016. *J Biomech Eng*. 138(2): 1-9.

COMPARISON OF IN-LAB AND OUT-OF-LAB GAIT AMONG HEALTHY YOUNG AND OLDER ADULTS AND OLDER ADULTS WITH KNEE OSTEOARTHRITIS

Mayumi Wagatsuma[1], Julien A. Mihy[1], Stephen M. Cain[2], and Jocelyn F. Hafer[1]
[1]University of Delaware, [2]West Virginia University
Email: mayumiw@udel.edu

Introduction

Walking speed, stride length, and range of motion (ROM) during gait vary between healthy young and older adults and older adults with knee osteoarthritis (OA) [1,2]. Gait data collected inside the lab has been used to understand more about aging and pathology and to design clinical training programs. However, interventions that are meant to affect real-world gait may be better informed by gait analysis out-of-lab due to longer walking durations and uncontrolled environment compared to a controlled in-lab environment. Studies comparing in-lab and out-of-lab gait found that spatiotemporal variables and joint range of motion (ROM) differ between the two settings. [3-6]. However, we do not know if gait differs between settings to the same extent among healthy young and older adults and older adults with knee OA. Any changes between in-lab and out-of-lab settings across groups may lead to different intervention effects across populations. Therefore, the purpose of this study was to compare spatiotemporal and joint ROM variables between in-lab and out-of-lab settings among older adults with knee OA, healthy older adults, and young adults. We hypothesized that older adults with and without knee OA would have larger between-setting changes compared to young adults.

Methods

Ten young adults (28.8±4.8yrs), 5 healthy older adults (60.8±2.2yrs), and 3 older adults with knee OA (63.7±4.2yrs) wore 4 inertial measurement units (IMUs): pelvis and one each on the right thigh, shank, and foot. Participants performed straight-line walking at their comfortable speed inside the lab followed by ~10 minutes of supervised out-of-lab walking at a comfortable speed. The out-of-lab walk included straight-line walking, turning, and stairs in open, public campus buildings. We used a zero-velocity update algorithm to calculate walking speed and stride length from foot-mounted IMU data [7]. A functional sensor-to-segment alignment procedure was used to define medial-lateral segment axes for the pelvis, thigh, shank, and foot data. For all strides that were level, steady-state, and did not contain a turn, we extracted walking speed, stride length, and hip, knee, and ankle ROM. Spatiotemporal variables and joint ROMs were compared between in-lab and out-of-lab among young adults, healthy older adults, and older adults with knee OA using a 2-way ANOVA (α=0.1). Due to the small knee OA group, we were not able to report interaction effects.

Results and Discussion

There were significant differences among groups in knee (p=0.006) and hip ROM (p=0.05). Post-hoc analysis revealed that young adults had larger knee ROM compared to older adults with knee OA (Young: 70.0±5.3°, Knee OA: 61.3±4.4°). There were no significant post-hoc differences for hip ROM among groups (Fig.1). Out-of-lab walking speed was slower than in-lab walking speed (p=0.098; In-lab: 1.26±0.15m/s, Out-of-lab: 1.18±0.13m/s) (Fig.1). All other comparisons were not significantly different. Contrary to our hypothesis, older adults with and without knee OA didn't appear to have larger differences between settings compared to young adults. The finding of slower out-of-lab walking speed agrees with previous findings [5], but interestingly, adults with knee OA appeared to have smaller differences in walking speed between settings compared to healthy adults. In addition, a larger range of walking speed was observed in older adults with knee OA.

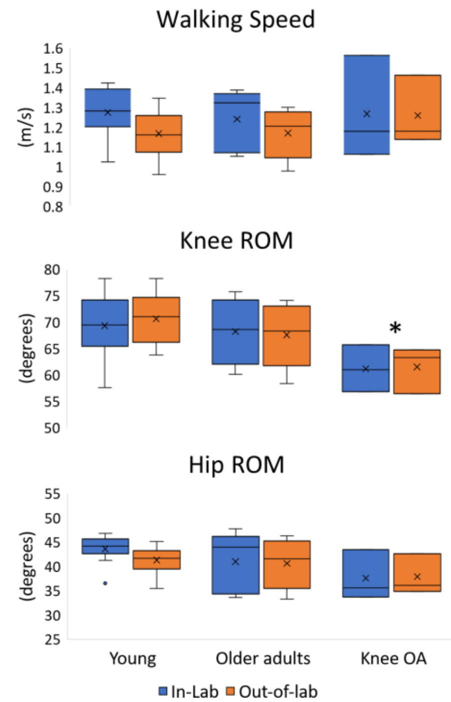

Figure 1: Comparison of in-lab and out-of-lab gait characteristics among healthy young adults, healthy older adults, and older adults with knee OA. * indicates significant difference from young.

Significance

IMUs enable gait measurement in and out of the lab, allowing researchers and clinicians to understand how groups of people walk differently depending on setting. The difference in walking speed between settings appeared to be driven by the healthy groups, with the knee OA group maintaining a similar speed in- and out-of-lab. These populations may not have the same changes in behavior between settings. Between-setting differences may be more apparent in a truly uncontrolled (i.e., real-world) environment. Changes in environment were accompanied by changes in walking speed. Therefore, environment should be carefully considered when conducting gait analyses outside of traditional laboratories or clinics.

References

1. Boyer, KA. Et al., *Experimental gerontology*, 2017, 63-70
2. Mills, K. et al., *Arthritis care & research*, 2013, 1643-1665
3. Carcreff, L et al., *Scientific reports* 2020, 10(1), 2091
4. Del Din, S et al., *J Neuroeng Rehabil* 2016, 13(1):46
5. Renggli D et al., Front Physiol 2020, 11, 90
6. Foucher et al., *Arch Phys Med Rehabil* 2010, 91:1390-5
7. Rebula, JR et al., *Gait & Posture* 2013, 38, 974-980

DIFFERENCES BETWEEN MALES AND FEMALES IN THE RELATION BETWEEN MUSCLE STRENGTH AND KNEE JOINT MOMENTS FEATURES ACROSS CLINICAL OSTEOARTHRIS SEVERITY

Cheryl L. Hubley-Kozey[1,2*], Dianne Ikeda[2], Bernadette McCann[2], Janie L Astephen Wilson[2] and William D Stanish[2,3]
[1]Schools of Physiotherapy and [2]Biomedical Engineering, [3]Department of Surgery Dalhousie University, Halifax NS, Canada
email: *clk@dal.ca

Introduction

Osteoarthritis (OA) is more prevalent in females with evidence that females with knee OA have a more systemic pathology than males. Muscle strength, in particular quadriceps strength, has been linked to knee OA initiation in females with varying reports of lower knee flexion angle (KFA), KF moment (KFM) and late stance knee extension moment (KEM) magnitude during walking in females with knee OA compared to males. These gait features are consistent with a stiff knee gait pattern shown to increase risk of clinical progression to total joint arthroplasty (TKA)[1]. Pain worsening and functional decline have been shown to be greater in females with OA than males, yet our understanding of sex-specific OA progression trajectories remains unclear. Understanding sex differences along an OA severity spectrum in biomechanical gait features, muscle strength, and muscle activation features linked to progression might shed light on the greater functional decline and burden of reported symptoms in females with knee OA.

Our goal was to determine if differences between males and females in muscle strength, KF angle and moment and muscle activation features linked to more rapid clinical progression trajectories were systematic across clinical OA severity levels.

Methods

Data from 324 participants between 40 and 65 years old with and without a knee OA diagnosis who self-reported no other major musculoskeletal, cardiovascular, or neurological gait-altering conditions included demographic (age, sex BMI). Participants were categorized into: Asymptomatic (**ASYM**) with no OA diagnosis (n=118); Moderate OA (**MOA**) knee OA diagnosis, met functional criteria and were nonsurgical candidates (n=141); Severe OA (**SOA**) knee OA diagnosis, scheduled total joint arthroplasty (TKA) within one week post testing (n=65).

Clinical measures included self-reported pain, stiffness and function and knee X-rays scored (WDS) using Kellgren Lawrence (KL) criteria. Participant completed 5-7 walking trials at self-selected speed. 3D segment motion, ground reaction forces and electromyograms (EMG) from medial/lateral quadriceps, hamstrings, and gastrocnemius muscles were collected from the most symptomatic OA limb and a random ASYM limb. Torque and EMG were collected during knee extensor/flexor and plantar flexor maximal voluntary isometric contractions (MVIC) against a dynamometer to calculate muscle strength and for EMG amplitude normalization. Moments and strength were normalized to mass (Kg) with EMG normalized to % MVIC. Principal components (PCs) were scored for KFA and KFM magnitude and difference operators. Discrete metrics included muscle strength, KFM peak, KFM-KEM range, KFM peak/KE strength (%), stance phase EMG root mean squared (RMS) amplitudes (peak, overall and mid-stance). Two-factor (sex, severity group) ANOVAs tested for significant interactions and main effects for PCs and discrete measure as described above (α=0.05) using IBM SPSS Statistics software, V. 26.

Results and Discussion

Example gait waveforms are in Figure 1.

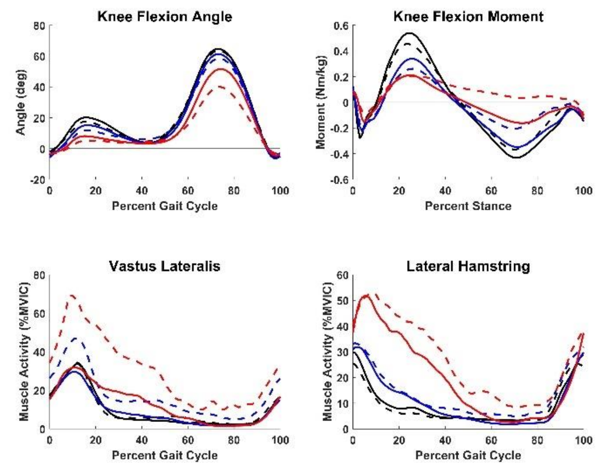

Figure 1: KFA, KFM, VL and LH EMG waveforms. Solid lines-males and dotted lines-females. **Black=AYM, Blue=MOA**, **Red =SOA**.

Key findings include group by sex interactions ($p<0.05$) for KFA magnitude PCs, KE strength, KFM peak/KE strength and all stance phase EMG RMS amplitudes except lateral hamstrings. SOA females had the lowest overall KFA and KE strength (0.67 Nm/Kg), with the highest percentage KFM peak/KE strength ratio (51%) that differed from SOA males, and with no sex differences in ASYM or MOA. SOA females had the highest vasti and hamstring %MVIC for all metrics, and SOA males had the lowest %MVIC for gastrocnemii. Significant group and sex main effects were found for all other variables except no sex differences for KFM peak and LH EMG. Lower KFM features in females indicates a systematic stiffer gait pattern across severity.

As expected, clinical measures and walking speed differed across severity, but no sex differences were found within each severity group for demographic or clinical measures. Despite similarities, the interactions show that sex differences are not systematic across severity for KFA, quadriceps strength and activation amplitudes for 5 of 6 six muscles. Generally, EMG amplitudes were higher for OA females than OA males, but SOA females had the lowest KF motion and activation amplitudes were two times higher than SOA males indicating greater and more prolonged co-activity which cannot be explained by quadriceps strength deficits alone.

Significance

The largest sex-specific differences were in the severe stages of knee OA, and this is an important consideration to understand timing of sex-specific interventions in preventing advanced progression or in end stage OA treatment.

Acknowledgments

CIHR funding support.

References

[1] Hatfield et al., 2015 Arthritis Care and Research

Validating *in-vivo* bone remodelling measurements in knee osteoarthritis

Daphne A. Kaketsis[1,2,3], Jason Werle[2,4], Nicholas Desy[4], Richard Ng[2,4], Emma O. Billington[1,2,3], Peter Salat[2,3], Sarah L. Manske[1,2,3]
[1]Biomedical Engineering Graduate Program; [2]McCaig Institute for Bone and Joint Health; [3]Department of Radiology, Cumming School of Medicine; [4]Department of Surgery, Cumming School of Medicine
Email: daphne.kaketsis@ucalgary.ca

Introduction:
Osteoarthritis (OA) is a whole-joint disease that involves multiple tissue pathologies, including abnormal metabolism in subchondral bone [1]. While early-stage OA can be difficult to diagnose, abnormal subchondral bone remodelling has been considered to have an important role in OA pathogenesis, and some propose that it could offer a target for OA treatment [2]. Clinically, measures of bone remodelling have been performed on iliac crest bone biopsies [3] which are invasive and do not capture local changes. Recently, high resolution peripheral quantitative computed tomography (HR-pQCT) has been utilized in several different ways to analyse bone dynamics [3][4], such as abnormal bone metabolism or bone remodelling in the subchondral bone. However, there are several factors that can affect these measurements [5], and therefore these measurements need to be validated in humans.

Total knee arthroplasty (TKA) patients offer a unique opportunity to acquire bone samples at the proximal tibia, a site accessible by HR-pQCT [6], as during surgery a portion of the proximal tibia is removed. The objective of this study is to validate HR-pQCT as a non-invasive method to measure bone remodelling in-vivo in humans.

Methods:
We recruited 4 participants with end-stage knee OA who intended to undergo TKA. Baseline and 4-month follow-up HR-pQCT scans of the proximal tibia were acquired prior to TKA (covering 30.3 mm in length). A scan-rescan protocol was implemented at one study visit for reproducibility measures. Longitudinal image registration was conducted to align baseline and follow-up scans [7]. Bone remodelling analysis was then conducted following similar principles as a previously established method [8]. Each image was first filtered to reduce noise and then segmented to produce a binary image of bone using a threshold. Three thresholds (250, 320 and 337 HU) were tested. These segmentations were then added together voxel-by-voxel, to identify voxels 1) only present in the baseline image (presumed resorption), 2) voxels only present in the follow-up image (presumed formation), and 3) the overlapping area in both images where there was no presumed change. The percentages of voxels reflecting formation or resorption in the image were calculated. This analysis was also conducted on the scan-rescan images to determine whether changes measured over time were larger than the noise in the scans.

Results and Discussion:
Preliminary results show that bone changes detected between baseline and follow-up scans are of a larger magnitude overall than changes detected from a same day rescan. Figure 1 illustrates that increasing the threshold decreases the percentage of voxels changed between images, although the difference between scan-rescan and baseline-follow-up remained relatively constant regardless of the threshold. Although motion was not observed, noise and registration accuracy likely contribute to the error observed.

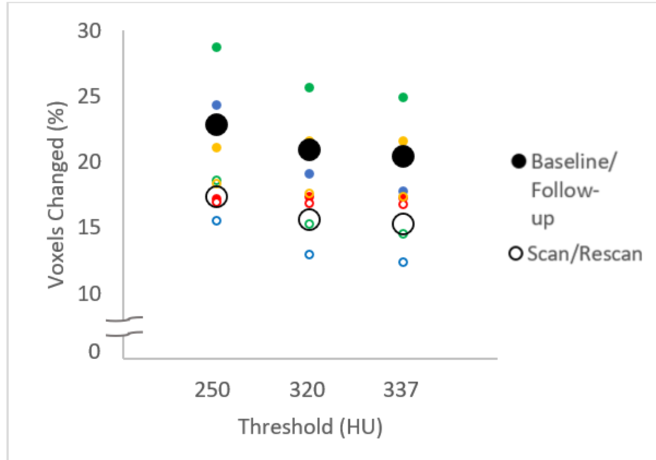

Figure 1: Percentage of voxels that are different between baseline and follow-up images, and between a scan and same day rescan. Black represents the mean, and each colour represents an individual participant.

Future work will include a larger sample size, refining the threshold and the registration process to ensure changes captured are true remodelling in the bone. Additionally in order to validate these measurements, they must be compared with dynamic histomorphometry measures that will be conducted on bone samples obtained from surgery.

Significance:
This study has the potential to advance the way bone remodelling is measured, and it has significant implications in the field of orthopaedics, as it would aid in assessment of joint health without the need for an invasive biopsy.

Acknowledgments
This research was funded in part by NSERC and the American Society for Bone and Mineral Research (ASBMR). We also thank our colleagues from the McCaig Institute for Bone and Joint Health at the University of Calgary for their continued support.

References:

[1] Loeser et al., 2012. *Arthritis & Rheumatism*, 64: https://doi.org/10.1002/art.34453.
[2] Lajeunesse, 2004. *Osteoarthritis and Cartilage*, 12: 10.1016/j.joca.2003.09.013.
[3] Armas et al., 2012. *Bone*, 50: 2011.09.055.
[4] Brunet et al., 2020. *BMC Medical Imaging*, 20: 10.1186/s12880-020-00437-8.
[5] Christenet al., 2018. *PLoS ONE*, 13: 0191369.
[6] Kroker et al., 2017. *Bone*, 97: 2016.12.015.
[7] S. C. Brunet *et al.*, 2021. *Scand. J. Rheumatol.*, 50: 10.1080/03009742.2020.1869303.
[8] S. C. Brunet *et al.*, 2020. *BMC Med. Imaging*, 20: 10.1186/s12880-020-00437-8.